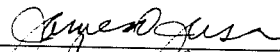



SEISMIC REHABILITATION USING PRECAST INFILL WALLS

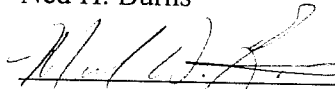
**Approved by
Dissertation Committee:**




James O. Jirsa, Supervisor




Ned H. Burns



Michael D. Engelhardt



Michael E. Kröger



Stelios Kyriakides

SEISMIC REHABILITATION USING PRECAST INFILL WALLS

by

Robert Joseph Frosch, B.S.E., M.S.E.

Dissertation

Presented to the Faculty of the Graduate School of

The University of Texas at Austin

in Partial Fulfillment

of the Requirements

for the Degree of

Doctor of Philosophy

The University of Texas at Austin

May 1996

To Mom and Dad

ACKNOWLEDGMENTS

I would like to thank Dr. James O. Jirsa, dissertation supervisor, for his guidance and assistance. He has been a source of motivation and support. I am grateful to have had the fortune of working with him. I would also like to thank Dr. Michael E. Kreger for his contributions to the project and for serving on my dissertation committee. His help and advice throughout the project were invaluable to the success of the project.

I want to extend my sincere thanks to Dr. Ned H. Burns, Dr. Michael D. Engelhardt, and Dr. Stelios Kyriakides for their help and advice and for serving on my dissertation committee.

I would like to thank Loring Wyllie, Jr. of Degenkolb Engineers and Tom Sabol of Englekirk and Sabol Consulting Engineers for their practical advice and assistance with the research. Their contributions to the project helped focus the project and maintain the research within the realm of the “real world.”

Thanks to all my fellow graduate students at the Ferguson Laboratory for their assistance and support. No part of this dissertation would be possible without their help. Special thanks to Michael Brack for his help in the research especially throughout the design and construction of the large scale model structure. I also want to thank Wanzhi Li for his assistance throughout the project. Also, the assistance of the entire staff of the Ferguson Laboratory is greatly appreciated.

I would like to thank my parents, Bessie and Warren Frosch, Jr., for their love and support throughout the years. They have taught me the joy of learning and the pursuit of excellence. Additionally, they have instilled in me drive and perseverance; allowing all my dreams to come true.

Finally, I would like to thank God for through Him all things are possible.
Crux Spes Unica.

This study was conducted at the Phil M. Ferguson Structural Engineering Laboratory and was sponsored by the National Science Foundation. I want to extend my gratitude to the sponsor for making this study possible. I would also like to thank the Earthquake Engineering Research Institute for additional support to my research provided through the EERI/FEMA NEHRP Graduate Fellowship.

Robert J. Frosch

December 26, 1995

SEISMIC REHABILITATION USING PRECAST INFILL WALLS

Publication No. _____

Robert Joseph Frosch, Ph.D.
The University of Texas at Austin, 1996

Supervisor: James O. Jirsa

Many existing reinforced concrete moment-resisting frames located in seismic zones lack strength and ductility. One approach for correcting these deficiencies is the construction of infill walls to strengthen and stiffen the structure. Cast-in-place construction is often used; however, there are conditions where cost, time constraints, or limiting disruptions to building operations may dictate other solutions. One possible modification is the use of infill walls constructed of precast concrete panels.

A precast infill wall system eliminates the need for large formwork during construction. Elimination or reduction of connection hardware between precast panels or between panels and the existing frame element can provide additional efficiency. Problems associated with casting large quantities of concrete in an existing building are eliminated. Construction time and inconvenience to occupants may be reduced along with the costs.

Three phases of experimental research were conducted. The first phase was investigation of the precast panel-to-panel connection. In the second phase, the precast panel to existing-frame connection was studied. In both phases, direct cyclic shear tests were conducted to determine minimum details for satisfactory connection performance. The third phase consisted of testing a large-scale model specimen. The test specimen, a two-story nonductile frame infilled with precast panels was used to

evaluate the overall system behavior, verify performance of connection details, and investigate the performance of post-tensioning used to provide column tensile capacity at the boundary elements of the wall.

Design and detailing guidelines were developed to enable designers to use the precast infill wall system as an alternative to cast-in-place construction. The precast system has the potential of reducing the overall costs of rehabilitating existing structures.

TABLE OF CONTENTS

CHAPTER 1: INTRODUCTION.....	1
1.1 Earthquake Resistant Design	1
1.2 Nonductile Reinforced Concrete Moment Frames	3
1.2.1 Nonductile Features	4
1.2.2 Typical Building	4
1.3 Current Techniques for Seismic Strengthening	6
1.3.1 Jacketing	7
1.3.2 Steel Bracing	9
1.3.3 Infill Wall.....	10
1.4 Need for Economic Rehabilitation Scheme	12
1.5 Precast Infill Wall	13
1.6 Objective and Scope	16
CHAPTER 2: PANEL TO PANEL CONNECTION	18
2.1 Introduction.....	18
2.2 Specimen Design	18
2.2.1 Panel Surface Preparation	19
2.2.2 Panel Reinforcement	19
2.2.3 Closure Strip	20
2.2.4 Test Variables	21
2.3 Specimen Construction	24
2.3.1 Precast Panel Construction	25
2.3.2 Wall Construction	25
2.3.2.1 Trough Method	26
2.3.2.2 Access Hole Method	27
2.4 Construction Materials.....	28
2.4.1 Precast Panel Concrete.....	28
2.4.2 Panel Grout	30
2.4.3 Reinforcing Steel	32
2.5 Test Setup and Procedure.....	33
2.6 Experimental Results	35
2.6.1 Series I-PC	37
2.6.1.1 PC-1 (Aligned, 1.0 Key Spacing)	38
2.6.1.2 PC-2 (Aligned, 1.5 Key Spacing)	38
2.6.1.3 PC-3 (Staggered, 1.0 Key Spacing)	38
2.6.1.4 PC-4 (Staggered, 1.5 Key Spacing)	39
2.6.2 Series II-PC.....	39
2.6.2.1 PC-5 (2#3 Bars)	41

2.6.2.2 PC-6 (4#4 Bars)	41
2.6.2.3 PC-7 (4#4 Bars, Low Grout).....	42
2.6.2.4 PC-8(4#4 Bars, Large Key)	42
2.6.2.5 PC-12(6 #5 Bars)	42
2.6.3 Series III-PC.....	43
2.6.3.1 PC-9 (4 #3 Bars)	44
2.6.3.2 PC-10 (2 #4 Bars)	44
2.6.3.3 PC-11 (4 #3 Bars, Large Key)	44
2.6.4 Series IV-PC	45
2.6.4.1 PC-13 (2 #3 Bars)	45
2.6.4.2 PC-14 (4#4 Bars)	46
2.7 Analysis of Test Results.....	46
2.7.1 Failure Surface Location.....	46
2.7.2 Shear Key Configuration	46
2.7.3 Shear Key Size	48
2.7.4 Spacing Between Panels	48
2.7.5 Concrete Strength.....	48
2.7.6 Panel Thickness	51
2.7.7 Vertical Steel Reinforcement.....	51
2.7.8 Other Failure Modes	51
2.7.9 Determination of Capacity.....	55
2.7.9.1 Adhesion Capacity	55
2.7.9.2 Peak Capacity.....	55
2.7.9.3 Residual Capacity	59
2.7.10 Design Rationale.....	60
2.8 Design and Detailing Recommendations.....	62
2.8.1 Precast Panel Design.....	62
2.8.2 Grout Strip Concrete	62
2.8.3 Grout Strip Reinforcement.....	62
2.8.4 Wall Design Considerations	63
CHAPTER 3: PANEL TO FRAME CONNECTION	64
3.1 Introduction.....	64
3.2 Specimen Design	64
3.2.1 Precast Panels.....	64
3.2.2 Existing Frame.....	65
3.2.3 Closure Strip	65
3.2.4 Test Variables	66
3.3 Specimen Construction.....	68
3.3.1 Precast Panel Construction	68
3.3.2 Frame Element.....	68

3.3.3 Wall Construction	69
3.4 Construction Materials.....	70
3.4.1 Existing Frame Concrete.....	70
3.4.2 Precast Panel Concrete.....	72
3.4.3 Panel Grout	72
3.4.4 Interface Steel	72
3.5 Test Setup and Procedure.....	73
3.6 Experimental Results	74
3.6.1 Series I-FC	75
3.6.1.1 FC-1	76
3.6.1.2 FC-2	77
3.6.1.3 FC-3	77
3.6.2 Series II-FC.....	77
3.6.2.1 FC-4	77
3.7 Analysis of Test Results.....	78
3.7.1 Interface Shear Failure	78
3.7.2 Pipe Failure Mode.....	78
3.7.3 Localized Bearing Failure.....	80
3.7.4 Determination of Capacity	80
3.7.4.1 Adhesion Capacity	80
3.7.4.2 Peak Capacity.....	80
3.7.4.3 Residual Capacity	81
3.7.5 Design Rationale.....	82
3.8 Design and Detailing Recommendations.....	83
3.8.1 Precast Panel Design.....	83
3.8.2 Pipe Design	83
3.8.3 Pipe Embedment.....	83

CHAPTER 4: STRENGTHENED NON-DUCTILE FRAME TEST	
STRUCTURE: DESIGN AND CONSTRUCTION.....	85
4.1 Introduction.....	85
4.2 Specimen Design	85
4.2.1 Existing Frame	85
4.2.2 Infill Wall.....	88
4.2.2.1 Design Shear Capacity	90
4.2.2.2 Wall-to-Frame Connection	90
4.2.2.3 Precast Panels.....	94
4.2.2.4 Panel Connection - Reinforcement Across Critical Shear	
Key Interface.....	96
4.2.2.5 Flexural Capacity, Post Tensioning Requirements.....	97
4.3 Specimen Construction.....	98

4.3.1 Existing Frame	98
4.3.2 Infill Wall Construction	100
4.3.2.1 Precast Panels.....	100
4.3.2.2 Core Holes	102
4.3.2.3 Panel Placement, Bracing, and Forming.....	102
4.3.2.4 Wall Construction Sequence.....	105
4.3.3 Post Tensioning Steel.....	109
4.4 Construction Materials.....	111
4.4.1 Existing Frame Concrete.....	111
4.4.2 Precast Panels.....	113
4.4.3 Panel Grout	114
4.4.4 Reinforcing and Interface Steel.....	115
4.4.5 Post-Tensioning Steel	116
4.5 Testing Setup	117
CHAPTER 5: EXISTING FRAME: TEST RESULTS.....	120
5.1 Introduction.....	120
5.2 Frame Analysis	120
5.3 Test Results.....	123
5.4 Cracking.....	124
5.5 Stiffness.....	125
5.6 Nonductile Elements.....	126
5.6.1 Beam Bottom Steel	126
5.6.2 Column Splice.....	127
5.6.3 Column Shear Failure	127
5.7 Conclusion	128
CHAPTER 6: PRECAST INFILL WALL SYSTEM: TEST RESULTS.....	129
6.1 Introduction.....	129
6.2 Test Results.....	129
6.2.1 Test 1: Flexural Hinge	129
6.2.1.1 Structural Behavior: Prior to Splice Failure.....	132
6.2.1.2 Structural Behavior: After Splice Failure (0.3-0.55% Drift)	134
6.2.2 Test 2: Shear Test - 500 kips Post-Tensioning	136
6.2.2.1 Structural Behavior	137
6.2.3 Test 3: Shear Test - No initial Post-Tensioning.....	139
6.2.3.1 Structural Behavior	139
6.3 Cracking.....	141
6.3.1 Flexural Cracking.....	141
6.3.2 Shear Cracking.....	141
6.3.3 Base Crack	143

6.3.4 Frame Boundary Cracks	145
6.4 Interface Slip.....	145
6.5 Capacity	147
6.5.1 Zero Tension	147
6.5.2 Decompression Load	148
6.5.3 Splice Failure	150
6.5.4 Flexural Strength.....	154
6.5.5 Shear Strength.....	155
6.6 Stiffness.....	157
6.6.1 Prior to Decompression Load	157
6.6.2 Decompression Load - Splice Failure.....	158
6.6.3 Post Splice Failure	159
6.7 Frame Connections	160
6.8 Precast Panels and Panel Connection	161
6.9 Observed Behavior versus Design Assumptions	162

**CHAPTER 7: PRECAST INFILL WALL SYSTEM: DESIGN AND
DETAILING GUIDELINES163**

7.1 Introduction.....	163
7.2 General Design Requirements	163
7.2.1 Design Philosophy	164
7.2.2 Effects of Modified Load Path on Existing Structure.....	165
7.3 Flexural Strength.....	165
7.3.1 Post Tensioning Anchorage	166
7.4 Shear Strength.....	166
7.4.1 Frame Connection.....	169
7.4.2 Precast Panels.....	173
7.4.3 Panel Connection	174
7.5 Performance Based Design Criteria.....	175
7.5.1 Drift Control.....	176
7.5.1.1 Decompression Moment	176
7.5.1.2 Splice Failure	177
7.5.1.3 Drift at the Collapse Limit State	178
7.5.2 Shear Strength Prior To Splice Failure	178

CHAPTER 8: SUMMARY AND CONCLUSIONS182

8.1 Introduction.....	182
8.2 Panel-to-Panel Connection.....	183
8.3 Panel-to-Frame Connection	184
8.4 Model Test Structure.....	185
8.4.1 Existing Frame	185

8.4.2 Precast Infill Wall System	186
8.5 Design Guidelines	187
8.6 Future Research	187
8.7 Conclusion	188
APPENDIX A: PANEL CONNECTION TEST RESULTS	189
APPENDIX B: FRAME CONNECTION TEST RESULTS	197
APPENDIX C: FRAME STRUCTURAL DRAWINGS	200
APPENDIX D: INFILL WALL STRUCTURAL DRAWINGS	211
APPENDIX E: LOADING AND BRACING SYSTEM DRAWINGS	215
BIBLIOGRAPHY	230
VITA	234

LIST OF FIGURES

Figure 1.1: Ground Motion Amplification.....	1
Figure 1.2: Structural Response.....	2
Figure 1.3: Hinging Mechanisms.....	2
Figure 1.4: Typical 1950's and 60's RCMRF Building.....	3
Figure 1.5(a): Beam Jacketing ^[15]	8
Figure 1.5(b): Column and Joint Jacketing ^[15]	8
Figure 1.6: Beam and Column Jacketing Construction.....	9
Figure 1.7: Steel Bracing.....	10
Figure 1.8: Infill Wall.....	11
Figure 1.9: Precast Infill Wall System.....	14
Figure 1.10: Out-of-Plane Resistance.....	15
Figure 1.11: Post-Tensioning System.....	15
Figure 2.1: Panel Connection Test Component.....	18
Figure 2.2: Shear Key Geometry.....	19
Figure 2.3: Panel Connection Specimen Details.....	20
Figure 2.4: Shear Key Alignment.....	21
Figure 2.5: Shear Key Spacing.....	23
Figure 2.6: Shear Key Size.....	23
Figure 2.7: Precast Panel Construction.....	25
Figure 2.8: Wall Construction.....	26
Figure 2.9: Trough Method.....	27
Figure 2.10: Access Hole Method.....	27
Figure 2.11: Precast Panel Concrete Strength Gain.....	29
Figure 2.12: Panel Grout Strength Gain.....	32
Figure 2.13: Test Setup.....	33
Figure 2.14: Self-Equilibrating Vertical Load System.....	34
Figure 2.15: Specimen Instrumentation.....	34
Figure 2.16: Panel Connection Test (PC-5).....	35
Figure 2.17: Failure Surface (PC-5).....	36
Figure 2.18: Series I-PC Specimens.....	37
Figure 2.19: Casting vs. Testing Position.....	40
Figure 2.20: Series II-PC Specimens.....	40
Figure 2.21: Series III-PC Specimens.....	43
Figure 2.22: Series IV-PC Specimens.....	45
Figure 2.26: Failure Plane (PC-7).....	48
Figure 2.30: Effect of Vertical Reinforcement on Peak Capacity.....	56
Figure 2.31: Effect of Compression on Shear Strength.....	57
Figure 3.1: Frame Connection Test Component.....	64
Figure 3.2: Existing Frame Element Details.....	65

Figure 3.3: Frame Connection Specimen Details	66
Figure 3.4: Frame Element Construction.....	69
Figure 3.5: Specimen Casting Position.....	69
Figure 3.6: Wall Construction.....	70
Figure 3.7: Core Hole for Shear Lug	70
Figure 3.8: Existing Frame Concrete Strength Gain.....	71
Figure 3.9: Specimen Instrumentation.....	74
Figure 3.10: Frame Connection Test Result (FC-3)	75
Figure 3.11: Series I-FC Specimens	76
Figure 3.12: Series II-FC Specimen.....	77
Figure 3.13: Flexural Yielding of Pipe (FC-2)	78
Figure 3.14: Shear Yielding of Pipe (FC-4).....	79
Figure 3.15: Embedment Determination.....	84
Figure 4.1: Existing Frame Specimen.....	86
Figure 4.2: Infill Wall Panel Layout.....	88
Figure 4.3: Infill Wall Specimen	89
Figure 4.4: Shear Distribution.....	90
Figure 4.5: Frame Connection Design.....	92
Figure 4.6: Check of Pipe Through Beam	93
Figure 4.8: Precast Panels.....	94
Figure 4.7: Precast Panel Design	95
Figure 4.9: Panel Connection Design	96
Figure 4.10: Footing Construction.....	99
Figure 4.11: First Story Construction	99
Figure 4.12: Completed First Story	99
Figure 4.14: Completed Structure.....	100
Figure 4.13: Second Story Construction.....	100
Figure 4.15: Panel Precasting Bed	101
Figure 4.16: Panel Storage.....	101
Figure 4.17: Panel Shrinkage Crack	101
Figure 4.18(b): Close-Up of Crane	103
Figure 4.18(a): Lifting System.....	103
Figure 4.19: Insertion of Lifting Inserts.....	104
Figure 4.21: Bottom Row of Panels in Position	104
Figure 4.20: Panels Supported by Lifting Inserts	104
Figure 4.22: Construction Sequence of Wall.....	105
Figure 4.23: Base Shear Lugs and Reinforcement.....	106
Figure 4.25: Grouting of Horizontal Shear Lugs in Column.....	106
Figure 4.24: Grouting of Shear Lugs in Footing.....	106
Figure 4.27: Vibration Through Access Holes	107
Figure 4.26: Closure Strips Formed.....	107

Figure 4.28: Simultaneous Operations.....	107
Figure 4.29: Installation of Shear Lug (Note Welded Joint).....	108
Figure 4.30: Vertical and Horizontal Strip Reinforcement Installed.....	108
Figure 4.31: Completed Wall Construction.....	108
Figure 4.32: Void at Beam/Column Corner.....	109
Figure 4.33: Stressing of Post-Tensioning Bars.....	110
Figure 4.34: Completed Infill Wall System.....	111
Figure 4.35: Existing Frame Concrete Strength Gain.....	112
Figure 4.36: Infill Panel Concrete Strength Gain.....	114
Figure 4.37: Infill Grout Strength Gain.....	114
Figure 4.38: 1 in. Dywidag Stress-Strain Curve.....	116
Figure 4.39: Testing Setup.....	117
Figure 4.40: Loading System.....	118
Figure 4.41: Bracing and Loading System.....	118
Figure 4.42: Displacement Gage Layout.....	119
Figure 4.43: Strain Gage Layout.....	119
Figure 5.1: Loading Pattern.....	120
Figure 5.2: Failure Sequence.....	122
Figure 5.3: Frame Loading Pattern.....	123
Figure 5.4: Existing Frame Test Result.....	123
Figure 5.5: Column and Beam +M Cracking.....	124
Figure 5.6: Beam -M Cracking.....	125
Figure 5.7: Analytical Model.....	125
Figure 6.1: Loading Distribution.....	129
Figure 6.2: Test 1 Loading History.....	131
Figure 6.3: Test 1 Response.....	131
Figure 6.4: Test 1 Response Prior to Splice Failure.....	132
Figure 6.5: Test 1 Response After Splice Failure.....	135
Figure 6.6: Loading Behavior After Splice Failure.....	135
Figure 6.7: Test 2 Loading History.....	137
Figure 6.8: Test 2 Response.....	138
Figure 6.9: Test 3 Response.....	140
Figure 6.10(a): Compression Strut Spalling Location.....	141
Figure 6.10(b): Close-Up of Spalled Concrete.....	141
Figure 6.11: Wall Cracking Pattern.....	142
Figure 6.13: Second Floor Cracking Pattern.....	142
Figure 6.12: First Floor Cracking Pattern.....	142
Figure 6.14: Crack at Wall Base.....	143
Figure 6.15: Crack Following Splice Failure (West Column).....	143
Figure 6.16: Pull-Out of Shear Lugs.....	144
Figure 6.17: Maximum Crack Width During Test 1 (East Bars Shown).....	144

Figure 6.18: Frame Boundary Crack (East Column Shown).....	145
Figure 6.19: Frame Boundary Cracking and Interface Slips	146
Figure 6.20: Slip at Base of Wall (Test 3)	146
Figure 6.21: Zero Tension Stress State	147
Figure 6.22: East Column Tension Steel (Test 1).....	148
Figure 6.23: West Column Tension Steel (Test 2)	149
Figure 6.24: Analysis of Decompression Load.....	149
Figure 6.25(a): East Column Splice Failure	151
Figure 6.25(b): West Column Splice Failure.....	151
Figure 6.26: East Post-Tensioning Strain Increase (Test 1).....	153
Figure 6.27: West Post-Tensioning Strain Increase (Test 2)	154
Figure 6.28: Strut and Tie Model.....	156
Figure 6.29: Nodal Point Analysis.....	156
Figure 6.30: Test 1 Model Comparisons.....	157
Figure 6.31: Test 2 Model Comparisons.....	158
Figure 6.32: Test 3 Model Comparisons.....	159
Figure 6.33: Post-Tensioning System Model	160
Figure 7.1: Precast Infill Wall System.....	167
Figure 7.2: Design Shear Distribution	169
Figure 7.3: Embedment Determination.....	170
Figure 7.4: Comparison of Frame Connection Recommendations.....	172
Figure 7.5: Shear Key Pattern.....	173
Figure 7.6: Base Shear Capacity Prior to Splice Failure	179
Figure 7.7(a): Assumed Failure Plane For Analysis.....	180
Figure 7.7(b): Wall Shear Capacity Prior to Splice Failure.....	181
Figure A.1: PC-1 Test Result.....	190
Figure A.2: PC-2 Test Result.....	190
Figure A.3: PC-3 Test Result.....	191
Figure A.4: PC-4 Test Result.....	191
Figure A.5: PC-5 Test Result.....	192
Figure A.6: PC-6 Test Result.....	192
Figure A.7: PC-7 Test Result.....	193
Figure A.8: PC-8 Test Result.....	193
Figure A.9: PC-9 Test Result.....	194
Figure A.10: PC-10 Test Result.....	194
Figure A.11: PC-11 Test Result.....	195
Figure A.12: PC-12 Test Result.....	195
Figure A.13: PC-13 Test Result.....	196
Figure A.14: PC-14 Test Result.....	196
Figure B.1: FC-1 Test Result.....	198
Figure B.2: FC-2 Test Result.....	198

Figure B.3: FC-3 Test Result	199
Figure B.4: FC-4 Test Result	199
Figure C.1: Isometric View.....	201
Figure C.2: Plan View.....	202
Figure C.3: North Elevation.....	203
Figure C.4: West Elevation.....	204
Figure C.5: Footing Plan.....	205
Figure C.6: Footing Details	206
Figure C.7: Floor Plan	207
Figure C.8: Column and Beam Details	208
Figure C.9: Floor Beam Reinforcement Detail.....	209
Figure C.10: Column Splices.....	210
Figure D.1: Isometric View	212
Figure D.2: Infill Wall Details	213
Figure D.3: Panel and Pipe Details	214
Figure E.1: Isometric View.....	216
Figure E.2: 2nd Floor Loading and Bracing System	217
Figure E.3: 3rd Floor Loading and Bracing System	218
Figure E.4: 2nd Floor Load Transfer System	219
Figure E.5: 3rd Floor Load Transfer System	220
Figure E.6: Detail 'A'	221
Figure E.7: Detail 'B'	222
Figure E.8: Detail 'C'	223
Figure E.9: Detail 'D'	224
Figure E.10: Detail 'E'.....	225
Figure E.11: Wall Gusset Plate.....	226
Figure E.12: Angle Connection Shims	227
Figure E.13: Bearing Plate.....	228
Figure E.14: Lateral Brace	229

LIST OF TABLES

Table 1.1: Typical Design Loads	5
Table 1.2: Design Requirements for Infill Wall System.....	16
Table 2.1: Panel Connection Test Details.....	22
Table 2.2: Precast Panel Mix Design.....	29
Table 2.3: Panel Grout Mix Design	31
Table 2.4: Panel Connection Reinforcing Steel.....	32
Table 2.5: Panel Connection Test Results	36
Table 2.6: Peak Capacity Analysis	58
Table 2.7: Residual Capacity Analysis	60
Table 2.8: Comparisons of Test Results with Design Method	61
Table 3.1: Frame Connection Test Details	67
Table 3.2: Frame Element - Concrete Mix Proportions.....	71
Table 3.3: Frame Connection Test Results.....	75
Table 3.4: Peak Capacity Analysis	81
Table 3.5: Residual Capacity Analysis	82
Table 3.6: Comparisons of Test Results with Design Method	82
Table 4.1: Existing Frame Concrete Mix.....	112
Table 4.2: Precast Panel Concrete Mix.....	113
Table 4.3: Infill Grout Mix	115
Table 5.1: Frame Section Properties.....	121
Table 6.1: Loading to Reach Zero Tension.....	147
Table 6.2: Decompression Moment Analysis.....	150
Table 6.3: Splice Failure Test Results	151
Table 6.4: Splice Capacity Analysis	153

CHAPTER 1

INTRODUCTION

1.1 Earthquake Resistant Design

Earthquakes are caused by a rupture in the earth's crust. The initial rupture and propagation of the rupture cause ground vibrations that propagate from the source as seismic waves. These waves carry energy at different frequencies and can be modified as they propagate due to distance and soil effects. For a specific earthquake, structure location, and soil condition; the frequency content of the ground motion varies. As shown in Figure 1.1, ground motion amplification can occur when the frequency content of the ground motion matches the vibration characteristics of the structure. The maximum amplification (a_{max}) results when the fundamental period of the structure (T_2) is the same as the peak period of the ground acceleration.

The ground accelerations induce displacements to the structure. Earthquakes, therefore, do not directly apply forces as is normally considered in design for loads such as gravity and pressure.

Rather, the forces are set-up or induced by the displacements. It can conveniently be viewed that an earthquake applies a displacement Δ_{EQ} to a structure. As shown in Figure 1.2, if the structure responds elastically, a lateral force resistance F_1 is required. If ductility is

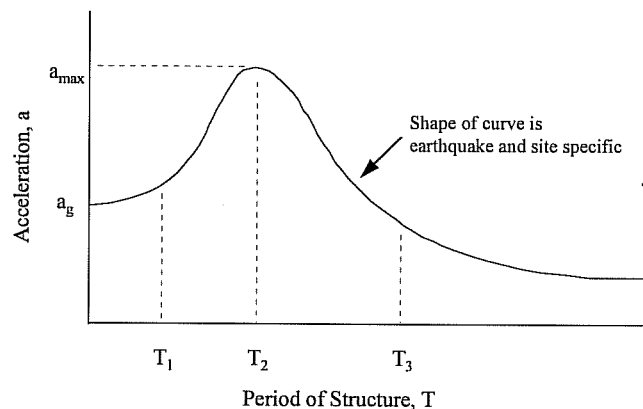


Figure 1.1: Ground Motion Amplification

provided, however, the structure can reach the same displacement with a lower lateral force level. For example, if a ductility of four ($\mu = 4$) is provided, the force resistance can be reduced by a factor of four. Assuming equivalent displacements is often termed the equal displacement principle which is approximately correct for structures with periods longer than T_2 on the descending branch of the amplification curve.^[32]

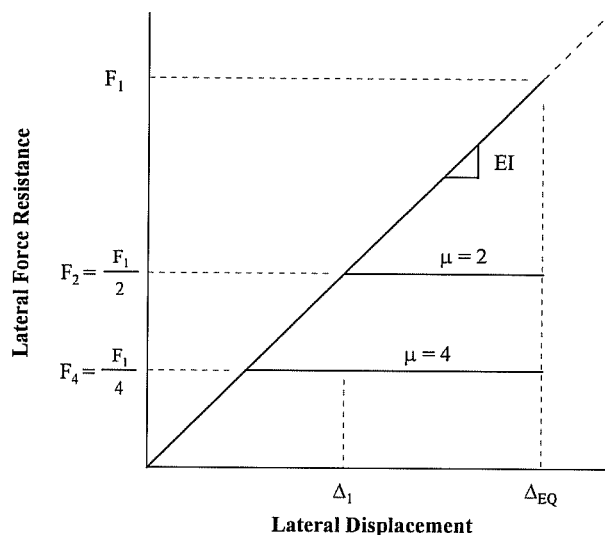


Figure 1.2: Structural Response

Overall structural ductility is provided by allowing a stable mechanism to form within the structure. Figure 1.3 shows the philosophy known as strong column - weak beam hinging (Mechanism 1) which is generally followed in earthquake design. The beams and column bases are allowed to hinge to provide for large lateral deformations while the gravity load capacity is maintained. If, however, the columns are allowed to hinge before beam hinging occurs (Mechanism 2), a loss of gravity load capacity can occur with a collapse of a single story at the hinging locations. This undesirable hinging mechanism is known as a strong beam - weak column

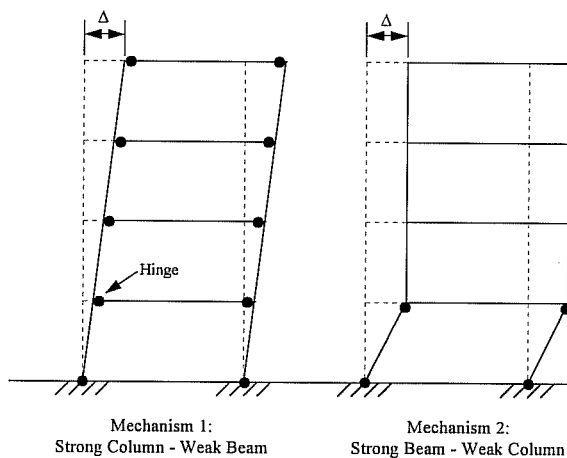


Figure 1.3: Hinging Mechanisms

system. It can also be seen by comparing the two mechanisms that for the same lateral displacement Δ , Mechanism 2 requires extremely large deformations and localized rotations to occur at the first story. Mechanism 1 spreads rotations and deformations across the entire structure to reduce the ductility demand on individual members.

1.2 Nonductile Reinforced Concrete Moment Frames

Many reinforced concrete moment resisting frame buildings in seismic zones lack strength and ductility. A large number of these buildings were designed and constructed during the 1950's and 60's and do not possess the deformation capacity required for the level of lateral strength provided. The codes at the time recognized earthquake loads as mentioned in ACI 318-56^[1] and ACI 318-63.^[2]

- (a) The resisting elements in structures required to resist wind and earthquake forces shall be limited to the integral structural parts.
- (b) The moments, shears, and direct stresses resulting from wind or earthquake forces determined in accordance with recognized methods shall be added to the maximum stresses which exist at any section for dead and live loads.
- (c) Members subject to stresses produced by wind or earthquake forces combined with other loads may be proportioned for unit stresses 33 1/3 percent greater than those specified ..., provided that the section thus required is not less than that required for the combination of dead and live load.

According to the recognized methods of the day, the lateral forces prescribed were much lower than that required for elastic behavior. Therefore, ductility must be present in the structure to sustain the imposed deformation. The building codes, however, did not specify detailing requirements to achieve inelastic deformation capacity and structural toughness under significant cyclic lateral deformations.

1.2.1 Nonductile Features

The principal deficiency in concrete moment frames is inadequate flexural ductility or shear capacity in beams or columns and lack of confinement, frequently in the joints.^[15] In addition, since structures were primarily designed for gravity loads, compression lap splices were typically used. Typical nonductile features (weak links) are summarized below. FEMA-178^[16] provides a method for evaluating existing buildings and identifying those that are likely to be seismically hazardous.

Beams and Columns:

- Inadequate flexural capacity
- Inadequate shear capacity
- Lack of confinement
- Lack of column tension lap splices

Beam-Column Joints:

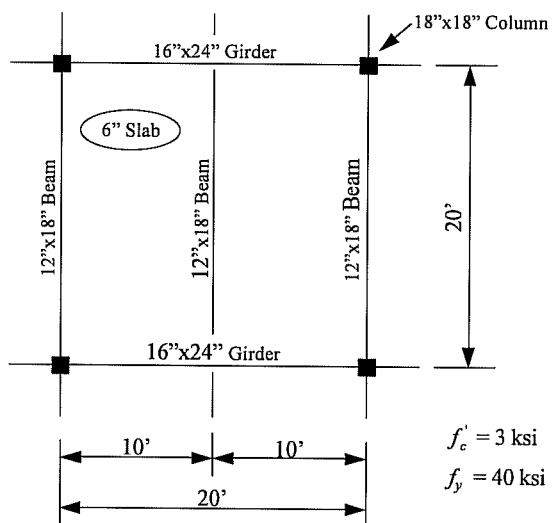
- Lack of confinement
- Inadequate joint shear capacity
- Strong Beam-Weak Column

1.2.2 Typical Building

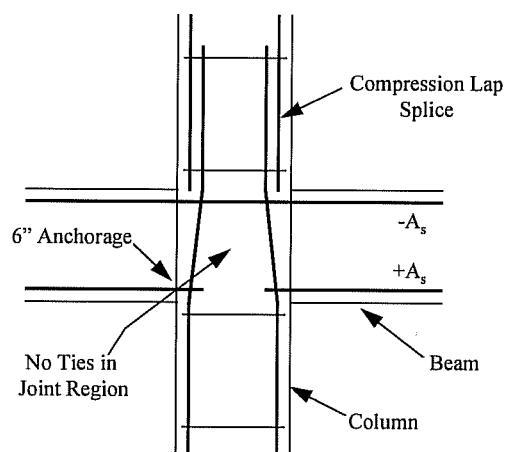
A typical reinforced concrete moment-resisting frame (RCMRF) building from the 1950's and 60's is presented in Figure 1.4. The gravity load system consisted of a one-way slab supported by a beam and girder system. There is a large inventory of this type of structure, particularly in the two to five story range as shown in the elevation view. Typical design loads for these structures are presented in Table 1.1.

Table 1.1: Typical Design Loads

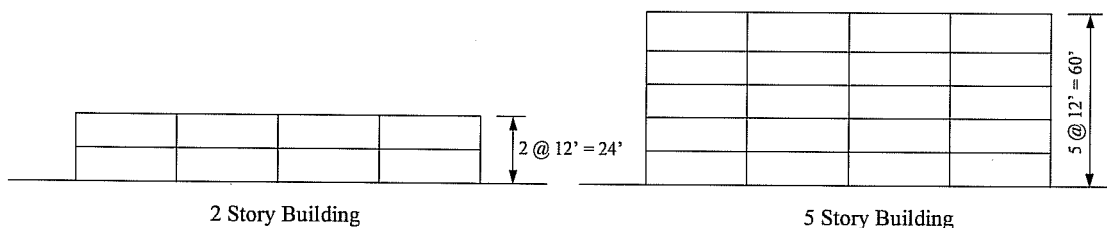
Dead Load		Live Load	
Partitions	20 psf	Apartment/	
Ceiling/Finish	10 psf	Office	50 psf
Services	5 psf		
Misc.	7 psf		



Typical Interior Plan



Typical Beam-Column Joint Detail



Elevation View

Figure 1.4: Typical 1950's and 60's RCMRF Building

1.3 Current Techniques for Seismic Strengthening

Structures can be rehabilitated by increasing the displacement capacity of the structure to meet the demands imposed by an earthquake Δ_{EQ} . As an example, a building may possess a lateral resistance F_4 and a ductility level of two ($\mu=2$) which provides a displacement capacity of Δ_1 as shown in Figure 1.2. The building may be strengthened by increasing the lateral force resistance to F_2 (assuming the ductility remains constant), by increasing the ductility to a level of four ($\mu=4$), or by a combination of the two. In other words, the building can be rehabilitated by increasing the strength, ductility, or a combination of the two.

Structures can also be rehabilitated by reducing the demands imposed by an earthquake. The structure's period can be modified by making the structure more stiff or more flexible to change the ground acceleration amplification as shown in Figure 1.1. For example, for a structure with a period T_2 , a shift to T_1 or T_3 will decrease the acceleration amplification. Depending on the period of the structure and the period shift, it is possible that the displacements may decrease or increase which can be determined from the displacement spectrum for the specific case investigated. There are many locations where ground motion characteristics require a change in the dynamic response of the structure to meet the performance requirements established for the structure. Generally, this can be done by changing the stiffness of the lateral load resisting system.

The effect of the rehabilitation scheme on the strength, ductility, and period must be considered together since modification of one can effect the others. The goal of the design or rehabilitation scheme is to provide for displacement capacity of the structure greater than the displacement demands of the earthquake.

A state-of-the-art report on seismic rehabilitation of existing structures is provided in the NEHRP Handbook for Seismic Rehabilitation of Existing

Buildings.^[15] The following three techniques are listed for rehabilitating reinforced concrete moment frame buildings.

1. *Increasing the ductility and capacity by jacketing the beam and column joints or increasing the beam or column capacities. (Jacketing)*
2. *Reducing the seismic stresses in the existing frames by providing supplemental vertical-resisting elements. (Steel Bracing)*
3. *Changing the system to a shear wall system by infilling the reinforced concrete frames with reinforced concrete. (Infill Wall)*

These common strengthening techniques are briefly discussed below.

1.3.1 Jacketing

Jacketing is used to modify the existing structure by encasing it with new reinforced concrete or steel. Strength can be increased by additional reinforcement while ductility can be improved by confinement provided by the jacket. In general, the period of the structure is not significantly altered. Figure 1.5 shows typical details of jacketing applied to an existing structure while Figure 1.6 shows typical beam and column jacketing construction performed during research conducted at the University of Texas at Austin.

Typically, most or all of the members must be strengthened to provide adequate ductility and strength to the frame system. Construction work, therefore, must be performed throughout the entire structure requiring relocation of building operations during construction. Additionally, “jacketing typically is not cost-effective because of the difficulty associated with providing the necessary confinement and shear reinforcement in the beams, columns, and beam-column connection zones.”^[15]

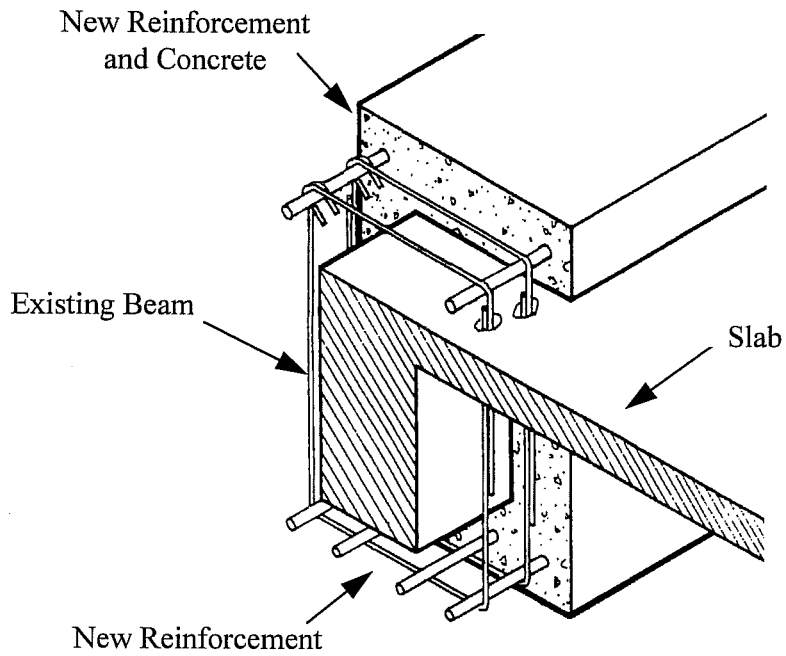


Figure 1.5(a): Beam Jacketing^[15]

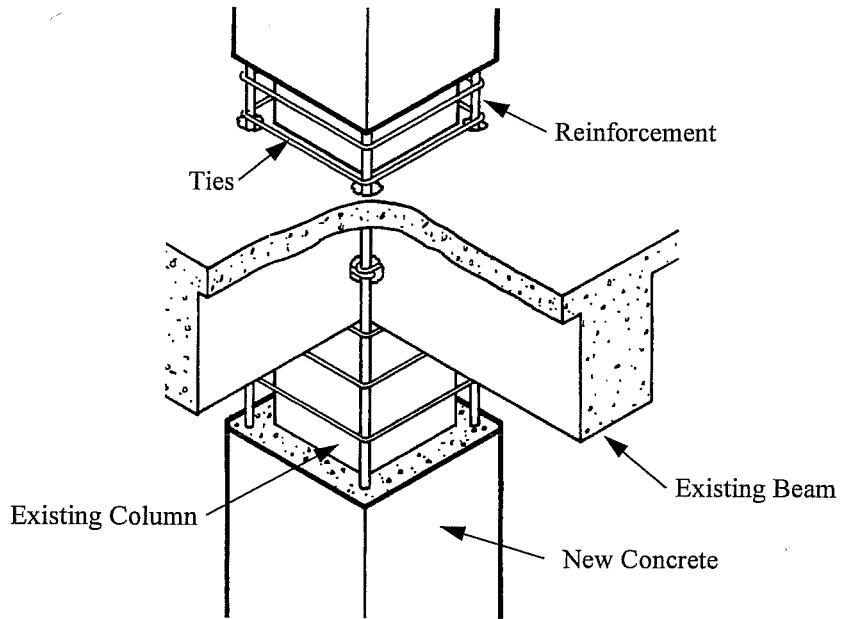


Figure 1.5(b): Column and Joint Jacketing^[15]

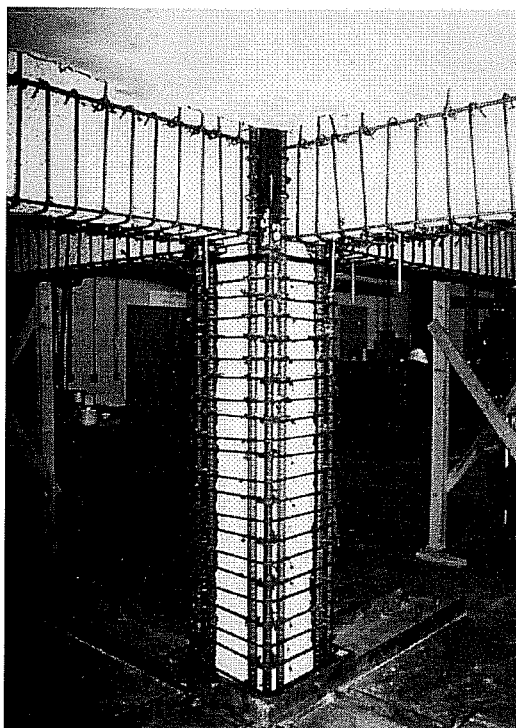


Figure 1.6: Beam and Column Jacketing Construction

1.3.2 Steel Bracing

Steel braces can be attached to the frame of an existing structure. The braces stiffen the structure to reduce the displacement demands of the existing moment frame while also reducing the period of the structure. An example of steel bracing used in a rehabilitation scheme is shown in Figure 1.7.

To provide adequate stiffness to limit deformations, it is typical for multiple frames throughout the building to require bracing. Therefore, bracing inside the building may not be feasible due to braces impeding access and functional circulation within the building. Additionally, connection of the braces to the existing frame is often difficult.

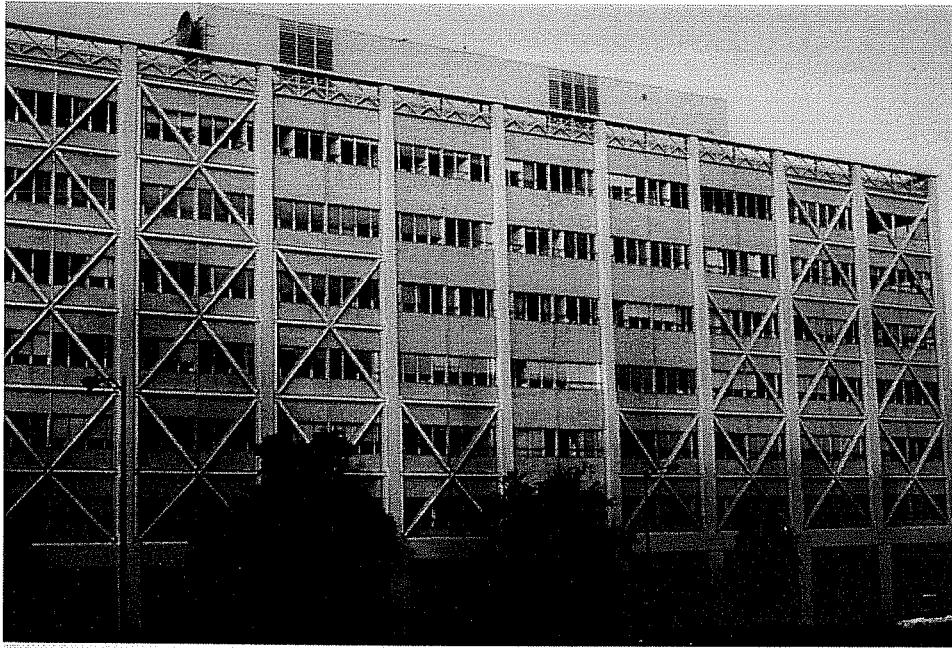


Figure 1.7: Steel Bracing

The building presented in Figure 1.7 is a good example of effective rehabilitation by bracing. The braces were attached to the exterior of the building to reduce inconvenience to occupants both during and after construction. Relatively easy attachment of the braces to the building frame was possible since the columns protrude from the face of the curtain wall. It should be noted, however, that the rehabilitation work altered the exterior appearance of the building. Therefore, this technique may not be feasible where architectural considerations control such as in historical rehabilitation or other projects where the appearance of the structure cannot be altered.

1.3.3 Infill Wall

The building frame can be infilled with a concrete wall to change the lateral load system to a shear wall (Figure 1.8). The addition of infills can dramatically

increase both the lateral strength and stiffness of the structure in addition to changing its dynamic response. Due to the high stiffness of the wall, the moment frames do not contribute to the lateral force resistance. Therefore, the weak links and problems exhibited in the existing structure are eliminated provided that the deformations are within the range which will not severely damage the existing columns, beams, or joints.

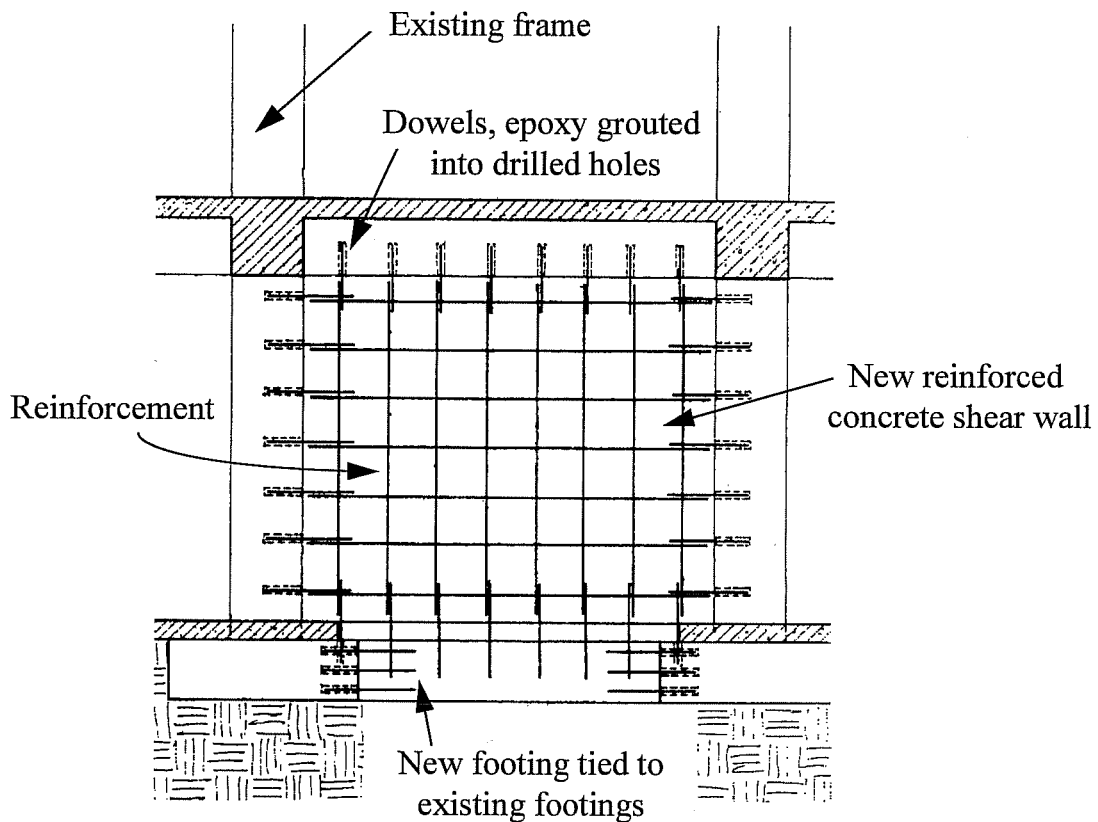


Figure 1.8: Infill Wall

Infill walls, however, subject the existing structure to various forces for which it was not designed. The performance of the infill wall depends on the existing columns to serve as boundary elements which carry large tension and compression forces. In many structures, as previously mentioned, the columns have been designed

for gravity loads and do not have sufficient tensile capacity to act as a boundary element for the new structural wall. Typically, tensile capacity is provided by jacketing or adding vertical reinforcement in the infill which is made continuous through the floors near the column. Additionally, the diaphragms must be capable of transferring the forces to the infill wall.

Infill walls can be costly if the foundation requires upgrading. Additionally, connections to the existing frame with interface dowels may be expensive and time consuming. Finally, the infill wall can also obstruct the functional use of the building by impeding access and functional circulation. However, due to the high stiffness of an infill wall, only a limited number of walls are typically required in a structure. Therefore, it is possible to locate walls to minimize disruption both during and after construction.

1.4 Need for Economic Rehabilitation Scheme

The techniques discussed have proven to be constructible, to be economically feasible for many structures, and are backed by some experimental data and field experience. However, the cost of such rehabilitation projects remains an obstacle for many owners. The costs may involve not only the actual construction, but the expenses associated with relocation of operations and loss of rental revenue or production during the period of construction.

Therefore, it is desirable to develop a rehabilitation scheme that will not only correct the “weak links” in a nonductile frame system, but will simplify the construction process; reduce the time, cost, and inconvenience of construction; and reduce the obstruction to functional use of the structure both during and after construction. The infill wall system meets many of the general objectives desired. However, as mentioned, there are several aspects that make the method inconvenient,

costly, and time consuming. The following objectives were identified to make the infill wall system a more economically viable rehabilitation solution.

1. Eliminate interface dowels.
2. Eliminate extensive concrete formwork
3. Eliminate movement and placement of large volumes of fresh concrete.
4. Increase column tensile capacity without column jacketing.

1.5 Precast Infill Wall

A precast panel system has been developed that will enable the panels to be assembled into an infill wall taking advantage of the infill wall system while achieving the objectives presented above. A precast system can be constructed rapidly without the need for extensive formwork and the relatively cumbersome and sometime difficult procedures associated with moving and placing large quantities of fresh concrete within an existing building. The precast panels can be brought into an existing structure through the use of elevators and light forklifts. The panels have shear keys along the sides to allow for force transfer and are connected to one another through the use of a reinforced grout strip. Panels are connected to the existing frame through the use of steel pipes (shear lugs) that eliminate the need for interface dowels. The existing structure is cored in selected locations to allow for insertion of pipes and continuity of the wall vertical reinforcement. A schematic of the proposed wall system is presented in Figure 1.9.

Out-of-plane resistance of the wall system is achieved through the combination of continuous vertical reinforcement in the grout strips, shear resistance of the steel pipes, and the constraint provided by the boundary elements that provides

capacity without using conventional jacketing. The post-tensioning system is illustrated in Figure 1.11.

From a study conducted by structural consulting engineers, the precast infill wall system was found to be most valuable for the rehabilitation of structures in the 2 to 5 story range. In addition, an analysis of typical floor slabs indicated that the maximum panel weight should be limited to 2,000 pounds. This conclusion was based on the capacity of the slab to support the panel and a light forklift/Bobcat (753 Series Bobcat (4730 pounds) was investigated). The limit of 2000

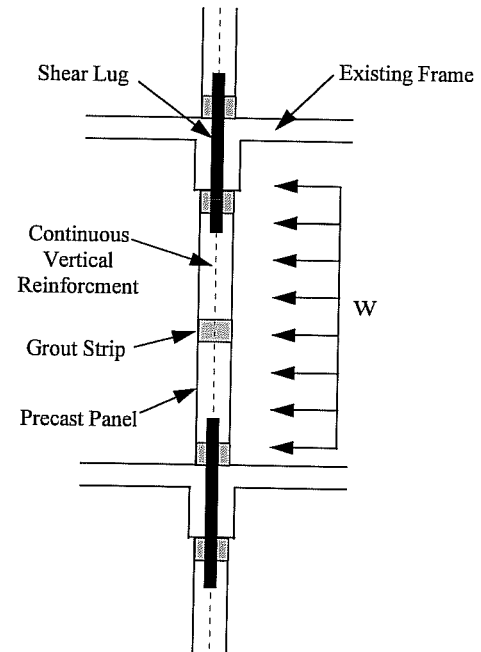


Figure 1.10: Out-of-Plane Resistance

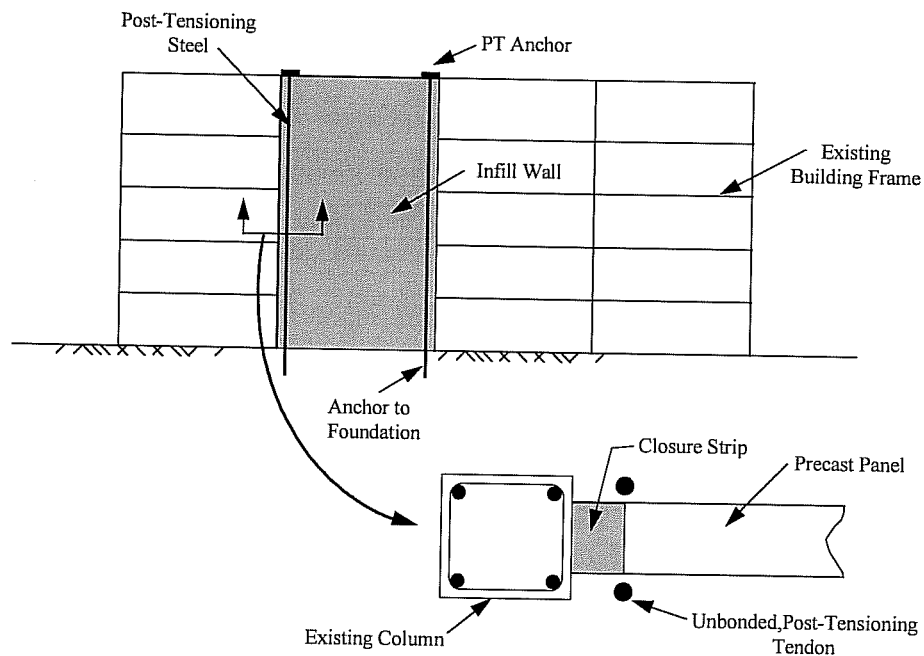


Figure 1.11: Post-Tensioning System

pounds was also consistent with typical elevator capacities. Furthermore, the study based on the typical frame previously presented indicated that multiple infill walls located throughout the structure could permit optimization of the system. Using the 1991 UBC^[37] with a seismic zone factor of 0.4, the base shears listed in Table 1.2 were computed along with the corresponding wall tributary area if uplift is prevented at the base for seismic loads. Since the base shears are approximately the same for the different height buildings, the precast wall system could be standardized using the maximum design force (123 kips). The size of the building and the number of stories would then determine the number of walls required. Standardization of precast wall panels may provide for an economic advantage in the precast system.

Table 1.2: Design Requirements for Infill Wall System

Stories	Wall Tributary Area (ft²)	Base Shear (kips)
2	2900	108
3	2100	116
4	1600	120
5	1300	123

1.6 Objective and Scope

The objective of this research was to develop minimum design and detailing requirements for the precast infill wall system. Current building codes do not provide guidance in designing rehabilitation systems such as that proposed; therefore, three phases of research were conducted to provide basic knowledge and understanding of the system. In the first phase, the connection of adjacent precast panels was investigated. In the second phase, connection of precast panels to the existing frame was studied. The final phase consisted of testing a large-scale, two-story model specimen infilled with the precast wall system to verify the performance of

connection details, investigate the post-tensioning system, and determine the overall system behavior.

CHAPTER 2

PANEL TO PANEL CONNECTION

2.1 Introduction

Fourteen tests were conducted to evaluate the connection between adjacent precast panels. The connections investigated were typical of interior connections made within the precast wall system. A representative detail of the panel connection is shown in Figure 2.1.

2.2 Specimen Design

The test specimens were designed to be representative of a full scale cut-out-detail of the panel connection illustrated previously in Figure 2.1. The overall size of the specimen was determined based on the constraints of an interface shear loading system available at the Phil M. Ferguson Structural Engineering Laboratory. The direct interface shear test does not simulate actual forces experienced on the joint within a shear wall. The shear test, however, does permit relative comparison of test variables involved in the connection design in addition to providing force resistance values that can be easily implemented for design purposes.

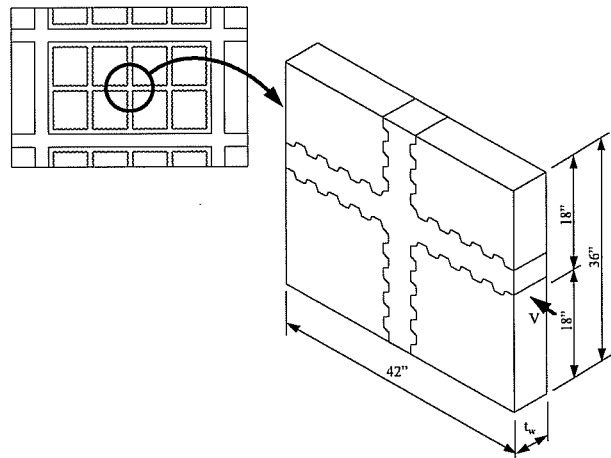


Figure 2.1: Panel Connection Test Component

2.2.1 Panel Surface Preparation

In keeping with the objectives of the research, the edges of the panel were designed to promote ease of fabrication and construction while providing an adequate force transfer mechanism. Shear keys were determined to be needed along the perimeter of the panel. A literature review of shear key technology^[5,23,39] provided the necessary background for design of the shear key geometry. The general key geometry shown in Figure 2.2 provides for force transfer around the perimeter of the panels. This shape was chosen to prevent crushing of the key edges exhibited by elongated keys and to prevent dislocation or overriding as would be expected with the edge of the key inclined less than 45 degrees. The key shape selected allows for complete shearing along the base of the key.

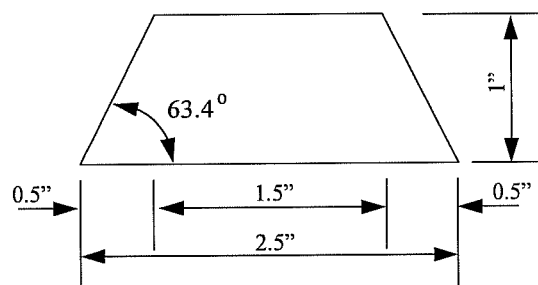


Figure 2.2: Shear Key Geometry

2.2.2 Panel Reinforcement

The panels were detailed with two layers of 4x4 - W2.9xW2.9 welded wire fabric. The level of reinforcement provided was consistent with the minimum reinforcement requirements of Chapter 21 of the current ACI-318-89^[3] code ($\rho_v = 0.0025$ along the longitudinal and vertical axes). A cover of 3/4 in. was provided. It should be noted that the shear keys were not reinforced and no reinforcement protruded from the panel. As indicated previously, direct continuity of panel reinforcement was eliminated to reduce construction and fabrication problems and to accelerate on-site erection.

2.2.3 Closure Strip

The panels were connected to one another through the use of a closure strip which allowed for tolerances in both the existing and new construction. In addition, it allowed for easy placement of the panels. Horizontal and vertical steel was placed in the joint to connect the panels and allow for force transfer through the grouted joint. For all tests conducted, the horizontal strips were reinforced with two #3 bars which meet minimum requirements for temperature and shrinkage. The horizontal and vertical strip steel was mechanically anchored through the use of steel plates welded to the ends of the bars. After the steel was placed, the joint was grouted. Details of the test specimen are shown in Figure 2.3.

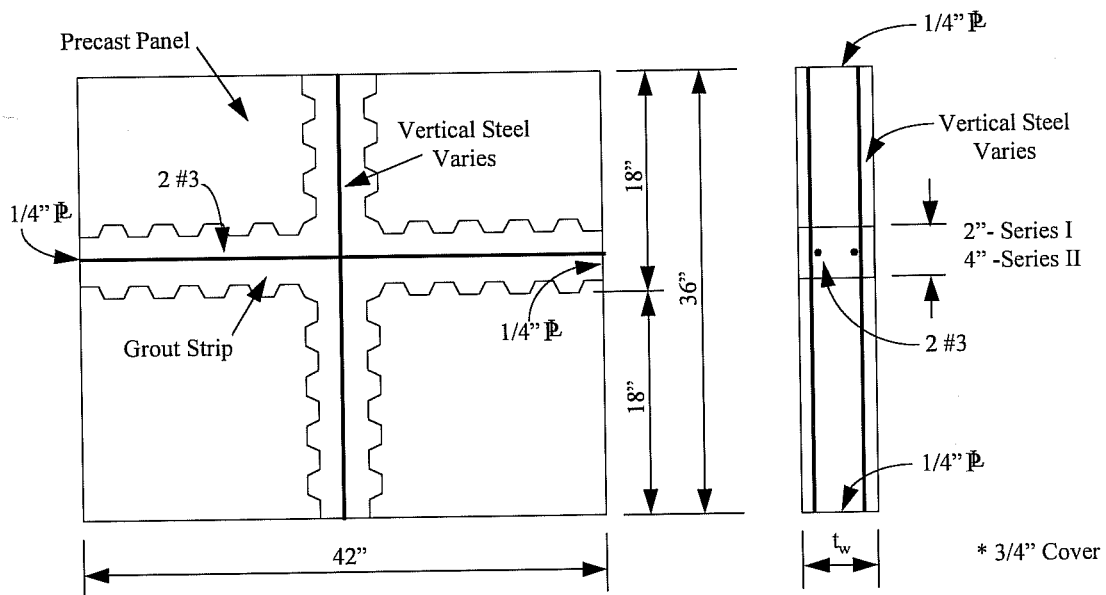


Figure 2.3: Panel Connection Specimen Details

2.2.4 Test Variables

A description of the test variables studied in this phase of the research is presented below. All specimens were identified by the description label PC (**P**anel **C**onnection) followed by the specimen number. A summary of the specimen variables is presented in Table 2.1. Tests were divided into four series in which the primary objective of each was as follows:

Series	Objective
I-PC	Shear Key Configuration
II-PC	Grout Strip Reinforcement, Grout Strength, Shear Key Size
III-PC	Grout Strip Reinforcement, Shear Key Size
IV-PC	Panel Thickness

Shear Key Configuration: The alignment of the shear keys with respect to one another was investigated. Two configurations were studied which represent the limits of alignment between panels. The limits were labeled aligned and staggered as shown in Figure 2.4.

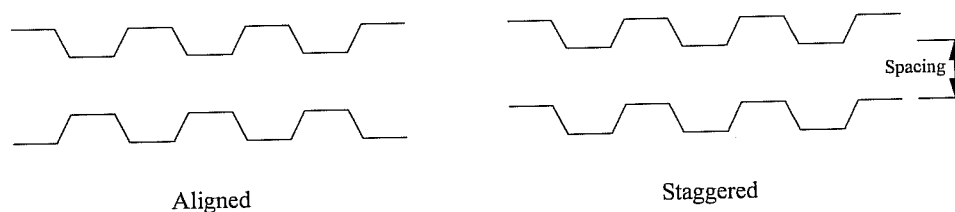


Figure 2.4: Shear Key Alignment

In addition, the spacing of the keys was also investigated. Two configurations were studied: a full spacing (1.0 spacing) with the length of the valley the same dimension as the peak, and a space and a half separation (1.5 spacing) with the

Table 2.1: Panel Connection Test Details

Series (PC)	Specimen	Panel			Shear Key			Grout Strip				
		Thickness (in.)	Age at Testing (days)	f_p (psi)	Alignment	Spacing	Size	Separation (in.)	Reinforcing	Strength	Age at Testing (days)	f_g (psi)
I	PC-1	6	136	5100	Aligned	1.0	Normal	2	2 #3	High	82	7200
	PC-2	6	125	5100	Aligned	1.5	Normal	2	2 #3	High	71	7200
	PC-3	6	119	5100	Staggered	1.0	Normal	2	2 #3	High	65	7200
	PC-4	6	111	5100	Staggered	1.5	Normal	2	2 #3	High	57	7200
II	PC-5	6	64	4000	Aligned	1.0	Normal	4	2 #3	High	37	6400
	PC-6	6	188	4300	Aligned	1.0	Normal	4	4 #4	High	161	6900
	PC-7	6	162	4300	Aligned	1.0	Normal	4	4 #4	Low	125	2650
	PC-8	6	170	4300	Aligned	1.0	Large	4	4 #4	High	143	6900
III	PC-12	6	184	4300	Aligned	1.0	Normal	4	6 #5	High	163	6900
	PC-9	6	190	4300	Aligned	1.0	Normal	4	4 #3	High	27	6000
	PC-10	6	175	4300	Aligned	1.0	Normal	4	2 #4	High	33	6000
	PC-11	6	181	4300	Aligned	1.0	Large	4	4 #3	High	36	6000
IV	PC-13	4	41	4500	Aligned	1.0	Normal	4	2 #3	High	24	6600
	PC-14	4	42	4500	Aligned	1.0	Normal	4	4 #4	High	25	6600

valley one and one-half times the peak length. The spacing configurations are shown in Figure 2.5.

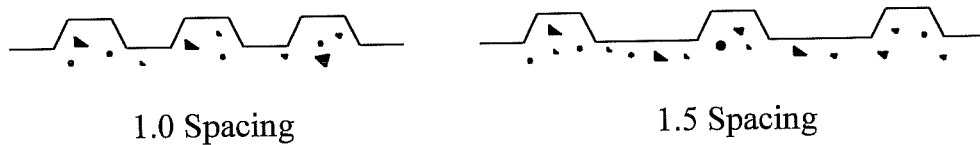


Figure 2.5: Shear Key Spacing

Shear Key Size: The key size as related to depth of the key was investigated. The overall geometry of the key, however, was maintained. The key size was studied to allow more fabricator freedom in constructing the formwork. As an example, the use of standard size lumber to construct the key void forms may reduce precasting costs. The depths chosen for the keys were the same as the thickness of readily available construction lumber. The key sizes used are shown in Figure 2.6.

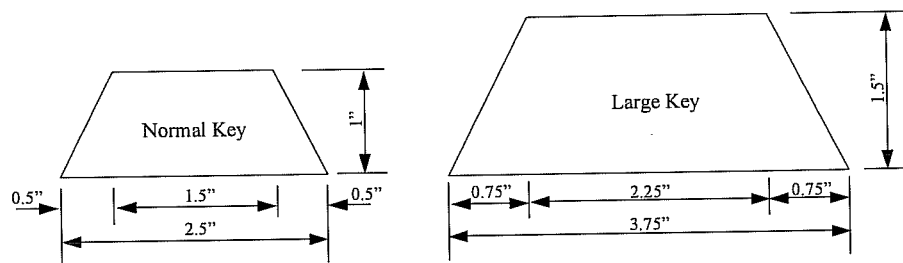


Figure 2.6: Shear Key Size

Panel Spacing: The effect of the separation between adjacent panels was investigated using 2 and 4 in. clear spacings.

Vertical Steel: The amount of vertical steel in the closure strip was investigated . A full range of reinforcing ratios was studied, from lightly reinforced (2 #3) to heavily reinforced (6 #5). The large range of bar sizes was chosen to evaluate the likely extremes of specimen behavior.

Grout Strength: The concrete strength of the precast panels (f_p) relative to the closure strip grout (f_g) was investigated. The strength of the precast panels remained constant throughout all specimens but the closure strip concrete was varied. Two extremes were studied; a grout strength that was lower (Low) and one that was higher than the precast panels (High).

Panel Thickness: The effect of thickness of the precast wall panels was investigated using 4 and 6 in. thick panels. The 6 in. panel represented a typical full scale wall installation; however, it is likely for varying wall thicknesses to be utilized in different rehabilitation projects.

2.3 Specimen Construction

The test specimens were constructed during four different casting operations. All specimens were not constructed at the same time in order to limit the number of tests to be performed at a given age and strength of concrete. Each series of tests were constructed and tested to assess specific variables that would provide information to assist in the development of design recommendations for the panel connection.

2.3.1 Precast Panel Construction

The wall panels were constructed in a flat precasting bed shown in Figure 2.7. The shear keys were fabricated from readily-available lumber. The normal (1 in. depth) keys were cut from 1-1/4 in. radius edge decking that has a dressed dimension of 1 in. The large (1-1/2 in. depth) keys were cut from 2 in. lumber that has a dressed dimension of 1-1/2 in. Shear keys were secured to the formwork with screws.

The panels were cast and cured for seven days using wet burlap. Companion concrete cylinders were cast and cured in the same manner for strength testing. The panels were removed from the casting bed and temporarily stored.

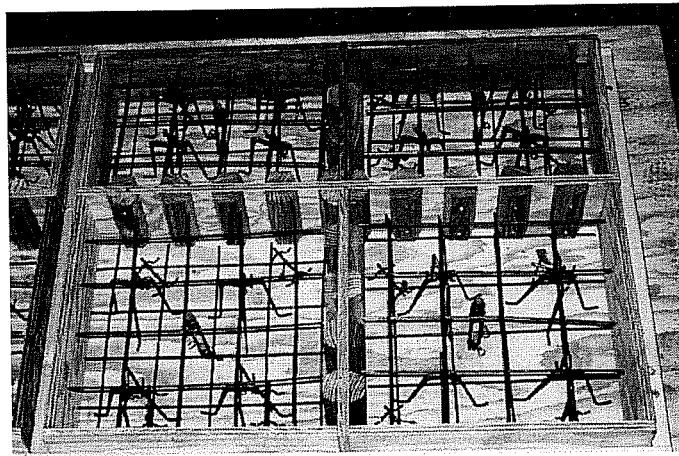


Figure 2.7: Precast Panel Construction

2.3.2 Wall Construction

The panels were assembled in an upright position as shown in Figure 2.8 simulating the actual wall assembly in a building frame. Reinforcing steel was placed through the joint. Plywood forms cut slightly larger than the joint width were placed along the joints and secured with all-thread. Nuts attached to the rods were tightened to ensure proper alignment of the panels. Clamping of the formwork through the joint also prevented the formwork from bowing during grouting operations. The vertical grout strips were enclosed from both sides while the horizontal strips were constructed using several techniques discussed below. The vertical strips were grouted by placing concrete into the joint at the top of the specimen, and

consolidation was achieved by direct insertion of a vibrator into the grout strip from the top of the specimen.

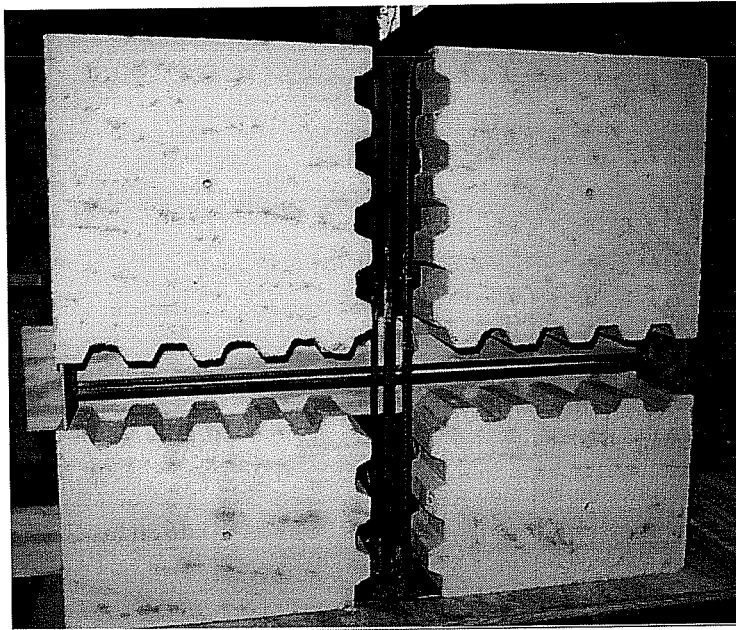


Figure 2.8: Wall Construction

2.3.2.1 Trough Method

The horizontal strip was formed and constructed using a plywood trough. The trough was provided along the length of the joint to allow for proper vibration of the joint. The trough allowed for easy vibrator access and visual inspection of the procedure. The main disadvantage, however, was that a substantial amount of concrete was wasted. Additionally, the method was fairly labor intensive since the surface of the wall at the location required finishing and the waste concrete remaining in the trough required early removal and disposal. The trough method is shown in Figure 2.9.

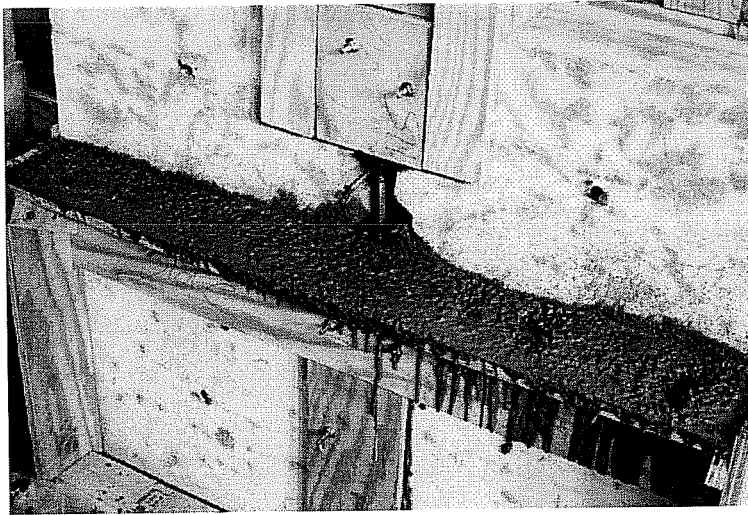


Figure 2.9: Trough Method

2.3.2.2 Access Hole Method

The main objective of the access hole method was to eliminate the finishing and removal of waste concrete as required by the trough method. Both horizontal and vertical grout strips were closed with formwork. Vibration was achieved through the use of small holes drilled into the formwork at select locations along the horizontal grout strip. The holes could be opened or closed through the use of a small wood block attached with a nail hinge. This method is shown in Figure 2.10.

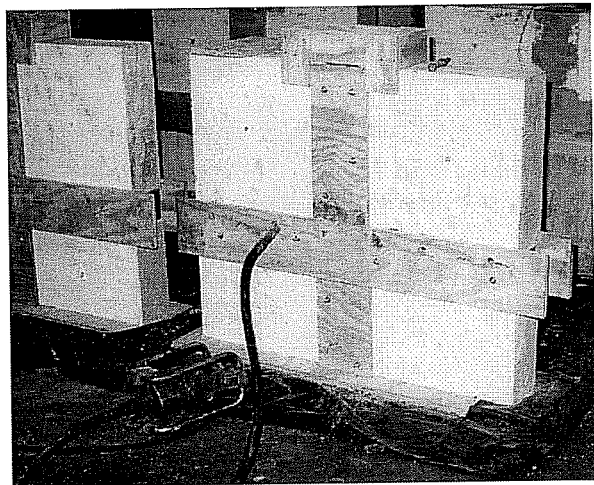


Figure 2.10: Access Hole Method

Method 1: The hole was maintained larger than the vibrator head to permit easy vibrator insertion, to eliminate clogging of the hole with aggregate, and to allow for angling of the vibrator to spread the area of vibrator influence. This method proved to work well in terms of good consolidation of the horizontal joint; however, backflow of the concrete occurred in the space not filled by the vibrator head. This method, therefore, wasted concrete and required the placement of more concrete than necessary. Additionally, there was a potential problem for voids at the top of the keys since material was being removed while backflow occurred.

Method 2: The hole was maintained approximately the size of the vibrator head to permit insertion of the head with a minimum of void space remaining around the head. Since only a small clearance was present upon insertion of the vibrator head, grout material did not backflow. This method also worked well with regard to good consolidation of grout material.

A few comments should be made, however. A small tool such as a slump cone rod or reinforcing bar should be inserted into the access hole to remove any coarse aggregate that may be clogging the hole to allow for easy vibrator insertion. Additionally, the vibrator should be removed slowly to permit grout to refill the void space left upon removal of the vibrator head.

2.4 Construction Materials

2.4.1 Precast Panel Concrete

The precast panels were constructed using a nominal 4000 psi concrete. A 3/8 in. gravel was used to promote good concreting in the shear key region. The mix

proportions are shown in Table 2.2. The exact proportions delivered varied slightly and were adjusted for moisture conditions of the aggregates. The mixes were adjusted at the jobsite to maintain a 6 in. slump. All panel concrete mixes were designated by the description label P (Panel) followed by the mix number. Strength gain curves are presented in Figure 2.11.

Table 2.2: Precast Panel Mix Design

Material	P-1 through P-4
Cement (Type I)	470 pcy
3/8" Coarse Aggregate (SSD ¹)	1625 pcy
Fine Aggregate (SSD ¹)	1655 pcy
Water	250 pcy
Admixture ²	20 ozcy

¹ Saturated Surface Dry

² For high temperature months (May-September), an admixture meeting ASTM C494 requirements for Type B retarding and for Type D water-reducing and retarding was used. During cooler months (November to April), an admixture meeting ASTM C494 for Type A water-reducing admixtures was used. The quantities of admixture used, however, remained constant throughout the year.

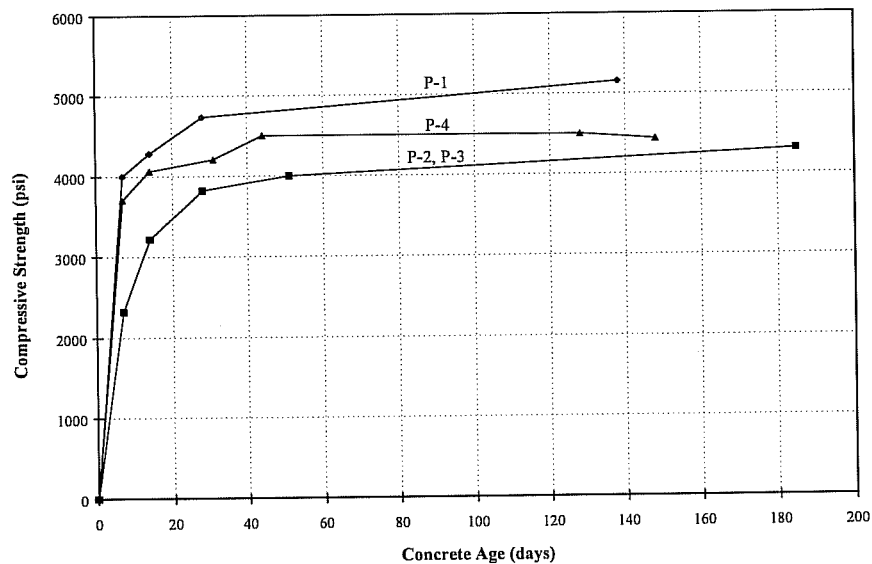


Figure 2.11: Precast Panel Concrete Strength Gain

2.4.2 Panel Grout

The cost of the material used to construct the closure strip was considered to be one of the overriding factors. Therefore, prepackaged grout materials as well as non-shrink admixtures would be unacceptable due to their costs. A normal grout using Portland Cement was considered ideal. To restrain shrinkage, however, it was deemed necessary to use a small coarse aggregate (3/8 in.) to provide dimensional stability to the mix in addition to providing better shear strength characteristics. The concrete used to fill the closure strip was referred to as grout. The word grout was used to differentiate between the panel concrete and was not used to indicate the absence of coarse aggregate. Several different grout mixes were used in the course of the research.

The first series of specimens were cast using a standard 5000 psi concrete with 3/8 in. aggregate obtained from a ready mix supplier. The mix was adjusted at the jobsite to obtain a 4 in. slump. A high range, water-reducing admixture (superplasticizer) meeting ASTM C494 requirements for Type A and Type F admixtures was added to adjust the slump to 8-10 in. prior to casting.

During casting, it was observed that the mixture was too rocky making it difficult to consolidate. In addition, the concrete did not flow well and clogging occurred. The concrete, ultimately, was properly placed and finished, however, increased work was required for good consolidation. Additionally, pumping of the concrete would not have been possible.

To increase the workability of the mix, several mix designs were developed and tested. The goal was to achieve a workable, pumpable mix that would not segregate. Suitable mixes were developed for both a low strength (2500 psi) and a medium strength (6000 psi) concrete. These mix designs were subsequently used in the connection tests. The medium strength mixes were obtained from a ready mix supplier and adjusted at the jobsite to obtain a 4 in. slump. Subsequently,

superplasticizer was added to obtain an 8-10 in. slump prior to casting. The low strength concrete, however, was mixed at the laboratory since only a small quantity was required. A 9 in. slump was obtained using water; no superplasticizer was added. Both mix designs provided a workable and flowable mix which required only minimum effort to place.

The grout mixtures were designated by the description label PG (**P**anel **G**ROUT) followed by the specimen series number. The low strength grout was labeled PLG (**P**anel **L**ow **G**ROUT) followed by the specimen series number. The mix proportions are presented in Table 2.3 while strength gain curves are presented in Figure 2.12.

It should be noted that PG-3 used the original mix design as cast in the first series. This mix was used for availability reasons. Use was justified since the concrete performs structurally as well as the modified mix, provided it is properly consolidated.

Table 2.3: Panel Grout Mix Design

Material	Original Mix PG-1, PG-3	Modified Mix PG-2, PG-4	Low Strength PLG-2
Cement	564 pcy	693 pcy	425 pcy
3/8" Coarse Aggregate	1625 pcy	1167 pcy	1167 pcy
Fine Aggregate	1469 pcy	1755 pcy	1945 pcy
Water	280 pcy	325 pcy	325 pcy
Admixture ¹	16.8 ozcy	27.6 ozcy	-
Superplasticizer ²	25 ozcy	25 ozcy	-

¹ For high temperature months (May-September), an admixture meeting ASTM C494 requirements for Type B retarding and for Type D water-reducing and retarding was used. During cooler months (November to April), an admixture meeting ASTM C494 for Type A water reducing admixtures was used. The quantities of admixture used, however, remained constant throughout the year.

² Exact addition amounts may have varied slightly to adjust the slump to 8-10 in..

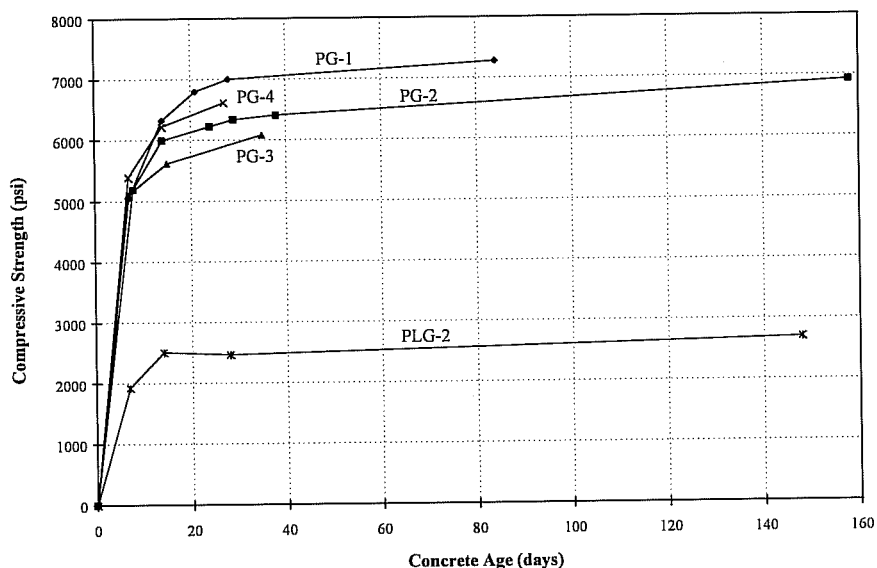


Figure 2.12: Panel Grout Strength Gain

2.4.3 Reinforcing Steel

Grade 60 reinforcing steel was used in all specimens along with Grade 60 welded wire fabric. Tensile tests were performed on representative coupons of all reinforcing steel used for construction of the specimens. Both yield and ultimate tensile strengths were obtained, and the results are presented in Table 2.4. Testing was performed according to ASTM A370-94. The welded wire fabric had a tensile strength of 72.2 ksi; yielding of the steel did not occur. Instead, the wire fractured at the welded connection of the crossing wires.

Table 2.4: Panel Connection Reinforcing Steel

Series (PC)	#3 Bars		#4 Bars		#5 Bars	
	Yield (ksi)	Tensile (ksi)	Yield (ksi)	Tensile (ksi)	Yield (ksi)	Tensile (ksi)
I	63.6	100.5	-	-	-	-
II & III	61.8	101.6	73	112.8	61.9	102.3
IV	65.5	102.5	-	-	-	-

2.5 Test Setup and Procedure

The test setup (Figure 2.13) was designed to subject the specimens to direct cyclic shear along the connection interface. The connection specimen was seated, and a hydrostone grout was used to secure the specimen. Two 400 kip hydraulic rams at each end of the setup allowed for pushing the top portion of the wall relative to the bottom portion. A self-equilibrating load system was also available to apply compressive loading or to restrain the specimen vertically (Figure 2.14). In general, testing was conducted without compression across the interface to produce lower bound interface shear strengths.

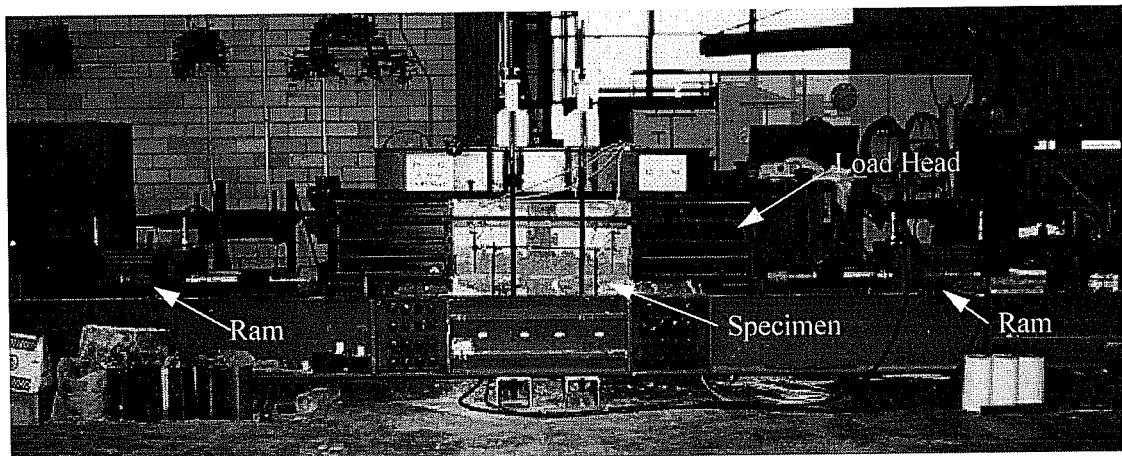


Figure 2.13: Test Setup

Load was monitored through the use of pressure transducers and gages. Interface slip and uplift were monitored by displacement transducers mounted along the interface. Additionally, strain gages were attached to the reinforcing steel at the testing interface to monitor steel stresses. The specimen instrumentation is shown in Figure 2.15.

The applied loading for the specimens was cyclic in nature. Load control was used up to the peak capacity of the specimen. Subsequently, displacement control

was utilized. Typically, three cycles at each load or displacement stage were completed. Cycles in 20 kip increments were used during load control, and cycles at 0.05, 0.1, 0.15, 0.2, and 0.3 in. were used during displacement control. The exact nature of the loading depended upon the specimen behavior.

When the vertical restraint system was utilized, the compressive load induced was monitored by strain gages attached to the connecting rods and by load cells mounted on the top loading head.

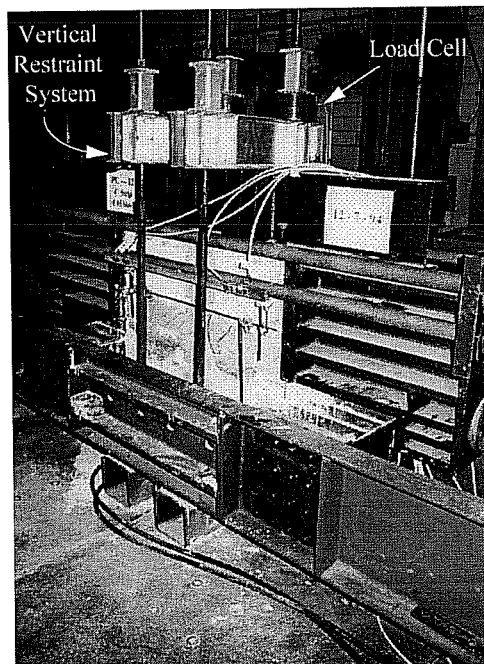


Figure 2.14: Self-Equilibrating Vertical Load System

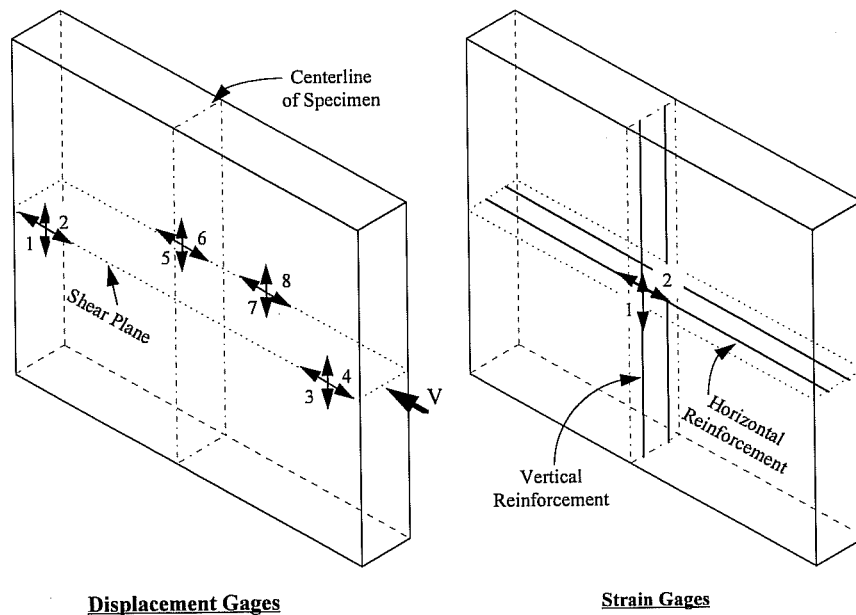


Figure 2.15: Specimen Instrumentation

2.6 Experimental Results

The general behavior of the test specimens is discussed, and a representative load-displacement relationship is shown in Figure 2.16. The specimen was very stiff initially and behaved monolithically up to the point where adhesion at the panel shear key/grout strip interface was lost. Uplift along the joint occurred and stresses were induced in the vertical joint reinforcement. Following adhesion loss, loading could be further increased until a failure occurred through the shear plane. When the peak capacity was reached, the vertical reinforcement was yielded. The failure surface is shown in Figure 2.17. After the peak capacity was reached, there was a transition to a lower load plateau or residual capacity which was maintained through large slip levels. A specific discussion of each test specimen follows. Test results for all specimens are presented in Appendix A and are summarized in Table 2.5.

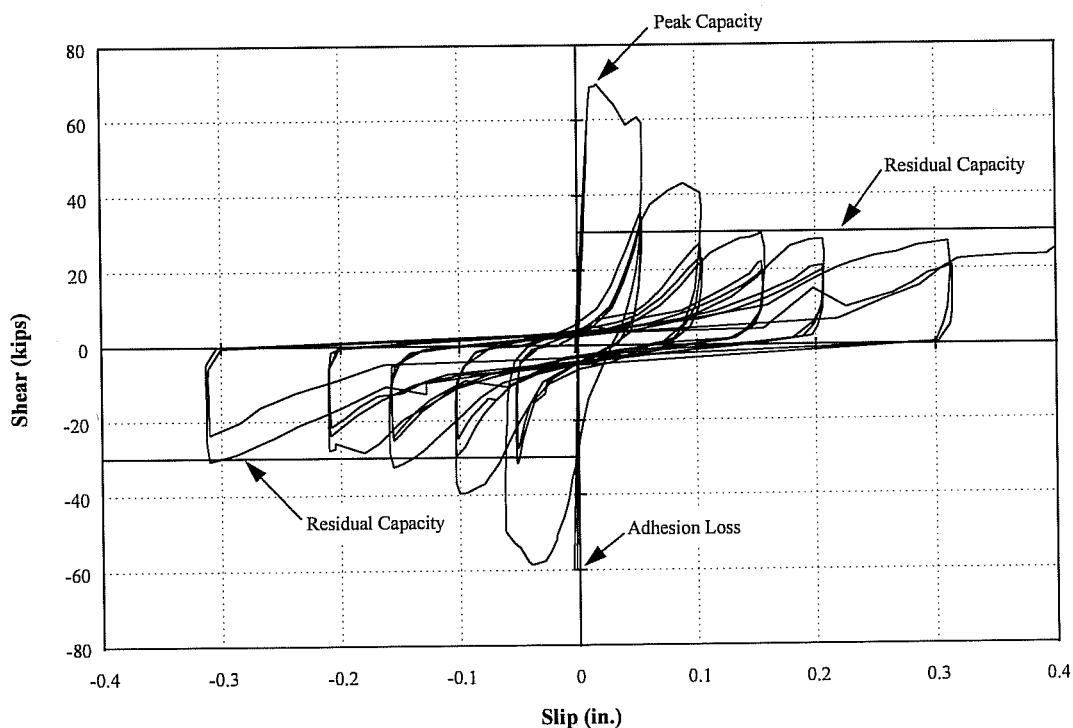


Figure 2.16: Panel Connection Test (PC-5)

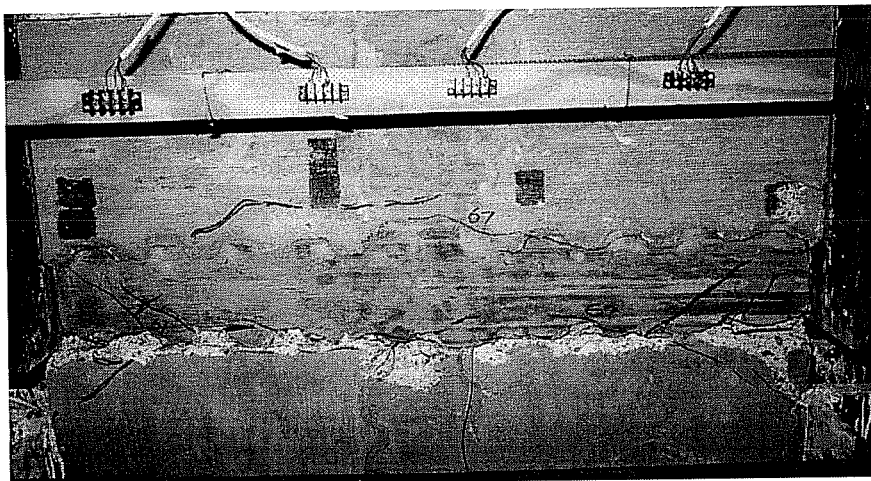


Figure 2.17: Failure Surface (PC-5)

Table 2.5: Panel Connection Test Results

Specimen	Recorded			Adjusted	
	Adhesion Capacity (kips)	Peak Capacity (kips)	Residual Capacity (kips)	Peak Capacity (kips)	Residual Capacity (kips)
PC-1	81	84	30	-	-
PC-2	59	62	30	-	-
PC-3	69	74	30	-	-
PC-4	50	70	30	-	-
PC-5	60	70	30	-	-
PC-6 ¹	60	179 ²	*	136 ²	*
PC-7	40	102	58	-	-
PC-8	40	153	50	-	-
PC-9	80	103	40	-	-
PC-10 ¹	80	109	58	90	52
PC-11 ¹	84	157	54	124	43
PC-12 ¹	70	202 ²	*	136 ²	*
PC-13	55	63	20	-	-
PC-14	25	74	25	74	25

¹ Vertical restraint system used.

² Interface shear failure did not occur. Wall failed in bearing from compression of loading head.

As will be mentioned later, four specimens required the use of a vertical restraint system that applied compression load across the interface. Therefore, both recorded and adjusted values are presented in the table. To eliminate the effects of compression on the interface shear strength, the recorded values were reduced by the applied compression multiplied by a coefficient of friction of 0.8 ($\mu=0.8$). A value of 0.8 is consistent with previous testing^[27,38] in which the effects of compressive loading on interface shear transfer were investigated.

2.6.1 Series I-PC

The first series of testing included specimens PC-1 through PC-4 as shown in Figure 2.18. The objective of this series was to determine the configuration of panel key geometry to use for the remainder of testing. The specimens were inserted into the test frame in the same upright position as cast with the plane of direct shear located at the bottom interface and at the base of the panel shear keys. All specimens in Series I had 2 #3 bars in both the vertical and horizontal strips. The panels were 6 in. thick with a 2 in.

clear separation between panels. The key variables investigated in each test are noted below.

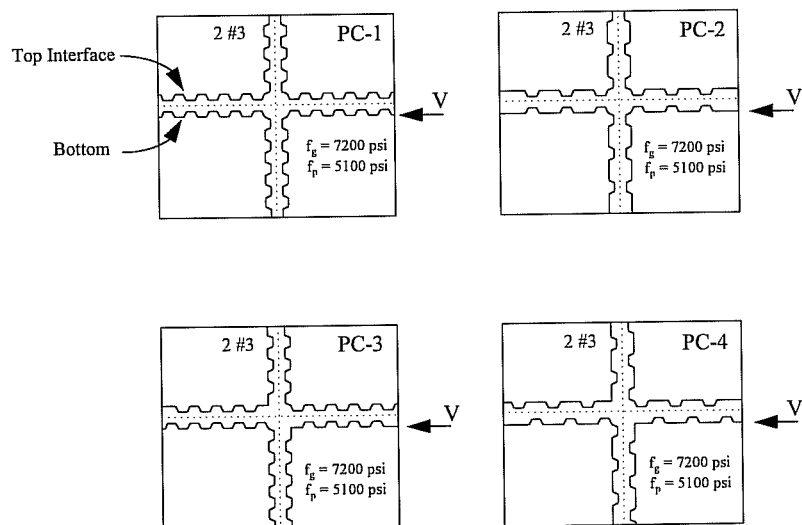


Figure 2.18: Series I-PC Specimens

2.6.1.1 PC-1 (Aligned, 1.0 Key Spacing)

Loss of adhesion at 81 kips was accompanied by a slight uplift along the interface. According to strain gage measurements, the stress in the vertical reinforcement at this load level was extremely small, approximately 4 ksi. However, when the load reached the cracking load and peak capacity of 84 kips, dramatic uplift occurred along the interface and the reinforcing steel yielded. The top interface (located 4 in. above the plane of direct shear) failed at the peak load since this interface was the top casting position. Inferior adhesion can be expected at this interface since air entrapment during casting of the grout can occur.

After testing of the top interface was completed, the bottom interface was tested. This interface was loaded monotonically in direct shear. The peak capacity across the bottom interface was 140 kips. Therefore, a significant difference between top and bottom interface capacities was noted.

2.6.1.2 PC-2 (Aligned, 1.5 Key Spacing)

Loss of adhesion was noted at 59 kips which was accompanied by a slight uplift along the interface. As loading continued to the peak load of 62 kips, the stress in the reinforcement increased to 59 ksi. When loading was reversed, approximately the same peak load was reached. In this direction, the uplift increased significantly and the reinforcing steel yielded. This interface also failed at the top surface.

After complete testing of the top interface, the bottom interface was tested monotonically to a capacity of 120 kips. Again, a significant difference between the top and bottom interface capacities was noted.

2.6.1.3 PC-3 (Staggered, 1.0 Key Spacing)

Loss of adhesion at 69 kips was accompanied by a slight uplift along the interface. As loading continued to the peak load of 74 kips, the stress in the

reinforcement crossing the interface increased to 20 ksi. The loading was reversed just at the initiation of failure. Upon reverse loading, a slightly lower peak load was reached with the reinforcing steel reaching yield. In this direction, significant uplift was noted. This interface also failed at the top surface.

2.6.1.4 PC-4 (Staggered, 1.5 Key Spacing)

Loss of adhesion along the interface at 50 kips was accompanied by a slight uplift along the interface. The loading was increased to 60 kips at which cracking was noted. Cycling at the cracking load resulted in increases in both slip and uplift in each subsequent cycle. Upon conclusion of the third cycle, the induced tension in the reinforcing bar was approximately 60 ksi. A peak load of 70 kips was reached which resulted in increased uplift and complete yielding of the vertical reinforcement. This interface also failed at the top surface.

2.6.2 Series II-PC

The second series included specimens PC-5 through PC-8 in addition to PC-12 as shown in Figure 2.19. All specimens in Series II had a panel separation of 4 in. and an aligned panel key configuration with a 1.0 spacing. Since the failure plane occurred at the top interface in all Series I specimens, the location where air entrapment can be expected, a modification was made to permit direct shear testing at the top interface as illustrated in Figure 2.20. The specimens were cast upside down so that they could be turned upright for the top casting interface to coincide with the plane of direct shear. Therefore, the top cast interface was at the plane of direct shear while the bottom cast interface was located 4 in. above. The specimens were tested in this manner to assure that the shear-moment interaction was not the cause of top interface failure in the first series of tests. This construction method was used in this series as well as all remaining test series. The key variables are noted.

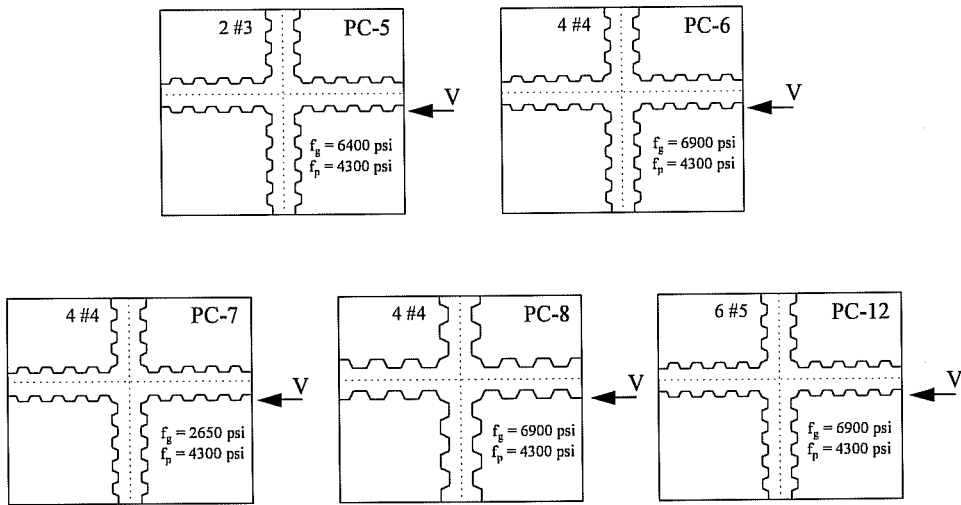


Figure 2.20: Series II-PC Specimens

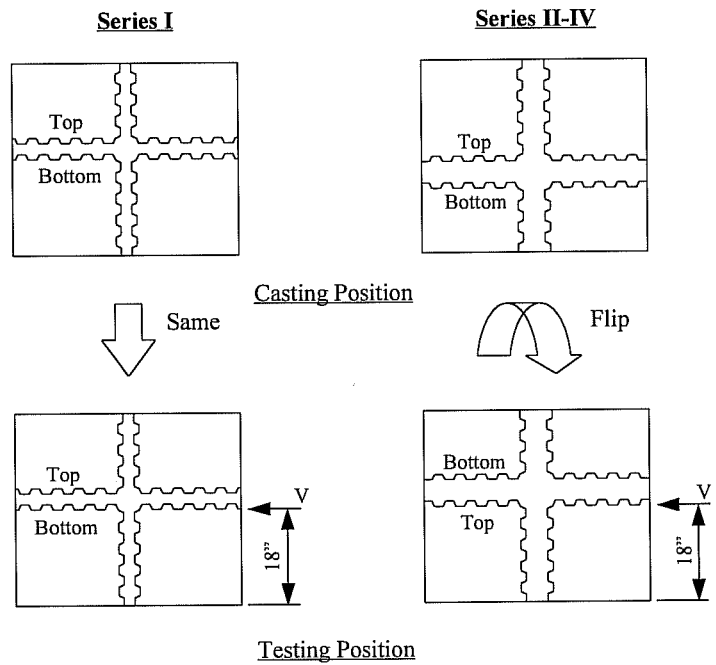


Figure 2.19: Casting vs. Testing Position

2.6.2.1 PC-5 (2#3 Bars)

Loss of adhesion along the interface occurred under reversed loading to a 60 kip level. As loading progressed, the load was increased to 70 kips which corresponded with the peak load. The failure in this case occurred through the precast panel keys at the location of direct shear. A residual capacity of 30 kips was noted. This specimen behaved similarly to PC-1 which had the same panel geometry and reinforcement. Consequently, the eccentricity of applied shear to the interface in Series I testing did not significantly affect the test results as demonstrated by this test.

2.6.2.2 PC-6 (4#4 Bars)

Loss of adhesion along the interface occurred at approximately 60 kips. Following loading at this level, the loading was increased to 100 kips at which the load was cycled. On applying load up to 100 kips during the completion of the cycle, the specimen managed to slip vertically out of the test frame so that further loading was not possible. The specimen was reseated, and the vertical restraint system was applied to prevent the specimen from again slipping. Testing was able to resume, and a peak load of 179 kips was reached. The interface, however, did not fail. Instead, a bearing failure occurred on the wall at both the loading head bearing location and the test frame support location. In other words, the specimen was being crushed; the wall had reached a limit other than the interface shear capacity.

According to strain gage readings, it appeared that an interface shear failure was close since the reinforcing steel was approximately at yield. In addition, there was a spread of diagonal cracking along the interface. It must be noted, however, that the peak load was reached with the vertical restraint system which applied compressive load into the wall at the interface. A compressive load of approximately 54 kips was applied across the interface. From previous testing conducted to evaluate effects of compressive loading on interface shear transfer,^[27,38] the enhancement in

shear capacity from the compressive loading was estimated at approximately 43 kips (0.8*54 kips). The maximum interface capacity reached was approximately 136 kips without the effect of the compression load.

2.6.2.3 PC-7 (4#4 Bars, Low Grout)

Loss of adhesion was noted at approximately 40 kips. As loading increased, a peak capacity of 102 kips was reached. The failure plane occurred 1 in. above the plane of pure shear since the failure occurred through the grout keys as opposed to the panel keys which has been previously encountered. Uplift occurred following loss of adhesion; however, it appeared to be restrained by the vertical reinforcement. Increased loading did not produce dramatic changes in uplift from cycle to cycle nor did the steel reinforcing stresses change significantly. A residual capacity of 58 kips was obtained.

2.6.2.4 PC-8(4#4 Bars, Large Key)

A loss of adhesion was noted at approximately 40 kips. Loading was increased to a peak capacity of 153 kips. The reinforcing steel was yielded at the peak load. The structure responded in much the same manner as PC-7 except the failure surface occurred through the panel keys. A residual capacity of 50 kips was noted.

2.6.2.5 PC-12(6 #5 Bars)

In order to test this specimen, it was decided that the vertical restraint system would be required. The restraint system was passive; the nuts to clamp the system were left loose so that the system would participate only if the specimen began slipping out of the setup.

A loss of adhesion was noted at approximately 70 kips. No compressive loading was induced by the system. However, as the loading proceeded to the peak

capacity, the restraint system became active. A peak capacity of 202 kips was reached with 82 kips of compressive load applied by the restraint system. The interface in this case did not fail, however. A bearing failure occurred in the wall due to compression at the loading and support heads. In approximating the peak capacity reached without compressive effects on the interface, an adjusted capacity of 136 kips was computed.

2.6.3 Series III-PC

The third series included specimens PC-9 through PC-11 inclusive as shown in Figure 2.21. In these specimens, the influence of the vertical steel and key size were further investigated. Since PC-6 did not experience a shear interface failure, the test results could not be compared directly with the other specimens. Therefore, the additional specimens in this series provided the necessary comparisons required for evaluating the test variables.

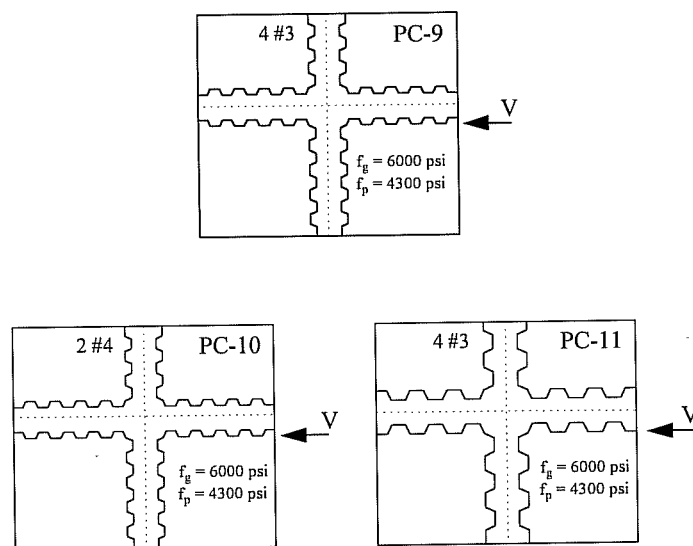


Figure 2.21: Series III-PC Specimens

2.6.3.1 PC-9 (4 #3 Bars)

Loss of adhesion occurred at 80 kips. A peak capacity of 103 kips was reached along with a residual capacity of 40 kips. Failure occurred through the panel concrete keys.

2.6.3.2 PC-10 (2 #4 Bars)

Loss of adhesion occurred at 80 kips. As loading increased, the specimen began slipping from the test frame; therefore, the vertical restraint system was used. A peak load of 109 kips was reached with a compressive load of 24 kips applied. Failure occurred through the panel shear keys along the plane of pure shear. A residual capacity of 58 kips was noted with 8 kips of applied compressive loading. Therefore, a corrected residual capacity eliminating the effects of compressive loading would be approximately 52 kips while a peak capacity of approximately 90 kips was calculated.

2.6.3.3 PC-11 (4 #3 Bars, Large Key)

Loss of adhesion occurred at 84 kips. As loading increased, the specimen also began slipping from the test frame; therefore, the vertical restraint system was used. A peak load of 157 kips was reached with a compressive load of 41 kips applied. Failure occurred through the panel shear keys, and a residual capacity of 54 kips was noted with 16 kips of applied compression. An adjusted peak capacity of 124 kips and a residual capacity of 41 kips were calculated.

In order to verify the adjustments made for the effect of compressive loading, an additional test was performed on this specimen. The vertical restraint system was removed to eliminate the effects of compression on the residual capacity. The specimen was reloaded to obtain the residual capacity without compression across the

interface. A capacity of 43 kips was obtained in this manner which correlated well with the calculated adjusted capacity of 41 kips.

2.6.4 Series IV-PC

The fourth series included specimens PC-13 and PC-14, shown in Figure 2.22, that were tested to determine the influence of panel thickness. A 4 in. wall was used for these tests.

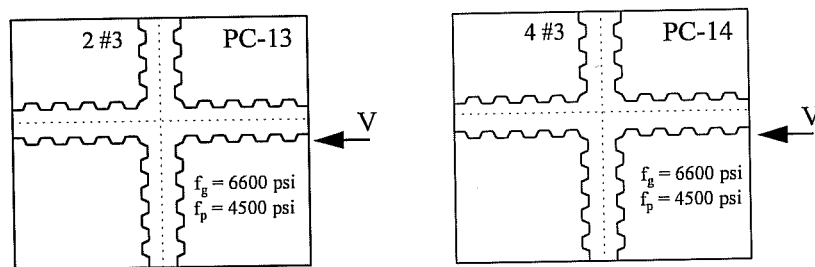


Figure 2.22: Series IV-PC Specimens

2.6.4.1 PC-13 (2 #3 Bars)

Loss of adhesion was noted at 55 kips. A peak load of 63 kips was measured. Additionally, it appeared that the residual capacity was approximately 20 kips. During negative loading to 0.1 in. displacement, the specimen was pushed significantly beyond the target displacement due to an instrument problem during testing. A plateau of 29 kips can be seen occurring from approximately 0.1 to 0.25 in. displacement. Since this load plateau was maintained to large displacement levels, it may be a better indication of residual capacity even though this plateau was not reached in subsequent loadings.

2.6.4.2 PC-14 (4#4 Bars)

Loss of adhesion was noted at 25 kips which was lower than in previous tests. Loading was increased to a peak capacity of 74 kips while a residual capacity of 25 kips was noted. In general, the behavior was typical of previous tests.

2.7 Analysis of Test Results

2.7.1 Failure Surface Location

Joint failure occurred at the top of the joint interface because adhesion was inferior at that location. The entrapment caused loss of adhesion and a lower peak capacity; however, it did not appear to influence the residual capacity. Air entrapment should be expected at the top surface regardless of grouting procedure since the geometry of the joint makes it difficult for air to escape during grouting.

2.7.2 Shear Key Configuration

There did not appear to be any significant effect of the key configuration. As shown in Figure 2.23, specimens PC-1 through PC-4 exhibited similar behavior. The peak capacity was slightly affected depending on the effect of the key pattern on the shearing cross section of the panel (total shear key area at the base of the keys). If the shear cross sectional area was larger, the peak load was slightly higher. It must be noted, however, that variations in the amount of air entrapment can also produce similar changes in peak capacity. Therefore, it is difficult to quantify the exact effect of the configuration. In terms of the residual capacity, however, the configuration did not have any significant effect. The same residual capacities were noted for all four specimens.

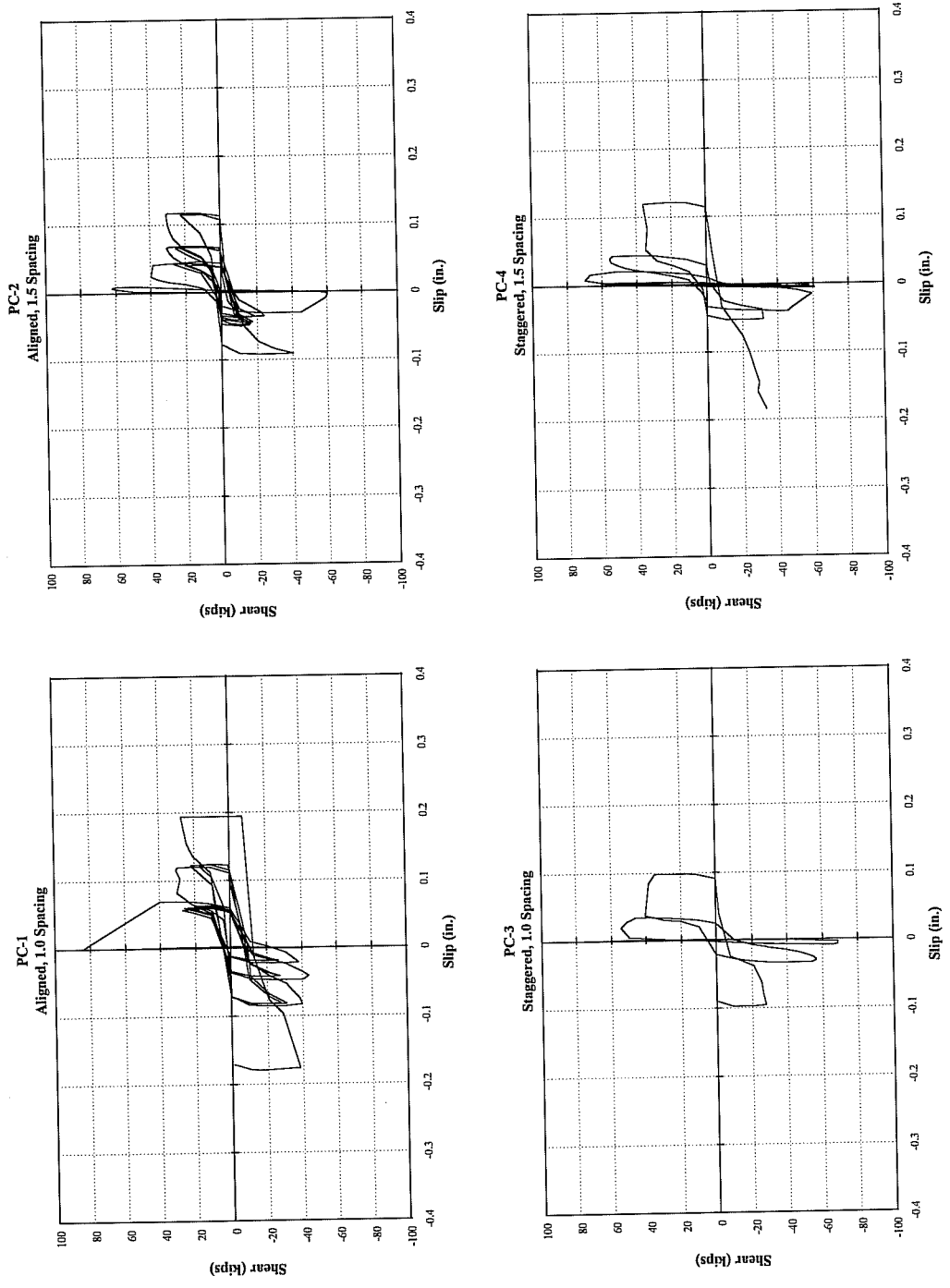


Figure 2.23: Shear Key Configuration Analysis

2.7.3 Shear Key Size

A comparison of specimen PC-9 and PC-11 are shown in Figure 2.24. The peak capacity of the large key was slightly higher since the panel key shear cross sectional area was larger. Behavior of both specimens beyond peak load was similar. The residual capacity was not affected. A comparison of PC-8 and PC-7 provides similar findings.

2.7.4 Spacing Between Panels

No effect of spacing between panels was noted. The specimens with 2 and 4 in. grout strips between panels responded with similar peak and residual capacities as shown in Figure 2.25. Since the panels failed at the grout/key interface and did not develop a strut mechanism through the grout joint between keys, the spacing between panels should have little or no effect. However, it was found that the 2 in. joint width was impractical for grouting operations and placement of reinforcing steel. A larger opening was required to prevent blockage as the grout flowed through the strip and to permit easier placement of the reinforcement. The 4 in. panel spacing was deemed adequate for these purposes.

2.7.5 Concrete Strength

The relative strength between the grout and panel concrete influenced the specimen behavior. For the case of grout strength weaker than the panel, failure of the joint occurred through the grout key (Figure 2.26). In cases where the grout was stronger than the panel, failure occurred through the panel keys as previously shown in

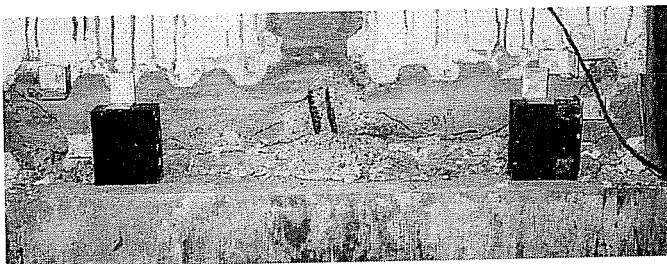


Figure 2.26: Failure Plane (PC-7)

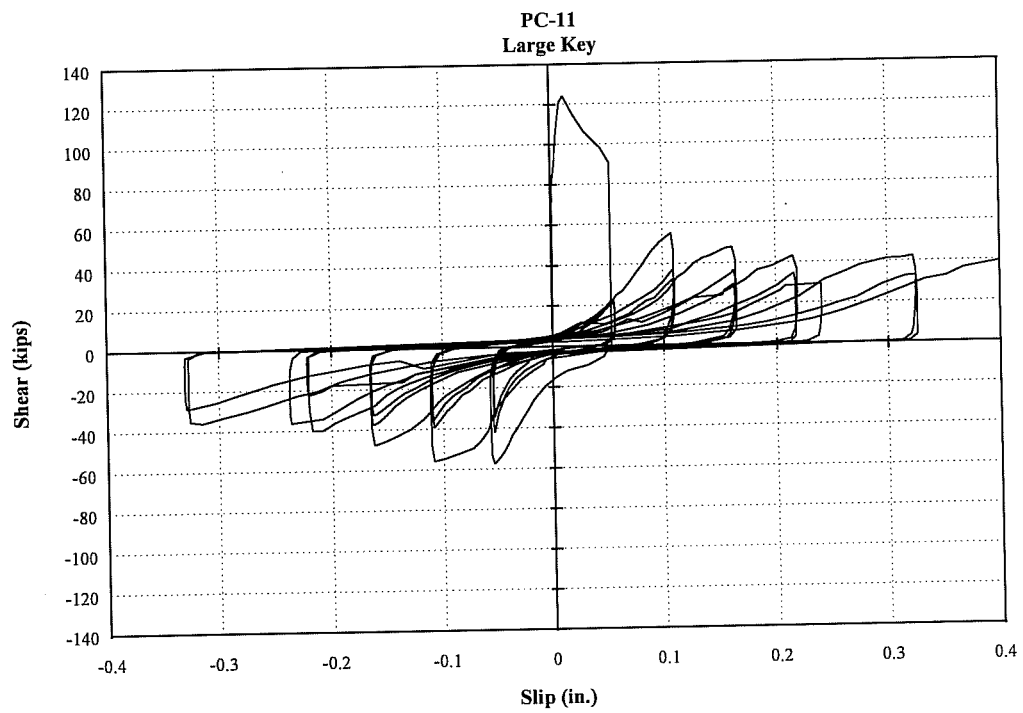
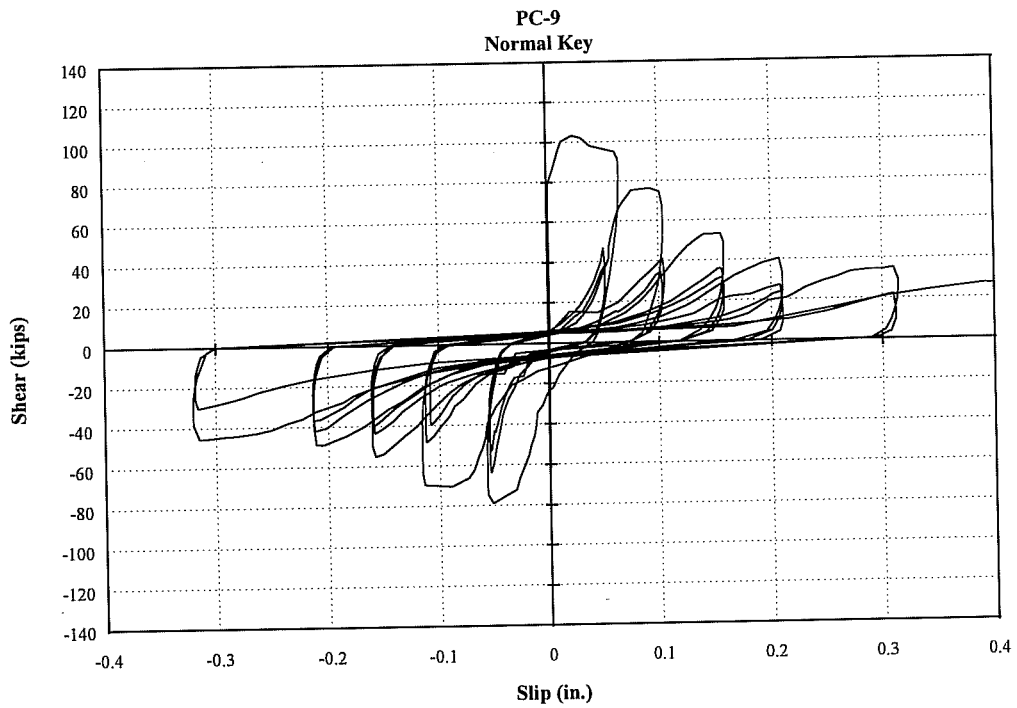


Figure 2.24: Shear Key Size Analysis

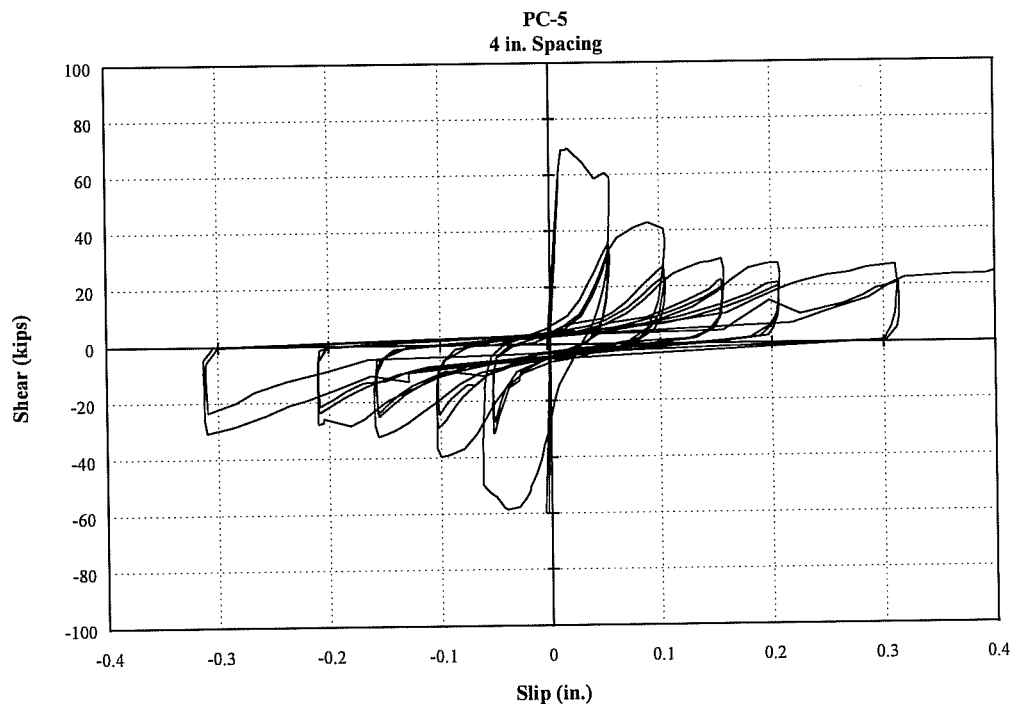
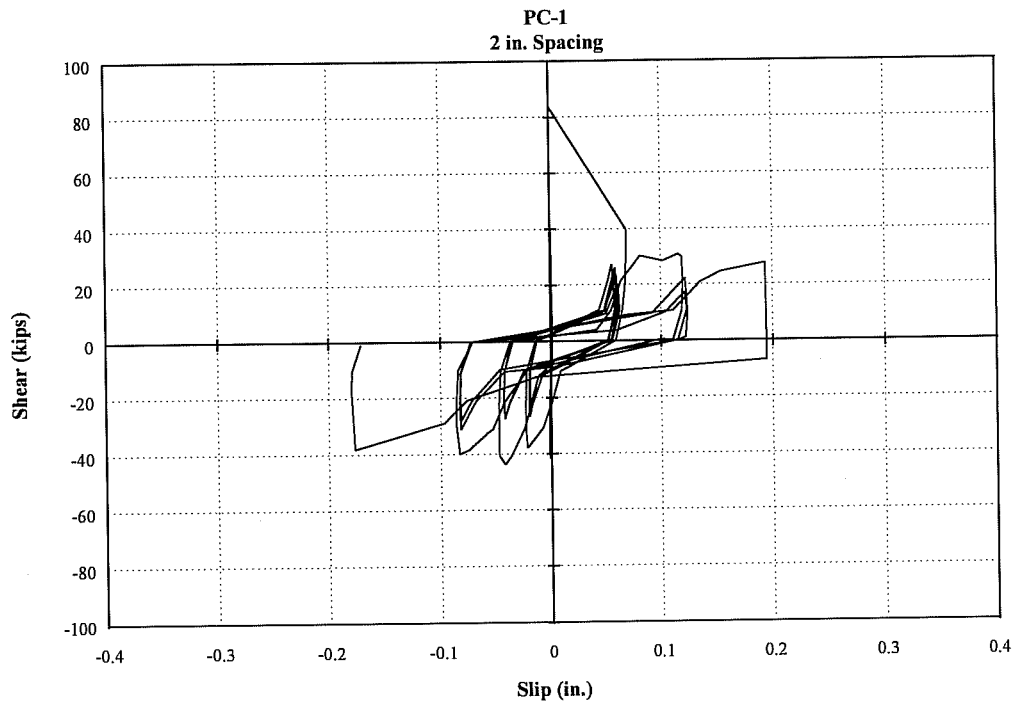


Figure 2.25: Panel Spacing Analysis

Figure 2.17. Therefore, the weaker unit (grout or panel) controlled the cracking strength of the joint and consequently the peak capacity. The concrete strength, however, did not affect the residual capacity as shown in Figure 2.27.

2.7.6 Panel Thickness

The thickness of the panel affected both the peak and residual capacity as shown in Figure 2.28. Due to the reduction in shearing cross section, there was a small reduction in the peak capacity. It is significant to note, however, that there was also a reduction in the residual capacity. The reduction was approximately in the same proportion as the panel thickness.

2.7.7 Vertical Steel Reinforcement

The amount of vertical reinforcement influenced both the peak load and the residual capacity as shown in Figure 2.29. As the reinforcement was increased, both the peak and residual capacity increased. A full discussion of these effects is presented later in Section 2.7.9.

2.7.8 Other Failure Modes

The capacity of the joint was controlled by failure modes other than an interface shear failure in specimens PC-6 and PC-12 which failed in bearing at the loading and support heads. The failure experienced in these tests is peculiar to laboratory testing due to the loading method and would not be expected in the field. In general, the shear strength of the specimen cannot be greater than the capacity of the wall to transfer forces to the joint.

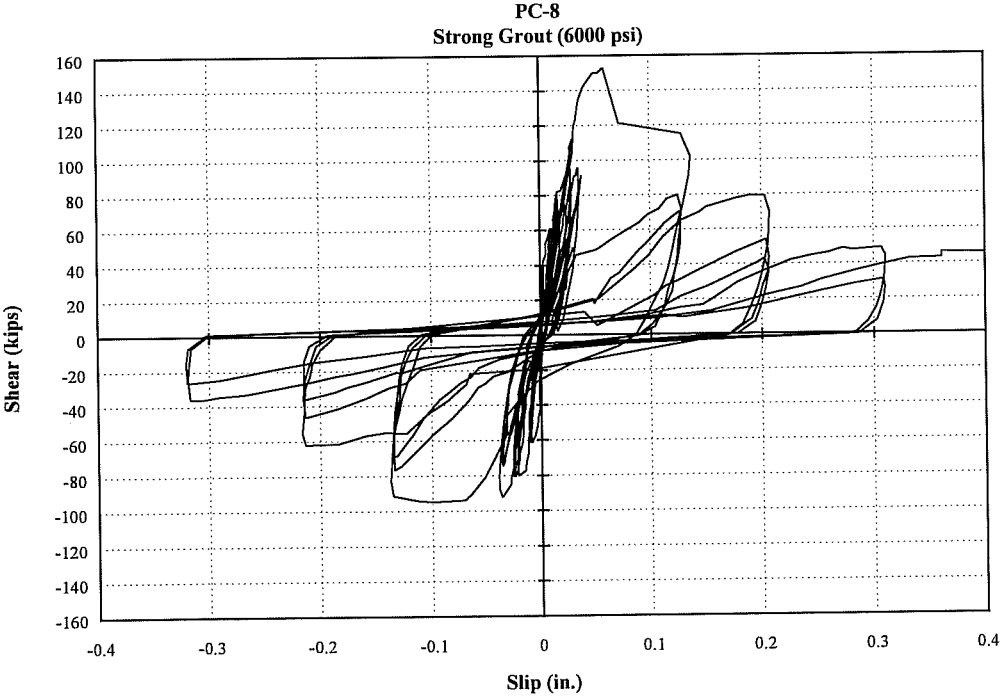
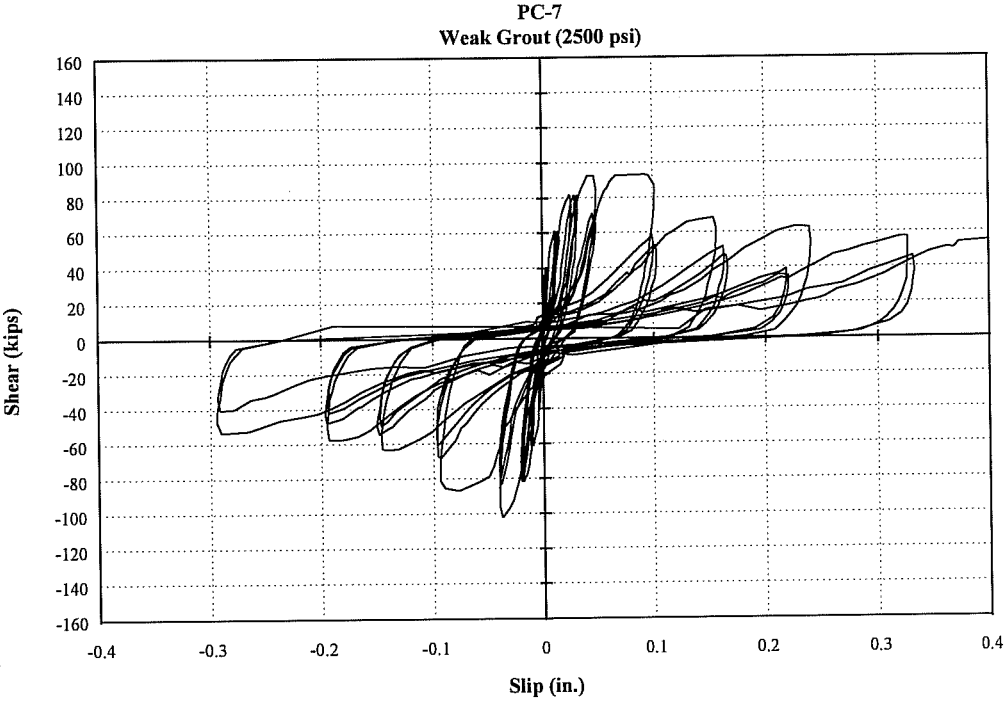


Figure 2.27: Concrete Strength Analysis

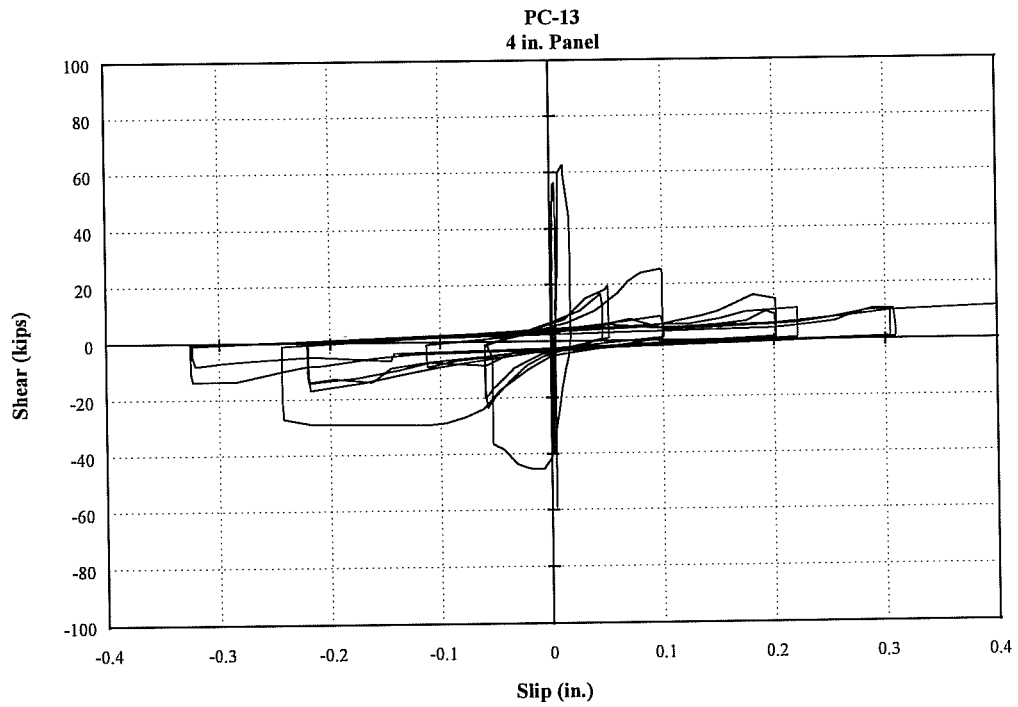
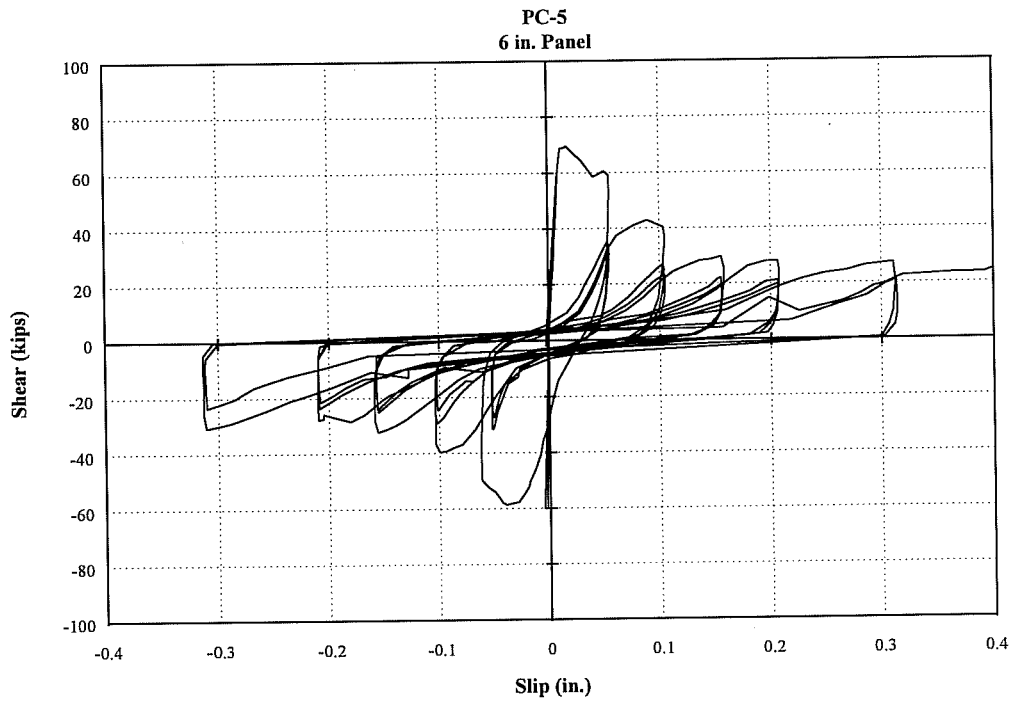


Figure 2.28: Panel Thickness Analysis

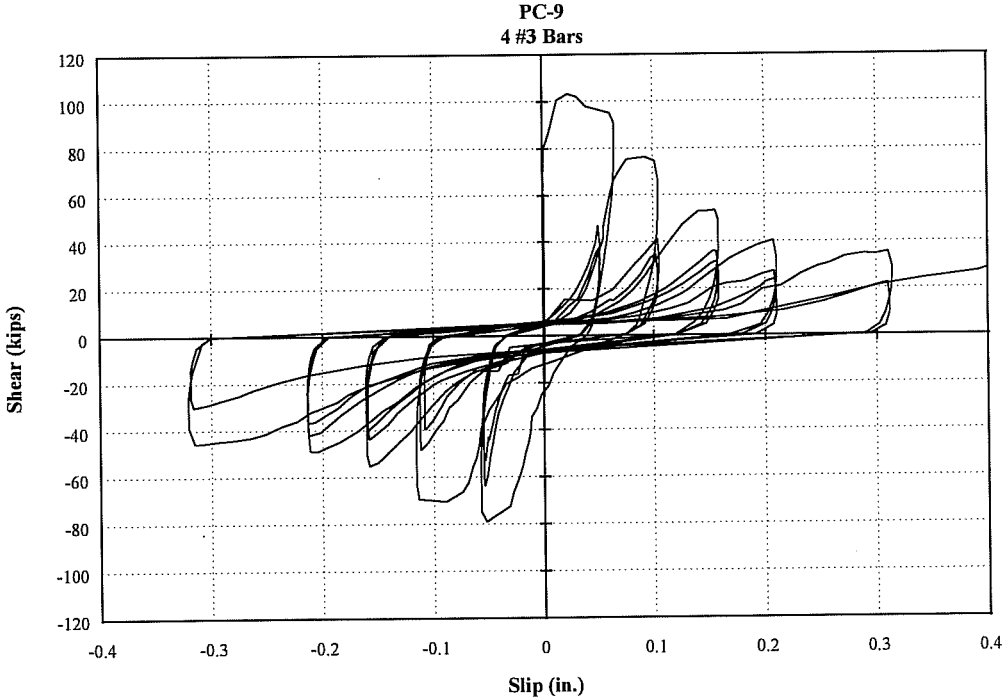
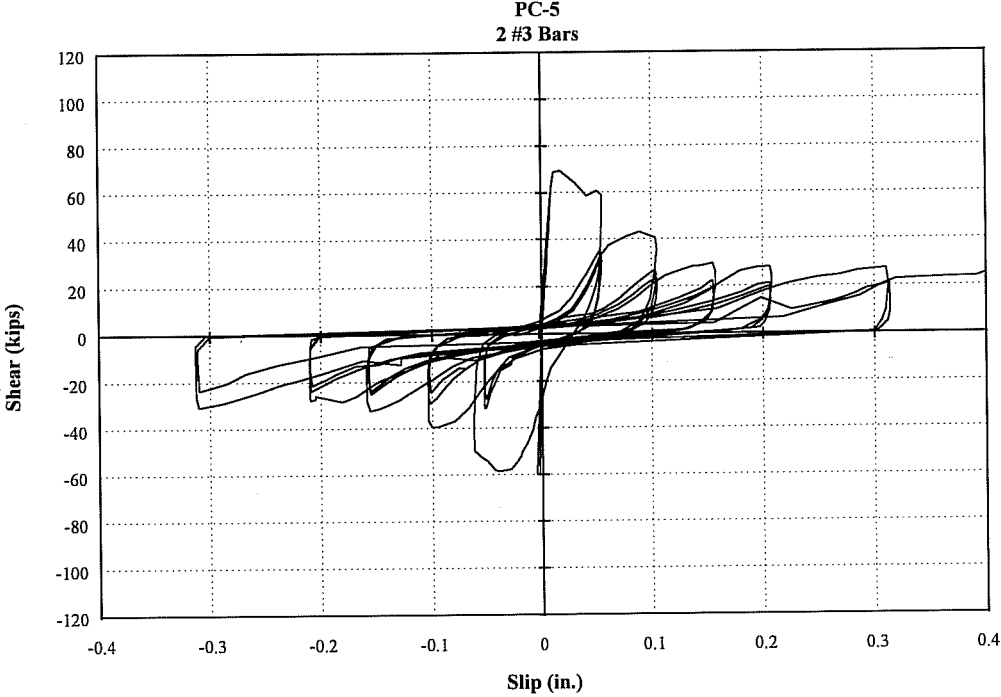


Figure 2.29: Vertical Steel Reinforcement Analysis

2.7.9 Determination of Capacity

2.7.9.1 Adhesion Capacity

Monolithic behavior of the specimen ceased when adhesion along the shear key/grout strip interface was lost. The adhesion capacity was highly variable as demonstrated by the variation between the top and bottom interface capacities in specimen PC-1 and PC-2 and the variation in the other tests presented. The variation is caused primarily by air entrapment that occurs during grouting. Adhesion cannot be reliably predicted and should be neglected for design considerations.

2.7.9.2 Peak Capacity

Cracking of the panel/grout interface occurred at the peak capacity. Therefore, the peak capacity appeared to be controlled by the shear strength of the concrete at the interface. While adhesion remains between the grout and the panel, the specimen behaves monolithically. Therefore, the entire specimen cross section can resist shear up to either the level at which adhesion is lost (adhesion capacity) or shear strength of the section is reached. It is most likely for the adhesion to be lost before a shear failure of the entire specimen occurs. After adhesion is lost, the specimen must resist shear with a reduced interface cross sectional area. Only the shear keys and vertical grout strip remain to transfer the shear through concrete. For most of the specimens studied, this results in reducing the interface cross section by about one half.

If the shear strength of the reduced interface cross section is less than the adhesion capacity, the specimen will crack across the interface and the peak capacity will be reached immediately once the adhesion capacity is reached. On the other hand, if the shear strength of the interface is greater than the adhesion capacity, increased loading is possible until the shear strength of the reduced interface cross

section is reached. In most cases studied, the shear strength of the reduced interface section was greater than the adhesion capacity. Therefore, the interface concrete shear strength determined the peak capacity.

Additionally, the shear strength of the concrete was affected by the vertical reinforcement as shown in Figure 2.30 where the peak capacity was plotted versus the amount of vertical steel. In all tests, the reinforcement was fully yielded in tension at the peak load. Therefore, compression was developed across the concrete interface to resist the reinforcement tension. This compression enhances the shear strength of the concrete due to biaxial effects as illustrated in Figure 2.31 using a Mohr's circle analysis with the Zia^[40] assumed failure theory for concrete. This approach has been used in previous research^[19] to explain the effect of vertical reinforcement in interface shear transfer. Elemental stresses at the interface are shown. As normal compression was increased, the analysis indicated that the concrete failure shear stress will increase. Furthermore, the analysis indicated that the shear stresses will increase approximately linearly with increasing compression.

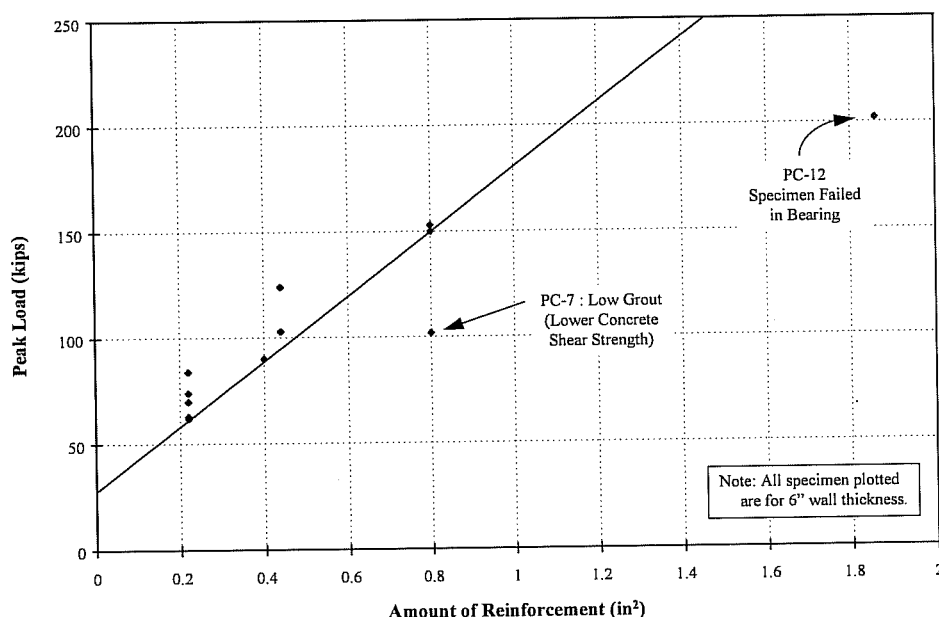
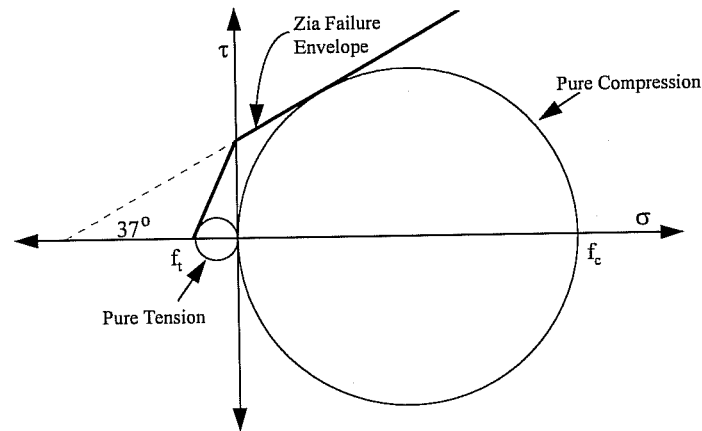
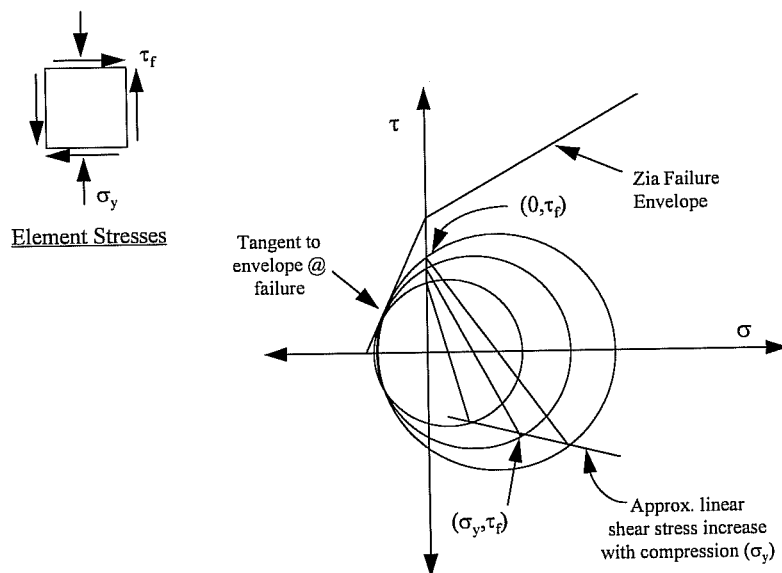


Figure 2.30: Effect of Vertical Reinforcement on Peak Capacity



Construction of Zia Failure Envelope

**Figure 2.31: Effect of Compression on Shear Strength**

The test results presented here also indicate similar findings. The peak capacity increased with the vertical steel amount, and the trend was approximately linear. Calculation of the concrete shear strength to predict the peak capacity, however, is extremely complicated. The compressive stress distribution along the

interface is nonuniform due to the concentration of steel reinforcement in the grout strip. In addition, the keyed interface is likely to result in a shear stress distribution that is complex and nonuniform. A consistent, reliable prediction of the shear strength and resulting peak capacity using this interface shear theory was not possible.

Table 2.6: Peak Capacity Analysis

Specimen	V_{Peak} (Kips)	$A_s f_y$ (Kips)	μ_{Peak}
PC-1	84	14.0	6.00
PC-2	62	14.0	4.43
PC-3	74	14.0	5.29
PC-4	70	14.0	5.00
PC-5	70	13.6	5.15
PC-6	*	58.4	*
PC-7	102	58.4	1.75
PC-8	153	58.4	2.62
PC-9	103	27.2	3.79
PC-10	90	29.2	3.08
PC-11	124	27.2	4.56
PC-12	*	113.9	*
PC-13	63	14.4	4.38
PC-14	74	28.8	2.57
Average:			4.05
Std. Dev.:			1.30

Due to the difficulties in applying the theory presented above, shear friction theory was used to provide a prediction of the peak capacity. Shear friction theory assumes that the reinforcement crossing the shear plane induces compression on the interface that provides for shearing resistance through friction. The coefficient of friction for each test was calculated based on the actual yield strength of the steel and is presented in Table 2.6. Specimens PC-6 and PC-12 were not included since they did not exhibit an interface shear failure. The average coefficient of 4.05 is

artificially high since the actual shear resistance in the test specimen was not due solely to friction. The high standard deviation (1.30) illustrates the high variability in the peak coefficient of friction. For reasonable use of this method in predicting the peak capacity, the average coefficient of friction should be reduced by one standard deviation to include a large percentage of the test results ($\mu=2.75$).

$$V_{Peak} = \mu_{Peak} A_s f_y$$

2.7.9.3 Residual Capacity

Residual capacity was maintained by shear friction which was directly dependent on the amount of vertical reinforcement. The vertical reinforcement induced compression on the interface that provided for shearing resistance through friction. The coefficient of friction for each test was calculated based on the actual yield strength of the steel and is presented in Table 2.7. Specimens PC-6 and PC-12 were not included since a residual capacity was not available. As can be seen in the large variation in the test results and the high coefficient of friction, other factors such as dowel action of the vertical reinforcement contribute to the shear resistance of the section. For reasonable use of this method in predicting the residual capacity, the average coefficient of friction should be reduced by one standard deviation to include a large percentage of the test results ($\mu=1.1$).

$$V_{Residual} = \mu_{Residual} A_s f_y$$

Table 2.7: Residual Capacity Analysis

Specimen	V_{Residual} (kips)	A_sf_y (kips)	μ_{Residual}
PC-1	30	14.0	2.14
PC-2	30	14.0	2.14
PC-3	30	14.0	2.14
PC-4	30	14.0	2.14
PC-5	30	13.6	2.21
PC-6	*	58.4	*
PC-7	58	58.4	0.99
PC-8	50	58.4	0.86
PC-9	40	27.2	1.47
PC-10	52	29.2	1.78
PC-11	43	27.2	1.58
PC-12	*	113.9	*
PC-13	20	14.4	1.39
PC-14	25	28.8	0.87
Average:			1.64
Std. Dev.:			0.53

2.7.10 Design Rationale

Design of the joint should be performed using a capacity on the descending branch of the load-slip curve such as the residual capacity. This capacity can be maintained at large slip levels while the peak capacity can only be achieved once in the loading history of the joint and cannot be maintained. Shear friction theory provides a relatively simple and reliable method for estimating the residual capacity of the joint as previously discussed.

For design calculations, a coefficient of friction of 1.4 ($\mu=1.4$) is recommended for shear friction calculations which is consistent with the highest coefficient permitted by ACI 318-89^[3] for shear friction design. This coefficient, slightly higher than the residual ($\mu=1.1$) is recommended to acknowledge the higher

peak capacity ($\mu=2.75$) since the peak must be reached before the residual capacity can be achieved. In addition, the specimen capacity did not reduce to the residual capacity until extremely large slip levels were reached. Therefore, the capacity at more reasonable slip levels would be higher than the residual.

Table 2.8 presents a comparison of the recommended design capacities with the test results. Calculations were made using the nominal strength of the reinforcing steel ($f_y = 60$ ksi). Since PC-6 and PC-12 did not experience interface shear failure, these tests were not included. However, even these specimens reached loads beyond the design levels presented here.

$$V_{Design} = 1.4A_s f_y$$

Table 2.8: Comparisons of Test Results with Design Method

Specimen	V_{Peak} (kips)	$V_{Residual}$ (kips)	V_{Design} (kips)	$V_{Peak} /$ V_{Design}	$V_{Residual} /$ V_{Design}
PC-1	84	30	18.5	4.45	1.62
PC-2	62	30	18.5	3.35	1.62
PC-3	74	30	18.5	4.00	1.62
PC-4	70	30	18.5	3.79	1.62
PC-5	70	30	18.5	3.79	1.62
PC-6	*	*	67.2	*	*
PC-7	102	58	67.2	1.52	0.86
PC-8	153	50	67.2	2.28	0.74
PC-9	103	40	37.0	2.79	1.08
PC-10	90	52	33.6	2.68	1.55
PC-11	124	43	37.0	3.35	1.16
PC-12	*	*	156.2	*	*
PC-13	63	20	18.5	3.41	1.08
PC-14	74	25	37.0	2.00	0.68
Average:				3.12	1.27

The shear friction method was extremely conservative in estimating the peak capacity for all test specimens. In addition, the method was also conservative for predicting the residual capacity of most of the tests conducted.

2.8 Design and Detailing Recommendations

The following recommendations are made concerning design of the grout connection between precast panels.

2.8.1 Precast Panel Design

Shear keys spaced in a 1.0 spacing pattern should be used along the perimeter of the panel. There does not seem to be a cost advantage in providing a wider spacing of keys. In addition, this key configuration provides for uniform shear transfer between the grout and the panel.

A minimum 4 in. clear separation should be used between adjacent panels since this dimension provides for placement of reinforcing steel and clearance for grout flow.

2.8.2 Grout Strip Concrete

The grout strength should be greater than the panel strength. This recommendation is made since a higher level of variability can be expected in the grout due to field mixing and grouting techniques. The precast panel is likely to be constructed under a more controlled environment where a higher quality product can be manufactured.

2.8.3 Grout Strip Reinforcement

The grout strip reinforcement can be designed using the shear friction provisions of ACI-318-89^[3] Section 11.7. The recommendations made here apply for

normal weight concrete since only normal weight concrete was investigated in this study.

$$V_n = A_{vf} f_y \mu$$

where:

V_n = Nominal joint shear strength

A_{vf} = Cross-sectional area of vertical joint reinforcement

f_y = Yield strength of reinforcing steel

μ = 1.4 (Coefficient of friction)

2.8.4 Wall Design Considerations

The shear strength of the wall cannot be greater than the capacity of the wall to transfer forces to the joint. Failure modes other than interface shear transfer may control and should be checked.

CHAPTER 3

PANEL TO FRAME CONNECTION

3.1 Introduction

Four tests were conducted to evaluate the connection of precast infill wall panels to elements of the existing structure. The connections investigated were typical of connections made along the columns or beams of the existing frame that bound the wall. A representative detail of the frame connection is shown in Figure 3.1.

3.2 Specimen Design

The test specimens were designed to be representative of a full-scale component or cut-out-detail of the frame connection previously illustrated in Figure 3.1. The overall size of the specimen was determined based on the constraints of the interface shear test setup discussed in Chapter 2.

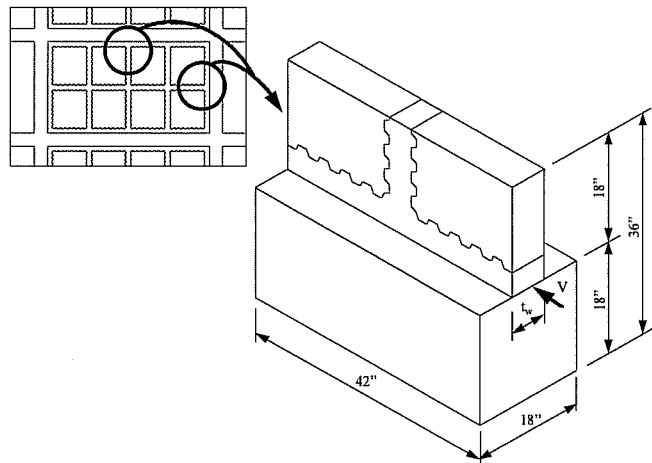


Figure 3.1: Frame Connection Test Component

3.2.1 Precast Panels

Precast infill wall panel details were developed in the tests of panel to panel joints presented in Chapter 2. The panels were reinforced in the same manner with

two mats of 4x4-W2.9xW2.9 welded wire fabric. The panel configuration used throughout the frame connection research was an aligned, normal key at a 1.0 spacing. A spacing of 4 in. between panels was utilized along with a 4 in. separation between the panels and the existing frame element.

3.2.2 Existing Frame

The existing frame element was designed as a column with reinforcement typical of design during the 1950's and 60's, was identical to the column details used in previous research at the University of Texas at Austin,^[38] and followed requirements of ACI 318-56^[1] and ACI 318-63.^[2] An 18x18 column was selected to fit within the loading system. One percent longitudinal column steel and #3 ties at 12 in. were used. The details are shown in Figure 3.2.

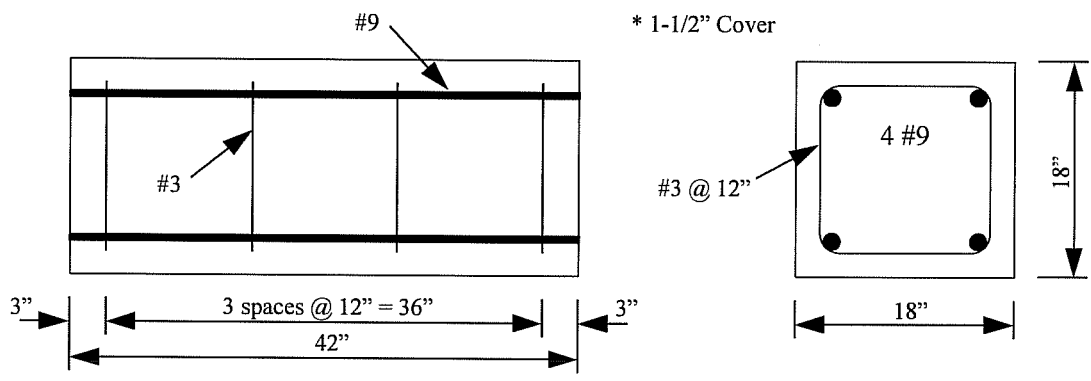


Figure 3.2: Existing Frame Element Details

3.2.3 Closure Strip

The panels were connected to the existing frame with a steel pipe section (shear lug) as shown in Figure 3.3. The pipe was inserted into a core hole made in the existing frame and was contained within the space provided by the grout strip of the panel connection. Reinforcing steel was placed parallel to the existing frame around the pipe. Two #3 bars, considered a minimum for temperature and shrinkage, were

used in all tests for this purpose. Bars perpendicular to the frame element were placed inside the pipe and extended out into the closure strip. For all tests, two #3 bars were used for the perpendicular bars. The horizontal and vertical strip steel was mechanically anchored through the use of steel plates welded to the ends of the bars. After the bars were in place, the joint was grouted. The pipe was installed at the end of grouting operations.

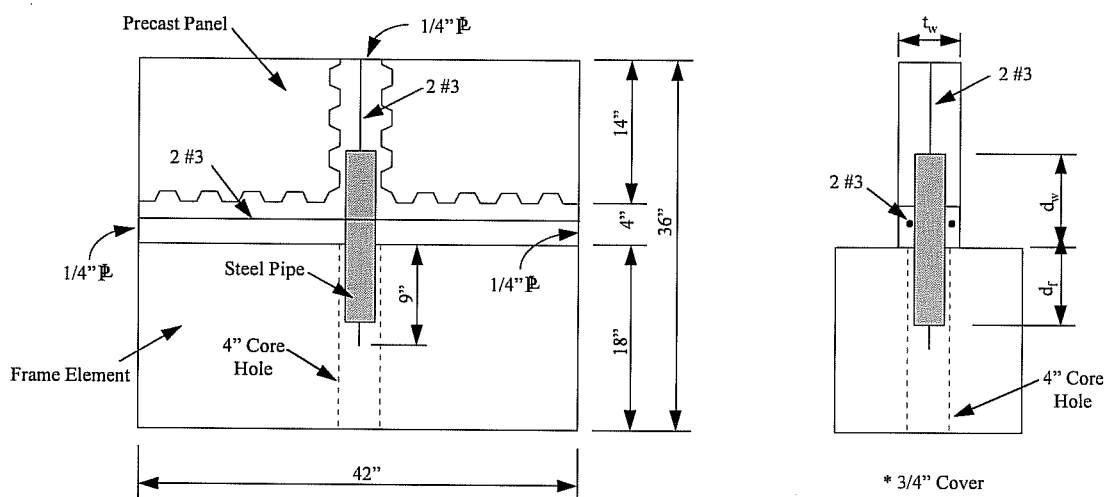


Figure 3.3: Frame Connection Specimen Details

3.2.4 Test Variables

A description of the test variables studied in this phase of the research is presented below. All specimens were identified by the description label FC (**F**rame **C**onnection) follow by the specimen number. A summary of the specimen variables is presented in Table 3.1. Tests were divided into two series as indicated in the table.

Panel Thickness (t_w): Two precast wall panel thicknesses were investigated. Both a 4 and 6 in. panel were selected to correspond with the work described in Chapter 2.

Table 3.1: Frame Connection Test Details

Series (FC)	Specimen	Existing Frame		Panel		Grout		Pipe			
		Age at Testing (days)	f_f (psi)	Thickness	Age at Testing (days)	f_p (psi)	Age at Testing (days)	f_g (psi)	Size	Frame Embedment (in.)	Wall Embedment (in.)
I	FC-1	239	3900	6	50	4000	23	6300	2-1/2" XS	9	4
	FC-2	245	3900	6	56	4000	29	6300	2-1/2" XS	9	9
	FC-3	251	3900	6	62	4000	35	6300	2-1/2" XS	4	9
II	FC-4	542	3900	4	45	4500	28	6600	2" XS	4	9

Steel Pipe Embedment Length (d_f , d_w): The embedment lengths of the steel pipe into the wall side of the interface and into the frame side of the interface were investigated. To limit the number of test specimens, preliminary calculations of embedment lengths were made by considering concrete bearing on the projected surface of the steel pipe. A bearing stress of $0.85 f'_c$ consistent with ACI 318-89.^[3] was used. The bearing strength was equated to the shear yielding strength of the corresponding pipe based on nominal yield. The tests were carried out to verify this design methodology.

Steel Pipe Size: The effect of the size of the pipe was investigated. A 2 in. extra strong pipe (2" XS) and a 2-1/2 in. extra strong pipe (2-1/2" XS) were studied. These pipe sizes were chosen because they represent maximum pipe sizes for typical installations in 4 and 6 in. walls, respectively. In addition, due to the bearing requirements, the pipe thickness also corresponded to a maximum practical size. The double extra strong (XXS) pipe for the equivalent pipe sizes would require extremely large embedment lengths that would typically not be practical.

3.3 Specimen Construction

3.3.1 Precast Panel Construction

The wall panels were constructed by the same method presented in Chapter 2.

3.3.2 Frame Element

The frame element was constructed as a column in a vertical casting position as shown in Figure 3.4. A 4 in. core hole required for the shear lug was cast into the column using a 3-1/2 in. PVC pipe as a void form. The PVC pipe was placed across

the width of the column through the formwork to produce a core hole through the section. The PVC pipe was removed prior to placement of the steel pipe sections.

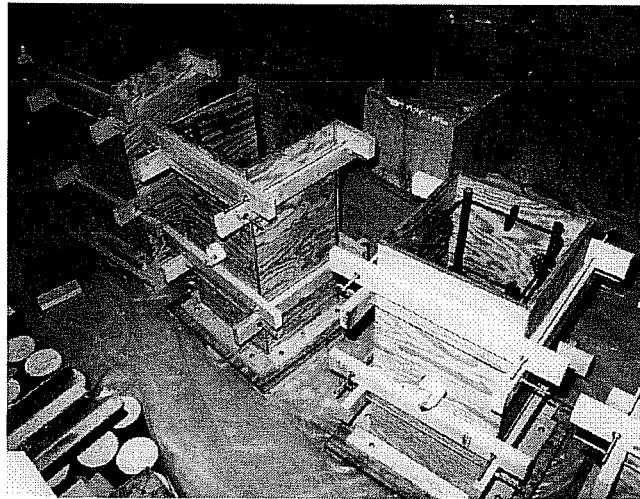


Figure 3.4: Frame Element Construction

3.3.3 Wall Construction

All specimens were constructed in the top cast position (Figure 3.5) since this position was deemed to be the most difficult and would produce lower-bound test results. The interface surface would likely have the lowest adhesion due to slumping effects and air entrapment. The wall panels were placed under the frame element with a 4 in. clear separation as shown in Figure 3.6. A close-up view is shown in Figure 3.7 where the core hole for placement of the grout and steel pipe can be seen. All grout was placed through the core hole

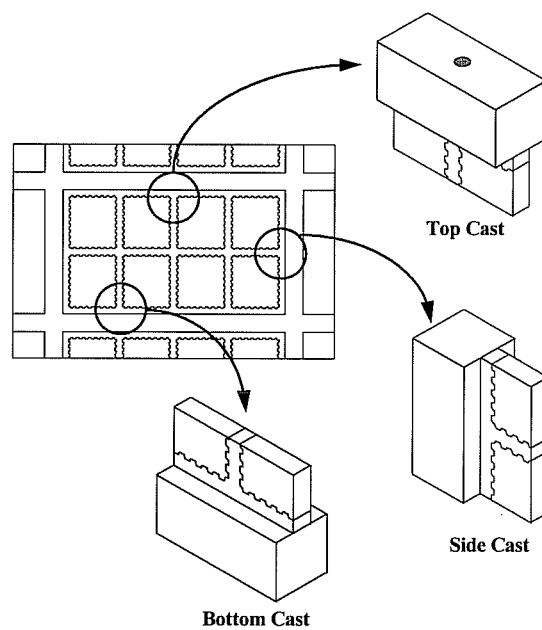


Figure 3.5: Specimen Casting Position

at the top of the frame element. The grout was vibrated in the vertical joint through the core hole while proper consolidation was ensured in the horizontal joint by vibration through access holes (see Chapter 2).

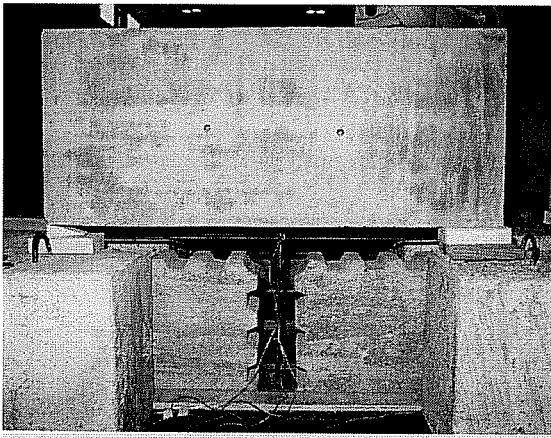


Figure 3.6: Wall Construction

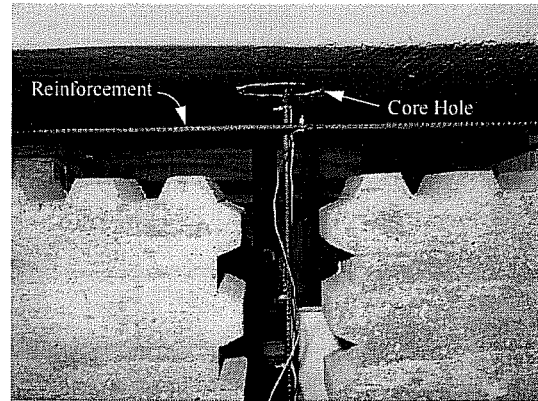


Figure 3.7: Core Hole for Shear Lug

Following placement of the grout, the steel pipe was inserted through the core hole. Final positioning of the pipe was achieved by providing vibration in the core hole. An all-threaded rod was inserted in the formwork at the design pipe embedment length to ensure proper pipe location. The bottom stop prevented settling of the pipe during construction which would result in the wrong embedment length being provided.

3.4 Construction Materials

3.4.1 Existing Frame Concrete

The existing frame element was constructed using a nominal 3000 psi concrete with 3/4" aggregate. A 3000 psi mix was used since this strength is typical of existing structures from the era under consideration. The mix proportions are

shown in Table 3.2. The exact proportions delivered varied slightly and were adjusted for moisture conditions of the aggregates. The mix was adjusted at the jobsite to maintain a 6 in. slump. All frame elements were constructed at the same time. The strength gain curve is presented in Figure 3.8.

Table 3.2: Frame Element - Concrete Mix Proportions

Material	Quantity
Cement (Type I)	400 pcy
3/4" Coarse Aggregate (SSD)	1625 pcy
Fine Aggregate (SSD)	1619 pcy
Water	275 pcy
Admixture ¹	12 ozcy

¹ For high temperature months (May-September), an admixture meeting ASTM C494 requirements for Type B retarding and for Type D water-reducing and retarding was used. During cooler months (November to April), an admixture meeting ASTM C494 for Type A water-reducing admixtures was used. The quantities of admixture used, however, remained constant throughout the year.

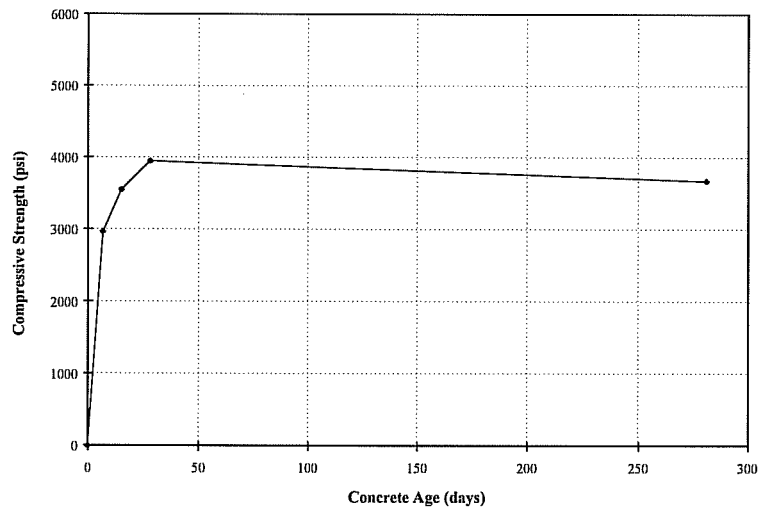


Figure 3.8: Existing Frame Concrete Strength Gain

3.4.2 Precast Panel Concrete

The precast panels were constructed using a nominal 4000 psi concrete with 3/8 in. aggregate. The panels for use in the frame connection tests were constructed with those for the panel connection tests. The panels used in Series I-FC specimens were constructed with mix P-2 while panels used in Series II-FC were constructed with mix P-4. See Chapter 2, Section 2.4.1 for panel concrete (P) information.

3.4.3 Panel Grout

The frame connection specimens were grouted with the panel connection test specimens. Series I-FC specimens were constructed with mix PG-2 while Series II-FC was constructed with mix PG-4. See Chapter 2, Section 2.4.2 for panel grout (PG) information.

3.4.4 Interface Steel

Number 3, Grade 60 bars were used in all specimens. Tensile tests were performed on representative coupons of the bars to obtain both the yield and ultimate tensile strength. Testing was performed according to ASTM A370-94. The test results are presented below. The reinforcing steel used in Series I-FC and II-FC corresponded with the reinforcing steel used in Series II-PC and IV-PC of the panel connection tests, respectively. The same welded wire fabric was used in panel construction as was used for the panel connection tests (Chapter 2).

Series	Yield (ksi)	Tensile (ksi)
I-FC	61.8	101.6
II-FC	65.5	102.5

The steel pipes used for the interface shear transfer were ASTM A-53 Grade B which has a minimum specified yield of 35 ksi. Coupon tests were conducted

according to ASTM A370-94 to determine the yield and ultimate tensile strengths. The results are presented below. As can be noted, the yield strengths are significantly above the minimum specified yield of 35 ksi, especially for the 2-1/2 in. pipe.

Pipe Size	Yield (ksi)	Tensile (ksi)
2" XS	40.4	55.7
2-1/2" XS	53.6	71.6

3.5 Test Setup and Procedure

The test setup was designed to subject the specimens to direct cyclic shear across the frame to wall connection interface. Two 400^K hydraulic rams at each end of the setup allowed for pushing the wall segment relative to the frame element which was hydrostoned into the loading frame. The setup was the same as used for the panel connection tests (Chapter 2).

Load was monitored through the use of pressure transducers and gages. Interface slip and uplift were monitored by displacement transducers mounted along the interface. Additionally, strain gages were attached to the reinforcing steel and the steel shear lug to determine steel stresses during testing. The specimen instrumentation is shown in Figure 3.9.

The applied loading for the specimens was cyclic in nature. Load control was used up to the peak capacity of the specimen. Subsequently, displacement control was utilized. Typically, three cycles at each load or displacement stage were completed. During load control, 20 kip increments were applied; and during displacement control, increments of 0.05, 0.1, 0.15, 0.2, and 0.3 in. were imposed. The exact nature of the loading may have varied slightly depending upon the specimen behavior.

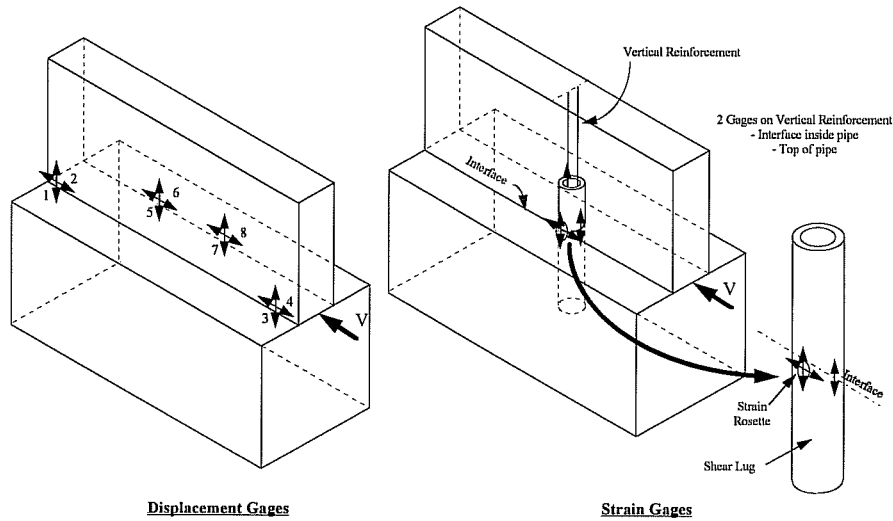


Figure 3.9: Specimen Instrumentation

3.6 Experimental Results

The general behavior of the test specimens is discussed, and a representative load-displacement relationship is shown in Figure 3.10. The structure responded in a monolithic fashion until loss of adhesion occurred along the wall/frame interface. The loss of adhesion was accompanied by uplift along the joint and by stresses being induced in both the steel pipe and the vertical joint reinforcement. Loading was increased until the peak capacity was reached. Following the peak, there was a transition to a lower load plateau which was maintained at a nearly constant level to extremely large slips. A specific discussion of each test specimen follows. Test results for all specimens are presented in Appendix B and are summarized in Table 3.3.

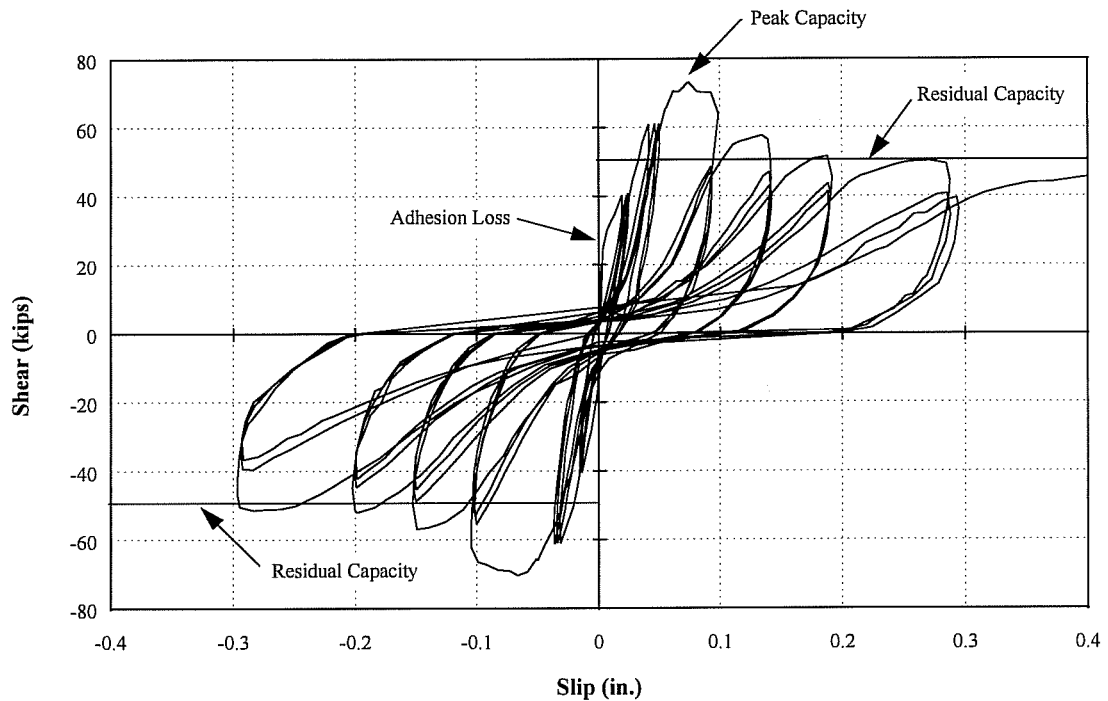


Figure 3.10: Frame Connection Test Result (FC-3)

Table 3.3: Frame Connection Test Results

Specimen	Adhesion Capacity (kips)	Peak Capacity (kips)	Residual Capacity (kips)
FC-1	30	62	34
FC-2	35	71	48
FC-3	30	73	50
FC-4	25	55	31

3.6.1 Series I-FC

In the first series, the use of the 2-1/2 in. extra strong pipe embedded into a 6 in. wall was investigated. The pipe embedment lengths were varied as discussed

previously. All three specimens in this series were constructed together and are shown in Figure 3.11.

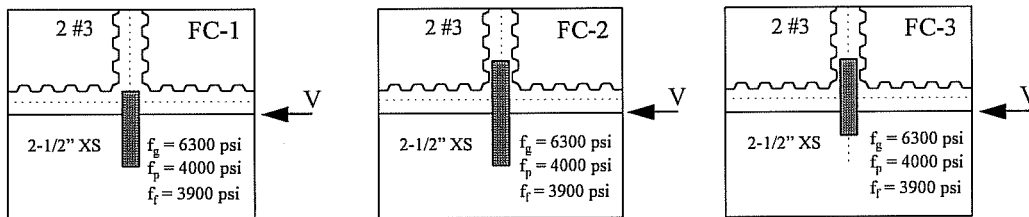


Figure 3.11: Series I-FC Specimens

3.6.1.1 FC-1

The specimen behaved in an extremely stiff or monotonic fashion up to a loading of 30 kips. At this level, slip occurred across the interface as the concrete adhesion at the existing frame/wall interface was overcome. The loss of adhesion at the interface was accompanied by uplift and stresses being induced in both the vertical strip reinforcement and the pipe. As loading continued, a peak capacity of 62 kips was reached. Full yielding of the vertical strip steel was achieved. In fact, yielding was evident when the load reached 60 kips. The failure surface at the peak capacity coincided with the shear key interface, 5 in. above the plane of pure shear. Since the pipe was only embedded 4 in. into the wall, it did not cross the plane of the grout-wall interface. Therefore, a failure mechanism identical to the panel connection tests resulted in which failure occurred on the shear key plane that was reinforced with 2 #3 bars. This test specimen, therefore, responded in the same manner as PC-5 which was also reinforced with 2 #3 bars in the vertical grout strip. After reaching the peak capacity, a transition to a lower load plateau occurred with increasing slip levels. A residual capacity of 34 kips was maintained to large displacement levels. The residual capacity was similar to that of specimen PC-5.

3.6.1.2 FC-2

Loss of adhesion occurred at 35 kips. Loading was continued to a peak capacity of 71 kips. The failure plane occurred at the wall-frame interface. There was a gradual transition with increasing displacements to a residual capacity of 48 kips.

3.6.1.3 FC-3

Adhesion loss occurred at 30 kips. A peak capacity of 73 kips was reached with a residual capacity of 50 kips maintained. Overall, this specimen behaved practically identical to FC-2 which is reasonable since both specimens had the same wall embedment length for the pipe. This test indicated that the 4 in. embedment into the frame element was adequate.

3.6.2 Series II-FC

Following the first series of frame connection tests, it was decided to investigate one additional specimen as shown in Figure 3.12. A 2 in. extra strong pipe was chosen along with a 4 in. wall. These changes were used to verify the behavior exhibited in Series I as well as verify the theory used to design this connection type.

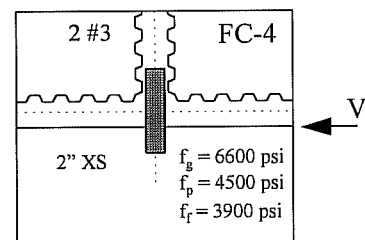


Figure 3.12: Series II-FC Specimen

3.6.2.1 FC-4

Loss of adhesion occurred at 25 kips. A peak capacity of 55 kips was reached followed by a gradual transition to a residual capacity of 31 kips. This specimen behaved as expected and according to the general behavior observed in the previous tests.

3.7 Analysis of Test Results

3.7.1 Interface Shear Failure

As exhibited by specimen FC-1, failure across the precast panel interface can occur depending on the embedment of the shear lug. Behavior corresponding to that of the panel connections was observed. To completely eliminate the possibility of failure at the panel interface, the pipe should be embedded for a depth greater than the grout strip width to ensure that the pipe crosses the precast panel-grout strip interface. Alternately, the section can be designed with proper reinforcement according to the design recommendation for the panel connection to maintain the joint capacity at the proper design load. Specimen FC-1 is not discussed further in this chapter since its behavior can be explained by the methods presented in Chapter 2.

3.7.2 Pipe Failure Mode

After testing, the wall concrete was removed to investigate the condition of the shear lug. The 2-1/2 in. pipe from specimen FC-2 was bent as shown in Figure 3.13. The deformed shape indicated that yielding of the pipe occurred. However, the mode of deformation appeared to be flexural since the deformed shape looked like a cantilever bending about the frame/wall interface. Therefore, shear yielding, as assumed in design, was not achieved. Similar behavior was exhibited in specimen FC-3.

Further analysis of the test data and material properties indicated that these pipes were not adequately embedded. Design for the embedment lengths was determined based upon the nominal

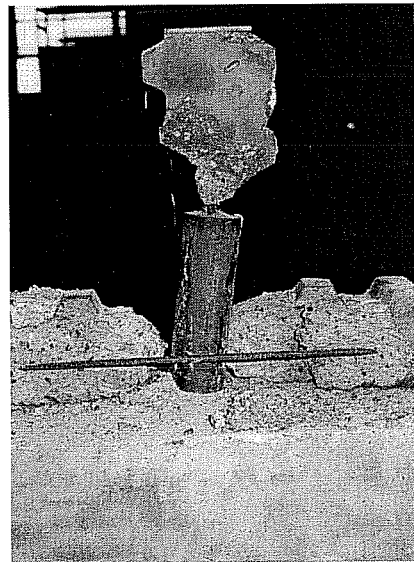


Figure 3.13: Flexural Yielding of Pipe (FC-2)

material yield strength of the pipe, but the actual yield strengths were significantly higher (1.53 times greater). Therefore, the design embedment lengths for the wall side were short by approximately 50 percent. Since embedment lengths provided were too short, shear yielding did not occur. In both tests, the concrete did have adequate bearing strength, however, to produce flexural yielding of the pipe.

Specimen FC-4 was provided adequate embedment length since the actual material strength was close to the nominal. Therefore, a shear failure was expected. The deformed shape of the pipe indicated that the design methodology for pipe embedment was acceptable since a shear yielding occurred as shown in Figure 3.14. The top half of the S shape, indicative of shear yielding, was evident. Additionally, after weathering, the localized yielding near the existing frame interface was evident from the rusted area. The extent of the yielding zone supported that shear yielding was the mode of deformation for this specimen.



Figure 3.14: Shear Yielding of Pipe (FC-4)

The test results presented here demonstrate that proper embedment was required to produce shear yielding of the pipe. Lack of embedment can cause a flexural failure that may reduce the capacity of the specimen. These tests also indicated that calculation using ACI 318-89^[3] bearing calculations on the projected surface of the steel pipe was acceptable. The shear lug designed on this basis was able to reach shear yielding of the pipe section. When embedment was shorter than that based on the bearing calculations, another mode of failure occurred.

3.7.3 Localized Bearing Failure

Local bearing failure at the interface was observed following testing. The bearing failure is evident in Figure 3.14 which shows localized crushing in the wall adjacent to the pipe at the interface. This localized crushing occurred since the bearing stresses were not uniform over the depth of the pipe. The localized bearing failure can be observed in the hysteresis curves. Pinching of the curve occurred since the pipe was required to engage sound concrete before loading could be increased during load reversals. Local failure did not affect the capacity of the section, but did increase slip levels required to regain the shear capacity.

3.7.4 Determination of Capacity

3.7.4.1 Adhesion Capacity

Monolithic behavior of the specimen ceased when the adhesion along the wall-frame interface was lost. The adhesive capacity was variable due to the amount of air that was entrapped during grouting and due to the quality of the grouting method. Adhesion cannot be reliably predicted and should be neglected for design considerations.

3.7.4.2 Peak Capacity

The peak capacity appeared to be approximated by the addition of the three components of shear strength at failure: steel pipe shear strength, vertical reinforcement shear strength, and friction developed by induced compression across the interface. A comparison of test results with the computed capacities is presented in Table 3.4 for specimen FC-4 since a shear friction failure occurred in this specimen. A coefficient of friction of 0.8 was used to estimate compression effects, and actual material strengths were used.

$$V_{Peak} = \text{Pipe Shear Yield} + \text{Reinforcement Shear Yield} + \text{Interface Friction}$$

$$V_{peak} = 0.6 A_{Pipe} F_y + 0.6 A_s f_y + 0.8 A_s f_y$$

Table 3.4: Peak Capacity Analysis

Specimen	Experimental V_{Peak} (Kips)	$0.6A_{Pipe}F_y$ (Kips)	$0.6 A_s f_y$ (Kips)	$0.8A_s f_y$ (Kips)	Calculated V_{Peak} (Kips)	Ratio Exp./Calc.
FC-4	54.6	35.9	8.6	11.5	56	0.98

3.7.4.3 Residual Capacity

The residual capacity across the interface was maintained by the steel pipe and can be approximated from the shear yielding capacity of the pipe as shown in Table 3.5 where the actual yield strength was used. Cycling of the specimen appeared to eliminate the contributions of the vertical reinforcing steel to shear strength and reduce the effectiveness of the cross-sectional shear area.

Due to composite action of the steel and concrete during loading to peak capacity, the entire cross sectional area of the pipe appeared to be effective in resisting shear. However, after cycling to achieve the residual capacity, the effective shear area appeared to be reduced. Crushing of the concrete inside the pipe may reduce the effectiveness of the composite action. A reduced shear area between the elastic solution for the pipe ($A_{sh}=0.54A_s$) and the full cross section area ($A_{sh}=1.0A_s$) seems more appropriate. The test result indicates $0.86A_s$ as the effective shear area assuming that the pipe provides the only contribution to shear strength.

$$V_{Residual} = 0.6 A_{pipe} F_y$$

Table 3.5: Residual Capacity Analysis

Specimen	Experimental $V_{Residual}$ (kips)	Calculated $V_{Residual}$ (kips)	Ratio Exp./Calc.
FC-4	31	35.9	0.86

3.7.5 Design Rationale

Design of the joint should be based on the residual capacity which can be maintained at large slip levels. The peak capacity can only be achieved once in the loading history of the joint and cannot be maintained. The method presented for calculating the residual capacity provides a simple and reliable method for estimating the capacity of the joint. Table 3.6 presents a comparison of the recommended design capacities with the test results. Values were computed using the nominal specified material strength as would be used for design. The design values provide a conservative estimate of the peak capacities while providing an extremely accurate estimate of the residual capacities. Specimens FC-2 and FC-3 are included to illustrate that the design method provides a conservative estimate of the shear capacity even though the proper embedment lengths were not provided to produce a shear yielding failure.

$$V_{Design} = 0.6 A_{pipe} F_y$$

Table 3.6: Comparisons of Test Results with Design Method

Specimen	V_{Peak} (kips)	$V_{Residual}$ (kips)	V_{Design} (kips)	$V_{Peak} /$ V_{Design}	$V_{Residual} /$ V_{Design}
FC-2	70.8	48	48.6	1.46	0.99
FC-3	73.1	50	48.6	1.50	1.03
FC-4	54.6	31	32.0	1.71	0.97
Average:				1.56	1.00

3.8 Design and Detailing Recommendations

The following recommendations are made concerning the design of precast panels to the existing building frame.

3.8.1 Precast Panel Design

A minimum 4 in. separation should be used between the adjacent panels at the frame connection location to provide clearance in the closure strip for the shear lug (pipe) to fit.

3.8.2 Pipe Design

The pipe should be designed based on the shear force required to be transferred at the interface. The design level should be based on the shear yielding capacity of the pipe which can be determined as follows:

$$V_n^{Pipe} = 0.6A_sF_y$$

where:

$$\begin{aligned} V_n^{Pipe} &= \text{Nominal pipe shear strength of one pipe} \\ A_s &= \text{Cross-sectional area of pipe} \\ F_y &= \text{Yield strength of pipe steel} \end{aligned}$$

3.8.3 Pipe Embedment

The pipe embedment lengths should be determined by the following method based on bearing of the pipe on the concrete (Figure 3.15). An overstrength factor of at least 1.25 is recommended to account for material overstrength of the pipe. It is recommended on the wall side to neglect any effects of the supporting surface being wider than the loaded area. Due to the small concrete cover near the pipe, it does not

seem reasonable to include this factor. On the frame side, however, it is possible to take advantage of the factor $\sqrt{A_2 / A_1}$.

$$\alpha V_n^{Pipe} = \phi \left(0.85 f'_c \sqrt{\frac{A_2}{A_1}} \right) \phi_{OD} d$$

where:

V_n^{Pipe} = Nominal pipe shear strength

$\alpha \geq 1.25$ (Overstrength factor)

$\phi = 0.7$ for concrete bearing

f'_c = Compressive strength of concrete

ϕ_{OD} = Outside diameter of steel pipe

d = embedment depth

$$\sqrt{\frac{A_2}{A_1}} \leq 2 \text{ (Confinement factor - See ACI}^{[3]}, \text{ Section 10.15)}$$

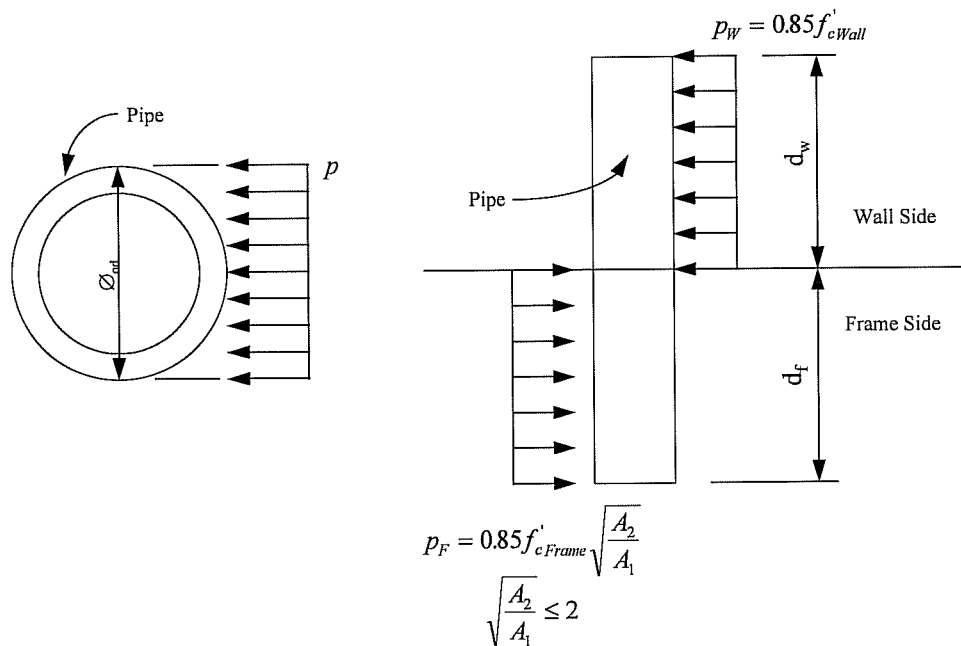


Figure 3.15: Embedment Determination

CHAPTER 4
STRENGTHENED NON-DUCTILE FRAME TEST STRUCTURE:
DESIGN AND CONSTRUCTION

4.1 Introduction

A two-story nonductile frame infilled with the precast infill system was used to evaluate the overall system behavior and verify the performance of the connection details discussed in the previous two chapters. The performance of a post-tensioning system used to provide column tensile capacity, typically deficient in nonductile reinforced concrete frames, was also investigated.

4.2 Specimen Design

The test specimen was designed in two stages. First the building frame was designed according to the building codes governing design during the period of construction of the original structure. Secondly, a rehabilitation scheme was designed utilizing present design codes and the recommendations for the infill panels developed as part of this project (Chapter 2, Section 2.8 and Chapter 3, Section 3.8).

4.2.1 Existing Frame

The five story nonductile frame building presented in Chapter 1 was typical of designs and details meeting the provisions of ACI 318-56.^[1] The prototype design was dimensionally scaled down using a 2/3 factor which resulted in a model with a 13 ft. - 4 in. bay spacing with 8 ft. story heights. For the test structure, a typical multistory interior frame was selected. The specimen selected represents a “cut-out”

section of the building and is shown in Figure 4.1. Complete structural drawings and details are presented in Appendix C.

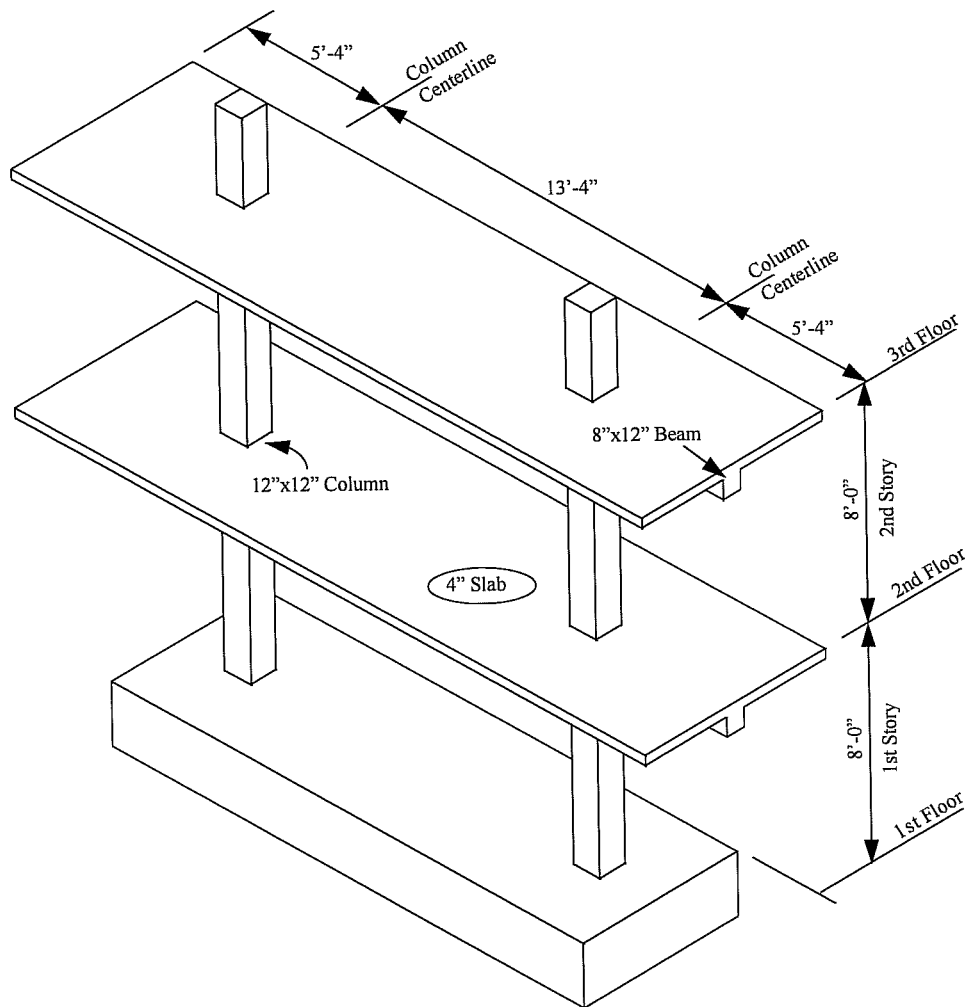


Figure 4.1: Existing Frame Specimen

Several features to simulate an interior frame can be noted. Cantilevers were provided on either side of the frame to simulate beam-column joint conditions in an interior frame. The cantilevers provide continuity across the column so that slab and beam reinforcement details simulate an interior column support. Similarly, column stubs were added above the top floor to permit extension of column reinforcement

through the joint. The column bars were spliced in the column stub as in the typical interior joints below. No special anchorages were required at the joints. Additionally, the cantilevers were designed to balance the beam moments at the column face to provide only axial load to the column under gravity loading.

The specimen was designed to be loaded through the slabs to simulate earthquake forces generated by the floor masses. The loads were transferred through the slab by diaphragm action. Additionally, the slabs provided for convenient access to the structure for use during construction and testing.

The building frame was attached to a footing that was anchored to the laboratory strong floor. The footing depth was determined by the structural dimensions and reaction wall geometry since the center line of the building slabs had to be aligned with the anchor points in the laboratory reaction wall to position the lateral load actuators.

The main nonductile features typical of 1950's and 1960's design contained in the test structure are presented below:

Column Lap Splices: Column splices were provided at the footing and at each floor level. They were designed as compression splices with a lap of 15 inches ($20 d_b$) for the #6 bars.

Column Ties: The columns were reinforced with #3 ties with 90° hooks spaced at 12 in.

Beam Reinforcement: The positive moment bars were discontinuous at the beam-column joint where a 4 in. embedment (6 in. in the prototype) into the joint was provided. Negative moment steel was also

discontinuous in the midspan regions where positive moment controls design. Shear reinforcement in the form of U stirrups was provided.

4.2.2 Infill Wall

The precast infill wall system was designed to strengthen and stiffen the model test structure. A general layout of eight precast panels per floor as shown in Figure 4.2 was selected. The resulting panel size was consistent with handling requirements for ease in transport and placement. In addition, a grid layout of 2 rows by 4 columns permitted shear lugs to be distributed in the closure strips around the frame boundary with three lugs along the top and bottom boundaries of the wall and one lug at the midheight of the column.

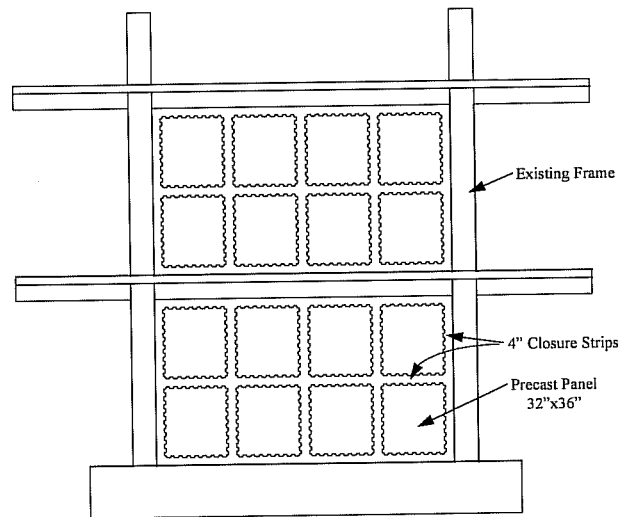


Figure 4.2: Infill Wall Panel Layout

The philosophy followed for design of the precast wall system was consistent with the seismic performance expectations stated in the SEAOC 1990 “Blue Book”^[35] upon which the current UBC^[37] provisions are based. The performance expectations are as follows:

Structures designed in conformance with these Recommendations should, in general, be able to:

1. Resist a minor level earthquake ground motion without damage;
2. Resist a moderate level of earthquake ground motion without structural damage, but possibly experience some nonstructural damage.

3. Resist a major level of earthquake ground motion having an intensity equal to the strongest either experienced or forecast for the building site, without collapse, but possibly with some structural as well as nonstructural damage.

The specific philosophy used in design was to provide for monolithic behavior of the precast infill wall system. Additionally, the infilled wall should have sufficient shear strength to permit the development of flexural yielding at the base of the wall. The shear strength of the wall should be controlled by the shear lugs provided around the interface since yielding of the lugs will provide some ductility. Since the column splices were not modified, a tension failure would be inevitable during a major seismic event. Therefore, shear resistance from the columns was neglected as was column tensile capacity in considering the collapse limit state design. The infill wall was designed using the design recommendations previously presented in Chapters 2 and 3 and in accordance with relevant sections of ACI 318-89^[3] and UBC 1991.^[37] Details of the infill wall design are presented below, and the design scheme for the rehabilitated structure is shown in Figure 4.3. Complete structural drawings and details are presented in Appendix D.

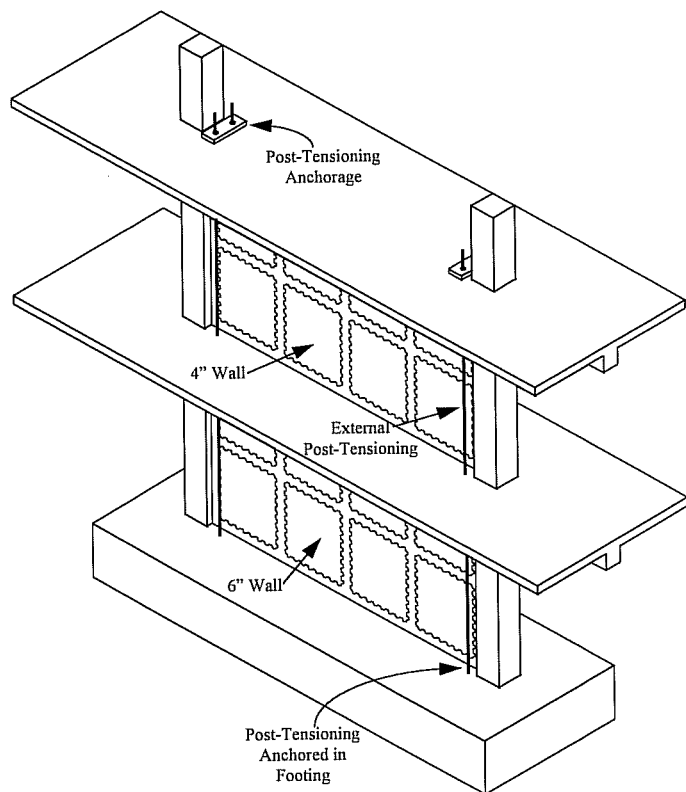


Figure 4.3: Infill Wall Specimen

4.2.2.1 Design Shear Capacity

To maximize the shear resistance available from the infill wall, the limits of the existing structure were assessed. The diaphragm strength was designed to be adequate for transferring shear to the new wall. However, in actual structures, the diaphragm capacity may control the loads that can be transmitted to the shear wall.

The design shear capacity of the new infilled wall was determined by the maximum pipe diameter that could be inserted through a beam core hole. Since the beam was supporting gravity load in the building, careful consideration of the core locations was required. In coring the beam, reinforcement is likely to be cut; therefore, the amount of reinforcement that might be cut and the necessity for shoring must be considered in a rehabilitation design. For the model test structure, the maximum hole size was determined to be 3-1/2 in. which required the cutting of a third of the positive and negative moment steel. Therefore, to permit insertion and grouting around the pipe, a 2-1/2 in. extra strong (2-1/2" XS) pipe was selected for use on the first story. The double extra strong (2-1/2" XXS) was deemed too strong since extremely large embedment lengths would be required to develop the shear strength.

4.2.2.2 Wall-to-Frame Connection

Following the selection of the pipe size to be used in the first story, the wall to frame connection was designed and detailed according to the design recommendations in Chapter 3, Section 3.8.

Forces in the shear wall were based on a triangular load distribution recommended by UBC 1991^[37] for the vertical distribution of force as shown in Figure 4.4. Since shear was constant in the

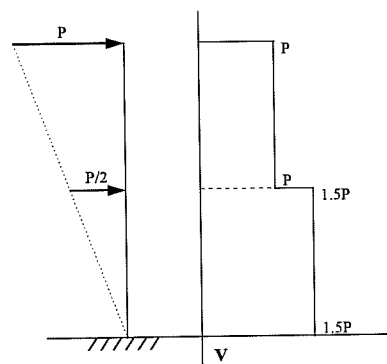


Figure 4.4: Shear Distribution

first story, the 2 -1/2 in. lugs were used along the beam/wall interface as well as at the base of the wall. The base interface shear capacity was determined from the combination of the pipe shear capacities at the interface. A maximum base shear of 145.8 kips was calculated.

Pipe Capacity:

$$V_n = 0.6 A_s F_y$$

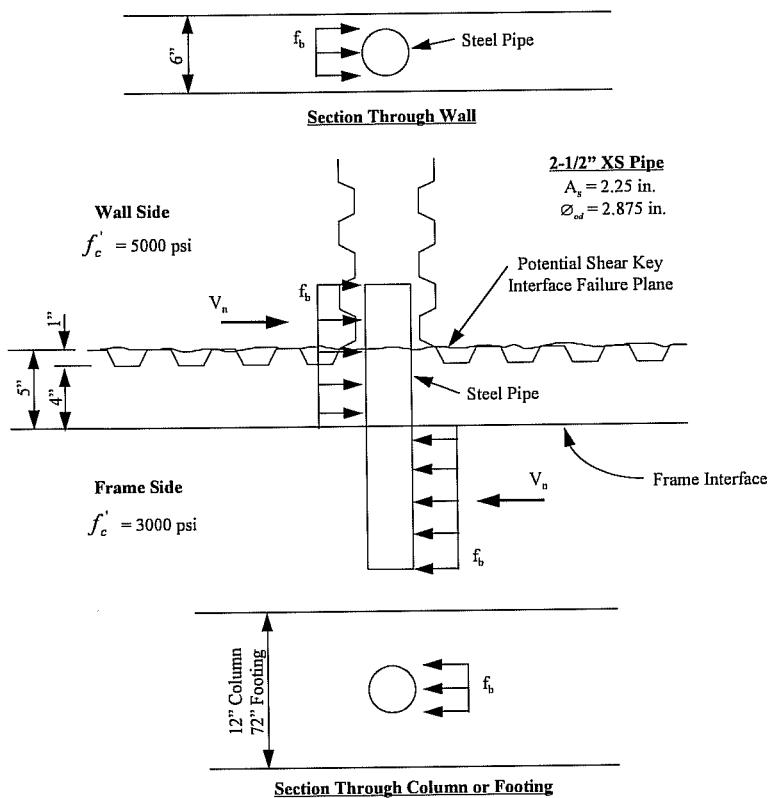
$$V_n = (0.6)(2.25)(36) = 48.6 \text{ kips}$$

$$V_{Base} = 3(48.6) = 145.8 \text{ kips}$$

Since no simple mechanical model could be established to determine the shear force required for the column frame connection, the same pipe size (2-1/2" XS) was used. Use of the same pipe throughout the story should also facilitate construction.

Embedment lengths for the pipes were determined based on the wall to frame connection design recommendations presented in Chapter 3, Section 3.8.3. The design for the first story connection is shown in Figure 4.5. The embedment lengths in the wall were measured beyond the shear key interface of the panel to eliminate the possibility of a shear key interface failure. Therefore, the wall embedment was increased by 5 in. to account for the 4 in. grout strip and the 1 in. key depth. A total wall embedment of 12 in. was used for the first story. As previously recommended, a confinement factor of one was used for embedment in the wall. For embedment in the frame, advantage was taken of the confinement provided by the width of the existing frame members.

As can be seen in Figure 4.6, connection through the beam is not as critical as the column and footing connection since the pipe continues through the beam into the wall above. The forces on the pipe from the wall above and below balance the majority of the shear; therefore, only the unbalanced shear generated at that floor



Bearing: $\alpha V_n^{Pipe} = \phi \left(0.85 f_c' \sqrt{\frac{A_2}{A_1}} \right) \phi_{OD} d$ $\alpha \geq 1.25$
 $\phi = 0.7$

Wall Side

Frame Side

$$\sqrt{\frac{A_s}{A_1}} = 1 \text{ per recommendations}$$

$$\sqrt{\frac{A_s}{A_1}} = \sqrt{\frac{12}{2.875}} = 2.04 \leq 2$$

Same for footing and column

$$(1.25)(48.6) = (0.7)(0.85(5)(1))2.875d$$

$$d = 7.1 \text{ in.}$$

$$(1.25)(48.6) = (0.7)(0.85(3)(2))2.875d$$

$$d = 5.9 \text{ in.}$$

$$d_{tot} = 7.1 \text{ in.} + 5 \text{ in.}$$

$$= 12.1 \text{ in.}$$

⇒ Use 12 in. Embedment

⇒ Use 6 in. Embedment

Figure 4.5: Frame Connection Design

must be accounted for by bearing on the pipe at the beam and should be checked. In general, due to the confinement provided by the slab and beam, bearing from the slab and beam, bearing from the unbalanced force at the beam should not control design.

The second story pipe was sized based on the shear diagram previously presented in Figure 4.4. Therefore, the pipe area required for the second story was two thirds (2/3) the first. The pipe size required was a 2 in. extra strong (2" XS).

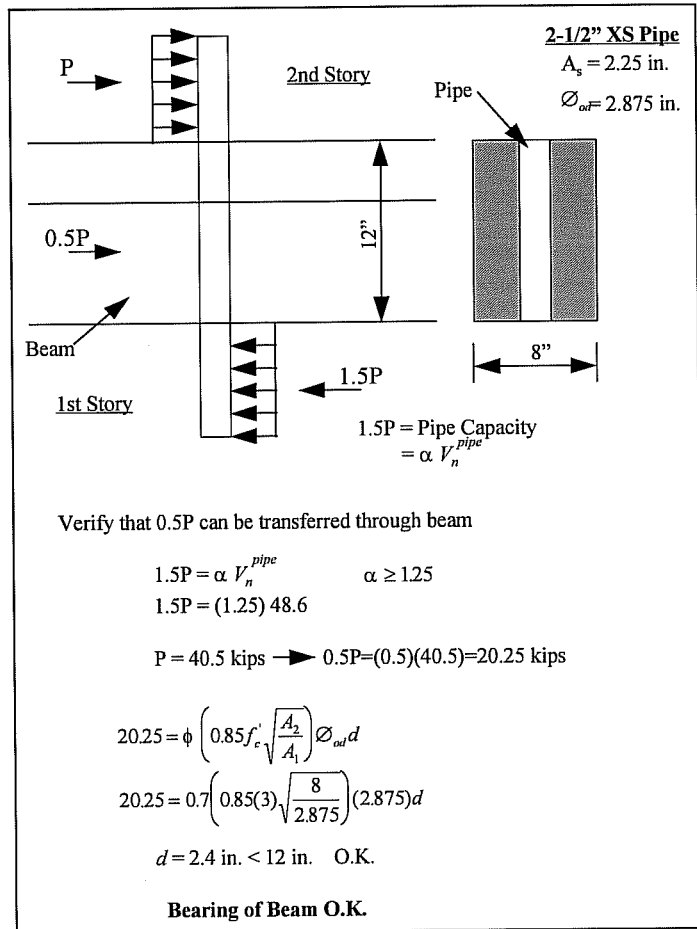


Figure 4.6: Check of Pipe Through Beam

lengths were determined in the same manner as presented for the first floor. The frame connection design is summarized below.

Story	Pipe Size (36 ksi)	Frame Embedment (in.)	Wall Embedment (in.)
First	2 1/2" XS	6	12
Second	2" XS	5	11

In practice, the pipes inserted through a beam between two stories would be continuous with the pipe size determined by the forces and dimensions of the story below. However, since the purpose of the infill wall test was to examine the design approach, different first and second story pipe sizes were utilized since these sections were optimized for the applied forces. Two different pipes were welded together to create a continuous pipe assembly for force transfer and ease of placement during construction. The welded joint was located at the midheight of the beam.

4.2.2.3 Precast Panels

As previously mentioned, it was assumed that at a collapse limit state, the existing frame columns would not be capable of transferring shear due to the splice failure. Therefore, the shear forces at the bottom of the wall were assumed to be carried by the shear lugs. In keeping with this design philosophy, the precast panels were designed to transfer shear forces to the shear lugs as shown in Figure 4.7 with three panels transferring the total shear force. The panels were designed with shear keys around the perimeter based on the recommendations previously presented. The resulting panel size and shape for use in the rehabilitation system is shown in Figure 4.8.

Panel shear strength was calculated according to ACI 318-89^[3] section 21.7.3.3, and the first story design calculations are presented in Figure 4.7. The panels were designed with an overstrength factor (1.25) applied to the pipe strength to eliminate panel failure prior to the development of yield in the pipes. The second floor panels were designed in the same manner. Panel details are summarized below.

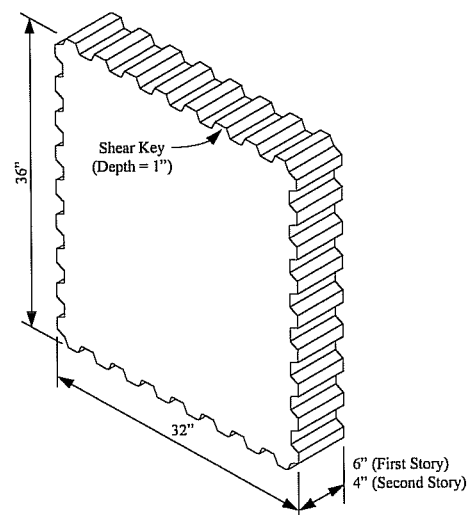


Figure 4.8: Precast Panels

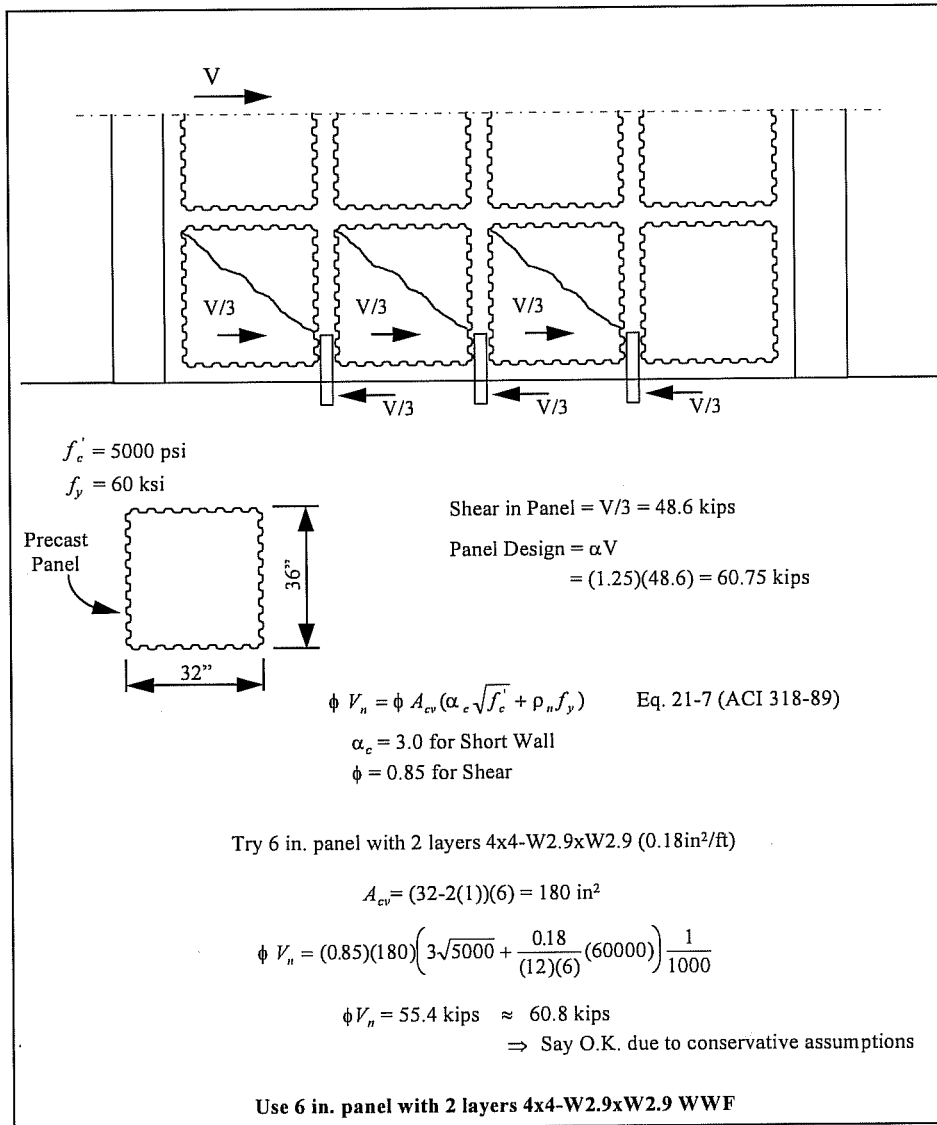


Figure 4.7: Precast Panel Design

Story	Panel Thickness	Panel Concrete Strength (psi)	Reinforcing Steel (2 Layers)
First	6	5000	4x4 - W2.9xW2.9
Second	4	5000	4x4 - W2.9xW2.9

4.2.2.4 Panel Connection - Reinforcement Across Critical Shear Key Interface

The panel connection was designed using the recommendations presented in Chapter 2, Section 2.8. The design forces were established using the same approach as for the precast panels. Since the shear force must be transferred through the grout strip from the adjacent panel, the connection was designed using the same force as required for the panel design. The design for the first story panel connection is presented in Figure 4.9. Since no simple mechanical model could be established to determine the reinforcement in horizontal panel connections, it was decided to use the same reinforcing in all panel connections in that story. Using the same reinforcement

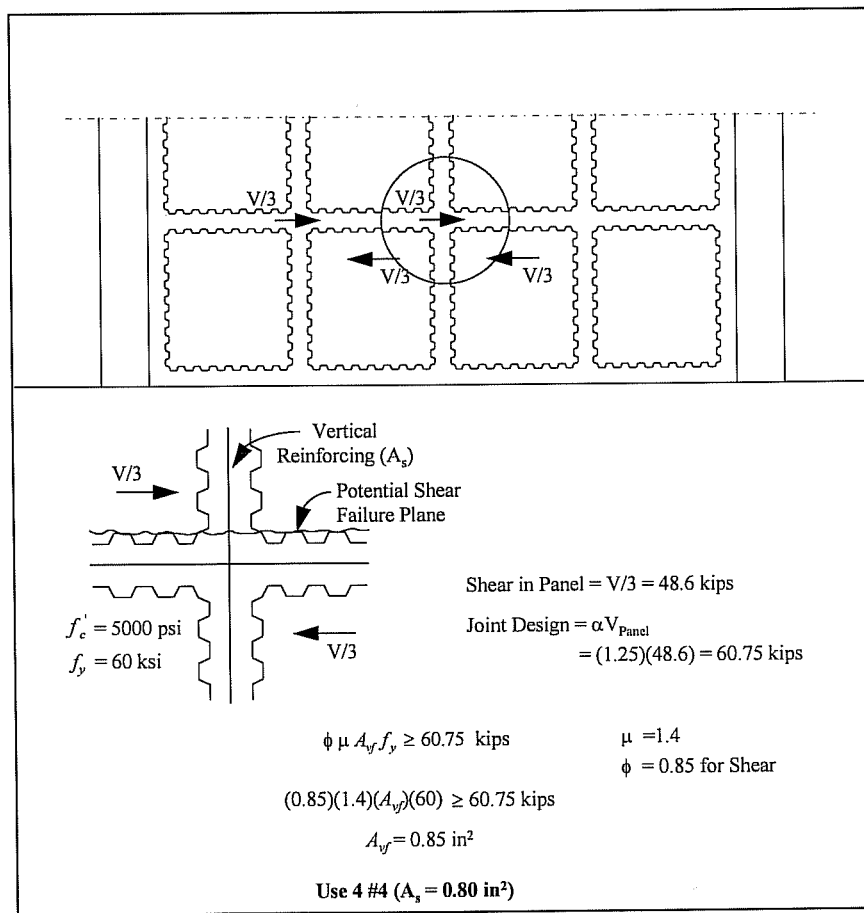


Figure 4.9: Panel Connection Design

for both vertical and horizontal strips should facilitate construction by eliminating placement errors.

The second floor panel connections were designed in the same manner as the first floor, and the panel connection design is summarized below.

Story	Closure Strip Reinforcement (in ²)
First	4 #4
Second	3 #4

Since many rehabilitated structures will require splicing of reinforcing steel to provide vertical continuity of the wall, the vertical strip steel was designed to be spliced in the test structure. The first and second story steel was spliced within the pipe that connects the two stories. Due to the change in pipe size, it was not possible to extend the first story steel up to the second story to allow splicing in the top region of the pipe for ease in construction. Therefore, the bottom steel was discontinued at the midheight of the beam. The bottom steel was designed to insert into the bottom section of the pipe. Due to the excellent confinement afforded by the pipe, extremely short development lengths were adequate. A design lap of 6 in. was used.

At the base of the structure, the strip steel was designed to extend 6 in. below the pipe to allow for development into the footing. The depth of the core hole was 12 in. to allow for pipe embedment and anchorage of reinforcing steel.

4.2.2.5 Flexural Capacity, Post Tensioning Requirements

When the infill panels are installed, it is assumed that the wall will resist overturning forces as a monolithic unit. The boundary elements, in this case the existing columns, are critical for mobilizing flexural strength. During a major level of earthquake ground motion, a column splice failure under tension in the boundary

column is expected. Since the column bars carry the tension force for overturning moments, a loss of flexural capacity would result. To overcome this problem, post-tensioning bars were designed to be located adjacent to the columns. The bars were designed to resist all tensile forces generated by the wall overturning moments at ultimate design strength (the column tensile capacity was ignored).

In addition to providing the moment capacity, the post-tensioning steel was designed to provide precompression forces to the wall to improve wall behavior during different stages of lateral loading. For a service limit state design, the post-tensioning was designed to provide for uncracked wall behavior so that the gross sectional properties of the wall could be used to reduce lateral drift. The high stiffness provided at this design level should maintain displacements at small values which may be necessary to meet building performance requirements based on continuity of operations. For a damage limit state design, the post-tensioning was designed to delay the column splice failure. The precompression force allows for an increase in the lateral loads before splice failure occurs.

Both the amount of post-tensioning steel and initial prestressing force were varied during testing to ascertain their effect on the behavior of the structure. Additionally, changing the amount of post tensioning steel allowed for evaluating both flexural and shear failure modes of the structure.

4.3 Specimen Construction

4.3.1 Existing Frame

The existing frame was constructed as a cast-in-place monolithic structure. Provision for the post-tensioning bars was made by using plate anchors in the footing and extending bars from the anchors so that they protruded from the top of the footing

to permit coupling later in the test program. The column bars were anchored with 90° hooks in the footing and extended above the footing. A construction joint for the columns was provided by roughening the surface. Footing construction is shown in Figure 4.10.

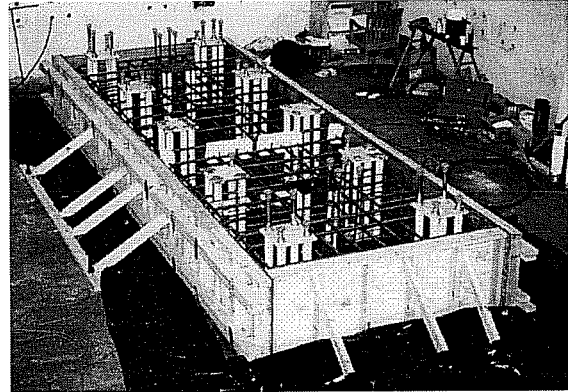


Figure 4.10: Footing Construction

The slab and beam forms were supported on the footing and laboratory floor with wood shoring as shown in Figure 4.11. The columns supporting the floor were formed and cast along with the beam and slab. Continuous monitoring of form alignment was conducted during construction to maintain tolerances within acceptable limits. The structure was cured with wet burlap for 7 days following casting to allow for strength gain which was monitored with companion cylinders. The shoring was then removed and the forms stripped. Figure 4.12 shows the completed first story of the building.

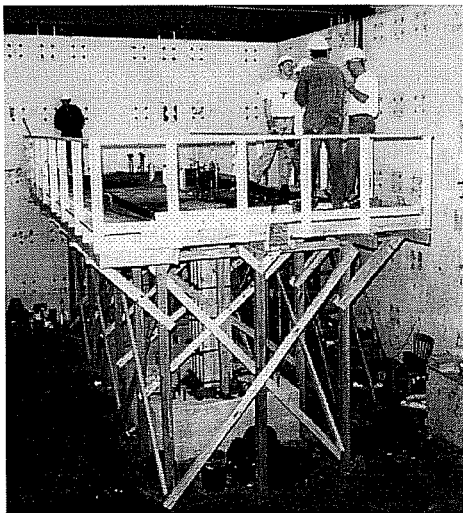


Figure 4.11: First Story Construction

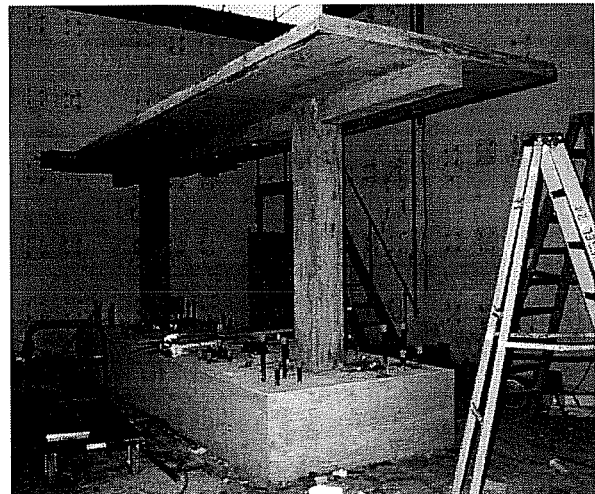


Figure 4.12: Completed First Story

The second floor was reshored on the footing and laboratory floor, and construction continued. The slab and beam forms for the third floor were supported by shoring placed on the second floor as shown in Figure 4.13. The third floor was constructed in the same manner as the second. After 7 days of curing, the formwork was stripped. In the final operation, the column stubs on the top floor were formed and cast. The completed structure is shown in Figure 4.14.

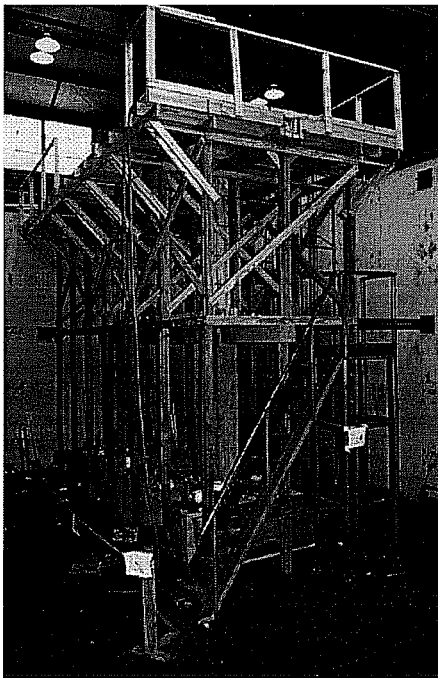


Figure 4.13: Second Story Construction

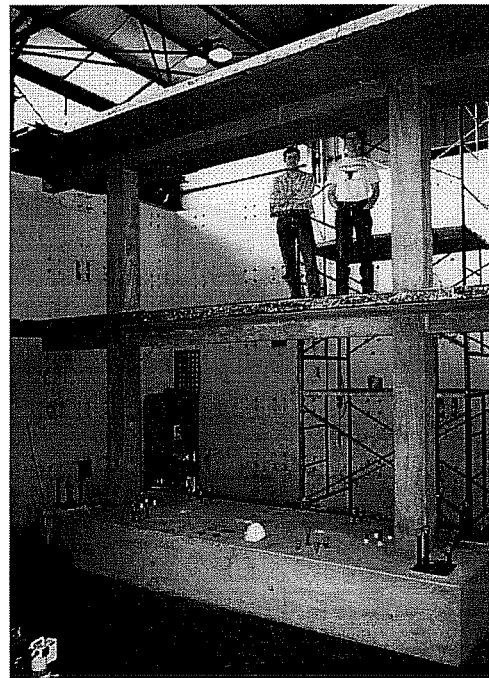


Figure 4.14: Completed Structure

4.3.2 Infill Wall Construction

4.3.2.1 Precast Panels

The precast panels were constructed in a flat precasting bed as shown in Figure 4.15. Two sets of forms were used to construct 4 in. and 6 in. panels. Lifting inserts were attached to the sides of the forms to allow for lifting and placement of the

panels as will be discussed later. In addition, a lifting insert with ferrules at either end was placed in the center of the panel to also assist in moving, placement, and bracing of the panels.

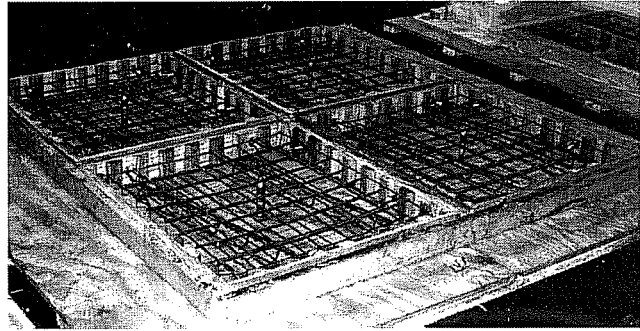


Figure 4.15: Panel Precasting Bed

The panels were cast and cured for seven days using wet burlap. Subsequently, they were removed from the casting bed and temporarily stored as shown in Figure 4.16. When removing the panels from the formwork, it was noted that several of the corner shear keys had shrinkage cracks. The shape of the formwork at the corners locked the key into the forms which restrained shrinkage as shown in Figure 4.17. Since the keys were unreinforced, the corners cracked off. A redesign of the corner key would eliminate

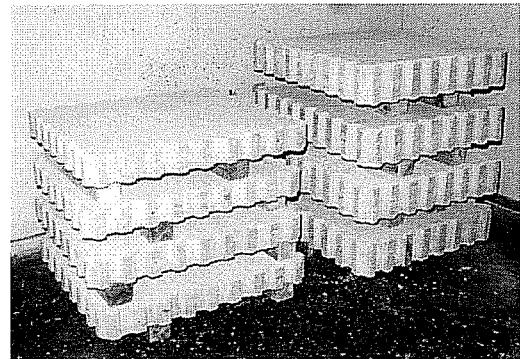


Figure 4.16: Panel Storage

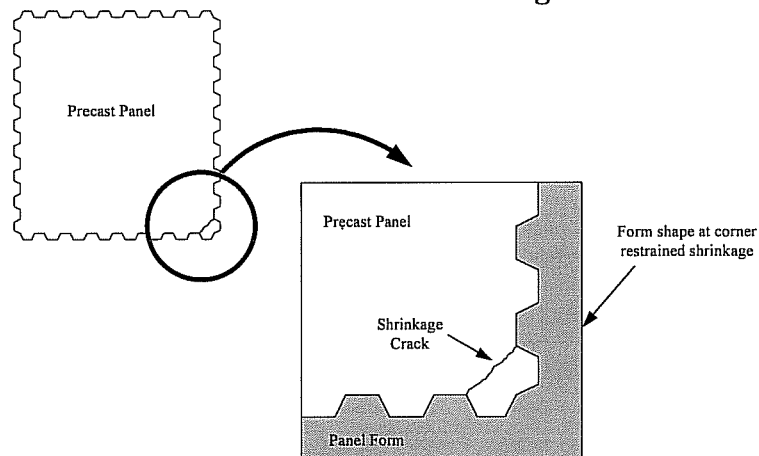


Figure 4.17: Panel Shrinkage Crack

this problem; the corner could be chamfered to enable shrinkage to occur unrestrained. Due to the grouting method used to install the panels, however, no adverse effects of the missing keys was anticipated.

4.3.2.2 Core Holes

Core holes for the shear lugs and the post-tensioning steel were provided during construction of the existing building frame using PVC pipe void forms placed in the forms prior to casting. Any steel crossing the location of the core hole was cut according to design requirements to simulate actual coring. The PVC pipes were slit along the edge, and a thin steel plate was inserted. Following construction of the building frame, the shear lug void forms were removed by removing the steel plate and collapsing the PVC pipe.

Several of the voided holes shifted slightly during concrete casting and required coring. Additionally, one of the column holes was too shallow since the hydrostatic pressure during casting pushed the void form 2 in. out of the formwork. All coring was performed with a concrete coring machine that could be mounted on horizontal and vertical surfaces. Vacuum suctioning was utilized for mounting the coring machine to the concrete.

Since the core holes were made during construction of the existing building, it was certain which reinforcing steel was cut to allow for the holes. In actual construction, however, it is imperative to locate the reinforcing steel to assure that only the specified steel is cut since a structural failure could result.

4.3.2.3 Panel Placement, Bracing, and Forming

The panels were moved into the existing frame with a light forklift. Due to restrictions created by the small size of the footing and slabs, however, the forklift could not be used to place the panels in the final position. The panels were lifted into

final position with a 2 ton crane that was mounted to the beam one story above the wall being constructed. A steel chain was placed through the core holes in the beam to support the crane. Chains were dropped through the core holes below to lift the wall panels using clevis plates attached to inserts along the edges of the panel. Figure 4.18 shows the lifting system used during construction. When construction reached the top floor, scaffolding was erected to allow mounting of the crane at a height sufficient to lift the panels into position. For this placement method, it was important that lifting inserts were located near the top edges of the panels. The inserts needed to be spaced far enough down the panel side, however, to provide clearance for the clevis plates. If the inserts were positioned too high, the lifting clevis would hit the bottom side of the beam which would prevent lifting to the proper height. Additionally, clearance between the adjacent panel was required for removal of the clevis plate following lifting. The 4 in. clearance provided by the panel spacing was sufficient for the lifting devices used in this project.

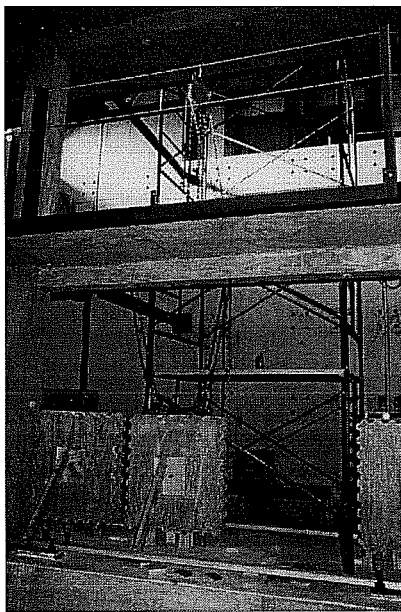


Figure 4.18(a): Lifting System

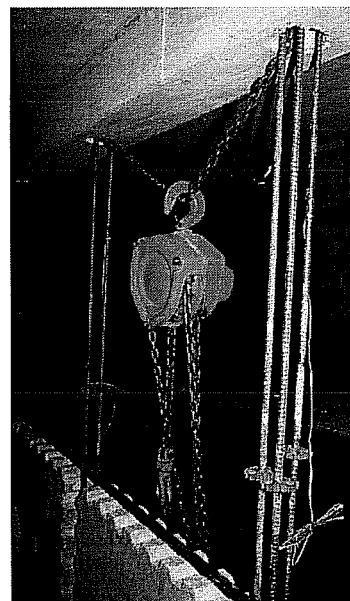


Figure 4.18(b): Close-Up of Crane

The panels were spaced from the existing structure and from one another using lag bolts to maintain the proper closure strip dimension. The bolts were inserted into the lifting inserts that were provided in the edges of the panel as shown in Figure 4.19. The inserts were also used for lifting the panels. The bolts were adequately sized to support the panel weight during construction as shown in Figure 4.20.

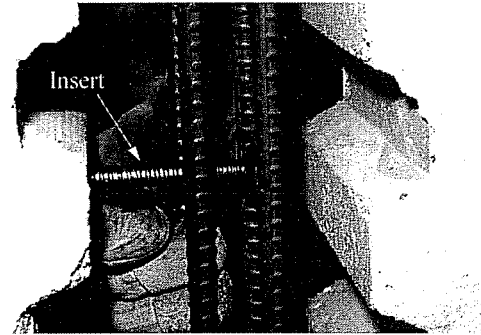


Figure 4.19: Insertion of Lifting Inserts

After placement of each panel, out-of-plane bracing was applied to secure the panel in position and prevent overturning. A panel surface insert allowed attachment of braces on both sides of the panel. The 2x4 braces were attached between the panel and a 2x4 that was anchored to the slab along the length of the wall as can be seen in Figure 4.20. Figure 4.21 shows the bottom row of panels positioned prior to grouting of the closure strips.

Following shear lug and grout strip reinforcement placement, the grout strips were formed using plywood one inch wider than the grout strip and attached by all-threaded rods and snap-ties. Complete details of the construction procedure and

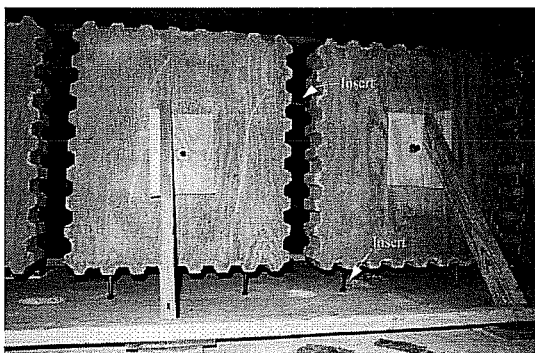


Figure 4.20: Panels Supported by Lifting Inserts

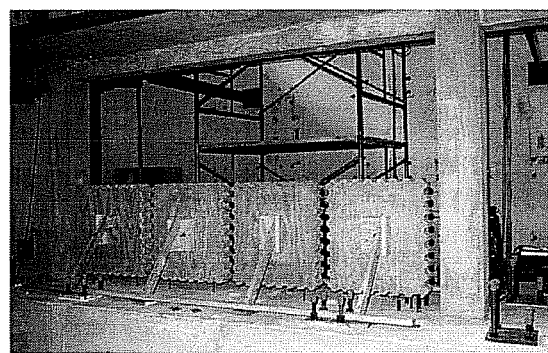


Figure 4.21: Bottom Row of Panels in Position

sequence are presented in the next section. All-threaded rods were utilized for the interior (panel-to-panel) closure strips since the formwork could clamp against the panels. Along the frame boundary closure strips, however, snap-ties were used to provide clamping support for the forms. Both attachment methods were secured with snap-tie holders. Tightening of the holders allowed for final aligning of the panels.

4.3.2.4 Wall Construction Sequence

Construction of the wall progressed in four stages and is illustrated in Figure 4.22. Details of the construction stages and sequence are presented below.

Following placement of the bottom row of panels, the base shear lugs were placed along with the grout strip reinforcement as shown in Figure 4.23. The shear lugs were grouted in the footing to ensure proper location (Figure 4.24). Following pipe grouting, the strips were formed and grouting proceeded from the top of the closure strips. Consolidation was achieved through the use of a vibrator in the vertical strips and simultaneously through vibration in access holes (described in Chapter 2 for the grout strip tests) provided in the horizontal strips. The access holes were spaced roughly at the third points of the panels with two access holes horizontally for each panel. Following grouting of the first row, the horizontal column shear lugs were grouted into position along with the horizontal strip steel as shown in Figure 4.25.

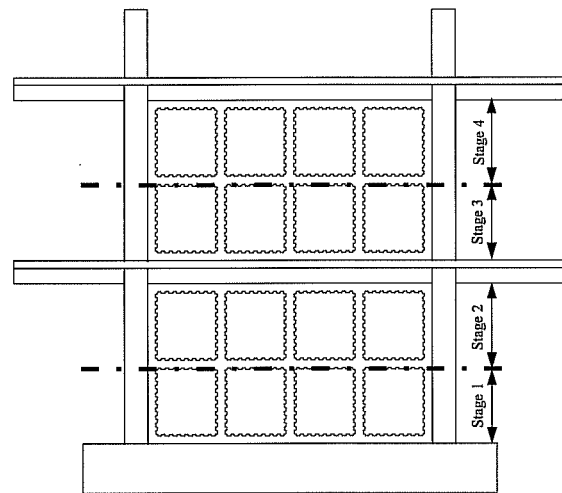


Figure 4.22: Construction Sequence of Wall

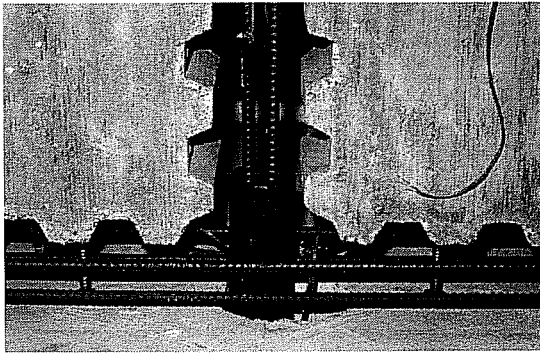


Figure 4.23: Base Shear Lugs and Reinforcement



Figure 4.24: Grouting of Shear Lugs in Footing

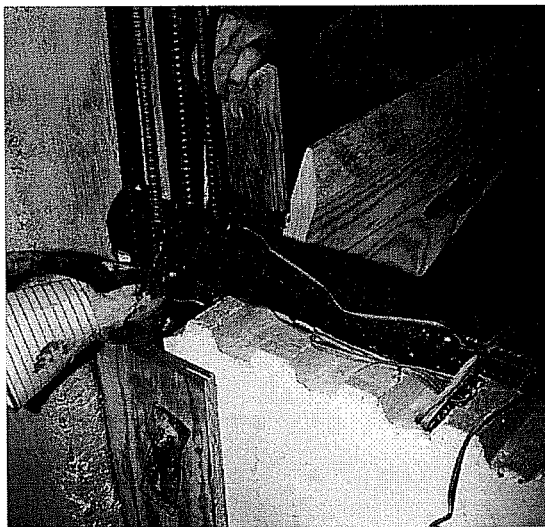


Figure 4.25: Grouting of Horizontal Shear Lugs in Column

Formwork was stripped the day after grouting, and the next level of panel construction commenced. The top row of panels for the first story was placed along with the reinforcing steel. Subsequently, all closure strips were formed (Figure 4.26). The grout was placed from the floor above through the beam core holes. The vertical strips were vibrated through the core hole while both the middle and top (below the

beam) horizontal strips were vibrated through access holes (Figure 4.27). Simultaneous horizontal and vertical vibration was essential for good grout flow. Figure 5.28 illustrates the simultaneous operations occurring on the two floor levels. The second floor pipe lugs (Figure 4.29) and the vertical strip reinforcing steel that was spliced

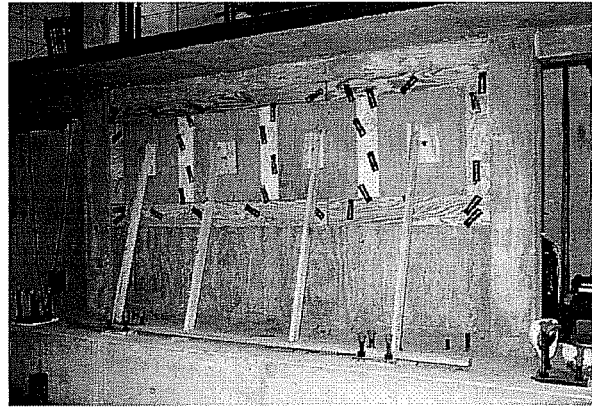


Figure 4.26: Closure Strips Formed

inside the pipe at this location (Figure 4.30) were installed after grouting of the strips in the panels below was completed. As noted previously in Chapter 3, a stop should be provided on or under the pipe lugs to ensure proper embedment lengths because vibration will cause the pipe to settle.



Figure 4.27: Vibration Through Access Holes

first. The strengthened structure after wall construction was completed is shown in Figure 4.31.

Construction proceeded for the second story in the same manner as the

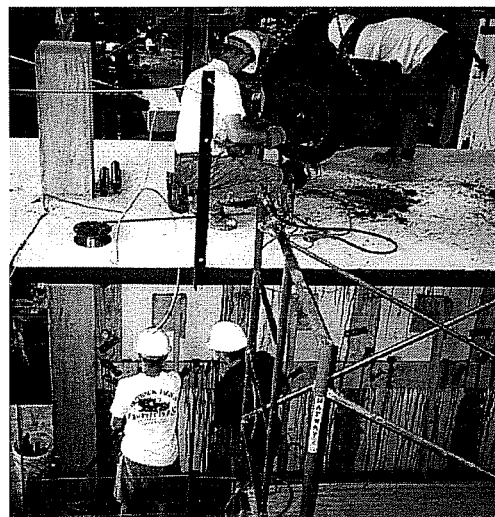


Figure 4.28: Simultaneous Operations



Figure 4.29: Installation of Shear Lug (Note Welded Joint)

Inspection of the grouting quality followed each stage of construction. Overall, the grout quality was excellent even in the strip underneath the existing beam where poor grouting is often seen. The only voids noticed along this interface were at one top beam/column corner on the first story as shown in Figure 4.32 where the corner was not completely filled. The other opposite corner, however, was in excellent condition. During grouting, it could not be determined if the corner was filled



Figure 4.30: Vertical and Horizontal Strip Reinforcement Installed

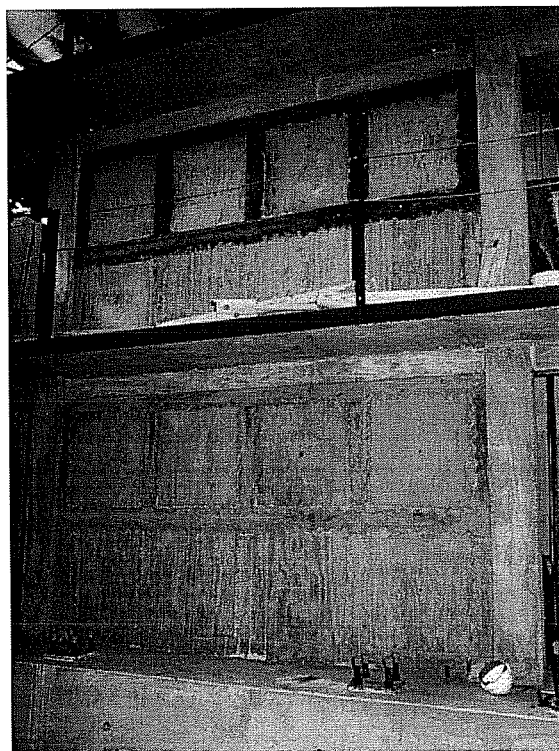


Figure 4.31: Completed Wall Construction

since formwork covered the region. To ensure proper grouting of the top beam/column corner for the second story wall, a small hole in the formwork provided at this location was used to check that the joint was filled. The observation hole worked well, and excellent grouting was achieved.

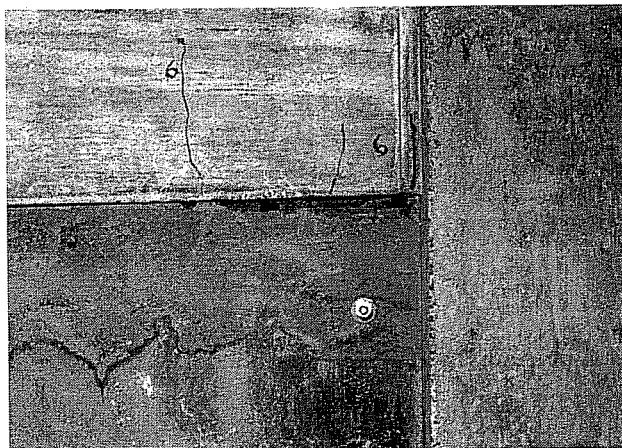


Figure 4.32: Void at Beam/Column Corner

Attention to detailing can simplify and ease construction. The vertical steel in the panel to panel connections (grout strips) was spliced inside the pipe lugs between the first and second stories to allow for continuity. Since the splice steel was discontinued at the middepth of the beam for testing reasons, the bars were inaccessible. During pipe installation, there was difficulty slipping the reinforcing bars inside the pipe since the bars could not be held together. After considerable effort, the bars were tied together inside the beam core hole to permit the pipe to be installed. In the field, the bars from the story below should be continued through the beam to allow for easy threading through the pipe.

4.3.3 Post Tensioning Steel

The post-tensioning steel was added to the structure using couplers to attach bars to those anchored in the footing. Bars were inserted from the top of the structure through holes in the slabs and installed one floor at a time. The bar lengths used were the same dimension as the floor to floor height; therefore, couplers were used approximately 1 ft. above each floor level. Alternately, the bars could have been inserted at each floor level, but the holes would have to be large enough to allow angling the bars into the holes and rotating the bar into a vertical position.

Because of the difficulty in installing long lengths of high strength bars and the large number of couplers required, prestressing strand may be a good alternative since it can easily be threaded through the floor slabs. However, providing anchorage for this system can be difficult. In addition, stressing losses cannot be controlled as easily as with threaded bars which can be properly stressed with minimal stressing losses even for short stressing lengths as would be used in frame structures 2 to 5 stories high.

The post-tensioning steel was anchored at the top of the structure with anchor plates and nuts. A bearing plate was used to distribute the anchor plate force to the structure and was sized based on concrete bearing requirements. The ultimate capacity of the bars was used to determine bearing area. The bearing plate was grouted to the concrete surface to reduce stress concentrations.

The post-tensioning steel was stressed from the top of the structure using 60 ton rams as shown in Figure 4.33. The bars were symmetric on either side of the beam; therefore, two rams were used in unison to prevent application of out-of-plane moments to the structure. The load was monitored with pressure gages and load cells. In addition, strain gages attached to the post-tensioning bars were calibrated with the load cells during stressing for use during seating and testing. After stressing, the anchorages were seated by tightening the nuts on the threaded bars. Anchorage losses were mitigated by tightening the nuts according to the calibrated strain gage readings. The completed infill wall system is shown in Figure 4.34.

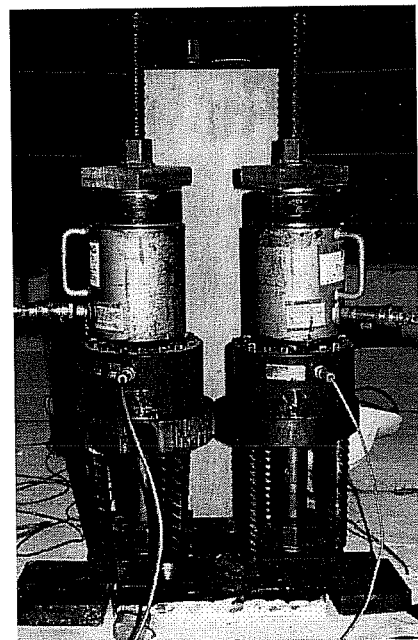


Figure 4.33: Stressing of Post-Tensioning Bars

4.4 Construction Materials

4.4.1 Existing Frame Concrete

The existing frame was constructed using a nominal 3000 psi concrete. The footing was constructed with 3/4 in. aggregate, but the rest of the structure was constructed using 3/8 in. aggregate. The 3/8 in. aggregate was selected because scaling required a reduction of clear cover and clear spacing between bars and was the aggregate size closest to that required (1/2 in.) for 2/3 scaling of 3/4 in. aggregate. A 3000 psi concrete was selected since the prototype structure constructed in the 1950's and 1960's would likely have had concrete with a relatively

low strength. The mix proportions are shown in Table 4.1. The exact proportions of the ready-mix delivered varied slightly and were adjusted for moisture conditions of the aggregate. The slump was adjusted at the laboratory to maintain a 6 in. slump. Strength gain curves for the second and third floors are presented in Figure 4.35. The strength was not monitored for the footing except at the time of testing the infill wall. The average footing strength was approximately 4600 psi at an age of 289 days.

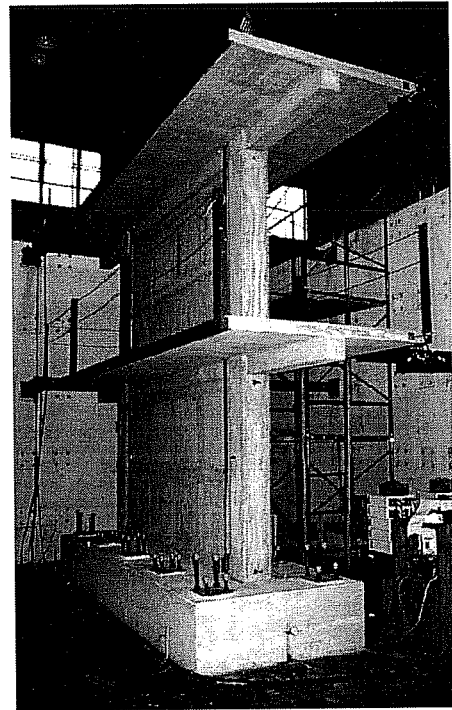
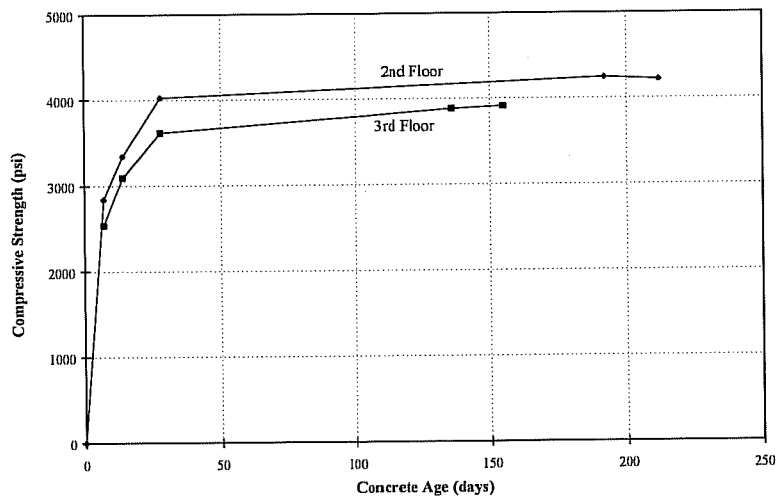


Figure 4.34: Completed Infill Wall System

Table 4.1: Existing Frame Concrete Mix

Material	Footing 3/4" Aggregate	Existing Frame 3/8" Aggregate
Cement	360	400
Coarse Aggregate (SSD)	1884	1625
Fine Aggregate (SSD)	1435	1619
Water	266	275
Admixture ¹	10.5	12

¹ For high temperature months (May-September), an admixture meeting ASTM C494 requirements for Type B retarding and for Type D water-reducing and retarding was used. During cooler months (November to April), an admixture meeting ASTM C494 for Type A water reducing admixtures was used. The quantities of admixture used, however, remained constant throughout the year.

**Figure 4.35: Existing Frame Concrete Strength Gain**

Split cylinder tests were conducted at the time of the infill wall tests to determine the average tensile strength of the second and third floor concrete. These tests were conducted at the time of the infill wall tests. The strengths are presented below along with the age of the concrete.

Floor	Age (days)	Tensile Strength (psi)
Second	214	498
Third	158	478

4.4.2 Precast Panels

In the precast panels, a nominal 4000 psi concrete with 3/8 in. gravel was used. The mix proportions are shown in Table 4.2. The exact proportions varied slightly and were adjusted for moisture conditions of the aggregates. The slump was adjusted at the laboratory to maintain a 6 in. slump for all mixes. The precast panels were designated by the description label IP (**I**nfill **P**anel) followed by the mix number. IP-1 was used for constructing the second row of panels on both floors while IP-2 was used for constructing the first row of panels. The strength gain curves are presented in Figure 4.36.

Table 4.2: Precast Panel Concrete Mix

Material	Quantity
Cement	470 pcy
3/8" Coarse Aggregate (SSD)	1625 pcy
Fine Aggregate (SSD)	1655 pcy
Water	250 pcy
Admixture ¹	20 ozcy

¹ For high temperature months (May-September), an admixture meeting ASTM C494 requirements for Type B retarding and for Type D water-reducing and retarding was used. During cooler months (November to April), an admixture meeting ASTM C494 for Type A water reducing admixtures was used. The quantities of admixture used, however, remained constant throughout the year.

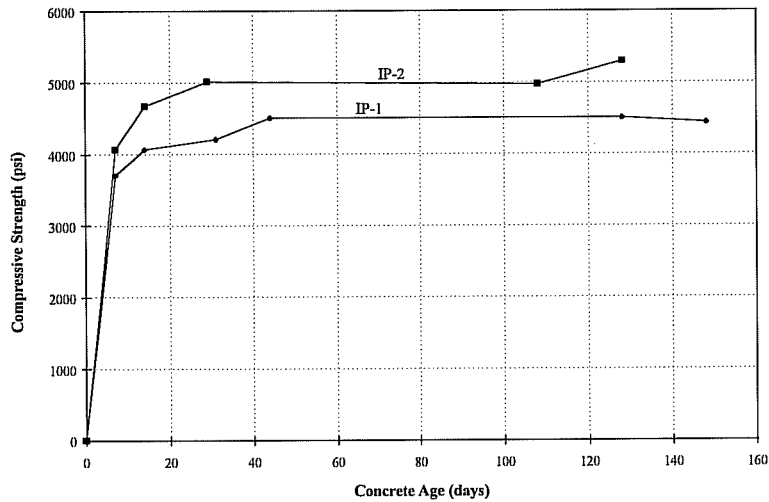


Figure 4.36: Infill Panel Concrete Strength Gain

4.4.3 Panel Grout

The panel grout was constructed using a nominal 6000 psi concrete with 3/8 in. aggregate. The mix proportions are shown in Table 4.3. The exact proportions varied slightly and were adjusted for moisture conditions of the aggregates. The slump was adjusted at the laboratory to maintain a 6 in. slump for all mixes. The panel grouts were designated by the description label IG (**I**nfill **G**ROUT) followed by the casting sequence number discussed under the wall construction. The strength gain curves are presented in Figure 4.37.

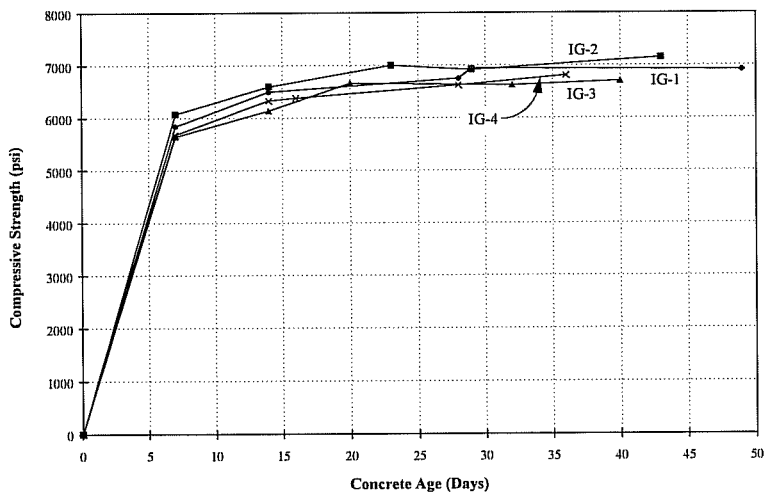


Figure 4.37: Infill Grout Strength Gain

Table 4.3: Infill Grout Mix

Material	Quantity
Cement	693 pcy
3/8" Coarse Aggregate (SSD)	1167 pcy
Fine Aggregate (SSD)	1755 pcy
Water	325 pcy
Admixture ¹	27.6 ozcy
Superplasticizer ²	25 ozcy

¹ For high temperature months (May-September), an admixture meeting ASTM C494 requirements for Type B retarding and for Type D water-reducing and retarding was used. During cooler months (November to April), an admixture meeting ASTM C494 for Type A water reducing admixtures was used. The quantities of admixture used, however, remained constant throughout the year.

² Exact addition amounts may have varied slightly to adjust the slump to 8-10 in..

4.4.4 Reinforcing and Interface Steel

Grade 60 reinforcing steel was used along with Grade 60 welded wire fabric. Tensile tests were performed on representative coupons of the bars to obtain both the yield and ultimate tensile strength. Testing was performed according to ASTM A370-94, and the results are presented below. The welded wire fabric had a tensile strength of 72.2 ksi; yielding of the steel did not occur. Fracture occurred at the welded connection of the crossing wires.

Reinforcing Steel	Yield (ksi)	Tensile (ksi)
<i>Existing Frame</i>		
#5 Bars	61.3	99.9
#6 Bars	61.1	98.7
<i>Infill Wall-Connection Strips</i>		
#4 Bars	63.0	102.8

Steel pipes used for interface shear transfer were ASTM A-53 Grade B with a minimum specified yield of 35 ksi and are the same as previously used in Chapter 3.

Coupon tests were conducted according to ASTM A370-94 to determine the yield and ultimate tensile strengths. The results are presented below. As can be noted, the yield strengths are significantly above the minimum specified yield of 35 ksi.

Pipe Size	Yield (ksi)	Tensile (ksi)
2" XS	40.4	55.7
2-1/2" XS	53.6	71.6

4.4.5 Post-Tensioning Steel

Grade 150, DYWIDAG Threadbars conforming to ASTM A722, Type II were used for post-tensioning bars. The bars were tested according to ASTM A370-94 to determine the yield and ultimate tensile strengths. The results are presented below, and a stress-strain curve is shown in Figure 4.38. As can be seen, the bars exhibited a true yielding plateau. The curve is shown up to the range of the extensometer used.

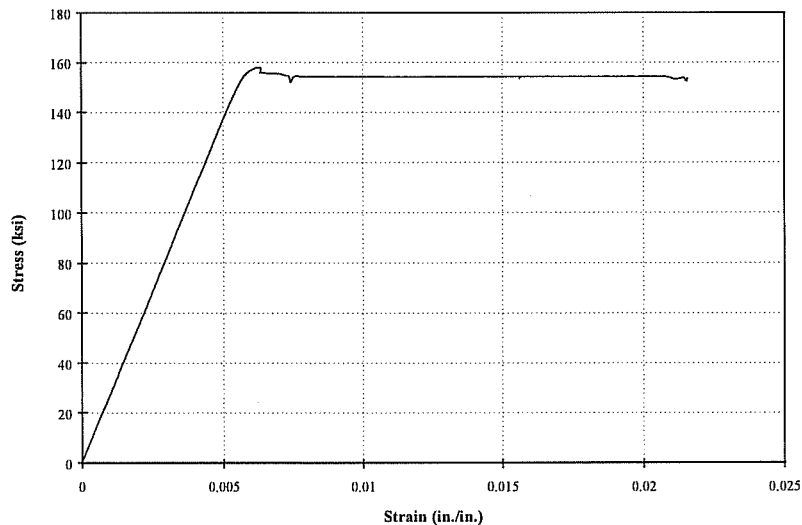


Figure 4.38: 1 in. Dywidag Stress-Strain Curve

Nominal Bar Size (in.)	A_s (in ²)	Yield (ksi)	Tensile (ksi)
1	0.85	152.9	170.6
1-1/4	1.25	146.0	160.4

4.5 Testing Setup

The testing setup consisted of a loading system used to subject the model test specimen to cyclic loading in the plane of the wall simulating earthquake effects as shown in Figure 4.39. The structure was loaded with four tension/compression hydraulic rams. Two 150 kip rams were used at the third floor level while two 100 kip rams were used at the second level. The rams were attached to the laboratory strong wall at buttress locations. Each buttress can resist 300 kips lateral load. The rams were attached to the test structure through a loading system that was cast into the edges of the floor slab. Steel angles with shear studs attached along the length were cast into the slab. A loading head was attached to the angle to permit attachment of the rams. With this system, load could be applied in both tension and compression. The loading system for both floors is shown in Figure 4.40.

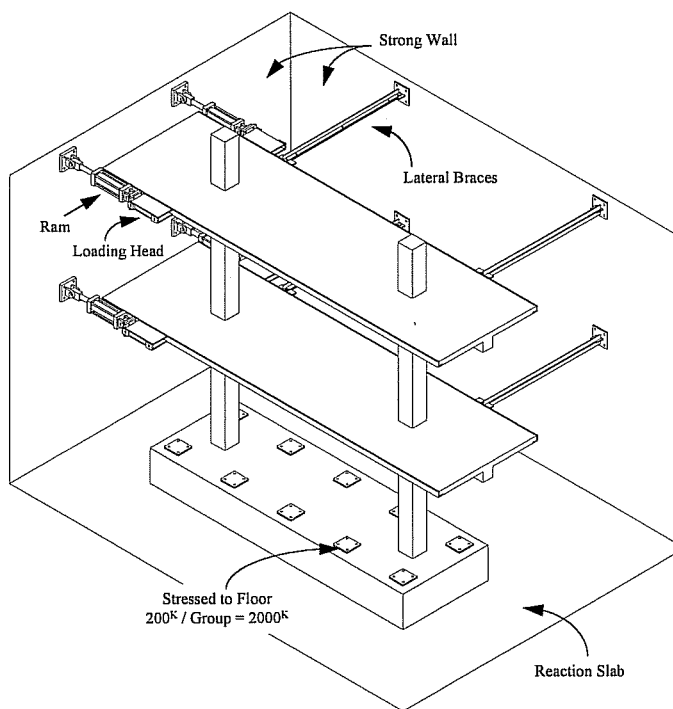


Figure 4.39: Testing Setup

The structure was laterally supported for out-of-plane forces by a double angle system. The system allowed for in-plane motion of the structure since the braces were attached with pinned ends to allow translation. The angles were attached to the slab with a plate welded to the angle at the slab edge. The angles were attached to the wall using a similar detail. The loading and bracing system is shown as constructed in Figure 4.41. The structural drawings for the loading and bracing systems are presented in Appendix E.

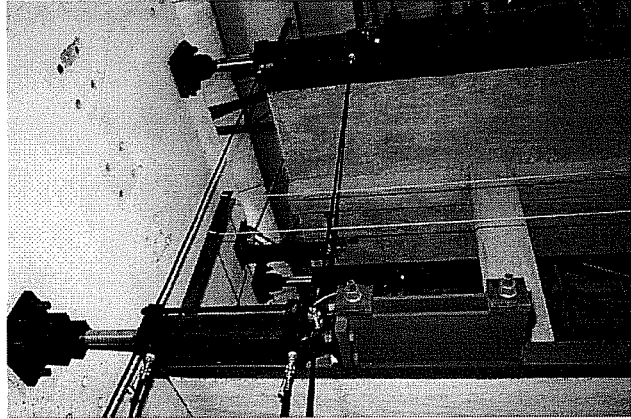


Figure 4.40: Loading System

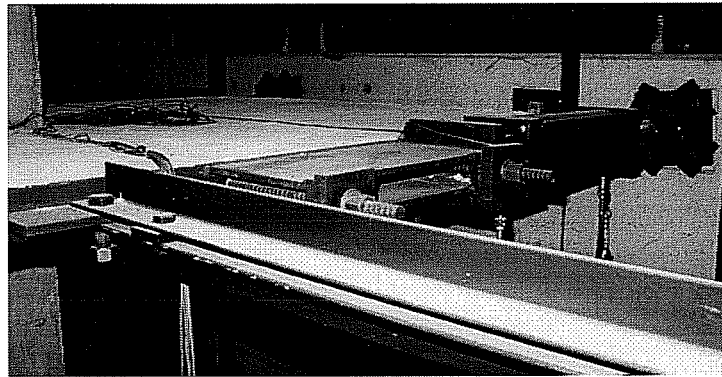


Figure 4.41: Bracing and Loading System

The second and third floor loads were controlled independently through the use of hydraulic hand pumps. The rams on one floor were connected to a single pressure manifold to permit equal loading on either side of the slab. Loads were monitored with shear pin load cells mounted to each ram. Additionally, pressures were monitored with pressure gages and transducers.

Structural displacements were monitored with displacement transducers and gages while steel strains on the reinforcing steel and steel pipes were monitored with strain gages located throughout the structure. The layout of the displacement instrumentation is shown in Figure 4.42 while Figure 4.43 shows strain gage locations. Due to the large number of gages monitored, two data acquisition systems were required. The first system monitored strain gages in the existing frame while the second system monitored gages in the infill wall.

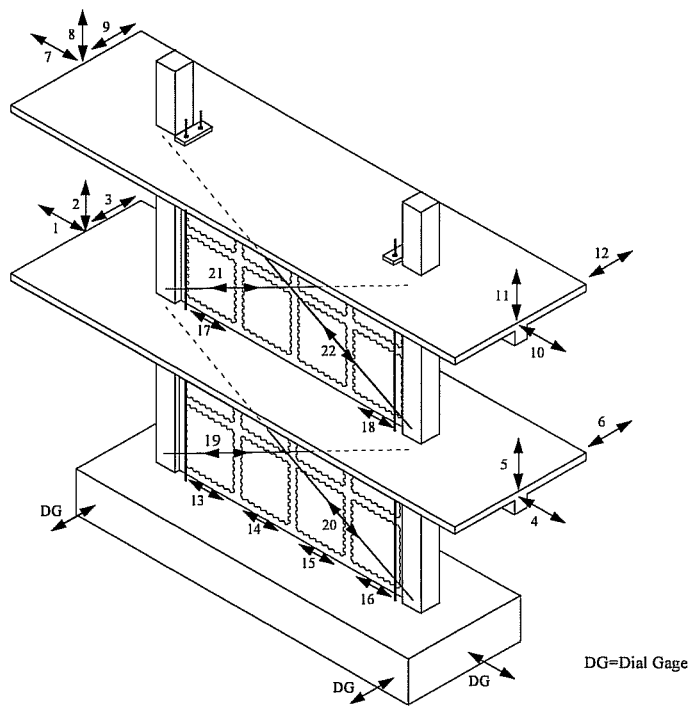


Figure 4.42: Displacement Gage Layout

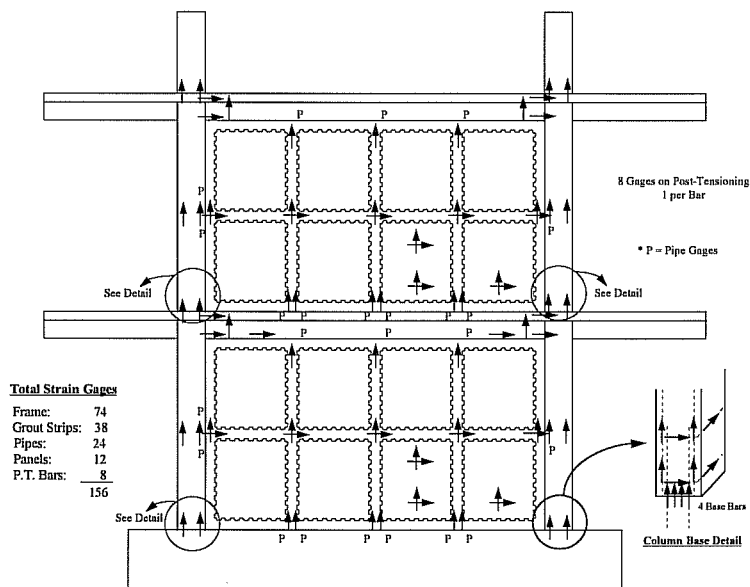


Figure 4.43: Strain Gage Layout

CHAPTER 5

EXISTING FRAME: TEST RESULTS

5.1 Introduction

Existing structures are typically found in a cracked condition due to forces the building frames have experienced in service. Therefore, the model structure was laterally loaded with a triangular load distribution applied at the two floor levels as shown in Figure 5.1 to produce cracking in the frame elements simulating the likely condition of a structure prior to rehabilitation. The existing frame was also tested to determine its overall behavior and to provide comparison of experimental results with those obtained analytically.

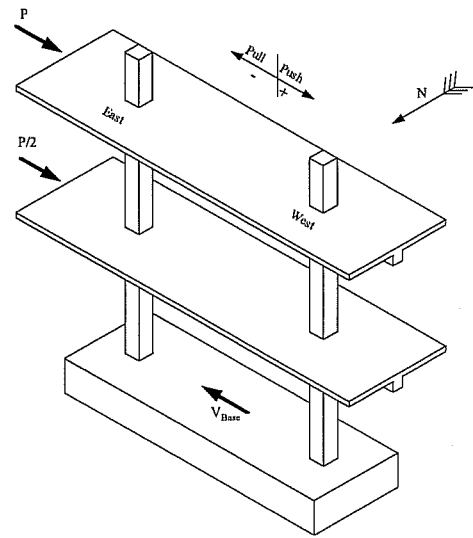


Figure 5.1: Loading Pattern

5.2 Frame Analysis

Elastic analyses were performed to predict behavior during testing and to identify loads that the structure could safely carry. The section properties used in the analyses are tabulated in Table 5.1; both uncracked and cracked moduli of elasticity were used as appropriate. Beam properties were computed using an effective flange width of 40 in. based on ACI 318-89^[3] recommendations, and cracking moments were based on a tensile stress of $7.5\sqrt{f'_c}$ (psi). All computations were based on the actual concrete strength of the building frame (4000 psi), and the concrete modulus of

elasticity was computed as $57,000 \sqrt{f'_c}$ (psi) also based on ACI^[3] recommendations. Shear deformations were neglected.

Review of the nonductile detailing provided in the structure suggested several “weak links” that could cause premature failure of the building frame. Bottom beam reinforcement could pull out of the column since an anchorage of only 4 inches was provided. In addition, the column splices at the base of the column could fail due to the short lap length provided. Finally, an unreinforced column shear failure could result since a wide tie spacing was provided. A specific discussion of these problems is presented later.

Table 5.1: Frame Section Properties

Element	I_{Gross} (in⁴)	I_{Cracked} (in⁴)	M_{Cr} (ft*k)	M_y (ft*k)
Column	1728	485	11.4	40.6
Beam (+M)	2200	610	10.5	44.7
Beam (-M)	2200	583	23.4	58.8

An analysis of failure modes of the test specimen for the triangular loading distribution selected predicted a base shear capacity of 11.4 kips. A pull out failure of the bottom reinforcing steel in the second floor beam is expected at a base shear of 10.8 kips. The subsequent moment redistribution causes an increase in moments at the base of the columns and in the forces on the bottom column splices. A slight increase in the lateral load (0.6 kips) causes failure in the download column splice which is immediately followed by failure of the other column. The sequence of events is shown in Figure 5.2. The maximum displacement at failure was calculated to be 0.89 in. using cracked section properties. The collapse sequence is nonductile; failure occurs with little or no warning.

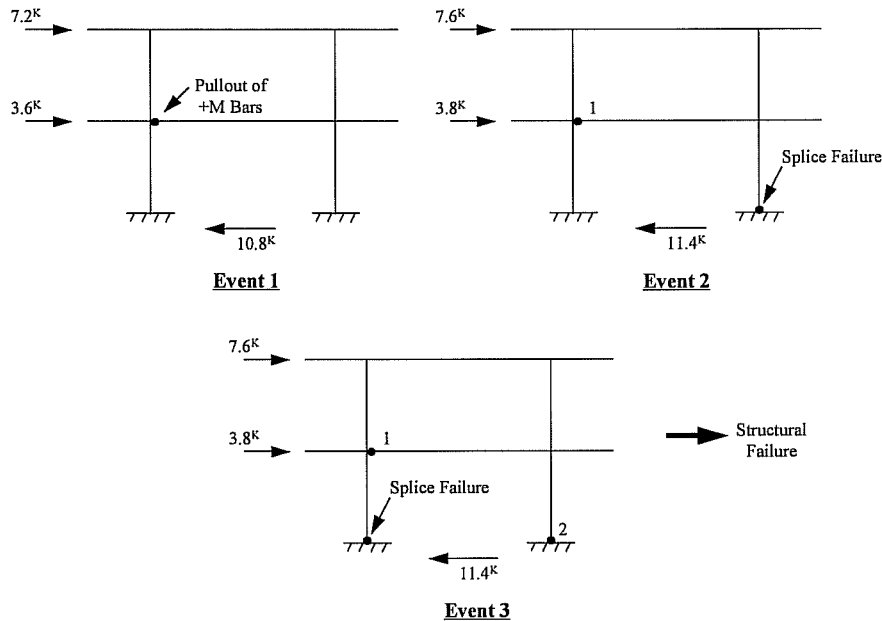


Figure 5.2: Failure Sequence

The limit capacity for the structure assuming ductile detailing was calculated as a base shear of 21.6 kips. This capacity was calculated assuming a complete mechanism could be achieved with full plastic hinging in the beams and at the column base. Because of the nonductile detailing in the existing frame, the lateral capacity of the structure is significantly reduced (only 53 percent of lateral strength achieved) as is the displacement capacity since hinge formation cannot occur. In general, the behavior of the existing frame is brittle; upon reaching a certain displacement, a loss of structural load capacity occurs.

Based on calculations of the structure's capacity, the maximum base shear applied during testing was limited to 10 kips. During testing, reinforcing steel stresses at critical sections were monitored to ensure that a brittle failure and excessive damage of the structure would not occur as predicted in the analysis.

5.3 Test Results

The existing frame was tested using a triangular load distribution as shown in Figure 5.1 (3rd floor load was twice the 2nd floor load) to simulate first vibration mode effects for the structure. This loading pattern was also consistent with current building code recommendations for analysis and design. The loading history is presented in Figure 5.3 while the load-displacement response is presented in Figure 5.4 while the load-displacement response is presented in Figure 5.4.

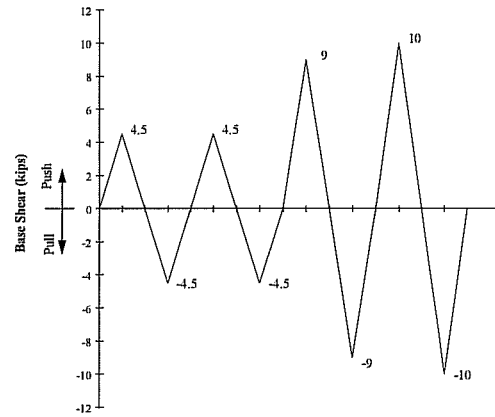


Figure 5.3: Frame Loading Pattern

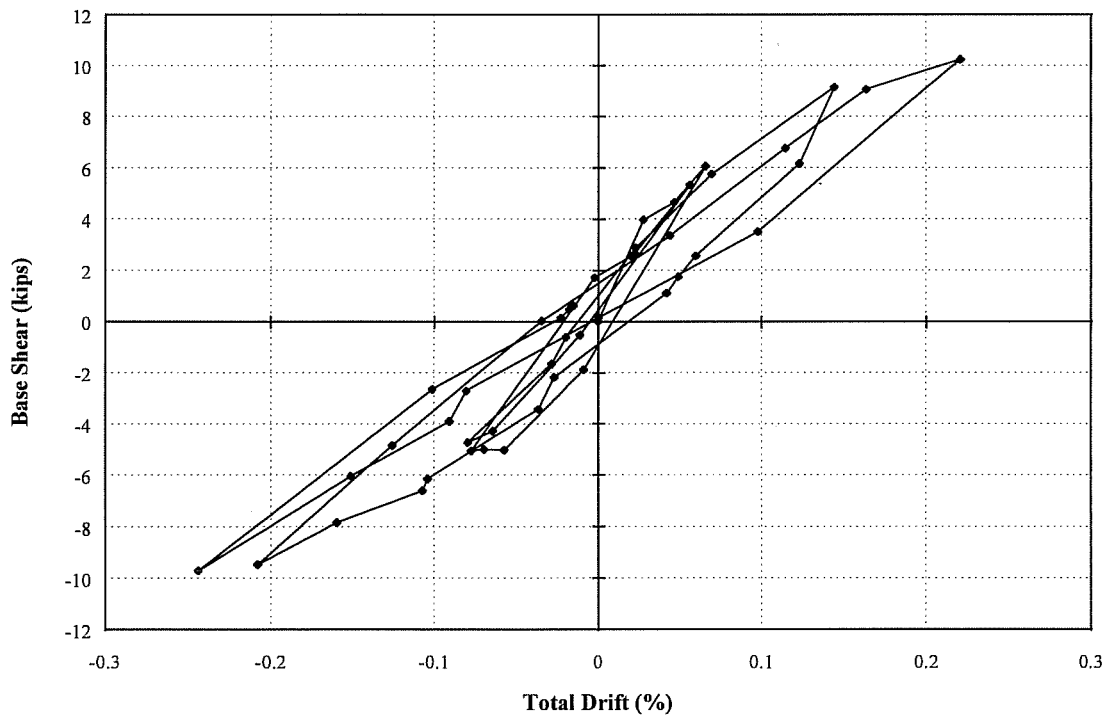


Figure 5.4: Existing Frame Test Result

The initial stiffness was substantially reduced at first cracking. As cycling and loading increased, however, the stiffness continued to decrease. The effect of cracking can be observed from the slopes and the hysteresis exhibited in the load versus displacement curve.

5.4 Cracking

Flexural cracking occurred in the columns at the base on both the first and second floors and at the face of the beam-column joints as shown in Figure 5.5. The cracking was isolated to these locations. From the cracking pattern, it can be seen that the column remained uncracked over its entire length. No shear or flexural shear cracking was observed.

Flexural cracking also occurred in the beams. The second floor beam experienced both positive and negative moment cracking. The cracking occurred at the beam-column joint and began spreading into the beam span. Since the core holes for rehabilitation were present in the structure at the time

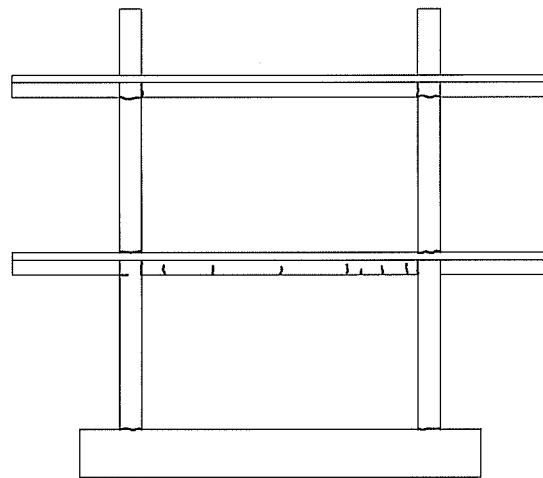


Figure 5.5: Column and Beam +M Cracking

of testing, positive moment cracking also occurred at these locations. Negative moment cracking occurred in the floor slabs; cracking extended across the entire width of the slab. As shown in Figure 5.6, slab cracks were limited to locations where peak negative moments were reached. The third floor beam experienced cracking only at the faces of beam-column joints in both the positive and negative moment regions.

All cracking was flexural in nature and extremely predicable from the analysis in terms of crack locations and cracking loads.

5.5 Stiffness

During initial loading, the structure behaved as an uncracked monolithic structure. The initial deflections match reasonably well with the analytical predictions based on gross sectional properties (I_g) as shown in Figure 5.7. As loading continued, the stiffness decreased due to the cracking that occurred at

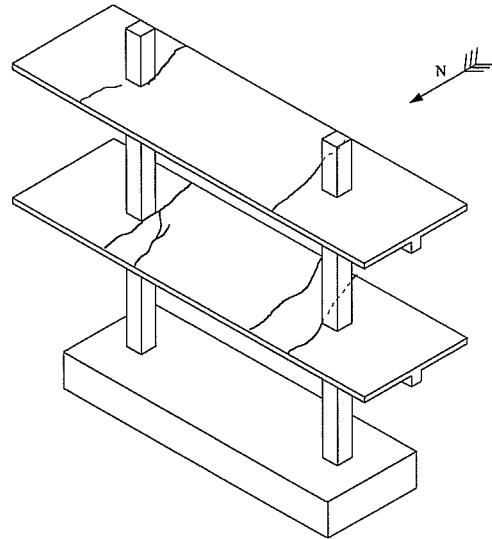


Figure 5.6: Beam -M Cracking

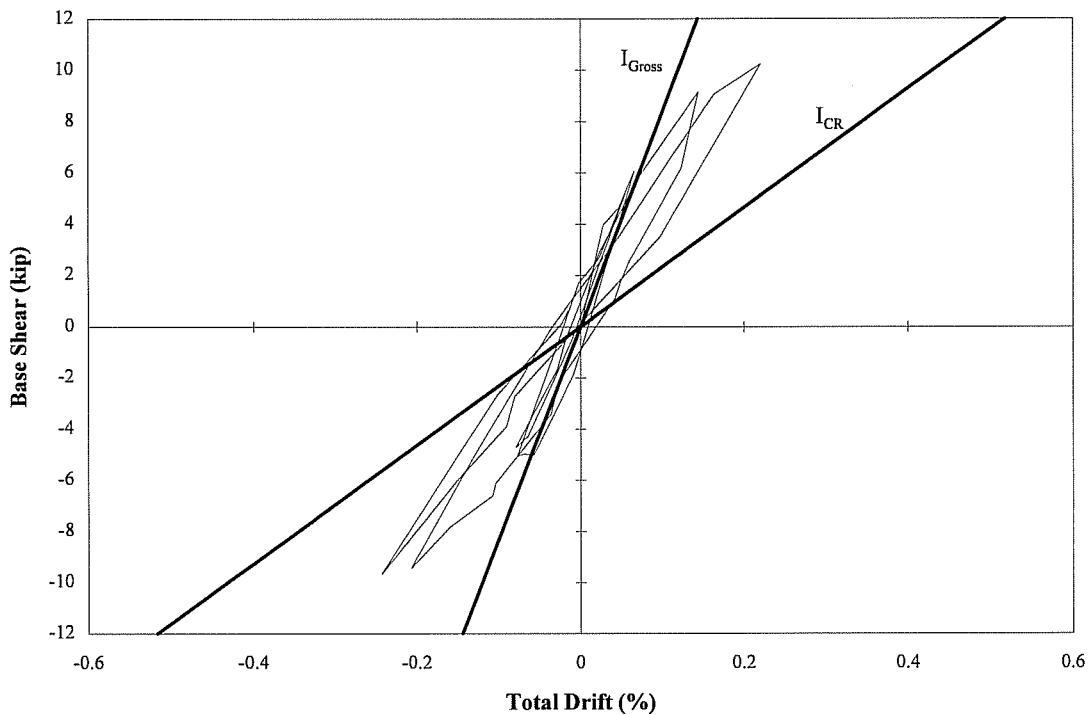


Figure 5.7: Analytical Model

the ends of the beams and the ends of the columns. As further cracking occurred with increased loading, the stiffness was further reduced. In comparing the stiffness with analytical results, it can be seen that the structure responded at a stiffness between gross and cracked stiffness values. Since the cracking was localized at the joints, the stiffness along the length of the members remained largely uncracked. Using cracked section properties (I_{cr}) over the length of the entire member overestimated the lateral deflection for the amount of cracking experienced in the model structure.

5.6 Nonductile Elements

From analysis of the structure, it was identified that nonductile elements present in the frame could cause premature failure of the frame. These “weak links” were monitored during testing to prevent localized failure and possible collapse of the structure.

5.6.1 Beam Bottom Steel

Pullout failure of the beam bottom reinforcement was analyzed using the Orangun^[29] bond stress equation given below.

$$u_{cal} = \left[1.22 + 3.23 \frac{C}{d_b} + 53 \frac{d_b}{l_s} \right] \sqrt{f'_c}$$

Using this equation, pullout failure was estimated at a reinforcing tensile stress of 28 ksi occurring at a base shear of 10.8 kips. During testing, the stress was monitored to prevent pullout of the reinforcement. Since the strain gage was zeroed with the frame under gravity loads, the stresses resulting from the lateral load could be directly read assuming elastic behavior which was reasonable for the applied load levels. Strain gage data indicated that the reinforcement reached a tensile range of 21 ksi at a base shear of 10.2 kips. The lateral load analysis at the same base shear indicated a steel stress of 35 ksi. The overestimation may have occurred because cracked section properties were used to determine the stress. The cracking was fairly

limited around the joint with only two cracks in the bottom of the beam. The first crack was located at the beam-column joint while the next was located 11 inches away. The section behaved between a cracked (I_{cr}) and uncracked section (I_g); therefore, an estimate of section properties between these two limits would produce results closer to the measured values. The cracked section analysis, however, resulted in a conservative estimate of the steel stress.

5.6.2 Column Splice

Analysis of the column splice failure was also conducted using the Orangun^[29] bond stress equation given below. An additional term was added to the equation previously presented to account for the effect of transverse reinforcement in the splice region.

$$u_{cal} = \left[1.22 + 3.23 \frac{C}{d_b} + 53 \frac{d_b}{l_s} + \frac{A_{tr} f_{yt}}{500 s d_b} \right] \sqrt{f'_c}$$

Using this equation, splice failure was estimated at 57 ksi occurring at a base shear of 14.9 kips. During testing, strain gage data indicated that at the maximum load of 10.2 kips, the reinforcement reached 30 ksi on the upload side and 40 ksi on the download side. A cracked section analysis resulted in a stress of 39 ksi for the 10.2 kip applied loading which corresponds well with the stresses measured in the column splices.

5.6.3 Column Shear Failure

Column shear failure was estimated using the ACI design strength for the contribution of concrete to shear strength.^[3]

$$V_c = 2\sqrt{f'_c} b_w d$$

The shear strength was calculated to be 15.6 kips per column for a base shear of 31.2 kips which is greater than the maximum load possible on the structure.

Therefore, a column shear failure for this structure would not control the specimen strength. During testing, no indications of column shear distress were evident.

5.7 Conclusion

Overall, the frame behaved as expected. The lateral force resistance of the frame was low. At the maximum load applied to the specimen, the stress in the positive moment steel was approximately 21 ksi which confirmed that pullout failure would occur at a low base shear. Pullout failure of bottom beam bars would occur suddenly and would be nonductile. Subsequently, forces would be redistributed to the columns leading to failure of the splices. The structure in this condition could not be expected to resist an earthquake producing significant ground motions. Structural rehabilitation, therefore, would be recommended to seismically upgrade the structure.

CHAPTER 6

PRECAST INFILL WALL SYSTEM: TEST RESULTS

6.1 Introduction

The infill wall system was tested to establish the behavior of the rehabilitation technique. The specimen was tested cyclically using a triangular load distribution applied at the two floor levels, shown in Figure 6.1, to simulate first vibration mode effects for the structure. Flexural and shear strength were investigated in order to examine the precast panel connection design recommendations previously presented, the infill wall design procedure, and the post-tensioning system.

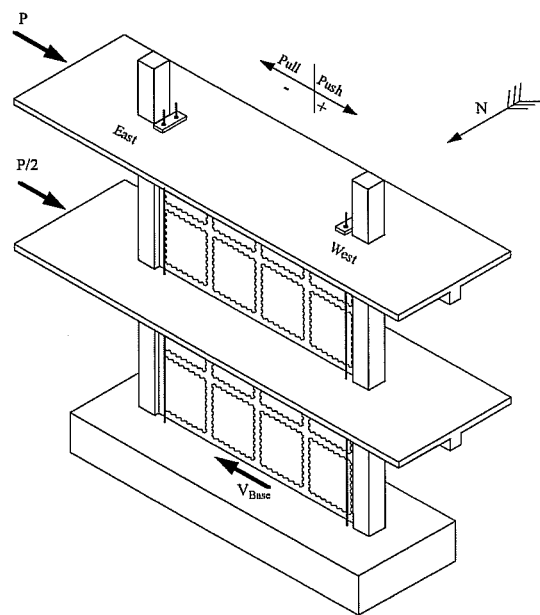


Figure 6.1: Loading Distribution

6.2 Test Results

6.2.1 Test 1: Flexural Hinge

Test 1 was performed to demonstrate that the infill wall system can be designed to achieve a ductile mechanism through the formation of a flexural hinge at the base of the wall. This mechanism allows the structure to sustain significant deformations while maintaining its lateral load capacity. The overall goal of the test

was to load the structure until the limit load of the structure was reached as determined by initial yielding of the post-tensioning bars.

Since the structure was tested cyclically in both directions, two different system characteristics could be determined in one test. Different post-tensioning bar sizes were used on opposite ends of the wall to assess the effect of the amount of steel. Two 1 in. post-tensioning bars were used adjacent to the east column while two 1-1/4 in. bars were used adjacent to the west column. The amount of reinforcement was selected so that the wall shear strength would be higher than the flexural strength, thereby, allowing the formation of a flexural hinge.

To investigate the effects of post-tensioning, an initial prestressing load of 56 kips per bar was selected. The same load was applied to all bars to produce uniform axial compression on the wall (moments eliminated). The post-tensioning loads after seating varied from the design levels and were measured by the bar strain gages. The stressing loads are tabulated below.

Wall Side	East End (Kips)	West End (Kips)
North	56.6	76.0
South	51.5	53.1
Total	108.1	129.1

The loading history used for Test 1 is shown in Figure 6.2, and the load-displacement relationship is presented in Figure 6.3. The results for different portions of Test 1 are discussed below. All loads are presented as base shear, and test cycles are designated by the load or displacement target level during testing superscripted by the cycle number. For example 45¹ is the first cycle to 45 kips.

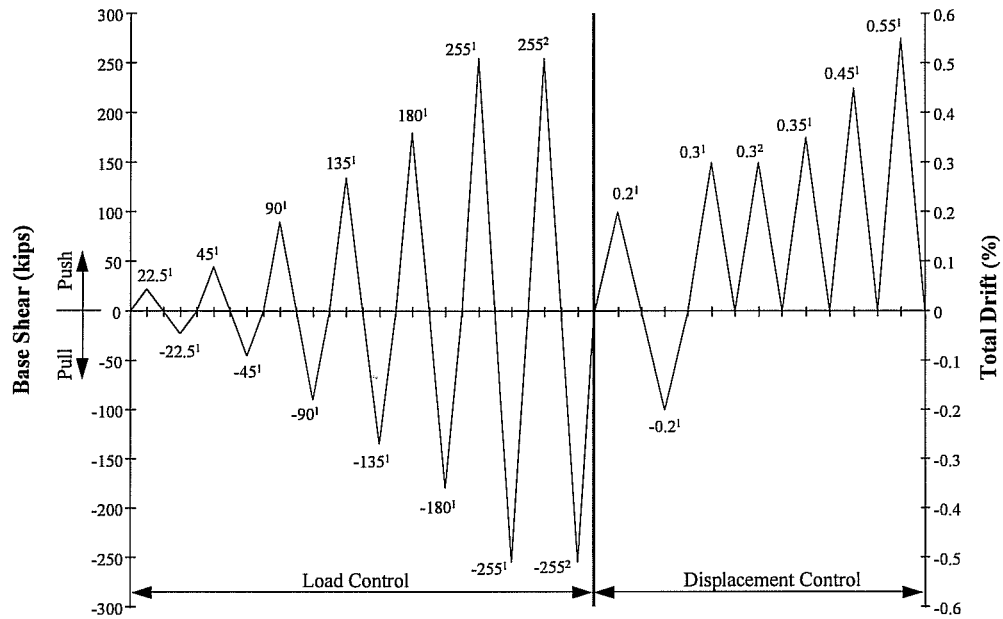


Figure 6.2: Test 1 Loading History

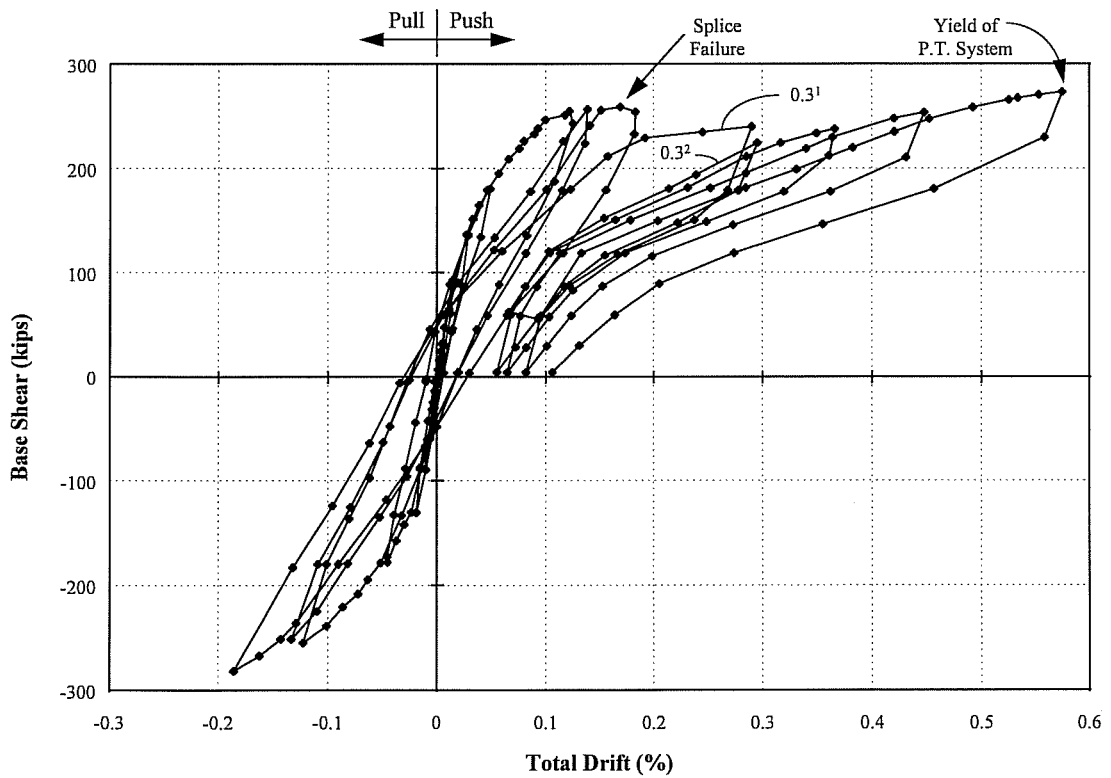


Figure 6.3: Test 1 Response

6.2.1.1 Structural Behavior: Prior to Splice Failure

Under initial loading, the structure was quite stiff as shown in Figure 6.4 which presents behavior prior to splice failure. Strain gage measurements indicated that compressive stresses across the interface from the post-tensioning were maintained in initial load cycles (22.5¹ and 45¹). The structural response was elastic, and the same stiffness was maintained in both loading directions.

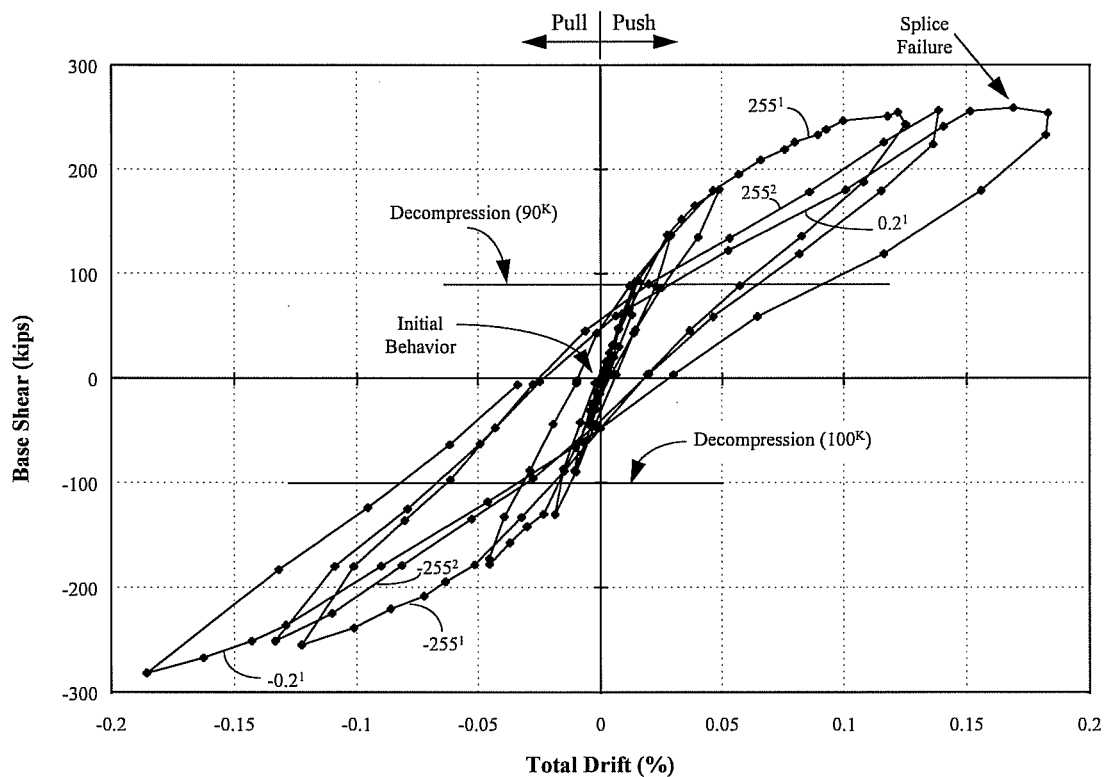


Figure 6.4: Test 1 Response Prior to Splice Failure

The column reinforcement strain gage measurements indicated that a zero tension stress state occurred in the push direction at 47.4 kips. In the pull direction, zero tension was indicated at 59.7 kips. In addition, the pre-existing crack at the base of the column was observed open during an inspection at 90 kips. The structural

response, however, as loading increased beyond the zero tension load remained the same; the same initial stiffness was maintained up until approximately 90 kips in the push direction and approximately 100 kips in the pull direction. The load at which the linear-elastic behavior changed was termed the decompression load for reasons to be explained later.

As loading increased beyond the decompression load, there was a gradual decrease in the stiffness. Cracking occurred on the bottom existing frame columns with the first crack occurring at the top of the column splice. As loading further increased, additional cracking was noted at intervals along the height of the column that progressed from the bottom of the column and moved upward. A detailed discussion of cracking is presented later.

When load in the push direction reached 255 kips (255¹), splitting cracks along the spliced bars were noted in the east column splice region indicating that failure was imminent. Therefore, it was decided to cycle at this load level to investigate behavior immediately prior to splice failure. Load in the pull direction to the same level did not produce splitting cracks in the west column. An additional cycle (255²) was completed at the same load level to further investigate the splice failure. Although cracking patterns did not change, significant changes in the hysteresis were noted. Additionally, the response beyond the decompression load in cycle (255²) was linear and did not exhibit the gradual change in stiffness that was observed in cycle 255¹. This reduction in stiffness was expected since flexural cracking occurred in the first cycle (255¹).

Following cycling at 255 kips, the load was increased to 259 kips in the push direction (0.2¹) when splice failure occurred in the east column. The structure was pushed to approximately 0.2 percent drift and unloaded. Loading was increased to 0.2 percent drift (270 kips) in the pull direction. Splice failure, however, did not occur because the initial post-tensioning in this column was slightly higher which

provided increased splice capacity. The structure was subsequently unloaded. Further testing was conducted in only the push direction to avoid failing the west column splice in this test.

6.2.1.2 Structural Behavior: After Splice Failure (0.3-0.55% Drift)

In Cycle 0.3^1 , the structure maintained good initial stiffness matching approximately the loading cycle to splice failure as shown in Figure 6.3. As loading increased beyond 120 kips, there was a slight decrease in stiffness; however, the load-displacement response was close to the original behavior with only a slight loss in load capacity. This response suggested that the splice bars were contributing to the tensile resistance of the structure and the overall stiffness. The structure was cycled at this displacement level to assess the contribution of the splice steel. The response in the second cycle (0.3^2) was much different than the first (0.3^1) as shown in Figure 6.5 which presents the post-splice failure response. It is clear that the splice bars were contributing to tensile capacity during cycle 0.3^1 , but the damage in the splice was sufficient to eliminate any significant tensile capacity for later cycles.

The structure responded in all cycles with the same initial stiffness (K_1) up to 60 kips (zero tension load). Figure 6.6 clarifies this finding since residual drifts were removed to illustrate the loading behavior (curves are shown originating at zero deflection). There was a gradual transition in stiffness until approximately 120 kips (slightly beyond the decompression load of 90 kips). Following this level, behavior in all cycles was fairly linear with approximately the same stiffness (K_2). There was a trend, however, of gradually degrading stiffness with increasing displacement cycles. In cycles up to 0.45 % drift, the post-tensioning steel remained elastic.

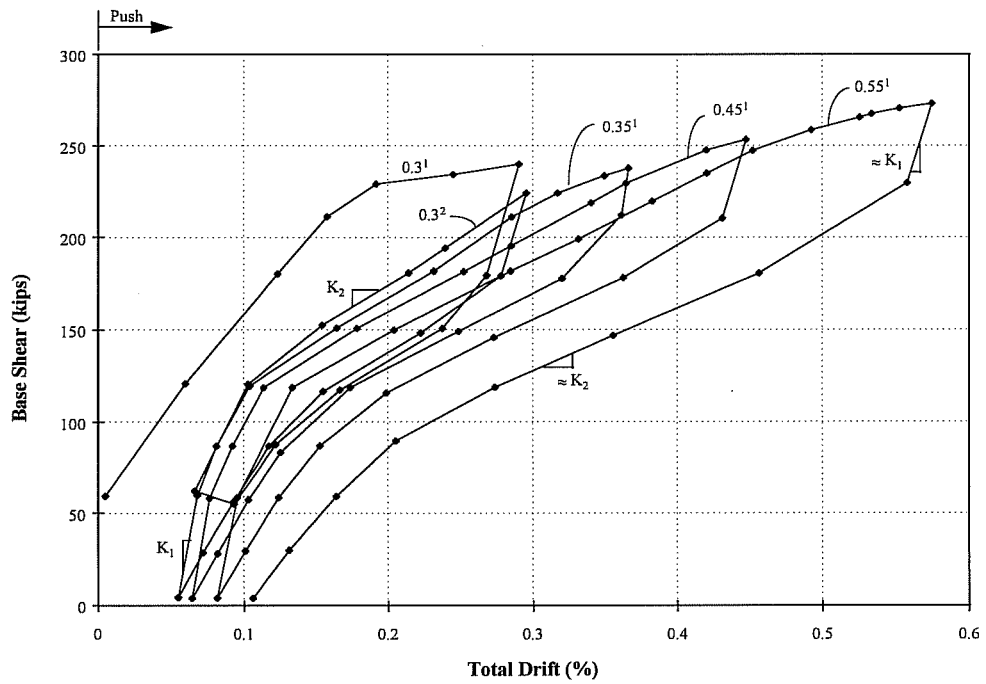


Figure 6.5: Test 1 Response After Splice Failure

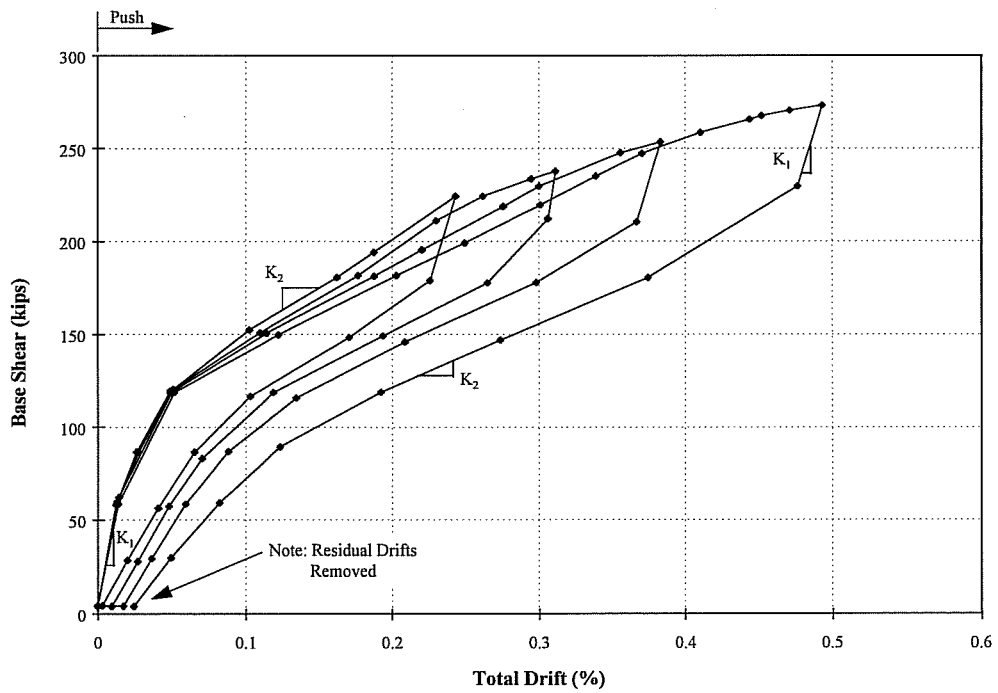


Figure 6.6: Loading Behavior After Splice Failure

Unloading curves followed the same general pattern of the loading curves and occurred at approximately the initial loading stiffness, K_1 , for approximately the same load range as the zero tension load (47 kips). Following that, the stiffness changed to a value nearly equal to that of loading after decompression, K_2 . As the structure reached approximately the decompression load, there once again was a gradual transition to an increased unloading stiffness. After complete unloading, the structure returned to approximately its original position; there was a small residual drift after each cycle caused most likely by the failed concrete in the column splice region and the cracking within the structure.

In the last cycle (0.55^1) of this test, the behavior was similar to the previous cycles. It is significant to note, however, that yielding of one east (north side) post tensioning bar was reached while the other bar remained elastic. The overall drift at this level was measured at 0.575 % as shown in Figure 6.5. After unloading, a larger residual drift remained since one of the post-tensioning bars yielded.

6.2.2 Test 2: Shear Test - 500 kips Post-Tensioning

Test 2 was designed to investigate the shear strength of the infill wall. Additionally, the effect of the prestressing force and the amount of post-tensioning steel were further investigated.

In order to produce a shear failure in the wall, an increase in the flexural capacity was required. Therefore, two 1 in. post-tensioning bars were added to each side of the wall. The bar configuration consisted of four 1 in. bars on the upload side and of two 1 in. and two 1-1/4 in. bars on the download side.

An initial prestressing load of 65 kips per bar was selected to further investigate the effects of the post-tensioning. The post-tensioning loads after seating varied slightly from the design levels and were measured by the bar strain gages. The stressing loads are tabulated below.

Wall Side	East Side		West Side	
	Out (Kips)	In (Kips)	In (Kips)	Out (Kips)
North	59.5	65.7	65.4	61.8
South	61.3	65.4	66.3	61.8
Total	251.9		255.3	

The loading pattern used for Test 2 is shown in Figure 6.7, and the response curve is presented in Figure 6.8.

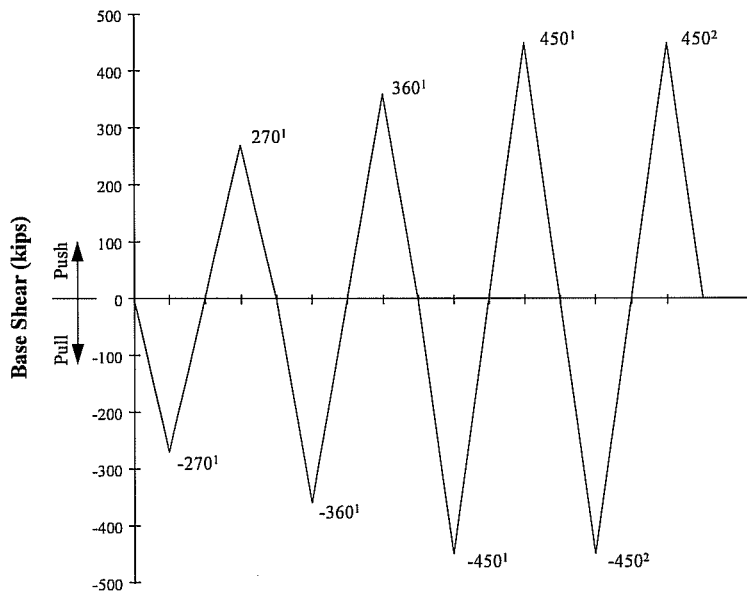


Figure 6.7: Test 2 Loading History

6.2.2.1 Structural Behavior

Test 2 commenced by loading in the pull direction, the direction in which splice failure in the column had not occurred. The zero tension stress state could not be determined from the column strain gage readings, but the slope of the response curve changed slightly at approximately 100 kips in both directions (point A)

indicating that the zero tension load had been reached. As load was increased beyond point A, there was a gradual change in stiffness up to point B (approximately 200 kips) where a distinct change in the load response was observed. Loading beyond point B occurred at a new slope and was fairly linear in both the push and pull directions. The distinct change in behavior occurring at point B was termed the decompression load as in Test 1. Loading beyond point B produced different behavior in both loading directions. The specimen was stiffer in the pull direction since the tension column splice was intact. In the push direction, a lower stiffness was expected since only the unbonded post-tensioning bars provided tensile capacity.

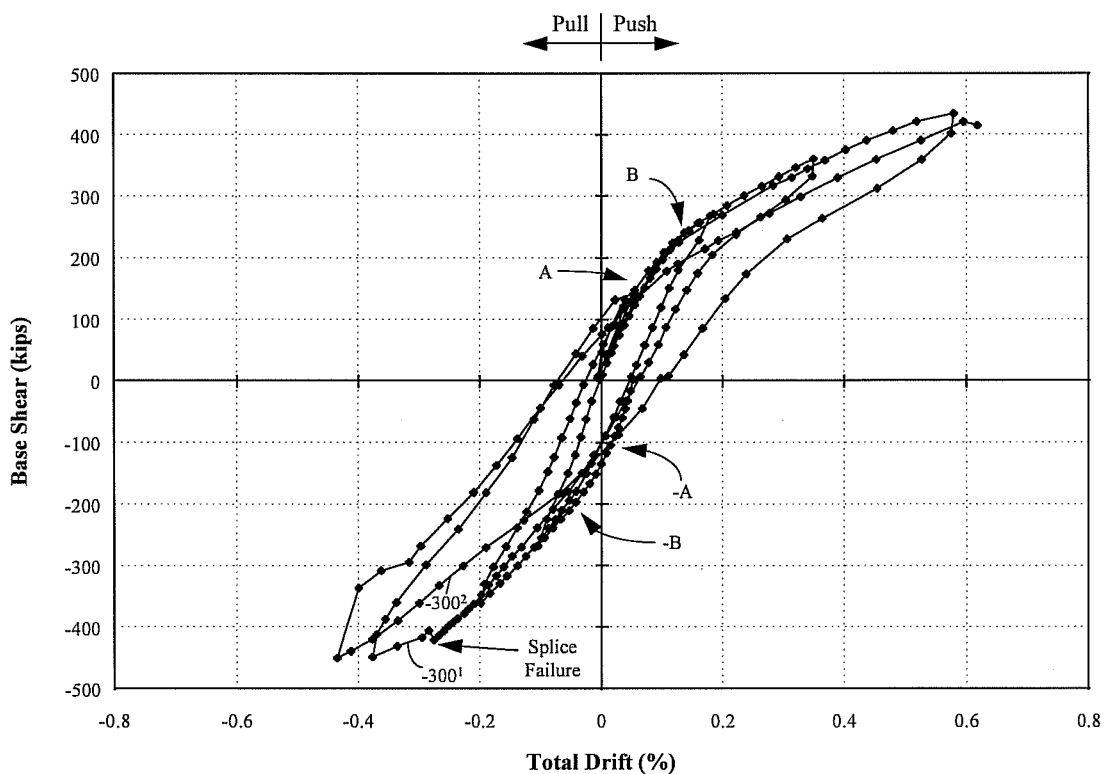


Figure 6.8: Test 2 Response

Loading in the pull direction (450¹) was continued until a base shear of 421 kips was reached when splice failure occurred in the west column. Loading was further increased beyond splice failure to 450 kips after which there was a slight

reduction in stiffness, but the base shear was still increasing very slightly. In cycle 450² in the pull direction, the difference in the hysteresis loops following splice failure can be noted. There was a distinct change in stiffness from the pre-splice behavior because the unbonded post-tensioning system was required to carry the tensile forces that previously had been carried by the tensile reinforcement in the column.

As noted from the overall response, there was some hysteresis in the loading loops due to cracking and column damage in the splice region. After unloading, however, the structure returned to approximately its original position with only small residual drifts since the post-tensioning steel remained elastic throughout testing. The load-displacement response formed an S shape, characteristic of non-linear elastic behavior.

6.2.3 Test 3: Shear Test - No initial Post-Tensioning

Test 3 was designed to investigate the shear strength of the wall in the absence of initial prestressing load. Since compressive stresses in the wall can enhance the shear strength, Test 3 was intended to obtain a lower bound shear capacity for the wall.

The same bar configuration used in Test 2 was maintained. The prestressing force, however, was released in all post-tensioning bars. The anchor nuts were reinstalled in the snug-tight position to permit loading of the structure. Monotonic loading to failure in the pull direction was used, and the response is presented in Figure 6.9.

6.2.3.1 Structural Behavior

The structure was loaded monotonically in the pull direction since a localized failure of the loading system prevented full testing in the push direction. The initial stiffness was maintained up to approximately 300 kips. The stiffness gradually

decreased with further loading as increased shear cracking occurred in the wall; the increased cracking increased the shearing deformations. The trend of stiffness degradation continued until approximately 460 kips where a distinct change in the slope of the curve was noticed. Fairly large deformations occurred with only a small increase in load.

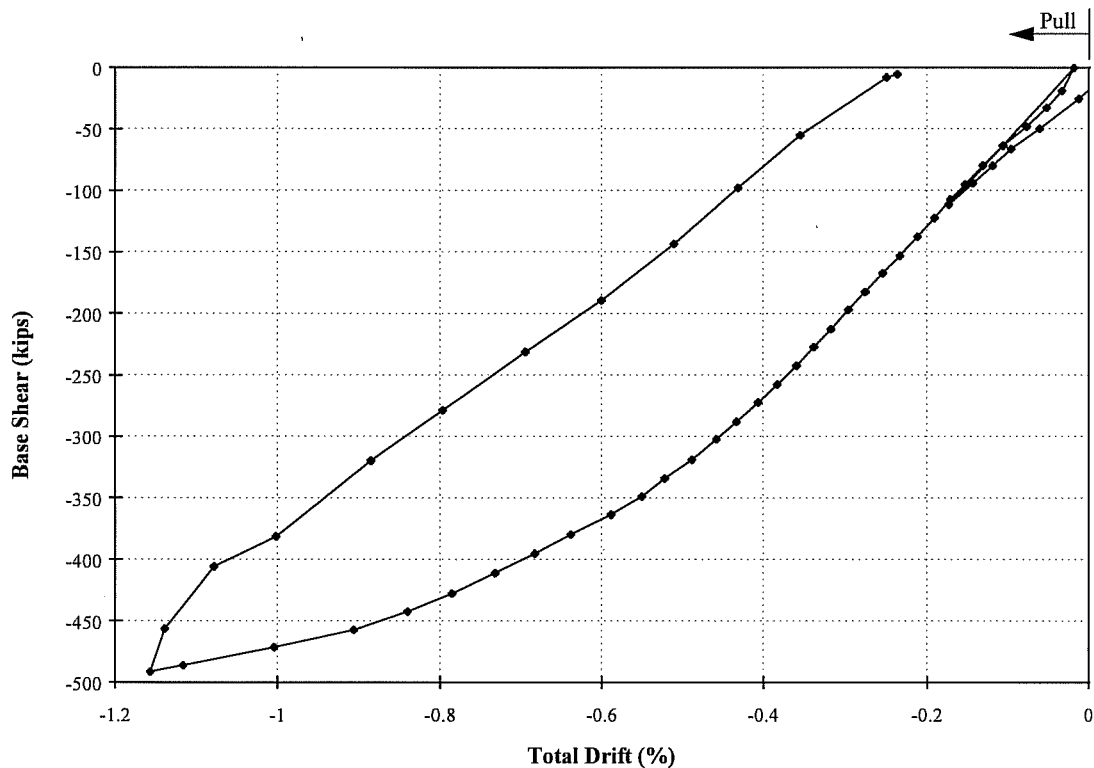


Figure 6.9: Test 3 Response

At 491 kips, concrete spalled in the wall at the top of the main compression strut as shown in Figure 6.10. The spalling occurred within the grout strip under the existing beam at the location of the west post-tensioning anchorage. Cracking patterns indicated that a primary compression strut directed from the “toe” of the wall to the post-tensioning anchorage had formed. It was within this strut that the wall spalled. From the flatness of the response curve at 491 kips and the crushing that

occurred in the compression strut, it was likely that the shear capacity of the wall was reached. Unloading occurred at approximately the initial loading stiffness.

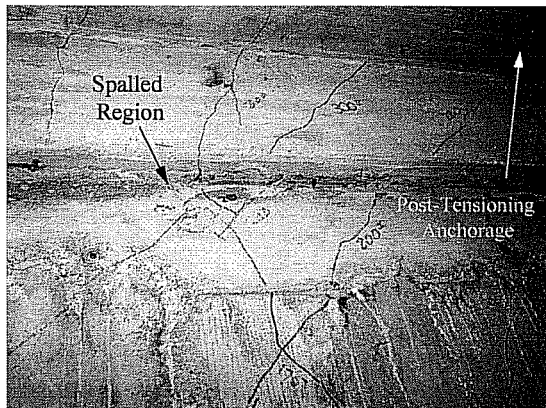


Figure 6.10(a): Compression Strut Spalling Location



Figure 6.10(b): Close-Up of Spalled Concrete

6.3 Cracking

6.3.1 Flexural Cracking

Prior to splice failure, flexural cracking occurred in the columns. Cracking initiated at the base of the structure and spread upward as loading increased. The flexural cracks, however, did not extend into the wall due to the jointed nature of the wall construction. Cracks were arrested at the column-wall interface when cracking extended through the column section. After splice failure, no further flexural cracking was noticed in the columns, and no flexural or flexural-shear cracking occurred in the wall.

6.3.2 Shear Cracking

Web shear cracking initiated at approximately a 45 degree angle in the middle first story wall ($V_{\text{base}}=248$ kips). A similar crack was also noted in the second story wall at slightly higher loads. As loading increased, shear cracks extended, and there

were additional cracks in both stories. The general orientation of all cracks was along a line connecting the column base to the top post-tensioning anchorage. The cracking pattern for the entire structure following testing is shown in Figure 6.11 while close up views of the first and second floors are shown in Figure 6.12 and Figure 6.13, respectively.

Diagonal cracks were continuous through panels and grout strips. There was no indication of distress along grout strips. The cracking pattern indicated that the wall behaved in a monolithic fashion even though it was constructed of smaller, individual units.

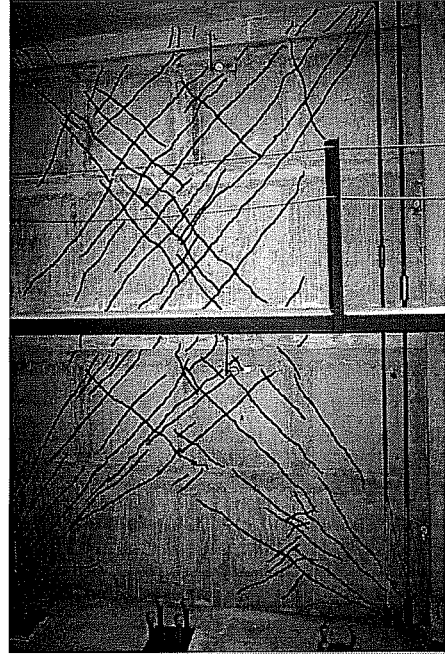


Figure 6.11: Wall Cracking Pattern

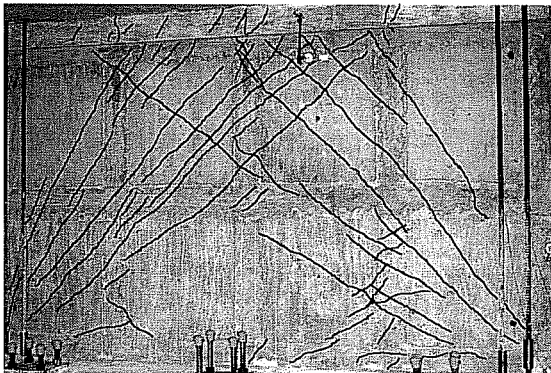


Figure 6.12: First Floor Cracking Pattern

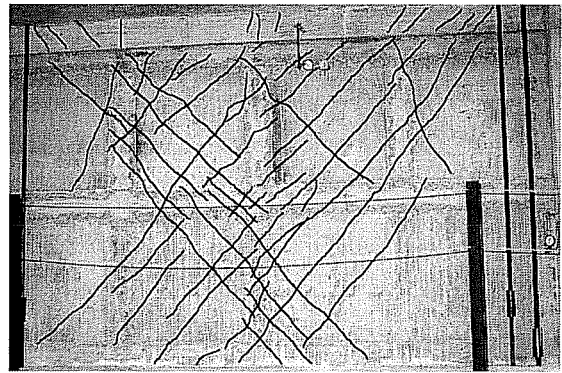


Figure 6.13: Second Floor Cracking Pattern

A maximum crack width of 0.8 mm was measured during testing. After reaching this width, it was noticed that additional cracks would open so that the initial crack would close slightly.

Web shear cracking was predicted using a Mohr's circle elastic stress analysis which included the effect of compressive stresses from the post-tensioning system. Cracking was assumed to initiate when the principle tensile stress reached $6\sqrt{f'_c}$ (psi). The cracking load was calculated to be 158 kips which was in excellent agreement with the test results.

6.3.3 Base Crack

The joint at the wall-footing interface opened as shown in Figure 6.14. The crack originated at the boundary element (existing column) and extended along the base of the wall. At the column, the crack was accommodated originally through flexural cracking of the column and following splice failure through the failed splice as shown in Figure 6.15. Prior to splice failure, the opening was small; but after splice failure, extremely large crack widths were noted (up to 3/4 in.). As loads were increased, the crack width also increased. Since the post-tensioning system which served as the tension steel at the boundary was unbonded, only one flexural crack formed in the structure; no flexural cracking occurred within the wall. Therefore, there was a concentrated rotation at the base of the structure

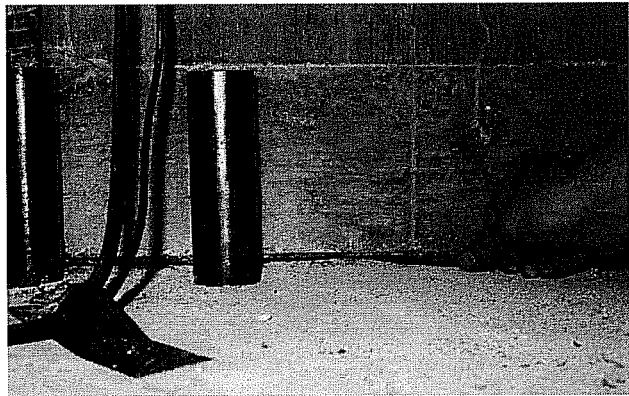


Figure 6.14: Crack at Wall Base



Figure 6.15: Crack Following Splice Failure (West Column)

as this crack was required to accommodate the flexural deformation. The structure appeared to rotate as a rigid body about the “toe” of the wall.

Due to the large vertical displacement required at the interface, the pipe shear lugs pulled out of the footing as shown in Figure 6.16. The pipes pulled out a cone of concrete from the footing. In addition, the vertical reinforcement also pulled out since it was anchored inside the pipe. The size of the crack coincided with the elongation of the post-tensioning steel which was about equal to the uplift at the second and third floor levels. In Test 1, at initial yield of the post-tensioning bars, the maximum crack width was measured at approximately 0.75 in. as shown in Figure 6.17. After unloading, the crack closed completely in all tests under the compressive force of the post-tensioning system.



Figure 6.16: Pull-Out of Shear Lugs

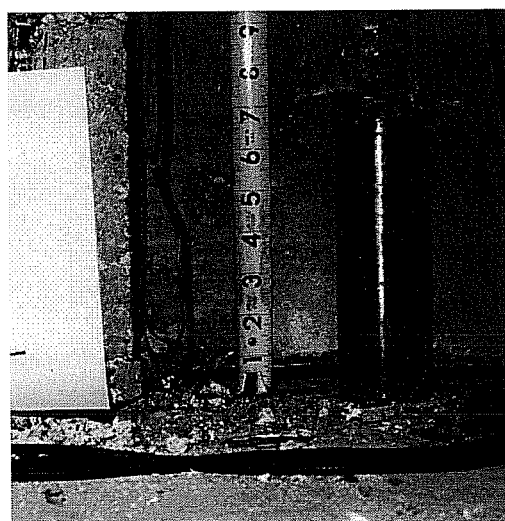


Figure 6.17: Maximum Crack Width During Test 1 (East Bars Shown)

6.3.4 Frame Boundary Cracks

Cracking occurred along the existing column-wall boundary and at the bottom of the beam-wall boundary as shown in Figure 6.18. The cracks were located at the corners opposite the formation of the compression struts (tensile stress corners) illustrated in Figure 6.19. The cracks originated at the midheight of the column and at the third point of the beam. These locations corresponded with the shear pipe locations. The tension steel at these locations appeared to arrest the cracking. Following unloading, residual crack openings were observed.



Figure 6.18: Frame Boundary Crack (East Column Shown)

6.4 Interface Slip

The relative motion of the existing building frame and the infill wall (interface slip) was measured, and the magnitude of the slip increased with the applied shear. Slips were consistent across the base of the wall. A maximum of 0.12 in. was measured at the maximum base shear of 491 kips as shown in Figure 6.20. A similar slip of 0.14 in. was measured at the top interface of the first story wall (beam bottom interface). Extremely small interface slips (0.01 in.) were measured at the base of the second story wall. Significant slip, however, of 0.11 in. was measured at the top of the second story wall. This slip was approximately the same as at the base of the structure. Maximum slips are indicated in Figure 6.19.

Slips along the column boundary were also measured. A maximum of 0.09 in. was measured in the first story and 0.04 in. was measured in the second.

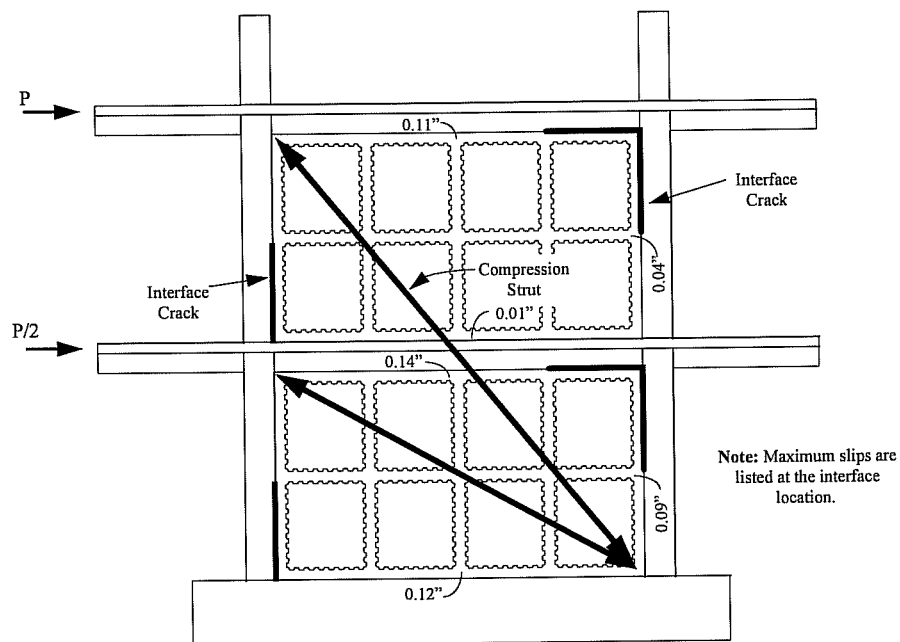


Figure 6.19: Frame Boundary Cracking and Interface Slips

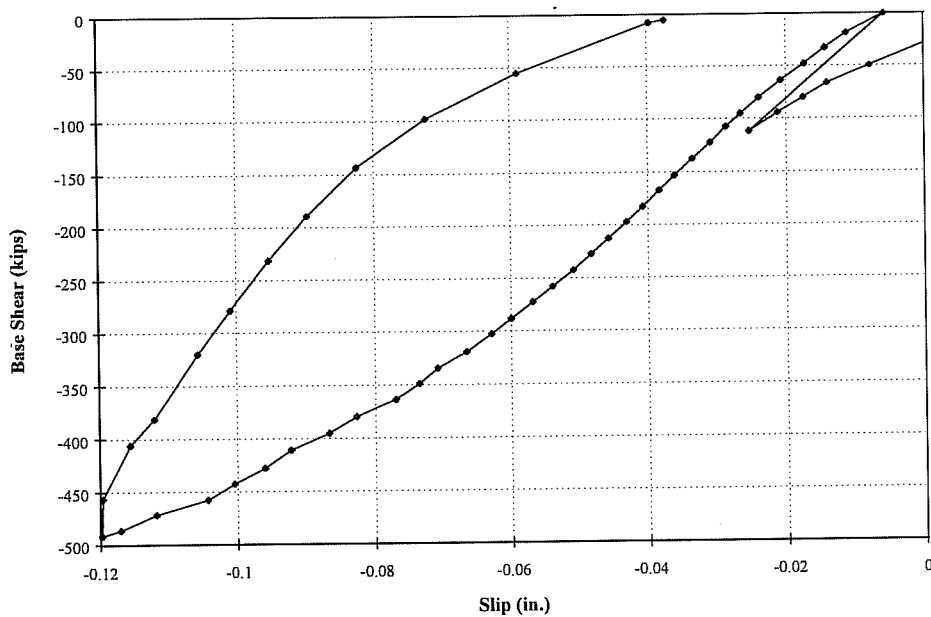


Figure 6.20: Slip at Base of Wall (Test 3)

6.5 Capacity

6.5.1 Zero Tension

The applied force required to produce zero tension (Figure 6.21) at the extreme fiber of the wall was measured as previously discussed. The load required to produce this stress condition was calculated using basic flexural mechanics and gross sectional properties of the flanged wall ($I_g=3,468,000 \text{ in}^4$, $A_g=1176 \text{ in}^2$). The equation for this stress state is presented below.

$$\frac{P}{A} + \frac{Mc}{I} = 0$$

A comparison of the experimental results with the theoretical calculations is presented in Table 6.1. The calculations were made assuming only axial compression. In reality, the post-tensioning system varied slightly from one side of the structure to the other producing applied moments. These moments could also be accounted for in the analysis which would provide for the different zero tension loads measured in the two directions in Test 1.

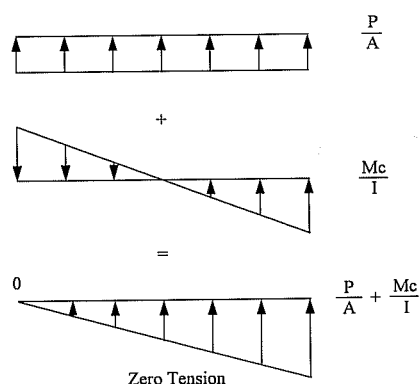


Figure 6.21: Zero Tension Stress State

Table 6.1: Loading to Reach Zero Tension

	Experimental (kips)	Calculated (kips)
Test 1		
Push	47	51
Pull	60	51
Test 2		
Push	100	108
Pull	100	108

6.5.2 Decompression Load

There was an abrupt change in stiffness at a load approximately double the zero tension load. Prior to this point, the structure maintained approximately the same stiffness even beyond the zero tension load. This behavior was not expected as a transition in behavior was anticipated when the structure reached the zero tension stress state.

It was discovered that the compressive stresses remaining in the structure at the zero-tension condition provide clamping forces to maintain the stiffness. The applied moment must fully overcome the pre-compression force or decompress the section before the stiffness of the section changes significantly. Before decompression, no significant tensile stresses are required to be resisted by the column tensile steel as shown in Figure 6.22 for Test 1 and Figure 6.23 for Test 2. A very small change in behavior was noticed after the zero tension load.

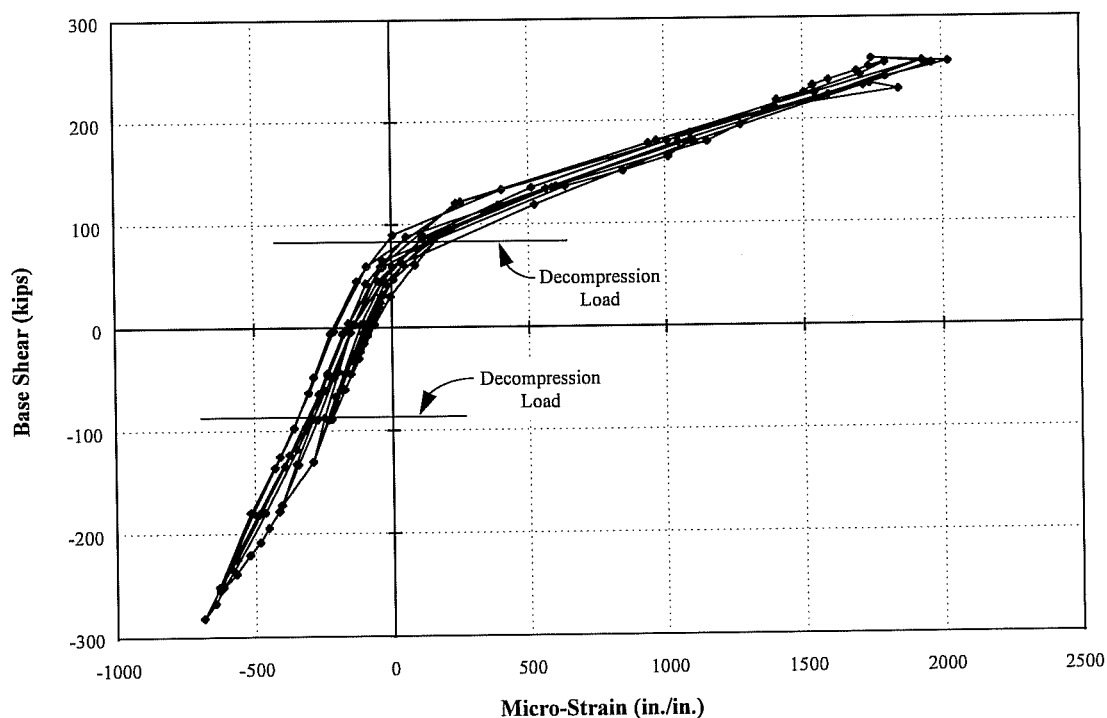


Figure 6.22: East Column Tension Steel (Test 1)

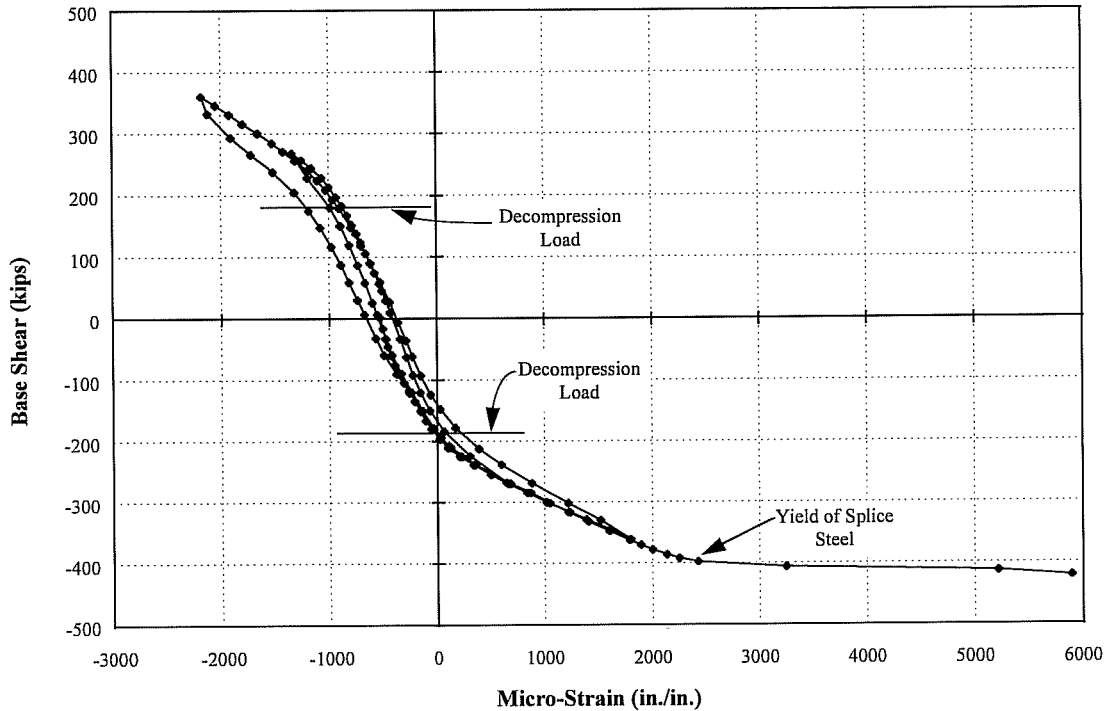


Figure 6.23: West Column Tension Steel (Test 2)

The system can be viewed by considering the applied moment as an eccentric axial load, P , where the axial load is the post-tensioning force as illustrated in Figure 6.24. As the axial load eccentricity increases, pre-compression across the interface is reduced. As P approaches the edge of the structure, the initial compression is eliminated and the moment on the section at this stage is termed the decompression moment in this report. The decompression moment can be calculated as follows.

$$M_{DC} = Pe$$

where $e = \text{Wall Length} / 2$

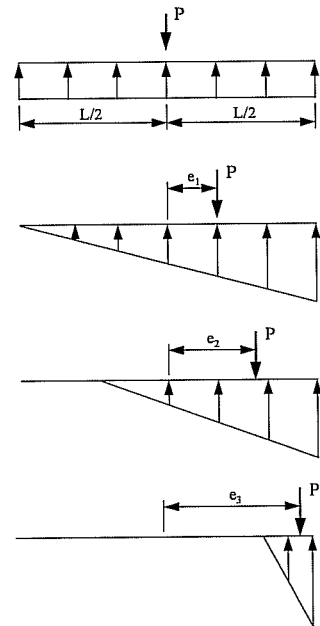


Figure 6.24: Analysis of Decompression Load

For this analysis, it was assumed that the section cannot resist tension. The column base was precracked prior to wall construction, and the wall was connected along an unroughened surface. In Table 6.2, calculated loads are compared with experimental results. The values were calculated assuming pure axial compression and neglecting any initial eccentricity of the applied pre-compression. The analytical results compare extremely well with those measured.

Table 6.2: Decompression Moment Analysis

Test	Experimental (kips)	Calculated (kips)
1	90	85
2	190	186

6.5.3 Splice Failure

The existing frame column acted as a boundary element of the infill wall; therefore, tensile stresses developed from the overturning moments were required to be resisted by the column reinforcement. As indicated in Chapter 5, the splice capacity was computed as 57 ksi using the Orangun^[29] equation. Since this capacity was less than yield, a nonductile splice failure was expected. A splitting tensile splice failure occurred in both columns due to the short compression lap length. Both columns failed in a face split as shown in Figure 6.25.

The reason that failures occurred in Test 1 and 2 at different lateral loads was the different initial post-tensioning forces applied. In general, as the initial post-tensioning increased, the lateral load to produce splice failure increased. The test results are presented in Table 6.3.

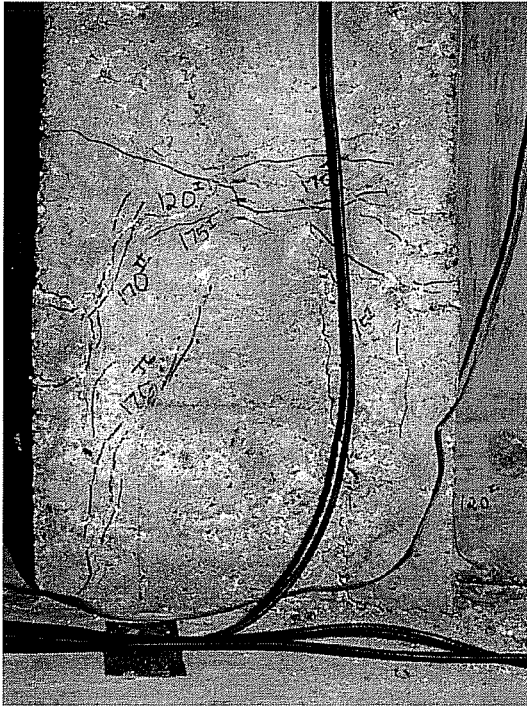


Figure 6.25(a): East Column Splice Failure



Figure 6.25(b): West Column Splice Failure

Table 6.3: Splice Failure Test Results

Column	Splice Failure V_{Base} (kips)	Initial Post-Tensioning (kips)
East	259	237.2
West	421	507.2

Stresses in the splice reinforcement and ties were determined from measured strains immediately prior to failure. In the east column, the column bars reached a stress of 59 ksi. From the load-displacement response, however, it appears that the bars probably reached yield as indicated by the load plateau. This seems highly likely since the bars had a yield strength of 61 ksi, and there was variability in the strain gage readings. Stresses in the two column ties in the splice region increased

significantly as the splice failure was approached, but did not reach yield. A maximum tie stress of 16 ksi was measured. The download column provided similar findings; two column bars apparently reached yield according to strain gage readings while the column ties reached 35 ksi. Even though several of the bars may have reached initial yield, the embedment lengths were too short to allow for any significant deformation capacity of the bars and any increase in stresses due to strain hardening.

For design and analysis purposes, the splice failure capacity can be calculated as follows.

1. Calculate the splice capacity with a method such as the Orangun equation.
2. Calculate the applied moment to produce the failure stress in the column reinforcement (M_{cr}). The moment was calculated using the cracked moment of inertia of the flanged wall (I_{cr}).
3. Since significant tensile stresses do not occur in the column bars until the decompression moment is reached, the calculated moment in Step 2 can be added to the decompression moment ($M_{cr}+M_{DC}$).
4. Use the calculated moment capacity to determine the lateral load based on the moment diagram.

The splice capacities were calculated according to the procedure presented, and the calculations are compared with the experimental results in Table 6.4. The procedure provided a conservative estimate of the splice failure capacity.

Table 6.4: Splice Capacity Analysis

Column	Splice Capacity (kips)	Decomp. (kips)	Calculated (kips)	Experimental (kips)	Ratio (Exp./Calc.)
East	99.3	84.9	184.2	259	1.41
West	99.3	186.3	285.6	421	1.47
Average:					1.44

As loading increased to produce splice failure, it was noted that stress in the post-tensioning bars increased as shown in Figure 6.26 for Test 1 and Figure 6.27 for Test 2. The post-tensioning force increased from the original stressing load by 29.7 kips in Test 1 and by 86.1 kips in Test 2. The stress increases in the post-tensioning tendons further extended the life of the splices by providing additional compression. The procedure suggested for calculating the splice failure should be conservative since the increased moment capacity due to the post-tensioning was neglected.

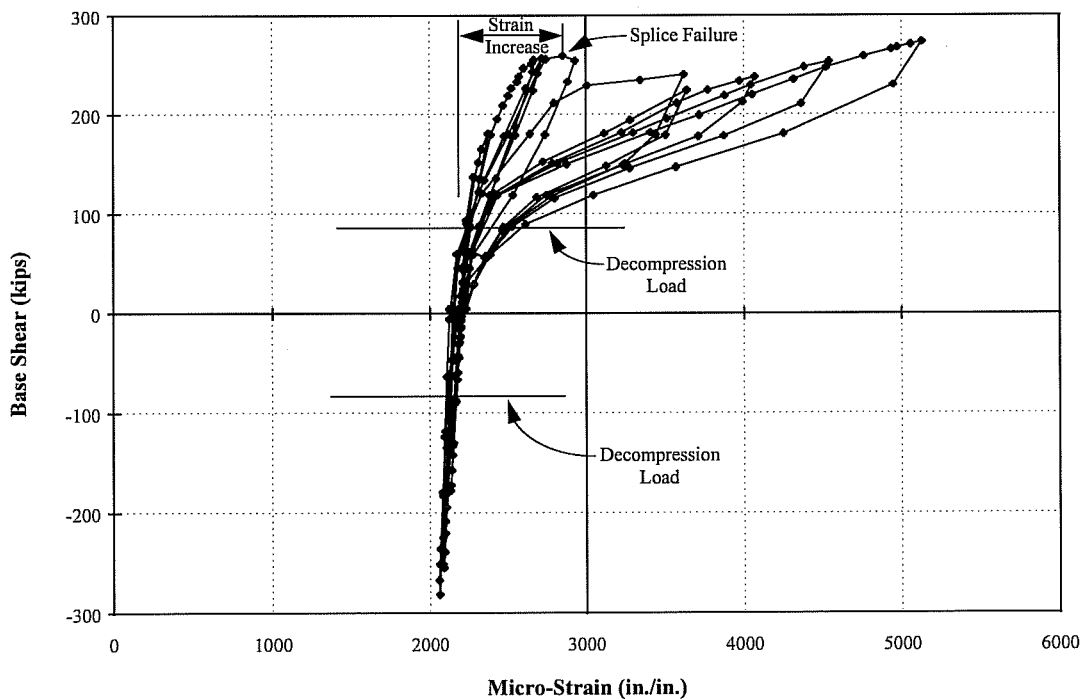


Figure 6.26: East Post-Tensioning Strain Increase (Test 1)

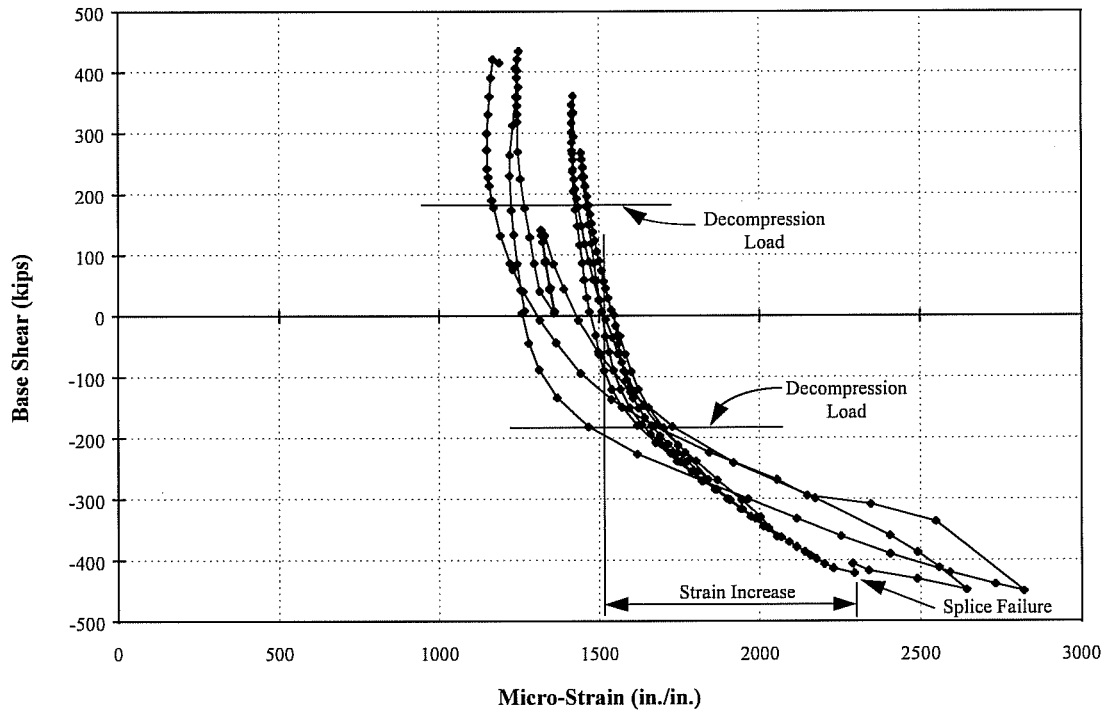


Figure 6.27: West Post-Tensioning Strain Increase (Test 2)

6.5.4 Flexural Strength

The ultimate flexural capacity of the structure following splice failure was achieved through yielding of the post-tensioning steel. The capacity can be computed from strength design procedures recommended by ACI 318-89.^[3] Since the high strength bars have a yield plateau, the yield strength of the material can be used to determine the moment capacity. The yield strength for the post-tensioning bars can be estimated as 90 percent of ultimate.

$$F_y = 0.9F_u$$

$$T = A_s F_y$$

$$a = \frac{T}{0.85f'_c b}$$

$$M_n = T \left(d - \frac{a}{2} \right)$$

A flexural strength of 273 kips was reached in Test 1 while the computed strength using the actual yield strength of the post-tensioning bar was 245 kips.

6.5.5 Shear Strength

The approximate shear strength of the wall was 491 kips. As previously mentioned, the load-displacement response for Test 3 and the initiation of compressive strut failure indicated that the shear strength had been reached. The test was not continued beyond this load level because the capacity of the loading system was reached.

The wall shear strength was controlled by concrete crushing in the primary compression strut. No interface or diagonal shear failures occurred that limited the shear capacity in either the first or second story wall. Both walls (6 in. and 4 in.) reached a shear stress of $7.1\sqrt{f'_c}$ (psi) which was calculated based on the lowest strength wall panels (4500 psi) and the entire length of the wall ($L_w = 172$ in.) as recommended by ACI 318-89^[3] Chapter 21, Section 21.7.3. The shear strength (492 kips) greatly exceeded the design strength of 146 kips.

By using a simple strut and tie model of the structure (Figure 6.28), prediction of the compression strut failure was possible. The crushing occurred in the wall below the top floor beam due to the reduction in cross sectional area created by the 4 in. wall. It was assumed that the bearing stresses from the post-tensioning anchorage spread out along a 45 degree angle as shown in Figure 6.29. By using this model and

the bearing strength of concrete ($0.85f'_c$) as recommended by ACI,^[3] compression strut failure was estimated at approximately 445 kips which compares reasonably well with the test result of 491 kips.

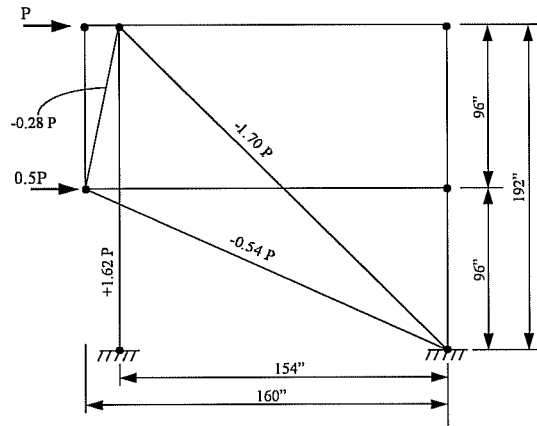
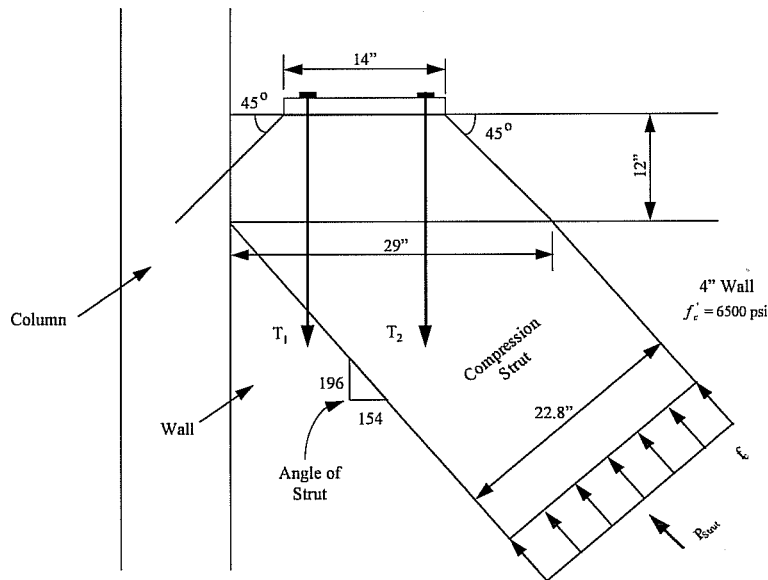


Figure 6.28: Strut and Tie Model



$$P_{Strut} = A_{Strut} (0.85f'_c)$$

$$= (22.8)(4)(0.85)(6.5) = 503.9 \text{ kips}$$

$$V_{Base} = 503.9 \left(\frac{1.5}{1.7} \right) = 445 \text{ kips}$$

$$V_{Base} = 445 \text{ kips} \approx 491 \text{ kips from Test 3}$$

Strut force from analysis

$$V_{Base} = 1.5 \text{ kips}$$

$$P_{Strut} = 1.7 \text{ kips}$$

Figure 6.29: Nodal Point Analysis

6.6 Stiffness

Analytical models for calculating the load-deflection response are compared with the experimental test results previously presented. Figure 6.30 through 6.32 present the comparisons for Test 1 through 3, respectively.

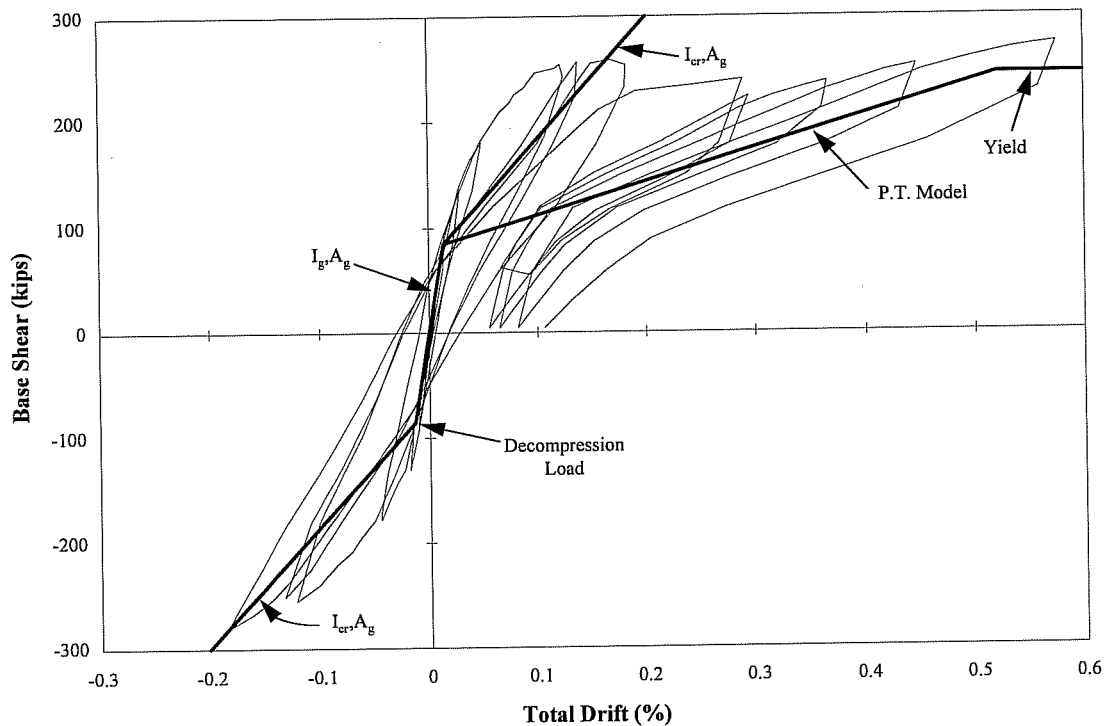


Figure 6.30: Test 1 Model Comparisons

6.6.1 Prior to Decompression Load

Before reaching the decompression load, the structure responded as an uncracked, monolithic wall. In this range of behavior, the structure can be modeled using gross sectional properties to obtain a load-deflection response. Due to the aspect ratio of the wall ($H_w/L_w = 1.12$), shear deformations are significant and should be accounted for in the analysis. The shear area used was calculated as the web area, and the sectional properties used are tabulated below.

Wall	I_g (in ⁴)	A_{sh} (in ²)
6 in.	3,468,000	888
4 in.	2,927,000	592

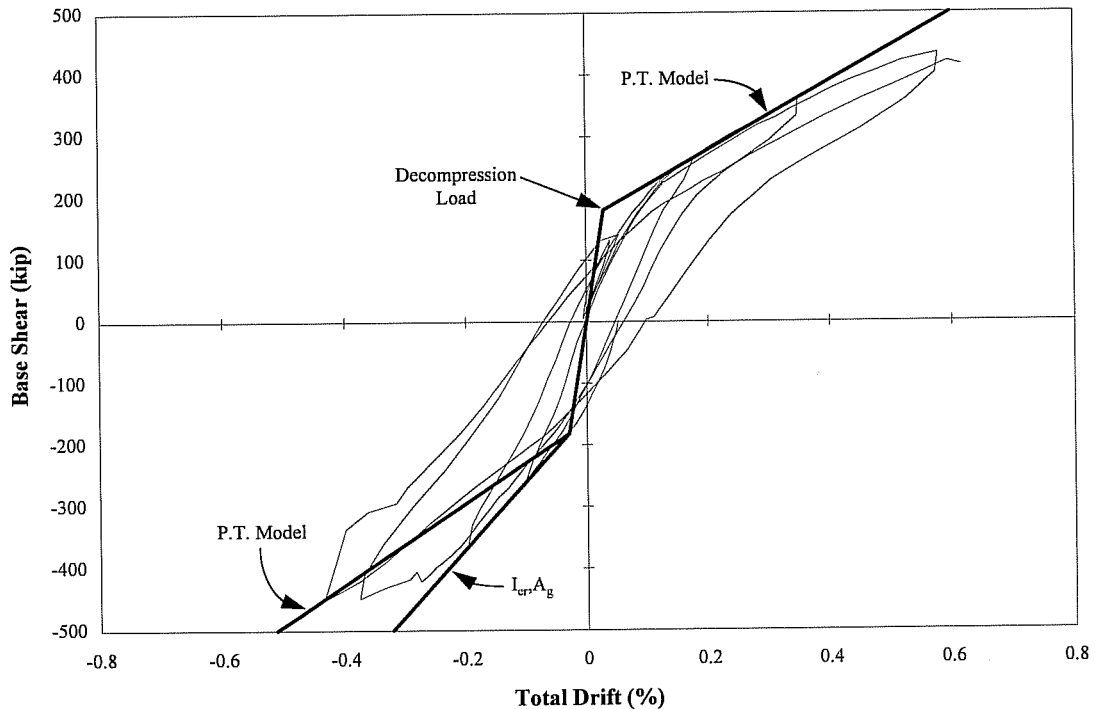


Figure 6.31: Test 2 Model Comparisons

6.6.2 Decompression Load - Splice Failure

Following the decompression load, there was a decrease in the stiffness. The structure experienced flexural cracking which indicated that behavior changed from the uncracked to a cracked condition. Therefore, this range of behavior can be modeled using cracked-sectional properties to obtain a load-deflection response. Shear deformations were accounted for by using the gross shear area used previously.

The sectional properties used are tabulated below. In this stage of behavior, the post-tensioning steel stress varies slightly under loading, but does not contribute significantly to the stiffness of the structure.

Wall	I_{cr} (in ⁴)	A_{sh} (in ²)
6 in.	331,000	888
4 in.	330,700	592

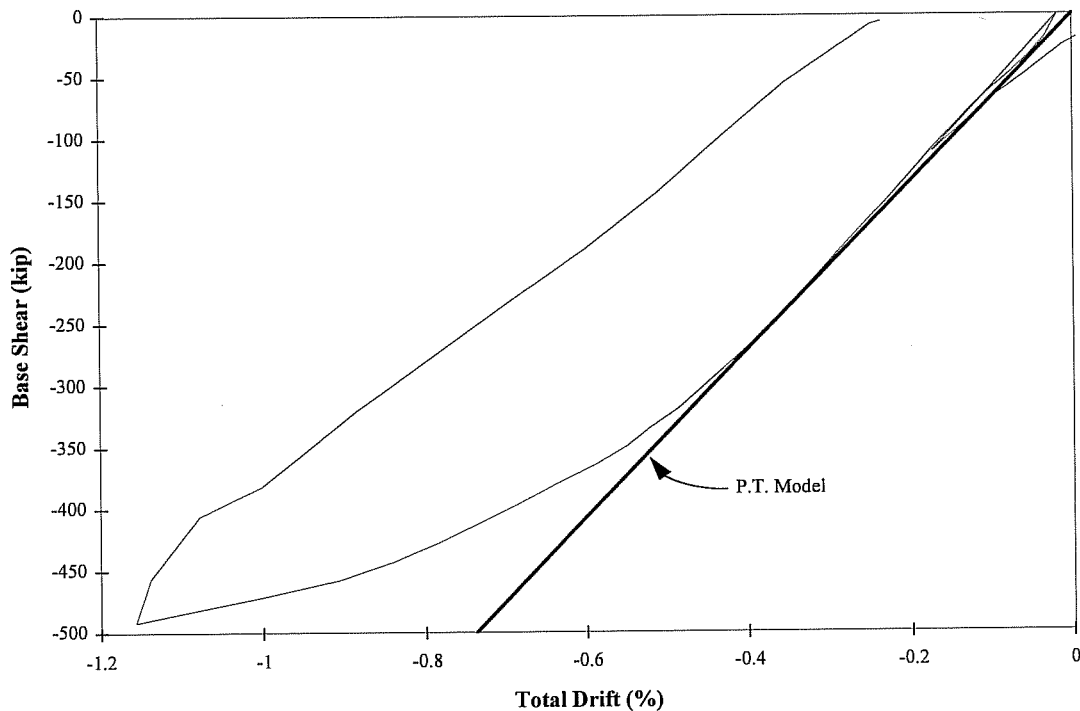


Figure 6.32: Test 3 Model Comparisons

6.6.3 Post Splice Failure

After splice failure, lateral resistance was provided by the unbonded post-tensioning system. In general, the response after reaching the decompression load was linear up to yield of the post-tensioning bars. Computation of the load-deflection

response can be made using a strut and tie model for the system. The model used in this research is shown in Figure 6.33. The size of the compression strut was determined by comparing the stiffness of test 3 with the analytical results. Once the model was calibrated in this manner, it was used in all three tests. It was determined that a strut area of 200 in^2 provided reasonable results. This strut area corresponds with 1/3 the length of the web

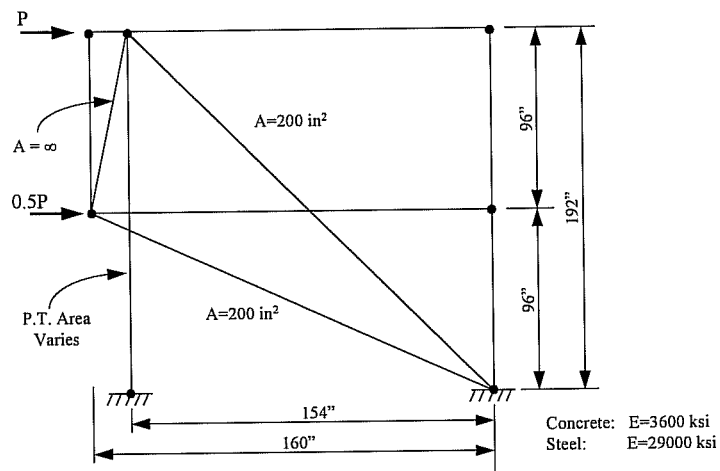


Figure 6.33: Post-Tensioning System Model

(148 in.) of the 4 in. wall. Both primary compression struts used the same area while the strut connecting the second floor to the third floor was given an infinite area since shortening of this strut should be negligible.

The upper bound to the post-yield behavior was either flexural hinging as exhibited in Test 1 or a shear failure.

6.7 Frame Connections

The frame connection in general performed excellently. Minor cracking was noted around several of the pipe connections, but no signs of distress were evident. The pipe lug, as previously mentioned, pulled out of the footing as evidenced by the large vertical opening that occurred at the base of the wall. Due to the pipe embedment length provided, however, the effectiveness of the pipe in transferring shear should not have been diminished.

It appeared that the 6 in. embedment of the grout strip steel in the footing was not adequate to eliminate pullout of the bars. For the unbonded post-tensioning system, however, large vertical displacements must be accommodated at the base of the wall. Therefore, it does not seem justifiable to fully anchor this reinforcing steel. If full anchorage was provided, either the bars must elongate enough through yielding or they must fracture. Anchorage of the steel, however, did seem to help the column splice prior to failure since tensile forces carried by steel in the vertical strips relieved the column steel slightly.

The magnitude of the interface slips were compared with the frame connection test results previously presented in Chapter 4. This comparison indicated that the shear lugs were working at approximately their peak strength. The capacities of the shear lugs (approximately 240 kips from test data), however, were not adequate to resist the total shear force (491 kips). Substantial shear resistance, therefore, must be obtained from friction along the base and from shear resistance of the column base. The shear cracking pattern also supports this theory since the main compression strut was directed at the toe of the wall. Cracking patterns did not suggest that compression struts formed adjacent to the shear lugs.

6.8 Precast Panels and Panel Connection

The precast panels and panel connections performed excellently. Inclined cracking occurred through the precast panels and panel joints without regard to the shear key interfaces. Crack widths remained fairly small throughout, and no signs of distress were evident.

6.9 Observed Behavior versus Design Assumptions

The infill wall was designed for a base shear of 146 kips assuming that the shear lugs were to carry the entire base shear. In reality, a large portion of the base shear was carried by a combination of friction from the compressive force acting at the “toe” of the wall and the shear resistance from the existing column at the failed splice. Even if it was assumed that the shear lugs were at their peak capacity, a large portion of the base shear would remain unaccounted as previously mentioned in the frame connection discussion.

The precast wall panels and the panel connections were designed to be consistent with the design assumption made for the frame connection. They were designed to transfer shear to the shear lugs without failure originating in either the panels or panel connections. The design of the panels worked according to design assumptions since no distress of the panels could be seen adjacent to the shear lugs. The cracking pattern, however, does not indicate struts forming adjacent to the shear lugs as was implicit in the design assumption. Instead, a primary compression strut was directed at the “toe” of the wall indicating that the entire wall was effective in transferring shear.

The infill wall reached a base shear of 491 kips which was 3.4 times greater than the design level.

CHAPTER 7
PRECAST INFILL WALL SYSTEM:
DESIGN AND DETAILING GUIDELINES

7.1 Introduction

Design guidelines for a precast infill wall system are presented for proportioning and detailing the various components of the precast infill wall system. The guidelines were developed for rehabilitation of nonductile reinforced concrete moment frame structures by extension of the research conducted in this report. Work is underway with FEMA sponsorship to develop design guidelines for seismic rehabilitation. The procedure developed here could become part of such a document in the future.

The general design requirements for the precast infill wall system are presented in Section 7.2 followed by specific requirements for both flexural (Section 7.3) and shear (Section 7.4) strength design. In general, the chapter uses a format of presenting the design criterion or objective followed by an explanation or justification of the criterion. The chapter concludes with a discussion of using the infill wall system for performance based design criteria (Section 7.5).

7.2 General Design Requirements

Design of the infill wall should conform to the recommendations presented in this chapter. Minimum design seismic forces shall be determined in accordance with UBC-1991^[37] or NEHRP recommended provisions.^[17] Additionally, any elements of the structure not part of the infill wall requiring rehabilitation shall be designed in accordance with provisions of UBC-1991^[37] or NEHRP.^[17]

In keeping with the intent of modern building codes, the structure should be designed to resist a major level of earthquake ground motion having an intensity equal to the strongest either experienced or forecast for the building site, without collapse, but possibly with some structural as well as nonstructural damage. Design for this level of performance is commonly referred to as a collapse limit state design.

7.2.1 Design Philosophy

The precast infill wall system should be designed to behave monolithically, and the infill wall should be designed with sufficient shear strength to develop flexural yielding at the base of the wall.

Discussion:

The infill wall should be designed to achieve a flexural hinge at the wall base since the formation of a hinge allows for ductile response of the wall. The ductility achieved through this mechanism can permit the structure to sustain large deformations that would be expected in a major level of ground motion.

The structure can be expected to behave inelastically in the collapse limit state; therefore, it is appropriate to reduce design force levels to account for this behavior. In the testing conducted in this research, the infill wall designed for flexural hinging at the base possessed excellent lateral deformation capacity. In general, the wall performed like a monolithic concrete shear wall. Due to the performance exhibited in this test, it is recommended that an R factor consistent with a reinforced concrete shear wall be used for design ($R_w=8$ for UBC and $R=5$ for NEHRP). It is not recommended to consider a dual system design because of the nonductile behavior generally exhibited by existing frames needing rehabilitation.

It may not always be possible to achieve flexural hinging of the wall such as in the case of low rise walls where large shear strengths are required due to the high flexural strengths. In this case, it may be acceptable to design the wall with the shear

strength controlling the lateral load capacity. Only elastic behavior should be considered in the design. In general, significant ductility in shear would not be expected with a shear failure. An R factor of one (R=1) should be used for a shear-controlled design.

7.2.2 Effects of Modified Load Path on Existing Structure

Design of the infill wall system should consider the effects of changes in the lateral load system on behavior of the existing structure.

Discussion:

Use of an infill wall system modifies the primary load path used for resistance of lateral forces. Therefore, structural diaphragms must be checked for adequacy in transferring forces to the wall. Additionally, the adequacy of the foundation must be considered.

7.3 Flexural Strength

Adequate flexural strength should be provided to resist wall overturning moments calculated from the design seismic forces. Design moments at collapse should be less than or equal to the ultimate moment capacity of the wall following splice failure. The ultimate moment capacity should be based on the yield strength of the post-tensioning steel.

$$M_{Collapse} \leq M_u = \phi M_n$$

$$M_n = T \left(d - \frac{a}{2} \right)$$

where:

$M_{Collapse}$ = Collapse limit state moment

M_u = Ultimate moment capacity

M_n = Nominal moment capacity

$\phi = 0.9$ for steel tensile yielding
 T = Yield strength of post-tensioning steel
 d = Effective depth of post-tensioning
 a = Depth of rectangular compressive stress block

Discussion:

For a severe ground motion, it should be assumed that splice failure will occur in the existing columns. The wall capacity; therefore, will be entirely dependent on the post-tensioning steel.

The lateral capacity in flexure following splice failure may be less than that producing splice failure in the existing columns. (See Chapter 6 for a discussion of splice failure capacity.) The splice performance must be checked since a higher strength (including splice strength) could lead to a shear failure in the wall. The wall shear strength should be designed to resist the highest lateral loads that can be developed in the structure to insure ductile response in flexure.

7.3.1 Post Tensioning Anchorage

The post tensioning system must be properly anchored to develop the full strength of the steel (and moment capacity of the wall) at all critical sections.

Discussion:

To eliminate local failures in bearing or in development, post-tensioning anchorages should be designed for the ultimate capacity of the post-tensioning steel.

7.4 Shear Strength

Shear strength is provided by the precast infill wall shown in Figure 7.1. The details of the design procedure are presented below, and an example design was presented in Chapter 4 where the design procedure was used for rehabilitation of the

model test structure. A capacity design approach is recommended for design of the elements comprising the infill wall with the shear lugs designed as the “ductile fuse.” The shear capacity should be computed considering the resistance of shear lugs installed along the interface at the base of the wall in the direction of applied shear.

$$V_{Design} = \phi \sum V_n^{Pipe}$$

where:

V_{Design} = Design shear capacity

V_n^{Pipe} = Nominal pipe shear strength

$\phi = 0.9$ for shear yielding of pipe

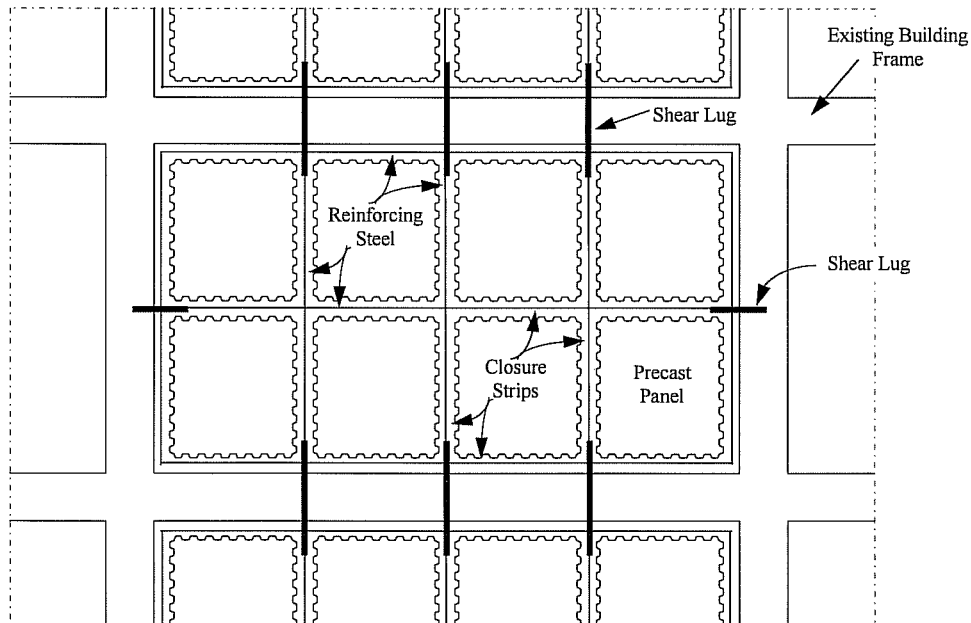


Figure 7.1: Precast Infill Wall System

Discussion:

In a capacity design approach, an element of the structural system is selected to control the design. The element selected generally displays ductility through deformations large enough to permit the structure to withstand the earthquake generated forces. This element is commonly referred to as the “fuse” of the system since the system strength is limited to the capacity of the selected element. Ductility provided in the “fuse” enables the system to maintain strength while exhibiting deformation capacity. All other elements in the system are designed for capacities greater than that associated with reaching the maximum feasible strength of the “fuse.” The intent is to protect these elements against failure. For the capacity design approach used here, the shear lugs are designed as the “fuses” of the system that controls the shear capacity of the wall. Shear yielding of the pipe was chosen as the “fuse” since it provides for reasonable ductility in shear.

Testing indicated that a substantial portion of the shear at ultimate capacity was resisted by friction along the base and by the existing column at the toe of the wall. However, since no physical preparation of the surface concrete is needed if shear lugs are used, the frictional resistance provided between the existing structure and infill wall could vary substantially due to varying concrete surface conditions and should be neglected. In addition, shear resistance from the existing columns should also be neglected due to the assumption that the column splice will fail. Failure of the splice in this region reduces the effectiveness of compression transfer through the boundary elements. In the worst case, compression and shear transfer is completely eliminated due to crushing of the “toe.” It is, therefore, recommended that only the capacity of the shear lugs across the interface be used to provide a conservative estimate of shear capacity.

The panels and panel connections should be designed to transfer shear to the lugs (pipes) to eliminate localized failure prior to ultimate shear lug capacity. Since

the entire shear force is assumed to be resisted by the steel pipes, the wall is effective only up to the last shear lug in the direction of applied shear (Figure 7.2).

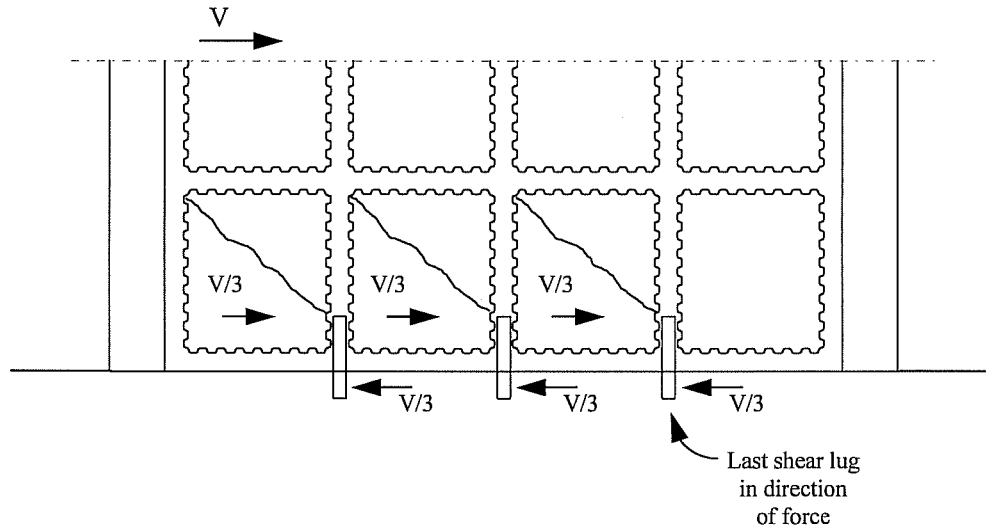


Figure 7.2: Design Shear Distribution

7.4.1 Frame Connection

Steel pipes (shear lugs) transfer forces between the infill wall/existing frame interface. The surface of the existing frame should be cleaned and laitence removed, but no roughening or scarification of the surface is required. The shear lugs shall be designed as follows.

$$V_n^{Pipe} = 0.6A_sF_y$$

where:

V_n^{Pipe} = Nominal pipe shear strength of one pipe

A_s = Cross-sectional area of pipe

F_y = Yield strength of pipe steel

The pipe must be properly embedded on each side of the wall/frame interface to ensure that the shear yielding capacity can be achieved. Proper embedment can be determined from concrete bearing on the projected area of the steel pipe as shown in Figure 7.3.

$$\alpha V_n^{Pipe} = \phi \left(0.85 f'_c \sqrt{\frac{A_2}{A_1}} \right) \phi_{OD} d$$

where:

V_n^{Pipe} = Nominal pipe shear strength

$\alpha \geq 1.25$ (Overstrength factor)

$\phi = 0.7$ for concrete bearing

f'_c = Compressive strength of concrete

ϕ_{OD} = Outside diameter of steel pipe

d = embedment depth

$$\sqrt{\frac{A_2}{A_1}} \leq 2 \text{ (Confinement factor)}$$

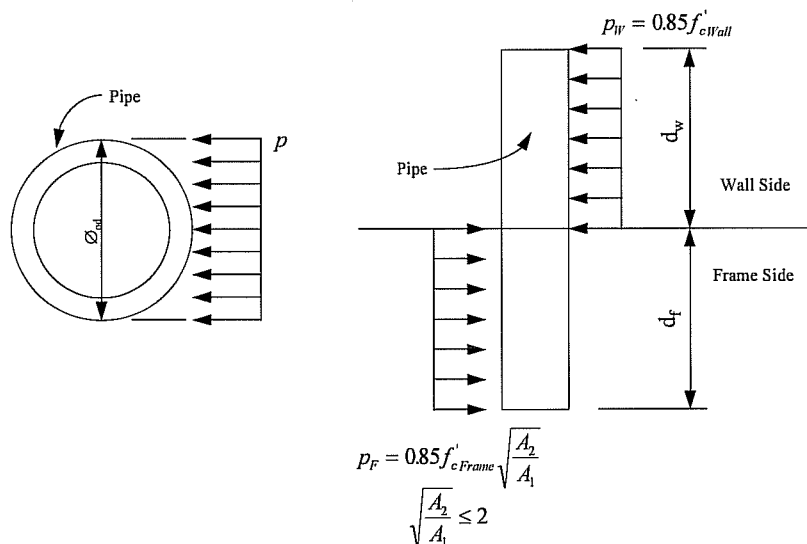
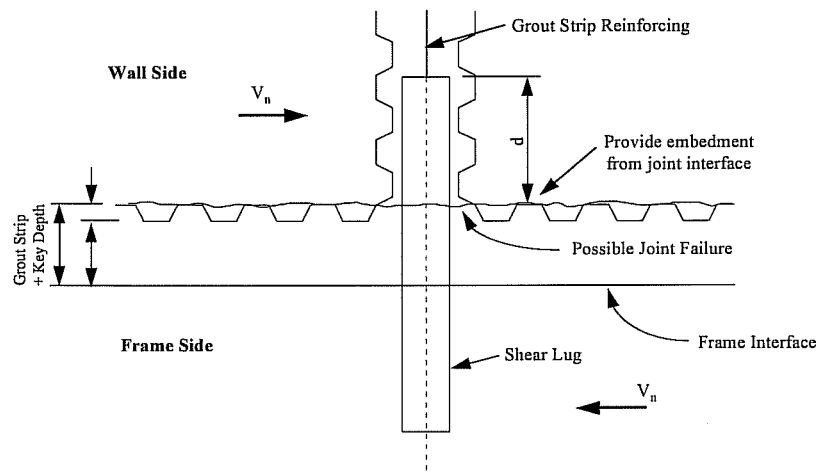


Figure 7.3: Embedment Determination

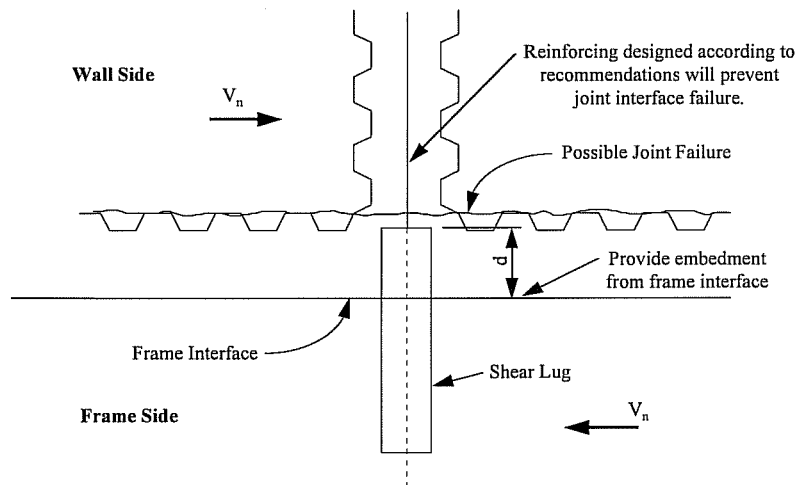
Discussion:

The capacity of the shear lugs is determined from the shear yielding capacity of the pipe. Proper embedment must be achieved on both the wall and frame side for shear yielding capacity to be reached. Proper embedment can be determined based on concrete bearing on the projected area of the steel pipe. Concrete bearing strength is calculated according to ACI 318-89,^[3] Section 10.15. An overstrength factor is applied to the nominal pipe capacity to account for material overstrength. A minimum of 1.25 is recommended, but higher values may be appropriate depending on the pipe stock. It is recommended that the $\sqrt{\frac{A_2}{A_1}}$ factor used to increase bearing strength for confinement effects be neglected in the wall side (grout joint) embedment calculation due to the small cover near the pipe. Background for these design recommendations can be found in Chapter 3.

It was previously suggested that the pipe embedment lengths begin above the grout strip joint to eliminate the possibility of failure at this location as shown in Figure 7.4. Using the capacity design approach recommended, it is found that the amount of vertical and horizontal strip reinforcement required according to the design recommendations for the panel connection (Section 8.4.1.3) provides adequate steel in the grout strip to eliminate an interface shear failure at the grout strip joint. Therefore, embedment lengths can be determined from the existing frame/wall interface and are not required to be increased by the dimension of the grout strip.



Original Recommendation to Prevent Joint Interface Failure



Final Recommendation

Figure 7.4: Comparison of Frame Connection Recommendations

7.4.2 Precast Panels

Shear strength of the individual precast panels shall be greater than the capacity of a shear lug. Panel shear strength shall be determined in accordance with ACI 318-89,^[3] Section 21.7.3.

$$\phi V_n^{Panel} \geq \alpha V_n^{Pipe}$$

where:

V_n^{Panel} = Nominal panel shear strength (ACI 318-89,^[3] Section 21.7.3)

V_n^{Pipe} = Nominal pipe shear strength

$\phi = 0.85$ for concrete shear strength

$\alpha \geq 1.25$ (Overstrength factor)

Shear keys spaced as shown in Figure 7.5 should be used along the perimeter of the panel to provide for force transfer between panels. Additionally, a minimum 4 in. separation should be used between adjacent panels.

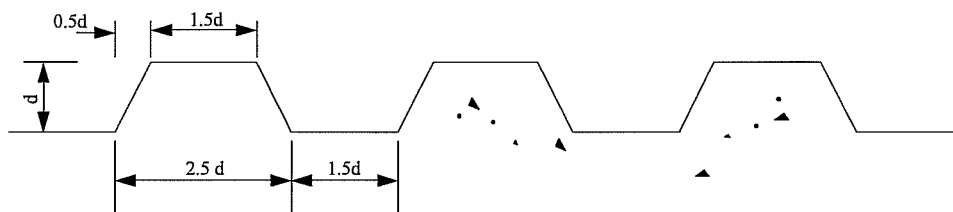


Figure 7.5: Shear Key Pattern

Discussion:

For the shear lugs to reach their shear yielding capacity, adjacent panels are required to transfer the force to the pipe as shown in Figure 7.2. Therefore, the panels should have a shear strength equal to or greater than the pipe capacity. An overstrength factor is used for the pipe strength to account for pipe yield capacities greater than the minimum specified strength.

There does not seem to be a cost advantage to providing a wide shear key spacing. The key configuration recommended provides for uniform shear transfer

between the grout and the panels. The depth of the keys can be varied for ease of construction. Testing indicated that the shear key size does not have a significant effect as long as the key geometry (same shape of key) is maintained. Key depths in the range of 1 in. to 1-1/2 in. are recommended. Finally, a minimum separation is recommended to provide adequate clearance for placement of reinforcing steel and grout flow.

7.4.3 Panel Connection

Panel connection joints shall be designed to provide adequate shear transfer between adjacent panels. Therefore, the joint can be designed to be the same as that of the precast panel. The grout strength used in the panel connection should be greater than the panel strength.

$$\phi V_n^{Joint} \geq \alpha V_n^{Pipe}$$

$$V_n^{Joint} = A_{vf} f_y \mu$$

where:

V_n^{Joint} = Nominal joint shear strength

V_n^{Pipe} = Nominal pipe shear strength

ϕ = 0.85 for shear

$\alpha \geq 1.25$ (Overstrength factor)

A_{vf} = Cross-sectional area of vertical joint reinforcement

f_y = Yield strength of reinforcing steel

μ = 1.4 (Coefficient of friction)

Discussion:

The strength of the connection between adjacent panels can be provided using interface steel crossing the joint. The amount of steel can be determined using the shear friction design approach. The coefficient of friction recommended (1.4) was verified by testing of the joint (Chapter 2) and by system testing (Chapter 6).

High variability can be expected in the grout due to field mixing and grouting techniques. The precast panels are likely to be constructed under a more controlled environment where a higher quality product can be fabricated. Therefore, the grout strength should be designed greater than the panel strength.

7.5 Performance Based Design Criteria

Designers are gradually adopting performance based design criteria also known as limit states for the design of new and rehabilitated structures. Using this approach, the structure can be designed to meet different performance requirements established by the owner and/or dictated by occupancy of the structure. Typical limit states commonly used are listed below.

Service Limit State: The building should remain functional without damage under an earthquake ground motion selected to represent service levels. Structural response should remain elastic for this limit state.

Damage Limit State: The building should experience no structural damage, but nonstructural damage is possible following earthquake ground motion at damage levels. Drifts producing damage to both structural and nonstructural elements should be identified so that the damage can be mitigated through design. Structural response for this limit state should also remain primarily in the elastic range.

Collapse Limit State: The building should resist an earthquake ground motion having an intensity equal to the strongest either experienced or

forecast without collapse. The collapse limit state has been previously discussed since this is the design basis for current building codes.

Several features of the precast infill wall system are discussed below that may be helpful to designers in achieving desired performance objectives in rehabilitation. In particular, drift control is discussed along with shear behavior prior to splice failure of the boundary elements.

7.5.1 Drift Control

7.5.1.1 Decompression Moment

In order to control drifts, the post-tensioning can be designed so that the decompression moment is greater than or equal to the moment applied to the wall. By keeping the applied moments below the decompression moment, test results indicate that the shear wall gross stiffness is effective in resisting lateral forces. The equation presented below for the decompression moment assumes pure axial compression on the wall due to the post-tensioning system.

$$M \leq M_{DC} = P \left(\frac{l_w}{2} \right)$$

where:

M = Applied moment

M_{DC} = Decompression moment

P = Post-tensioning force acting on wall cross-section

l_w = Length of wall

Deflection criteria can be checked based on elastic analysis of the wall using the gross moment of inertia (I_g) and an uncracked shear area equal to the web area (A_{sh}).

$$\Delta_T = \Delta_G$$

where:

Δ_T = Total deflection from lateral forces

Δ_G = Deflection up to decompression, (I_g, A_{sh})

7.5.1.2 Splice Failure

Post tensioning can be designed to maintain the design moment at or below moment corresponding to splice failure. Keeping the moment below the level at which splice capacity is reached can eliminate structural damage to the wall. Tests on the wall system demonstrated that behavior remained nearly elastic prior to splice failure and the wall maintained excellent stiffness characteristics thereby controlling structural as well as nonstructural damage in the existing structure.

$$M \leq M_{Splice}$$

where:

M = Applied Moment

M_{Splice} = Moment capacity of wall system at failure of column splice

Wall deflections can be computed through the addition of the deflection at the decompression load and the additional deflections generated for loading beyond the decompression load.

$$\Delta_T = \Delta_{DC} + \Delta_{Cr}$$

where:

Δ_T = Total deflection from lateral forces

Δ_{DC} = Decompression deflection, (I_g, A_{sh})

Δ_{Cr} = Deflections beyond decompression, (I_{cr}, A_{sh}) up to splice failure

Tests results presented in Chapter 6 indicated that the approach outlined above provides a reasonable estimate of the load-displacement response. Gross sectional properties should be used up to the decompression moment while cracked sectional properties should be used beyond the decompression moment. Shear deformations should be accounted for using a shear area corresponding to the web area or a reduced web area to account for shear cracking as deemed appropriate for the wall.

7.5.1.3 Drift at the Collapse Limit State

Design drift levels can be checked using a strut and tie model of the wall. Based on the research conducted, diagonal compression having a width of 1/3 the web length should provide a reasonable estimate of the post decompression stiffness.

$$\Delta_T = \Delta_{DC} + \Delta_{ST}$$

where:

Δ_T = Total deflection from lateral forces

Δ_{DC} = Decompression deflection, (I_g, A_{sh})

Δ_{ST} = Deflections beyond decompression (Strut and tie model)

Test results presented in Chapter 6 indicated that analysis based on the recommendations provided reasonable estimates of the load-displacement response. The calculations in Chapter 6 illustrate the use of the strut and tie method for deflection calculations.

7.5.2 Shear Strength Prior To Splice Failure

Prior to splice failure, interface shear capacity can be considered as the combination of shear resistance available from the shear lugs and the boundary element at the wall “toe.” Monolithic wall behavior can be assumed with the entire wall length considered effective in resisting shear.

The boundary elements should be intact without damage prior to splice failure. Therefore, shear transfer at the boundary elements should be available and can be accounted for in design. In most cases, the boundary element (existing column) will have a construction joint at the base that provides a roughened surface for consideration of shear friction. Shear at this location can be accounted for by the shear friction provisions of ACI^[3] Section 11.7. It is recommended that only the compression force contribution to shear friction be used since the column steel cannot be fully developed in tension. An example calculation of the base shear prior to splice failure is presented in Figure 7.6. In the calculations, a conservative estimate of the shear strength was determined by only accounting for the compression from the post-tensioning; compression from the overturning moment was neglected.

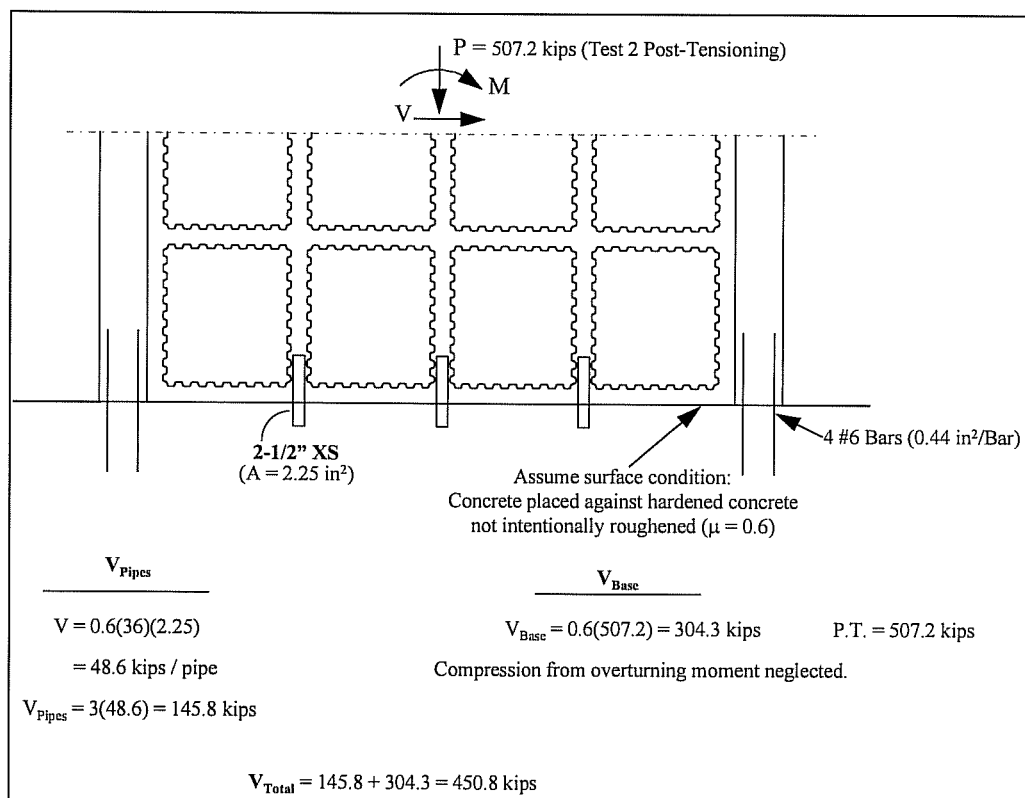


Figure 7.6: Base Shear Capacity Prior to Splice Failure

Additionally, the shear resistance was conservatively estimated using a coefficient of friction of 0.6 ($\mu=0.6$) which corresponds to concrete placed against hardened concrete not intentionally roughened.

The shear capacity of the wall can be checked according to ACI 319-89,^[3] Section 21.7.3 for shear strength of structural walls. The entire wall should be effective in resisting the shear and can be checked accordingly. Only the horizontal strip steel should be accounted for in design, however, since it provides the only continuous steel in the wall. An example calculation for the model test structure is presented in Figure 7.7. Considering the concentrated steel used in the grout strips, it is convenient to investigate a 45 degree failure plane as assumed in the code. Strip steel crossing the surface that can be fully developed may be assumed effective in resisting shear. As previously mentioned, the panel steel was neglected since it was not continuous. The concrete and steel contribution to shear strength were calculated separately.

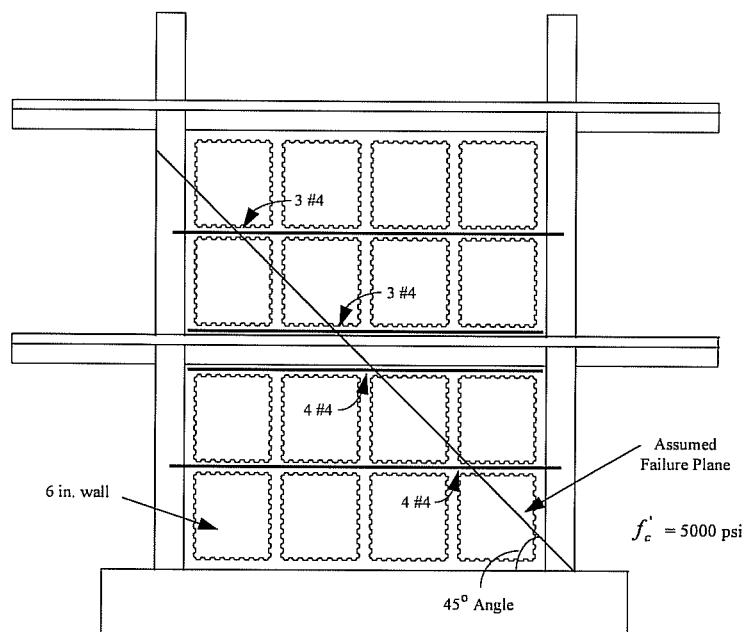


Figure 7.7(a): Assumed Failure Plane For Analysis

$$\phi V_n = \phi A_{cv} (\alpha_c \sqrt{f'_c} + \rho_n f_y) \quad \text{Eq. 21-7 (ACI 318-89)}$$

Concrete Contribution

$$\begin{aligned} V_c &= A_{cv} \alpha_c \sqrt{f'_c} & \alpha_c &= 3.0 \text{ for Short Wall} \\ &= (1032(3)\sqrt{5000}) \frac{1}{1000} & A_{cv} &= (6'')(172'') = 1032 \text{ in}^2 \\ &= 218.9 \text{ kips} \end{aligned}$$

Steel Contribution

$$V_s = A_{cv} \rho_n f_y \quad \longrightarrow \quad \text{Use steel in strips based on } 45^\circ \text{ failure plane.}$$

First Story: 8 #4

Second Story: 6 #4

$$14 \text{ #4 Bars} \quad (14)(0.2 \text{ in}^2)(60 \text{ ksi}) = 168.0 \text{ kips}$$

$$V_n = 218.9 + 168.0 = 387 \text{ kips}$$

$$V_n = 387 \text{ kips}$$

Figure 7.7(b): Wall Shear Capacity Prior to Splice Failure

CHAPTER 8

SUMMARY AND CONCLUSIONS

8.1 Introduction

Many reinforced concrete moment resisting frame buildings in seismic zones lack strength and ductility. Several rehabilitation techniques have proven to be constructible and economically feasible for many structures. However, the cost of such rehabilitation projects remains a major problem for many owners. The costs may involve not only the actual construction, but the expenses associated with relocation of operations and loss of rental revenue or production during the period of construction.

A new rehabilitation scheme is needed that will not only correct the “weak links” in a nonductile frame system, but will simplify the construction process; reduce the time, cost, and inconvenience of construction; and reduce the obstruction to functional use of the structure both during and after construction. To fulfill these objectives, a precast infill wall system was developed. The infill wall can be built of precast wall units that will allow facilitation of construction and elimination of many procedures required for cast-in-place construction.

To develop design and detailing guidelines for the precast infill wall system, three phases of experimental research were conducted. The first phase of research investigated the connection of precast panels to one another while the second phase investigated the connection of precast panels to existing frame members. The third phase assessed the overall behavior of the precast system and verified connection details developed in the first two phases.

8.2 Panel-to-Panel Connection

Fourteen specimens were tested to investigate the connection between adjacent precast panels. The specimens, representative of an interior wall joint, were tested by applying cyclic shear across the connection interface. In general, failure of the specimens consisted of sliding along the keyed interface with either grout or precast panel keys shearing depending upon the concrete strength in each. The ultimate capacity of the connection was controlled by the lower concrete shear strength (grout or panel) and the amount of vertical reinforcement crossing the joint. After the peak capacity was reached, there was a transition to a lower load plateau or residual capacity that was maintained through large slip levels. The residual capacity was maintained by shear friction which was directly dependent on the amount of vertical reinforcement. The following conclusions were made concerning primary variables investigated.

1. Joint failure occurred at the top of the horizontal grout interface due to lack of adhesion between the panel and the grout caused by air entrapment during grouting of the joint.
2. The shear key configuration (alignment and spacing) had no significant effect on the peak strength and no effect on the residual capacity.
3. The shear key size had no significant effect on the panel peak capacity and no effect on the residual.
4. The spacing of adjacent precast panels did not effect the peak or residual capacity.
5. The relative strength between the grout and panel concrete influenced the joint behavior. The lower strength material controlled the peak capacity and failure surface location. The residual capacity, however, was not affected.

6. The peak and residual capacity of the walls increased directly with the wall thickness.
7. Increasing the vertical reinforcement increased both the peak and residual capacities of the specimen. The capacities could be determined using shear friction theory even though the reinforcement was concentrated in the grout strip. The peak capacity could be determined using a coefficient of friction of 2.75 while the residual capacity could be determined using a coefficient of 1.1. A coefficient of friction of 1.4 was recommended for design.

8.3 Panel-to-Frame Connection

Four specimens were tested to investigate the connection between the precast infill wall panels to elements of the existing building frame. The specimens, representative of the wall boundary joint, were tested by applying cyclic shear along the frame boundary interface. In general, failure of the specimens consisted of interface sliding along with yielding of the steel pipe. Following a peak capacity, there was a transition to a lower load plateau or residual capacity that was maintained at a nearly constant level to extremely large slips. The following conclusions were made:

1. Failure across the precast panel interface similar to the panel connection failure can occur depending on the embedment of the steel lug. To eliminate the possibility of failure at the panel interface, the pipe should be embedded for a length greater than the grout strip to ensure that the pipe crosses the precast panel interface.

2. Proper embedment was required to produce shear yielding of the pipe. Lack of embedment can cause a flexural failure that may reduce the capacity of the specimen. Embedment lengths determined on the basis of concrete bearing on the projected surface of the steel pipe enabled the pipe to yield in shear.
3. Localized bearing failure occurred in the wall adjacent of the pipe at the interface since bearing stresses were not uniform over the depth of the pipe. The local failure did not affect the capacity of the section, but did increase slip level required to regain the shear capacity.
4. The residual capacity could be determined by the shear yield strength of the pipe. For design it is recommended that the entire cross section of the pipe can be considered effective in resisting shear.

8.4 Model Test Structure

A two-story nonductile frame was constructed and rehabilitated with the precast infill wall and post-tensioning system developed in this research. The model structure was constructed with details typical of 1950's and 60's construction. The test structure had a column spacing of 13 ft. - 4 in. and floor heights of 8 ft. which corresponded with a 2/3 scale for typical moment frame buildings investigated. A 6 in. wall was provided in the first story and a 4 in. wall in the second.

8.4.1 Existing Frame

The existing frame was tested to determine its overall behavior and produce cracking in the frame elements to simulate the likely condition of structures prior to rehabilitation. The structure was loaded with a triangular distribution simulating earthquake effects and behaved as predicted by analytical modeling. Analysis and testing demonstrated that the structure had a low lateral resistance and was

nonductile. Structural rehabilitation would be recommended to seismically upgrade a structure of this type.

8.4.2 Precast Infill Wall System

Three tests were performed on the rehabilitated model structure to evaluate the system behavior of the precast infill wall and the post tensioning system used to provide column tensile capacity. Primary variables included the amount of post-tensioning steel and the initial post-tensioning loads. Loads were cyclically applied to the floor slabs in a triangular distribution to simulate earthquake effects. Testing allowed examination of design recommendations for the precast infill wall, post-tensioning system, and panel connections.

The precast wall system performed exceptionally well. Diagonal cracks were continuous through panels and grout strips. There was no indication of distress along grout strips. Shear cracking extended along a line from the “toe” of the wall to the top post-tensioning anchorage. There was some cracking concentrated around the pipe shear lugs between the wall and frame, but failure did not appear to be imminent. Overall, crack patterns indicated that the wall behaved monolithically even though it was constructed of multiple units and both the panel and frame connections performed according to design. At ultimate, the shear strength of the structure was controlled by concrete crushing of the primary compression strut; no interface or diagonal shear failures occurred that limited the shear capacity in either the first or second story wall.

The post-tensioning system performed according to design. Testing demonstrated that the splice capacity of the existing frame could be controlled with the initial post-tensioning force. Following splice failure, a large crack formed at the base of the wall with the wall/frame system rotating nearly as a rigid body around the “toe” of the wall in the direction of applied load due to the unbonded tendons. The

flexural capacity of the structure during this stage of behavior was determined by the yield strength of the post-tensioning steel.

8.5 Design Guidelines

Design and detailing guidelines for the precast infill wall system were developed to provide designers with a method for proportioning various elements of the precast infill wall system. The guidelines presented in Chapter 7 cover design of the precast infill wall, connections between the infill and the existing frame, and the post tensioning system along with general design considerations. Additionally, a discussion of using the infill wall system for performance-based design criteria is presented.

8.6 Future Research

The research presented in this report was developed for the rehabilitation of nonductile concrete moment frame structures since these structures have been identified as a threat to life safety. Steel moment frame structures are also vulnerable to undesirable behavior during an earthquake. Frames designed for gravity or wind loads only and frames with questionable welded joints could be strengthened using precast infills.

Strengthening or repair of joints within an occupied structure pose problems similar to those experienced in the rehabilitation of nonductile concrete structures that were addressed in the development of the precast infill wall system. Therefore, the use of this rehabilitation method for retrofitting steel moment frame structures should be investigated. The infill wall system can be used as an alternate lateral force resisting system for the structure to eliminate the need for repair of inadequate connections or frame elements.

The primary focus of future research should address the connection of the infill wall to the existing steel frame. Connection methods such as studs welded around the perimeter may be viable alternatives to the use of a shear lug.

8.7 Conclusion

The precast infill wall system developed in this research may eliminate many of the costly and time-consuming procedures currently used in cast-in-place infill wall construction. The precast system should provide engineers with a technique that offers the potential to reduce overall costs of rehabilitating existing structures while allowing the rehabilitation to be tailored to the requirements of the owner. Furthermore, the system can be used to decrease nonstructural damage and costs associated with the damage and to increase life safety.

APPENDIX A
PANEL CONNECTION TEST RESULTS

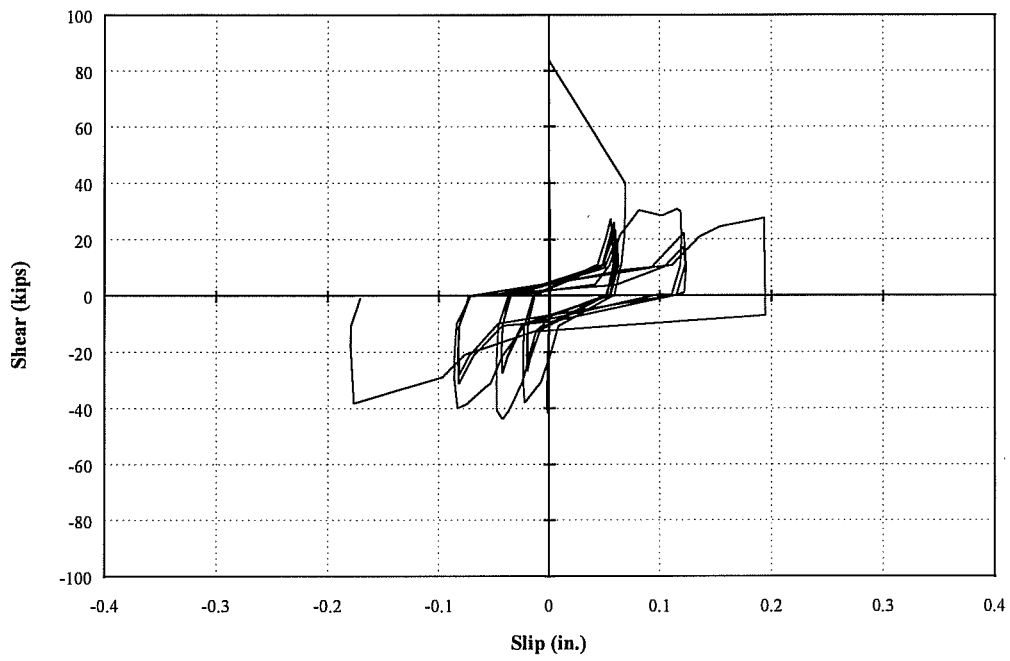


Figure A.1: PC-1 Test Result

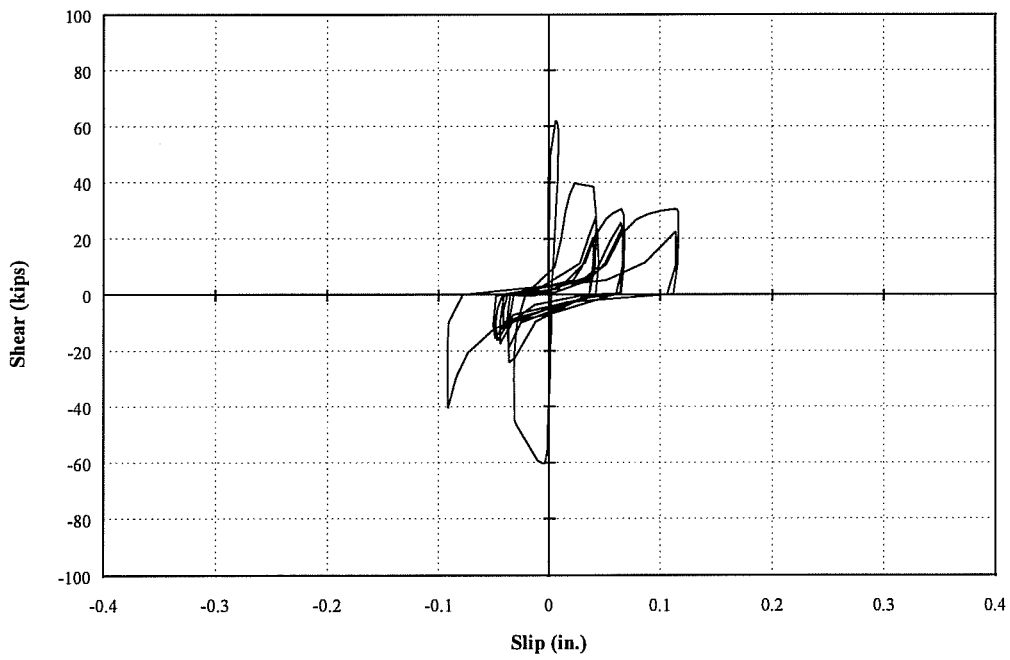


Figure A.2: PC-2 Test Result

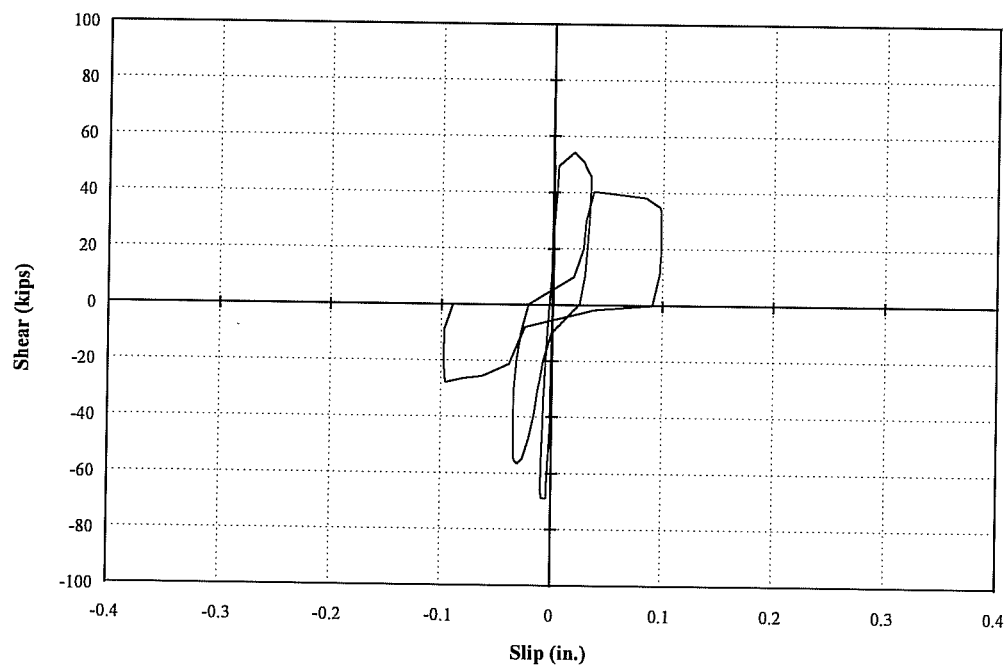


Figure A.3: PC-3 Test Result

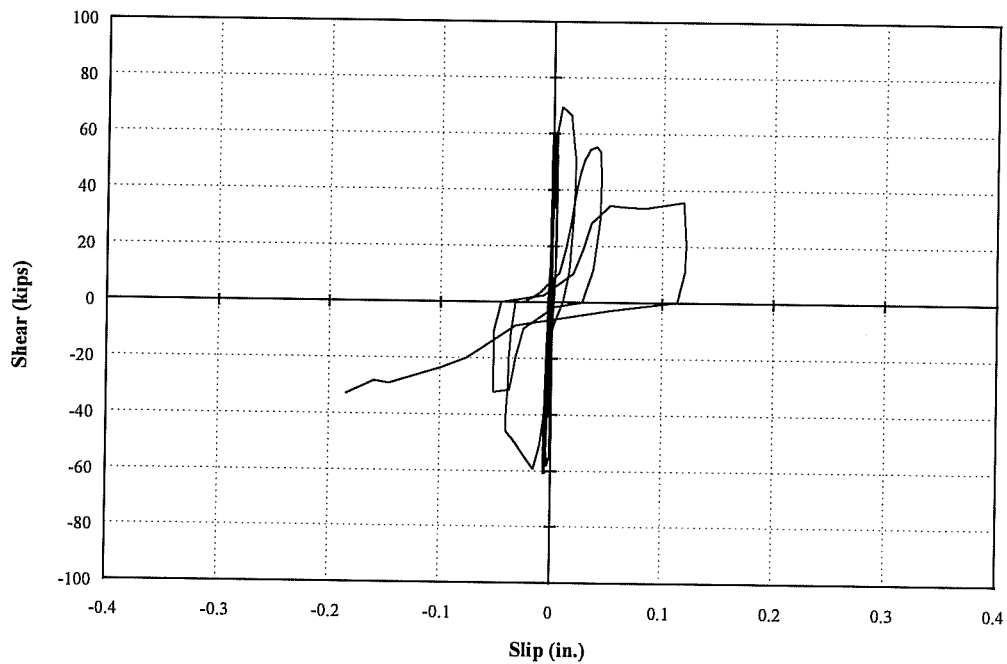


Figure A.4: PC-4 Test Result

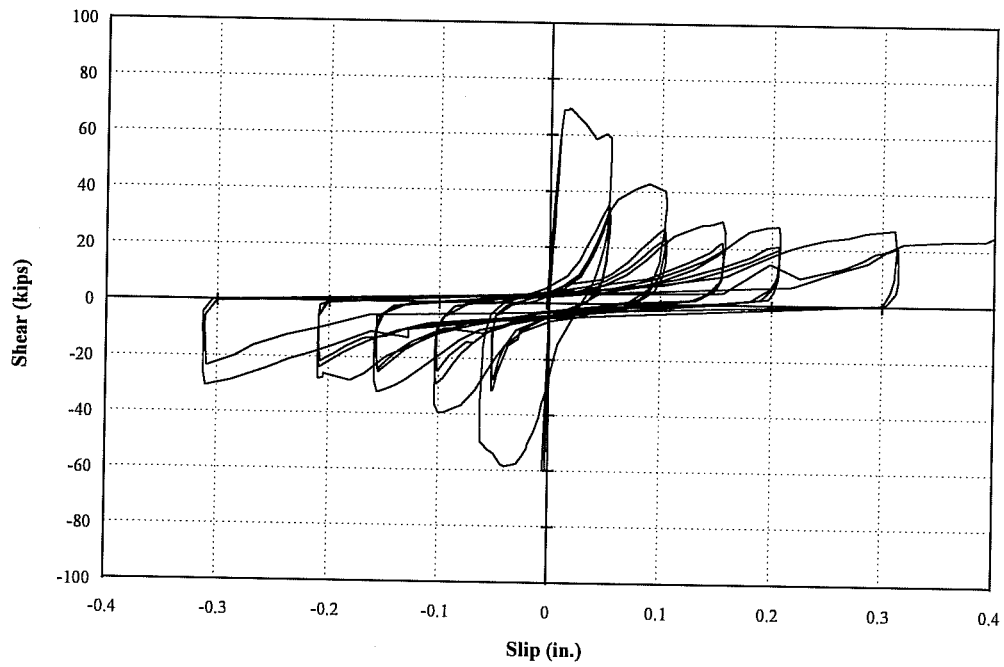


Figure A.5: PC-5 Test Result

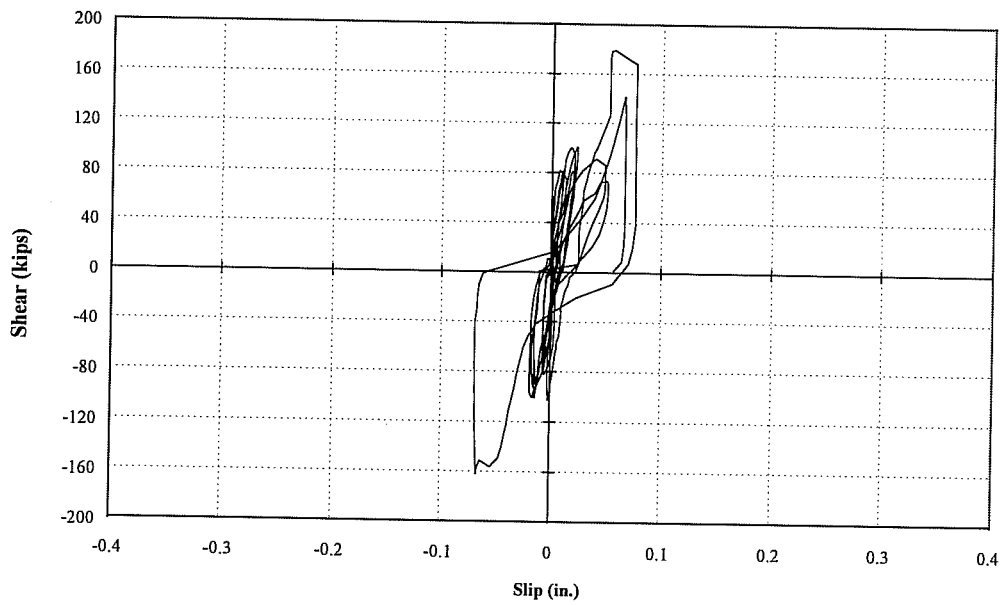


Figure A.6: PC-6 Test Result

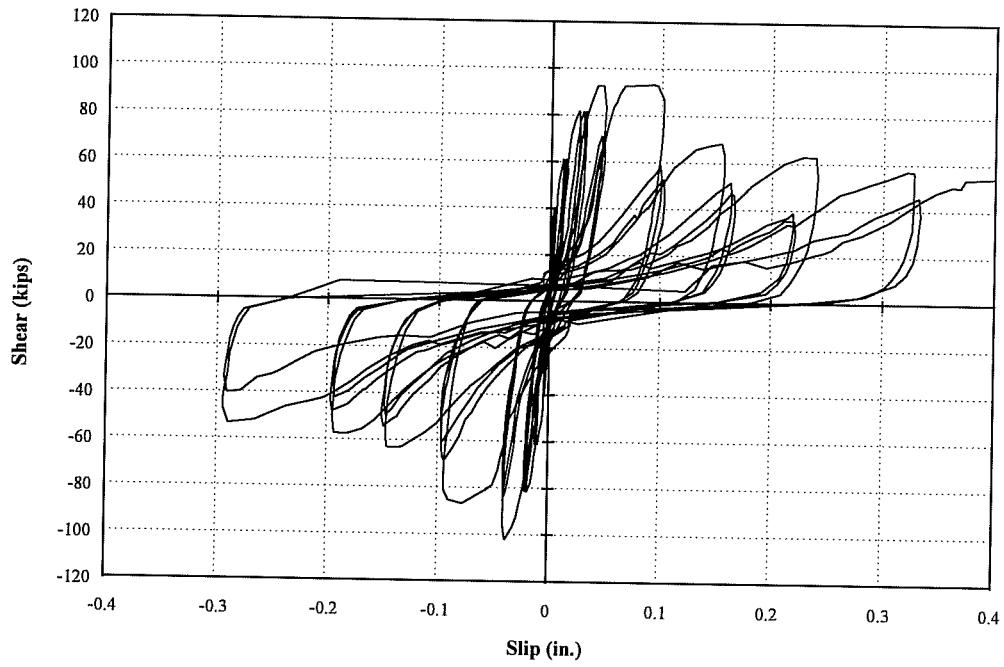


Figure A.7: PC-7 Test Result

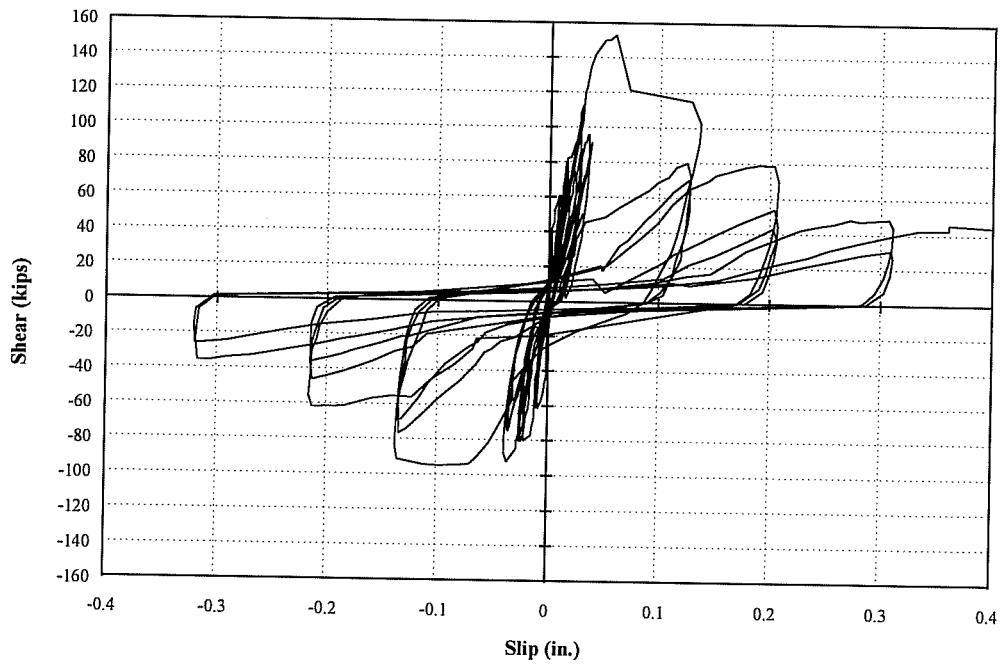


Figure A.8: PC-8 Test Result

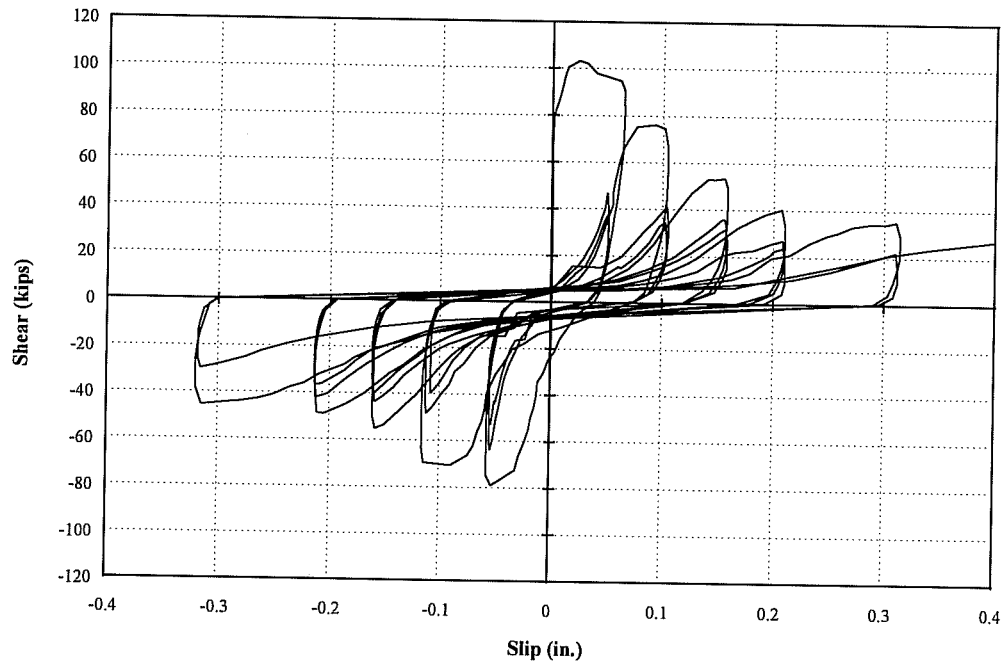


Figure A.9: PC-9 Test Result

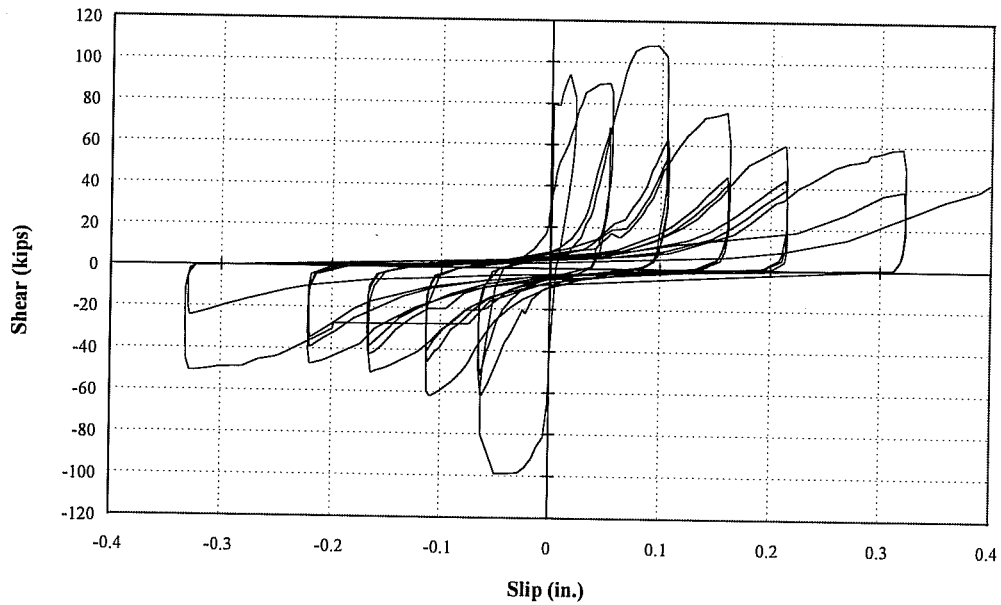


Figure A.10: PC-10 Test Result

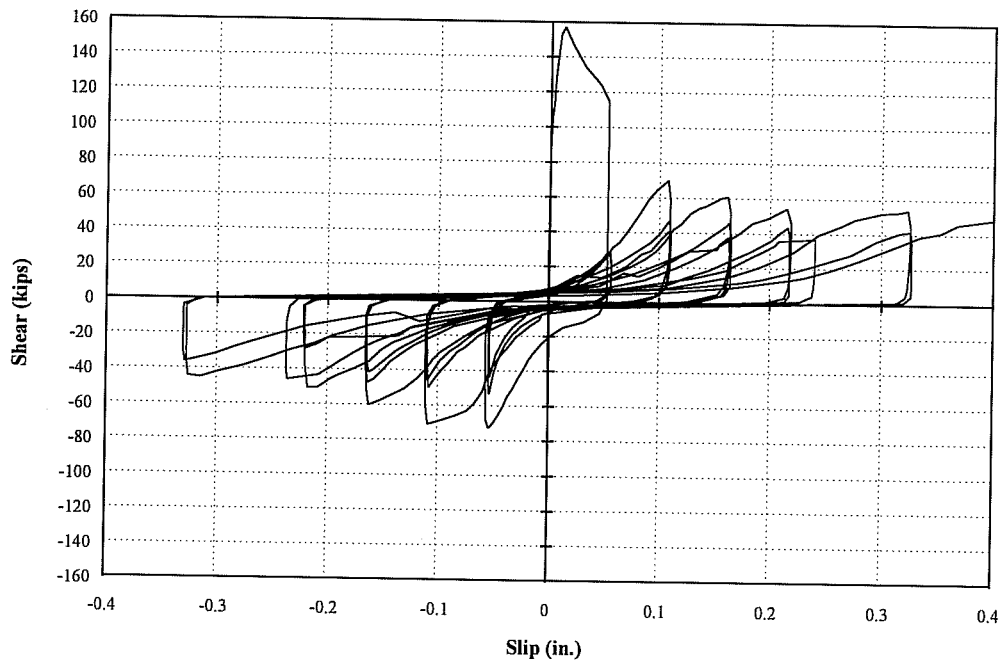


Figure A.11: PC-11 Test Result

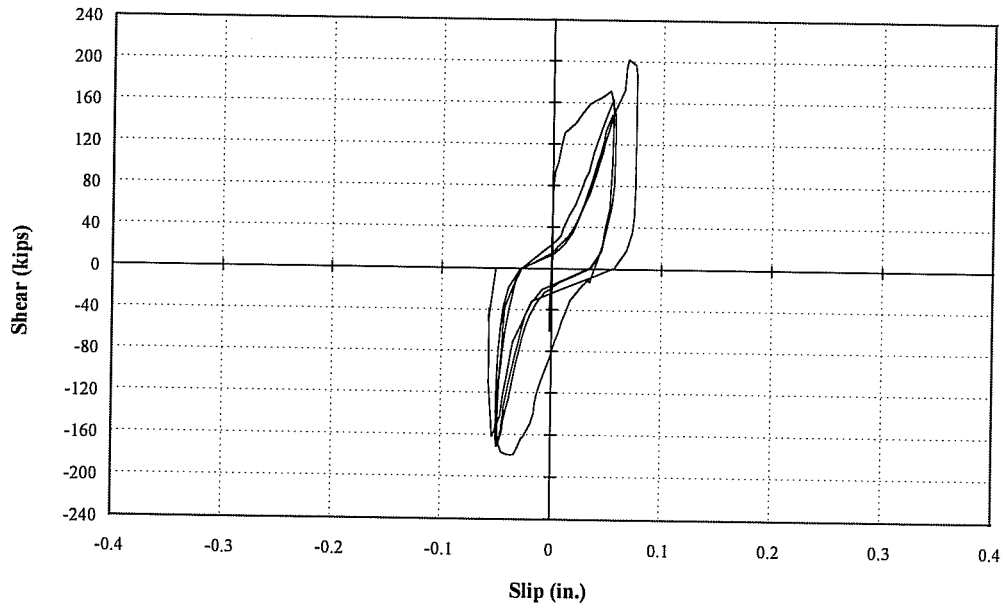


Figure A.12: PC-12 Test Result

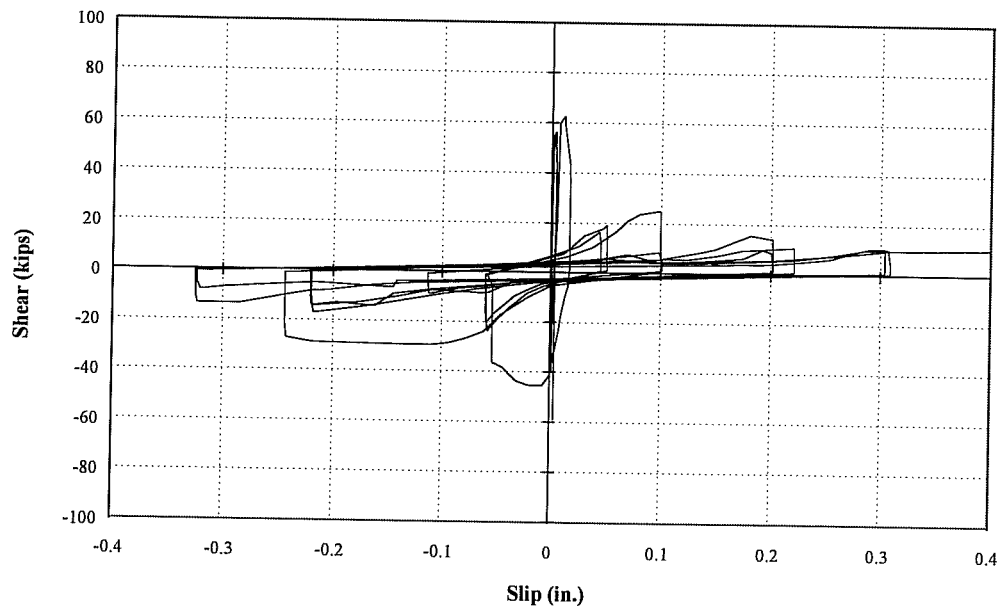


Figure A.13: PC-13 Test Result

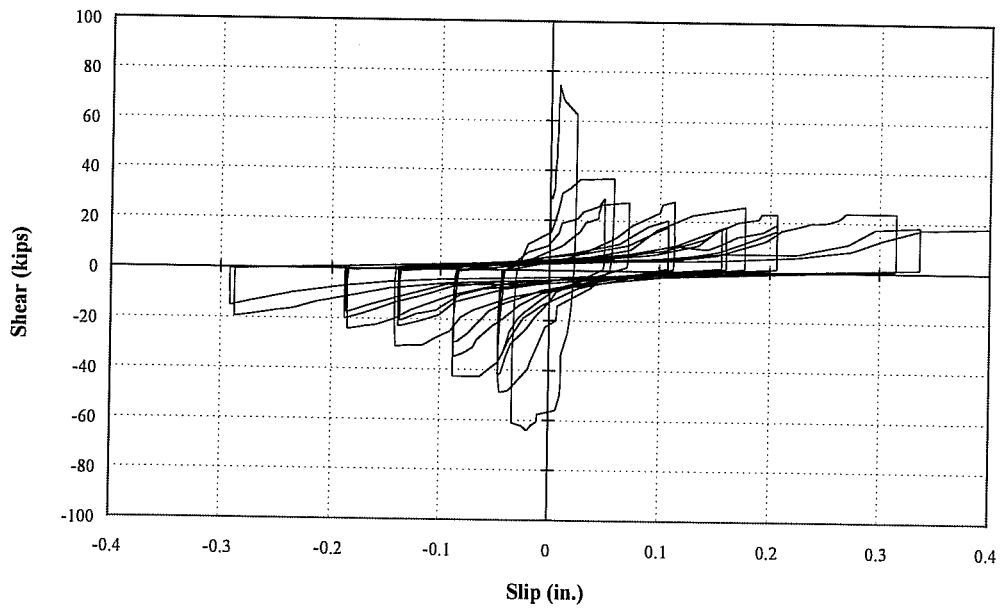


Figure A.14: PC-14 Test Result

APPENDIX B
FRAME CONNECTION TEST RESULTS

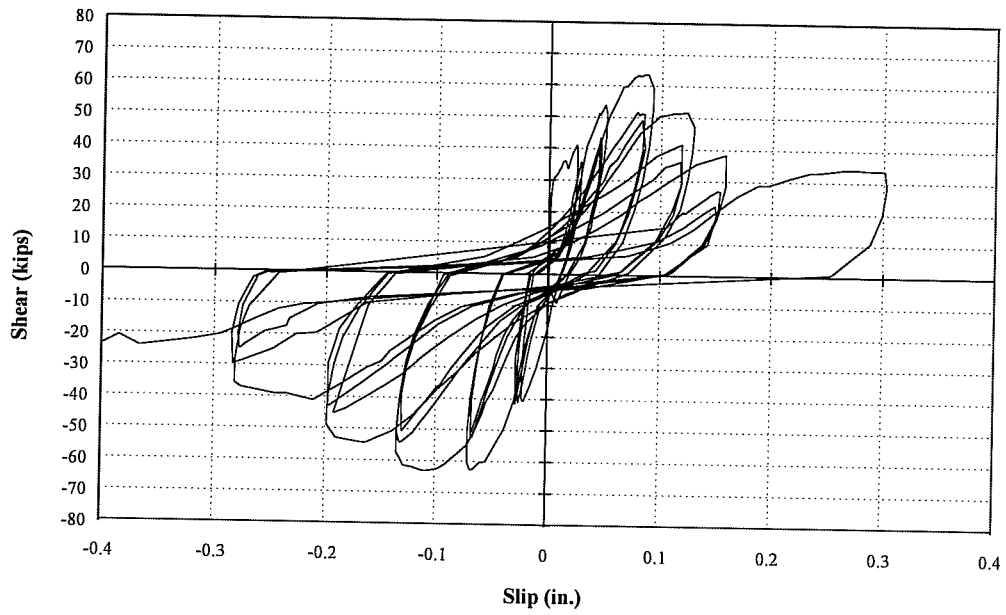


Figure B.1: FC-1 Test Result

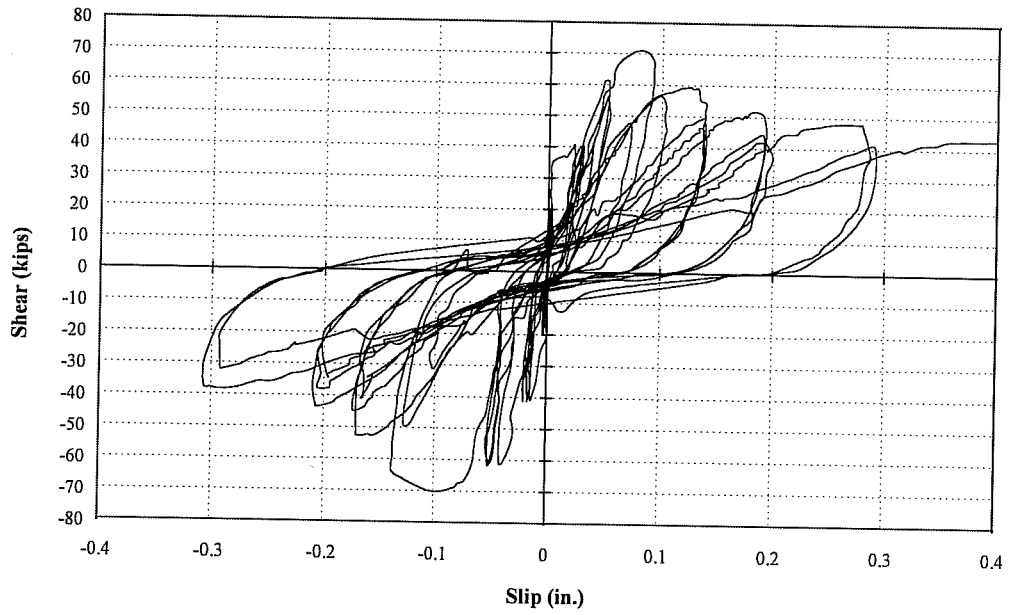


Figure B.2: FC-2 Test Result

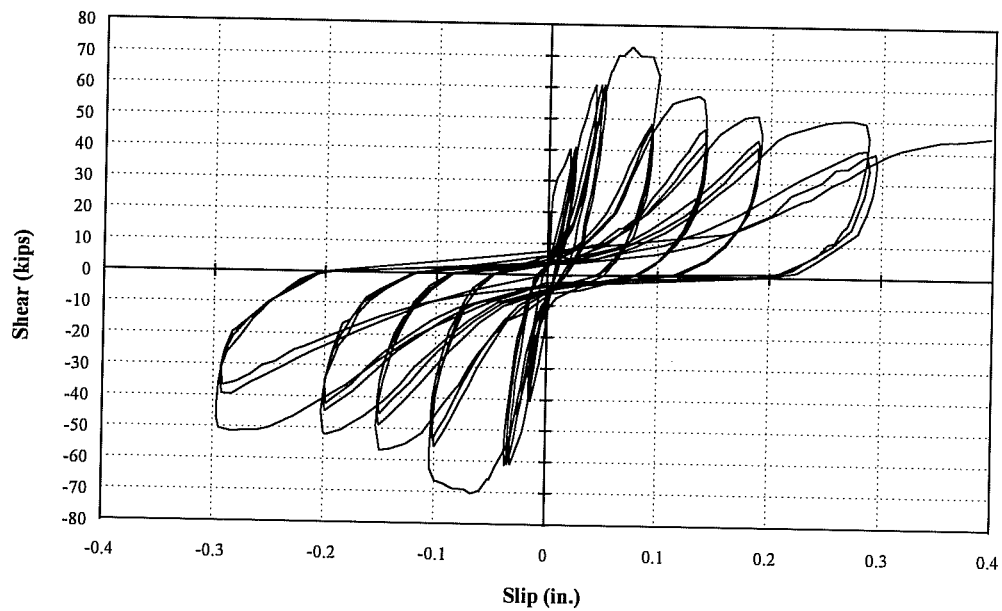


Figure B.3: FC-3 Test Result

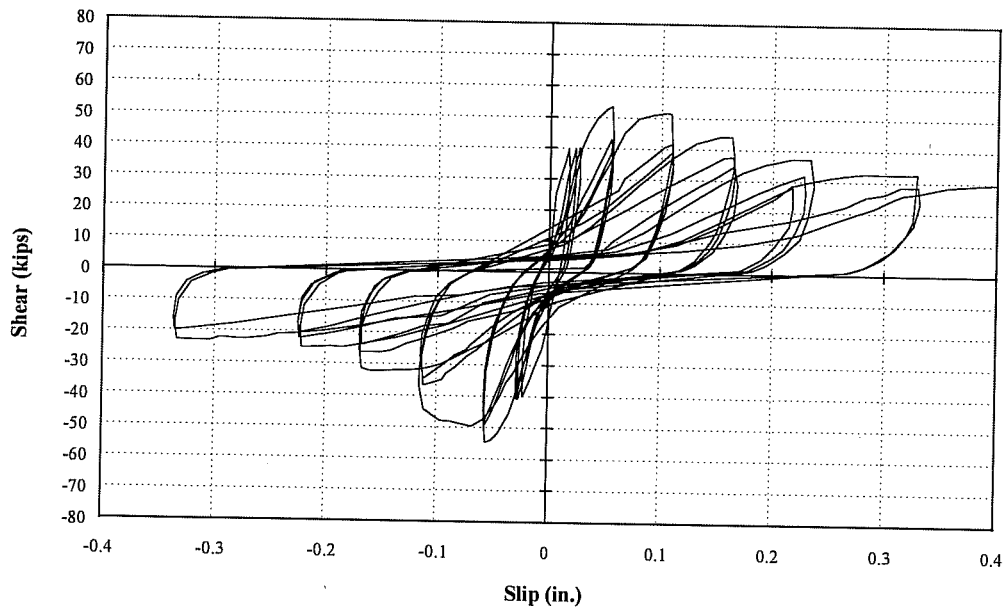
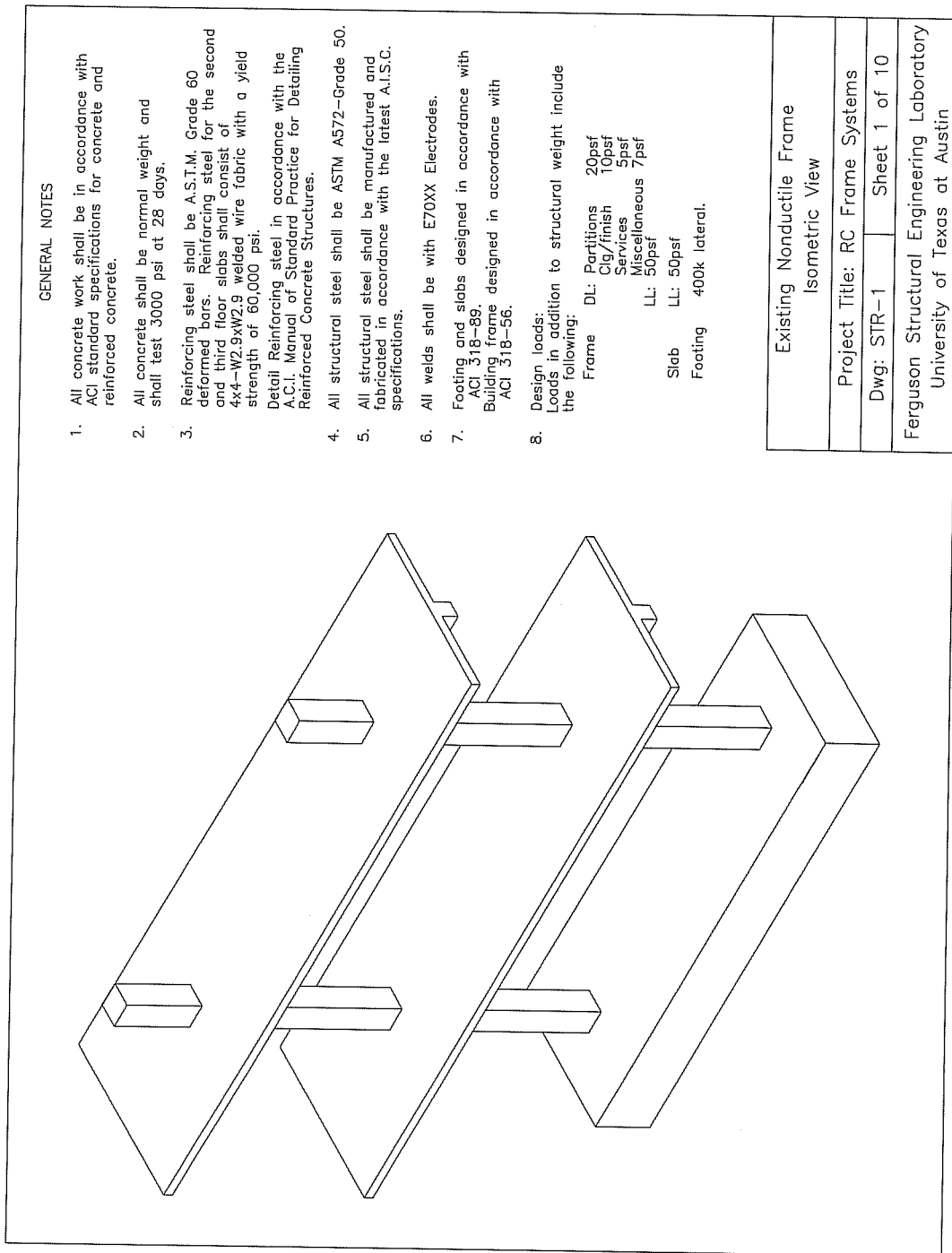


Figure B.4: FC-4 Test Result

APPENDIX C
FRAME STRUCTURAL DRAWINGS



GENERAL NOTES

1. All concrete work shall be in accordance with ACI standard specifications for concrete and reinforced concrete.
2. All concrete shall be normal weight and shall test 3000 psi at 28 days.
3. Reinforcing steel shall be ASTM Grade 60 deformed bars. Reinforcing steel for the second and third floor slabs shall consist of 4x4-W2.9xW2.9 welded wire fabric with a yield strength of 60,000 psi.
Detail Reinforcing steel in accordance with the A.C.I. Manual of Standard Practice for Detailing Reinforced Concrete Structures.
4. All structural steel shall be ASTM A572-Grade 50.
5. All structural steel shall be manufactured and fabricated in accordance with the latest A.I.S.C. specifications.
6. All welds shall be with E70XX Electrodes.
7. Footing and slabs designed in accordance with ACI 318-89.
Building frame designed in accordance with ACI 318-56.

8. Design loads:
Loads in addition to structural weight include the following:

Frame	DL: Partitions	20psf
	Clg/finish	10psf
	Services	5psf
	Miscellaneous	7psf
	LL:	50psf
Slab	LL:	50psf
Footing		400k lateral.

Existing Nonductile Frame	
Isometric View	
Project Title: RC Frame Systems	
Dwg: STR-1	Sheet 1 of 10
Ferguson Structural Engineering Laboratory University of Texas at Austin	

Figure C.1: Isometric View

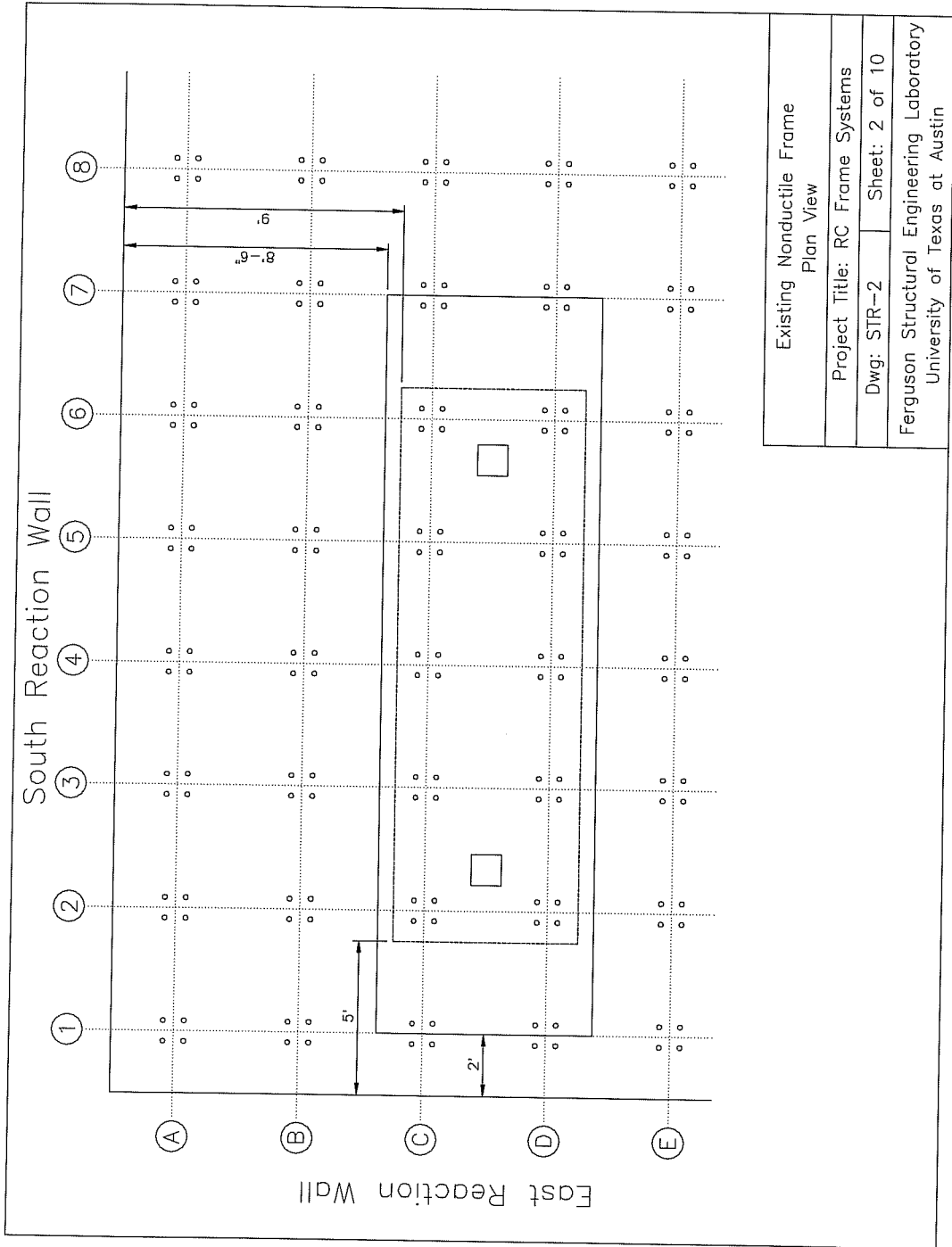


Figure C.2: Plan View

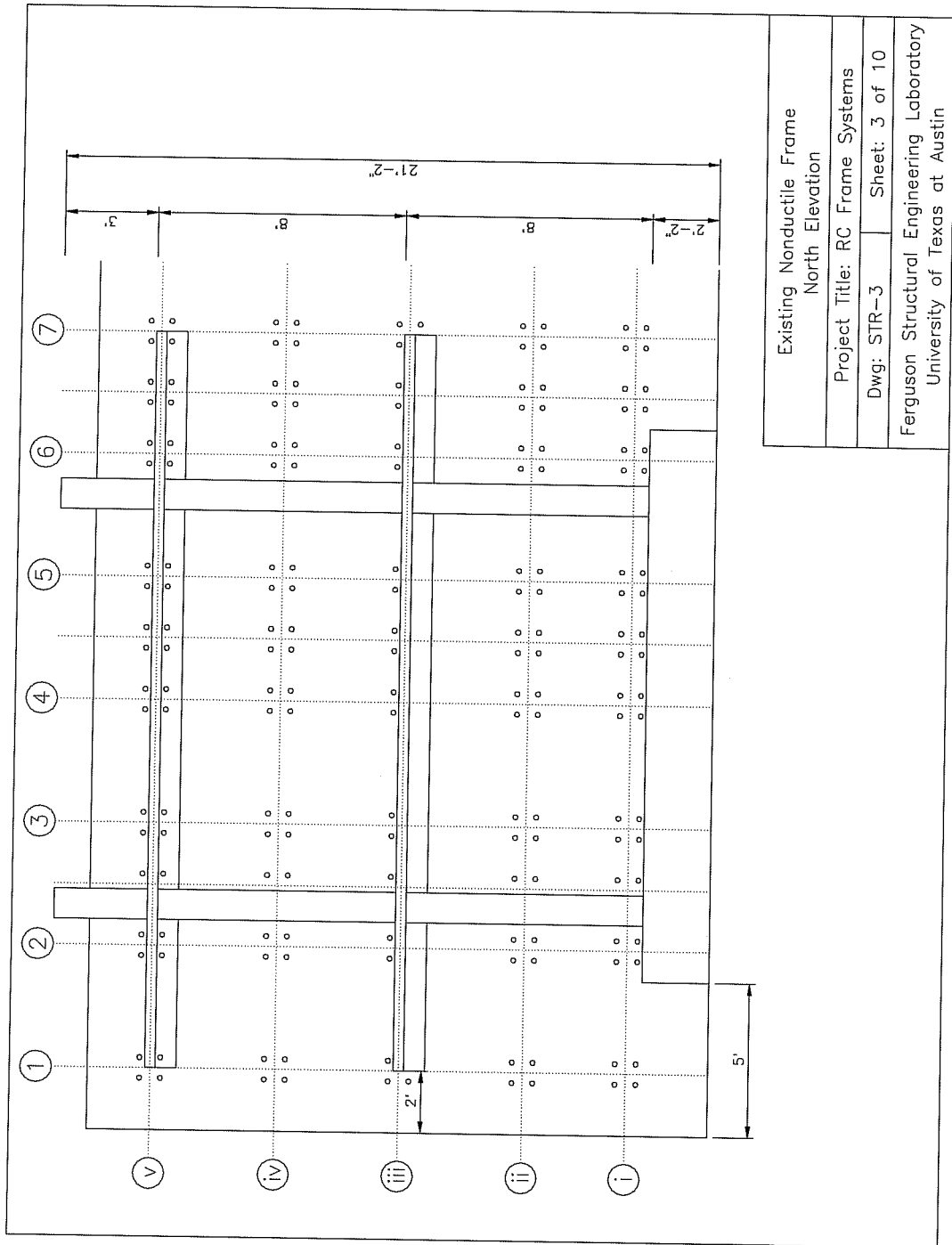


Figure C.3: North Elevation

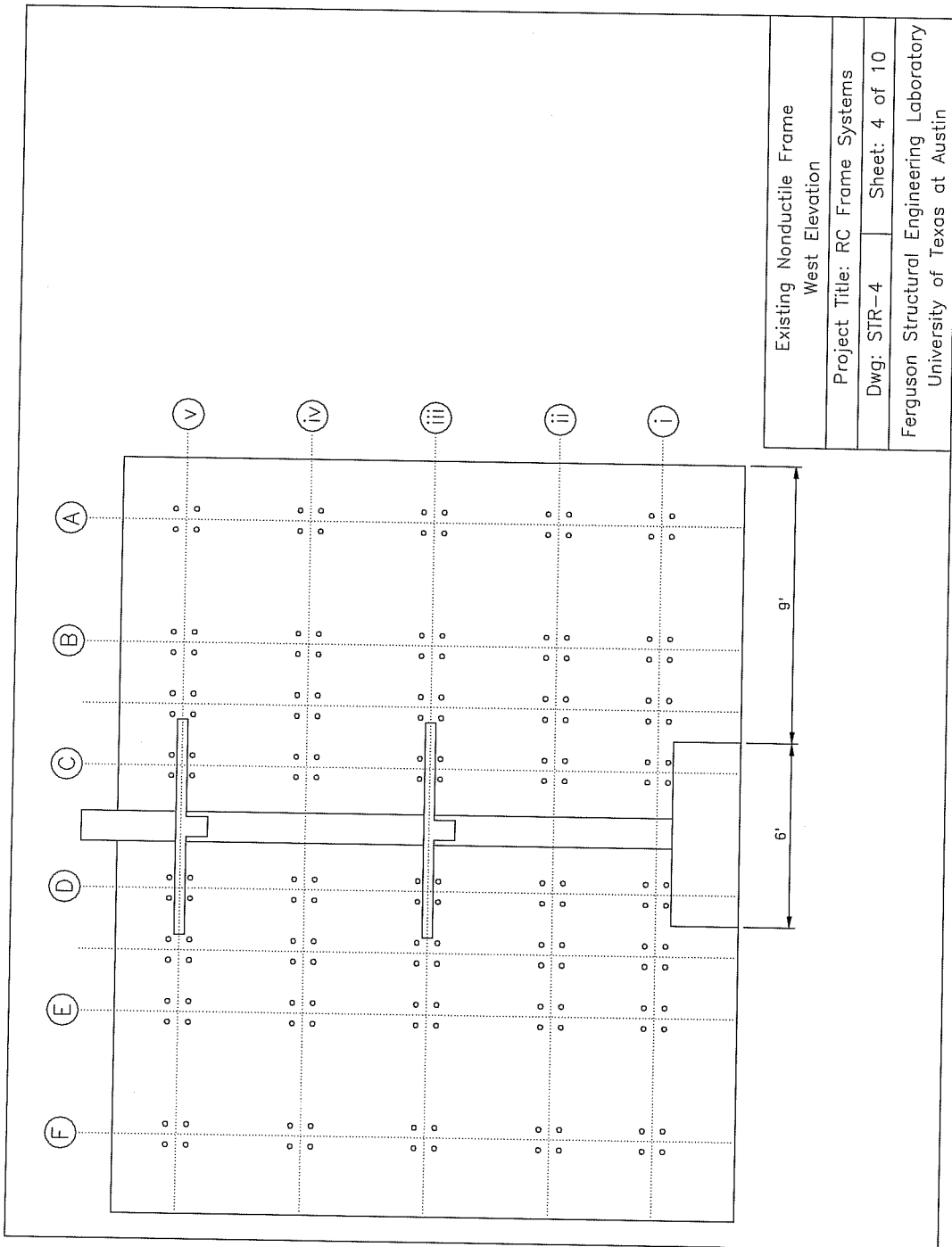


Figure C.4: West Elevation

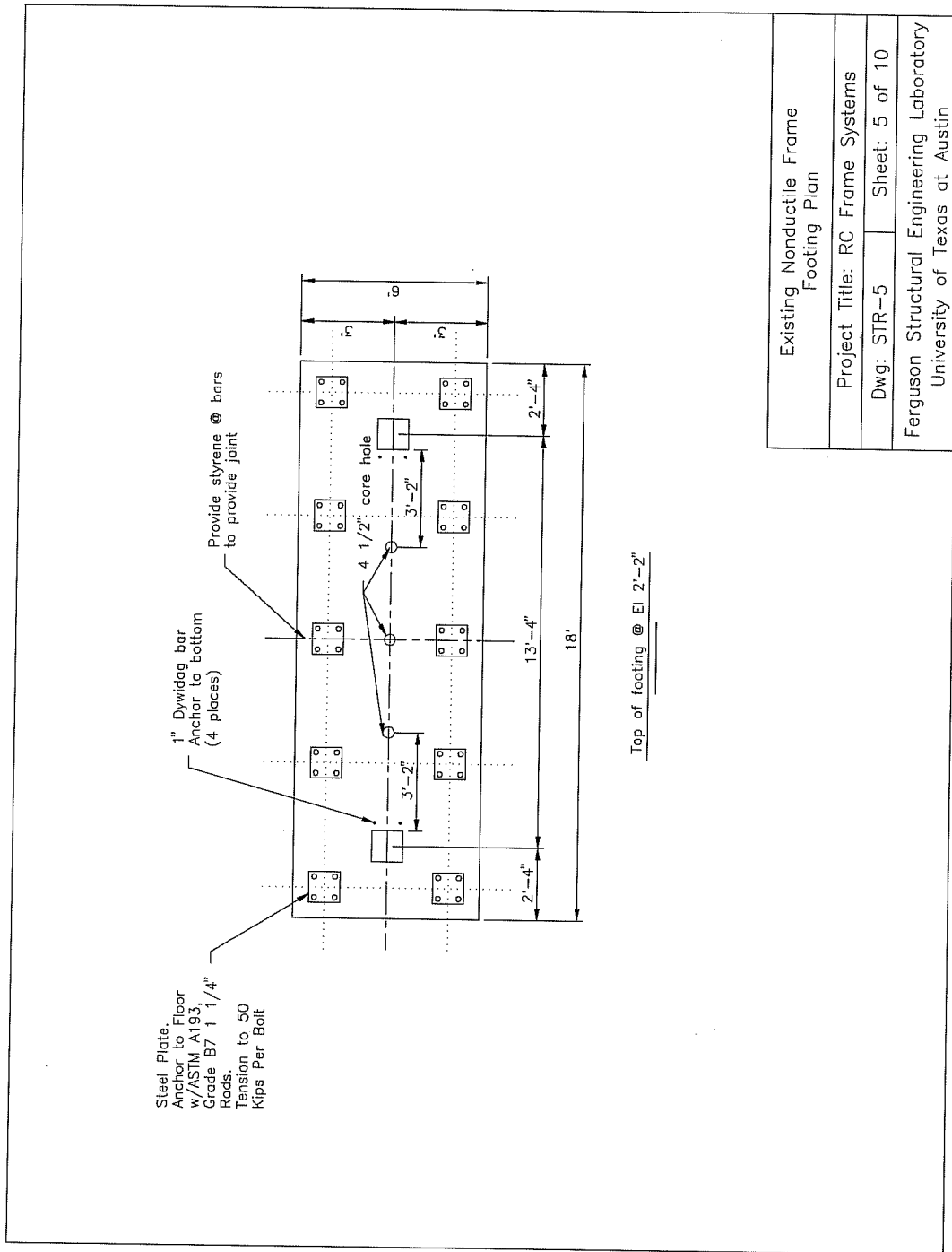
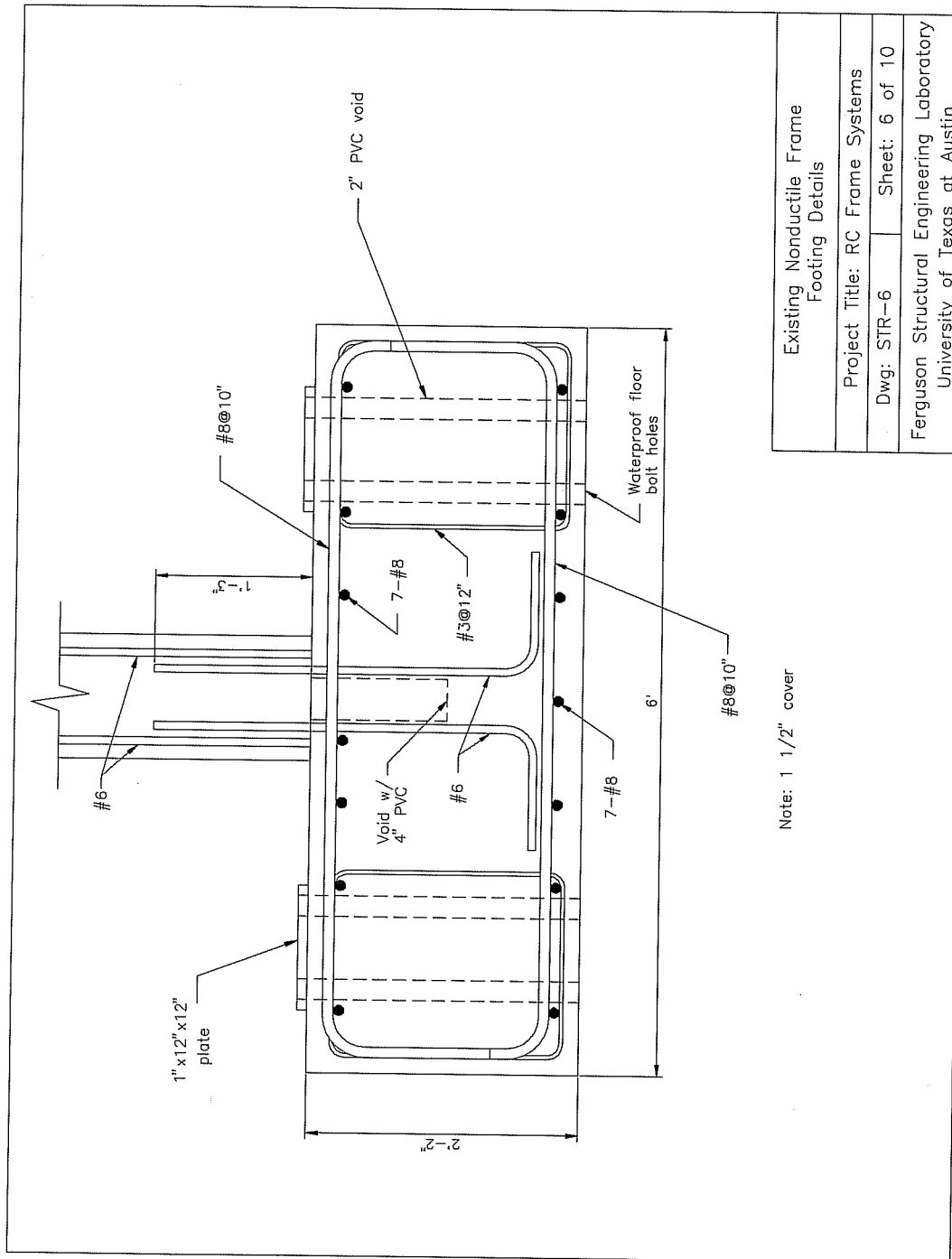


Figure C.5: Footing Plan



Note: 1 1/2" cover

Existing Nonductile Frame Footing Details	
Project Title: RC Frame Systems	
Dwg: STR-6	Sheet: 6 of 10
Ferguson Structural Engineering Laboratory University of Texas at Austin	

Figure C.6: Footing Details

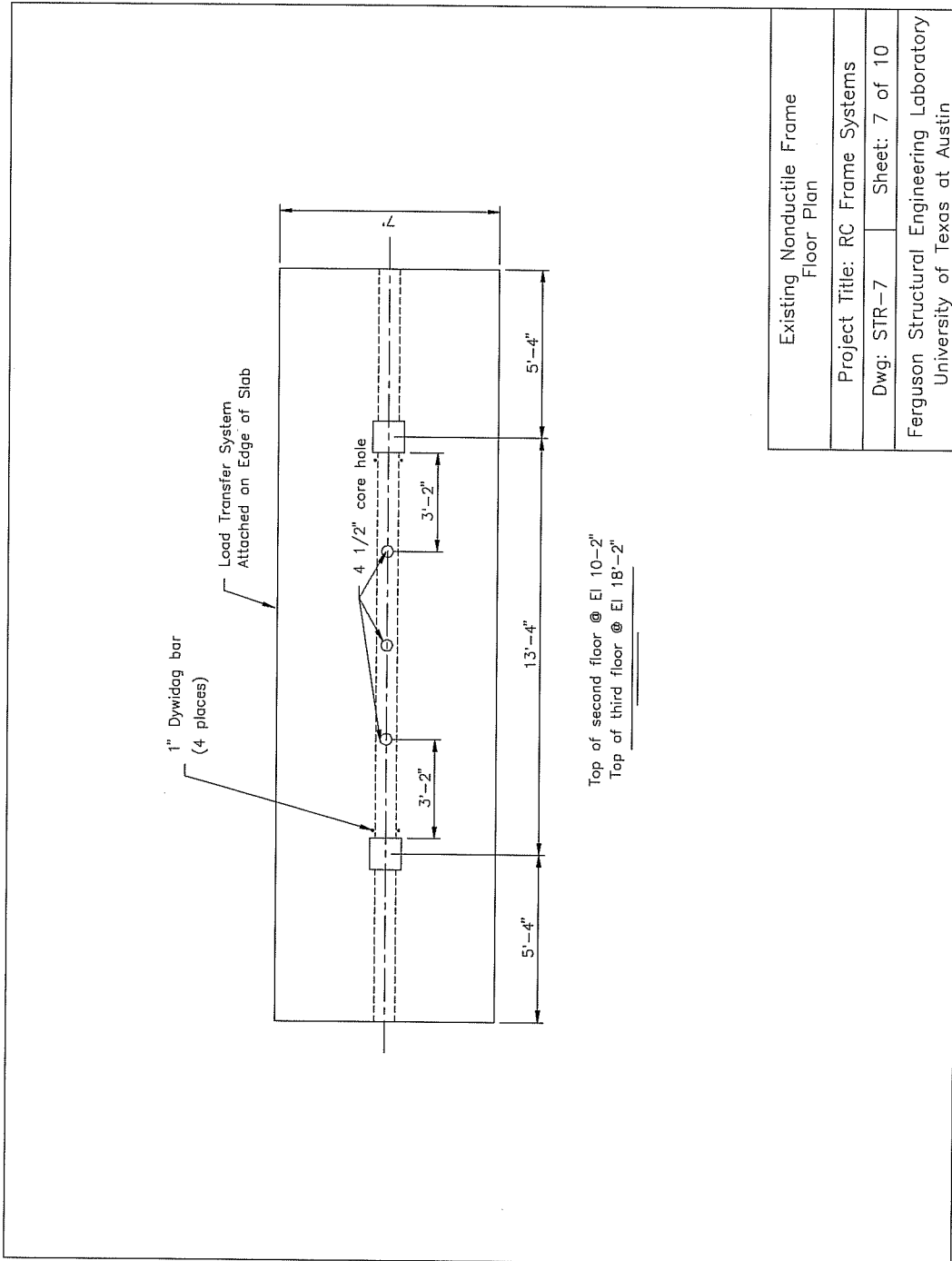


Figure C.7: Floor Plan

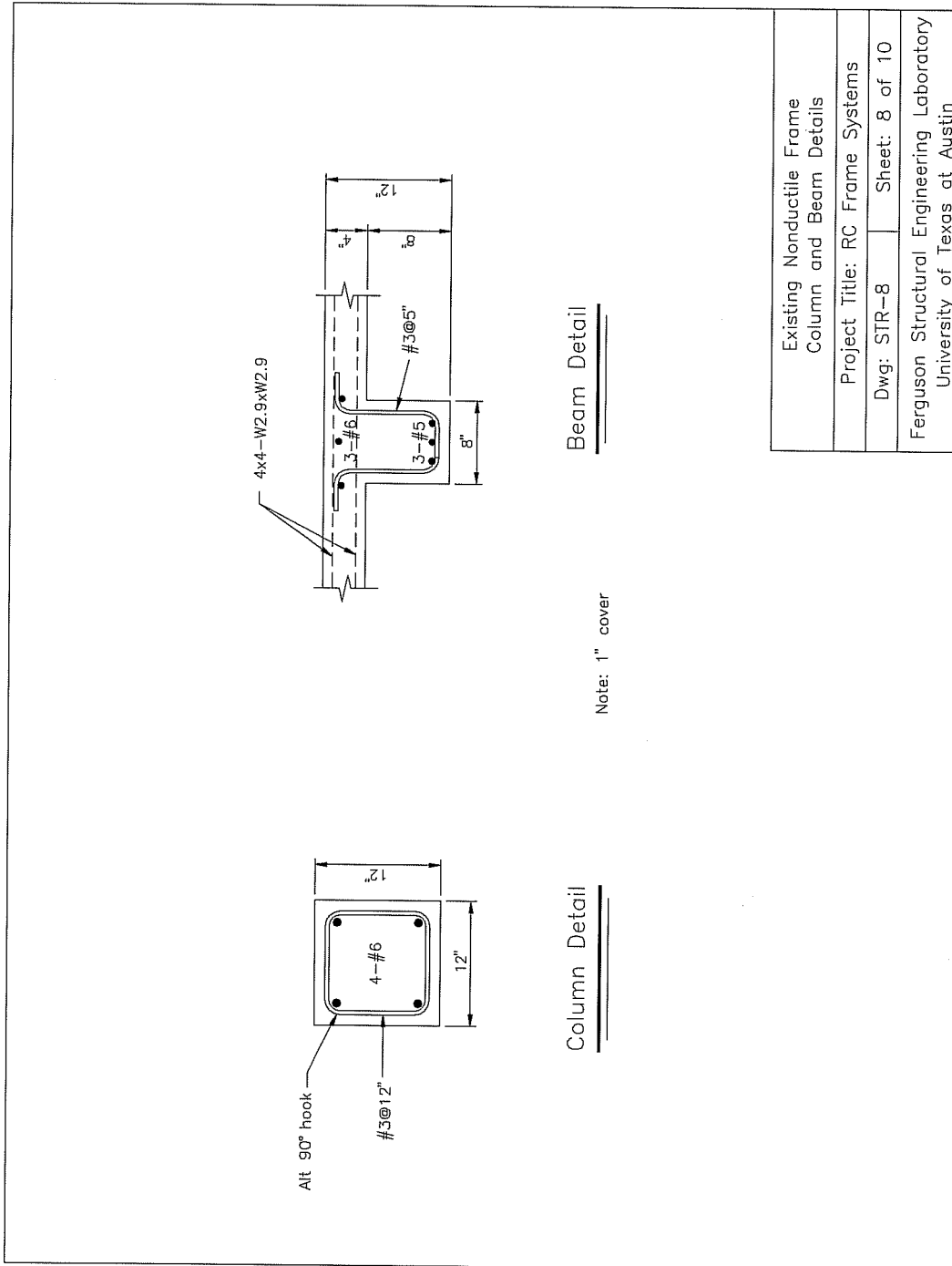


Figure C.8: Column and Beam Details

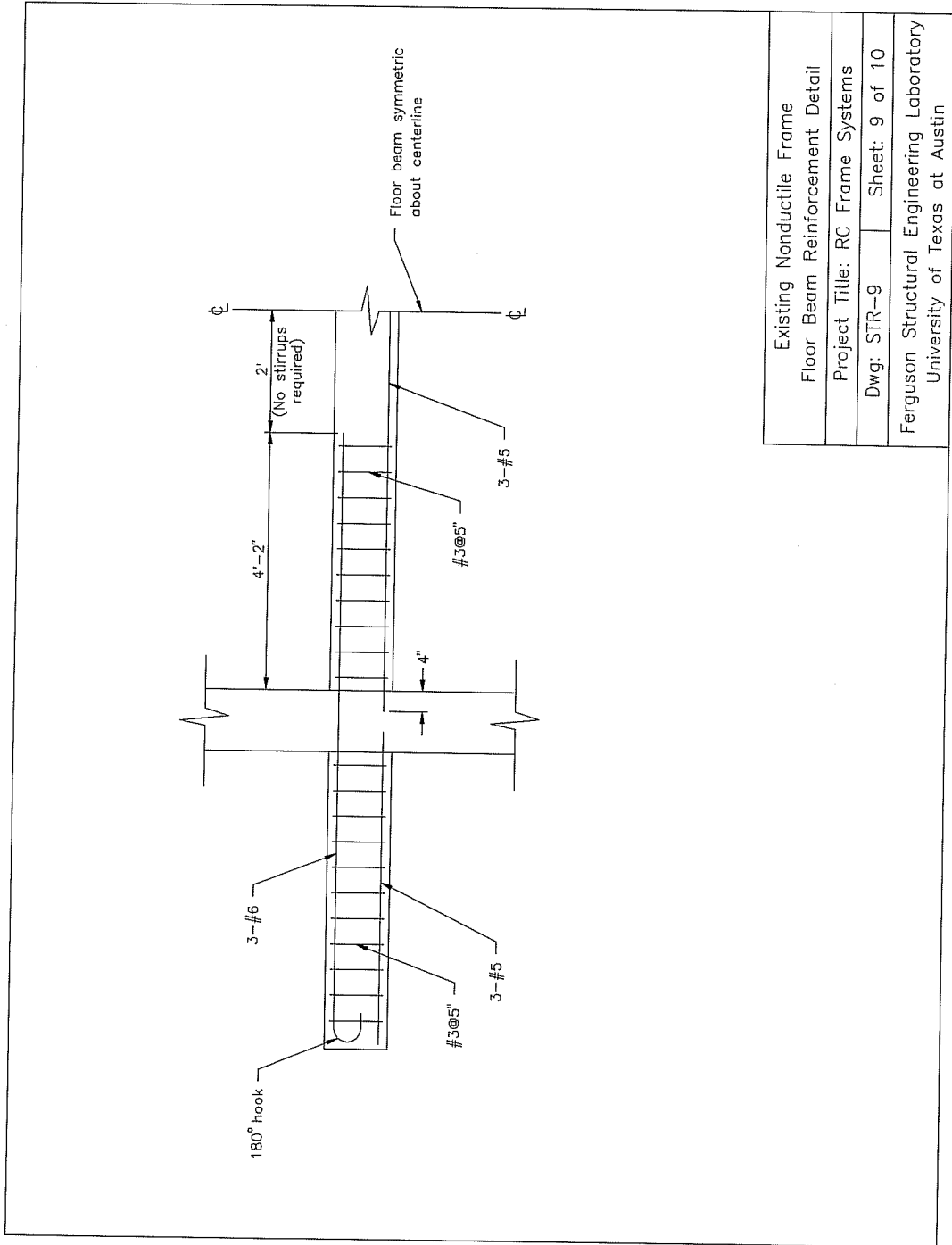


Figure C.9: Floor Beam Reinforcement Details

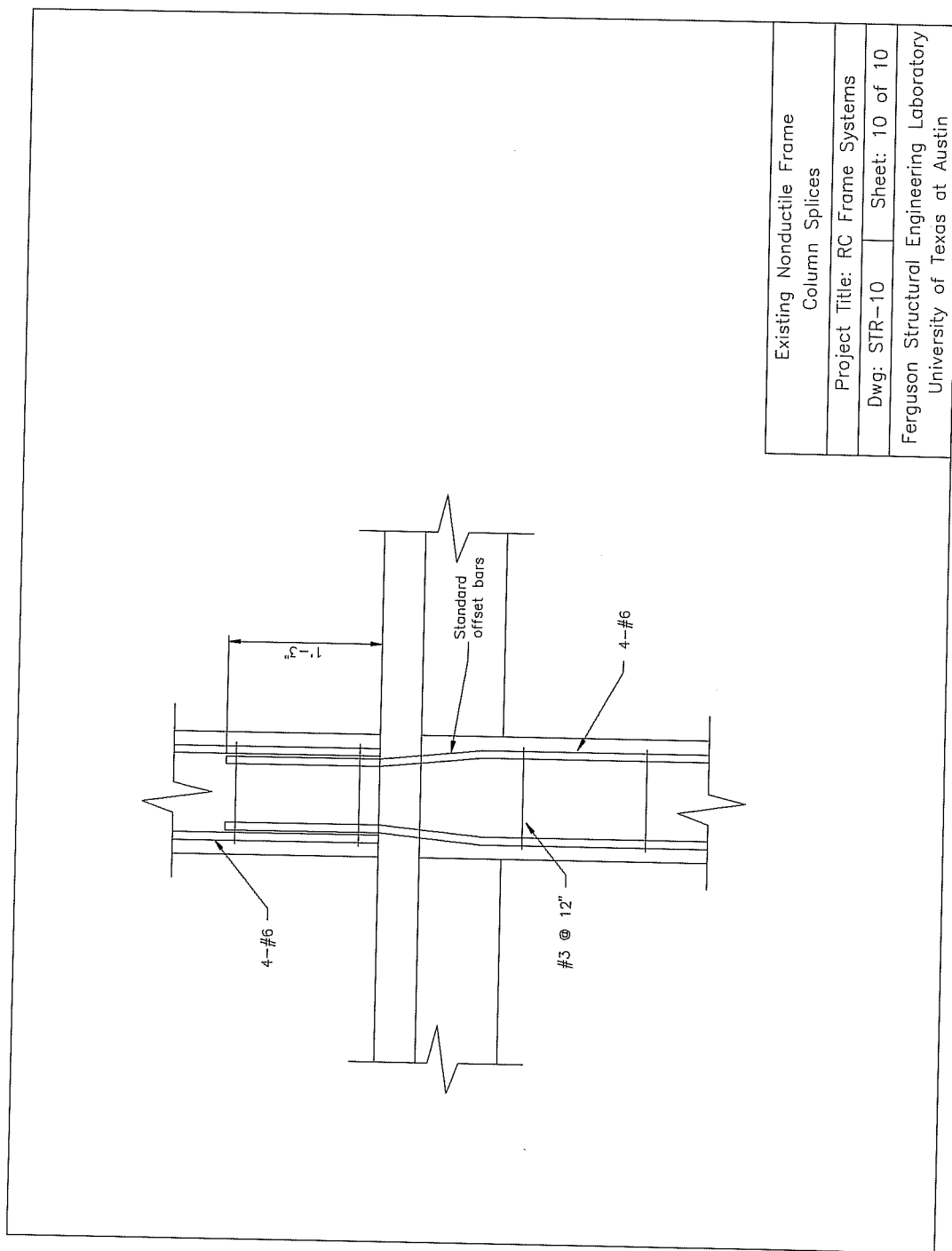


Figure C.10: Column Splices

APPENDIX D
INFILL WALL STRUCTURAL DRAWINGS

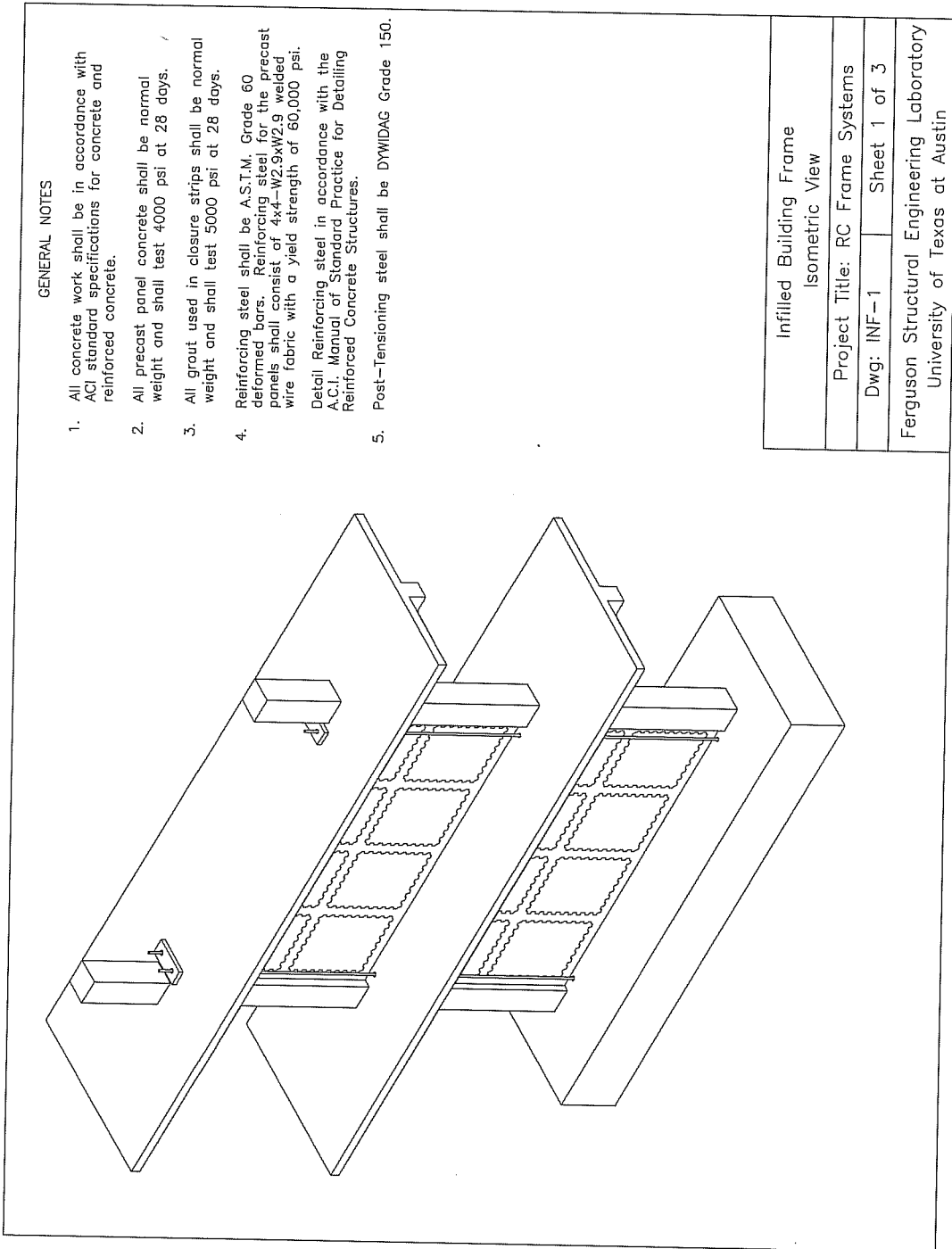


Figure D.1: Isometric View

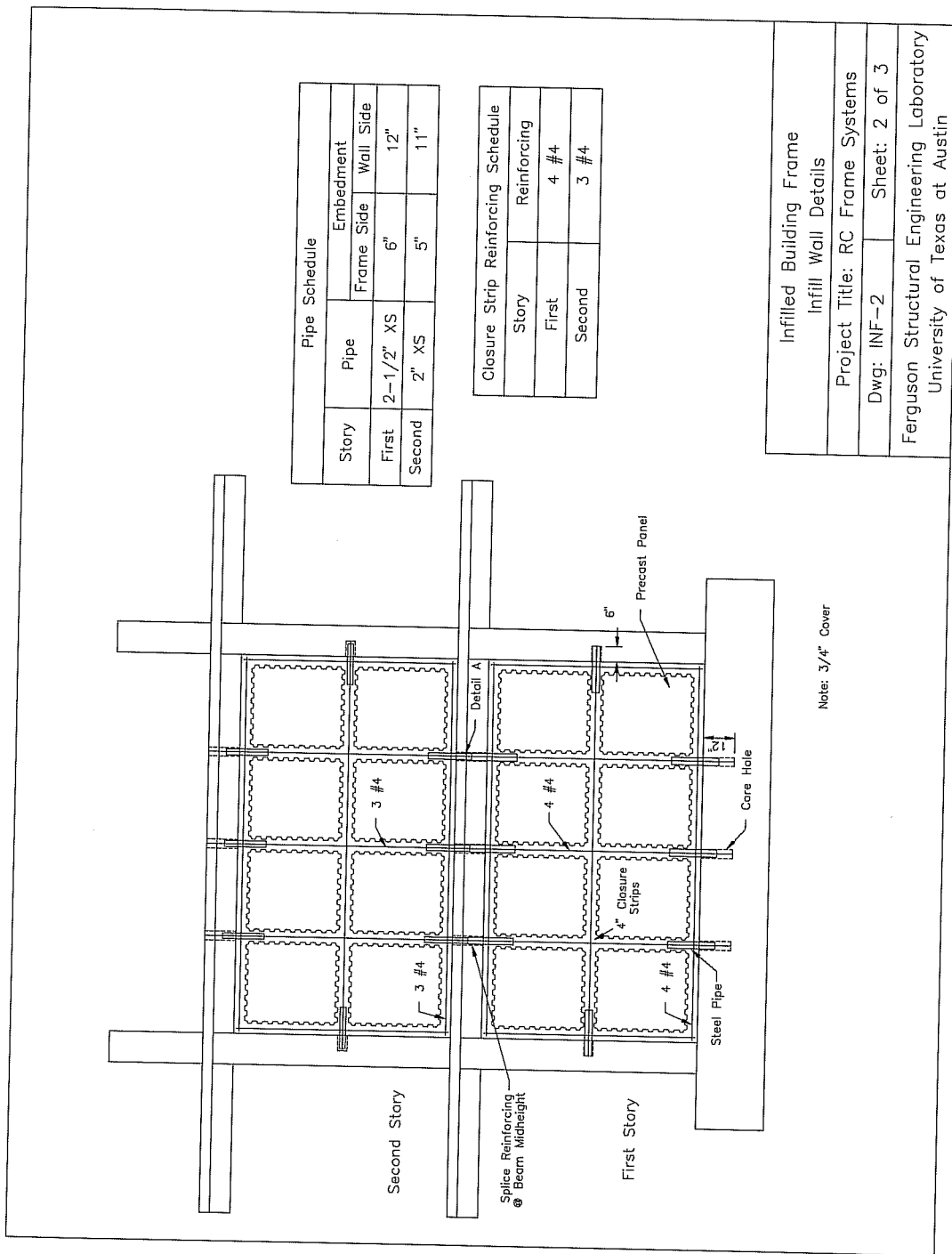


Figure D.2: Infill Wall Details

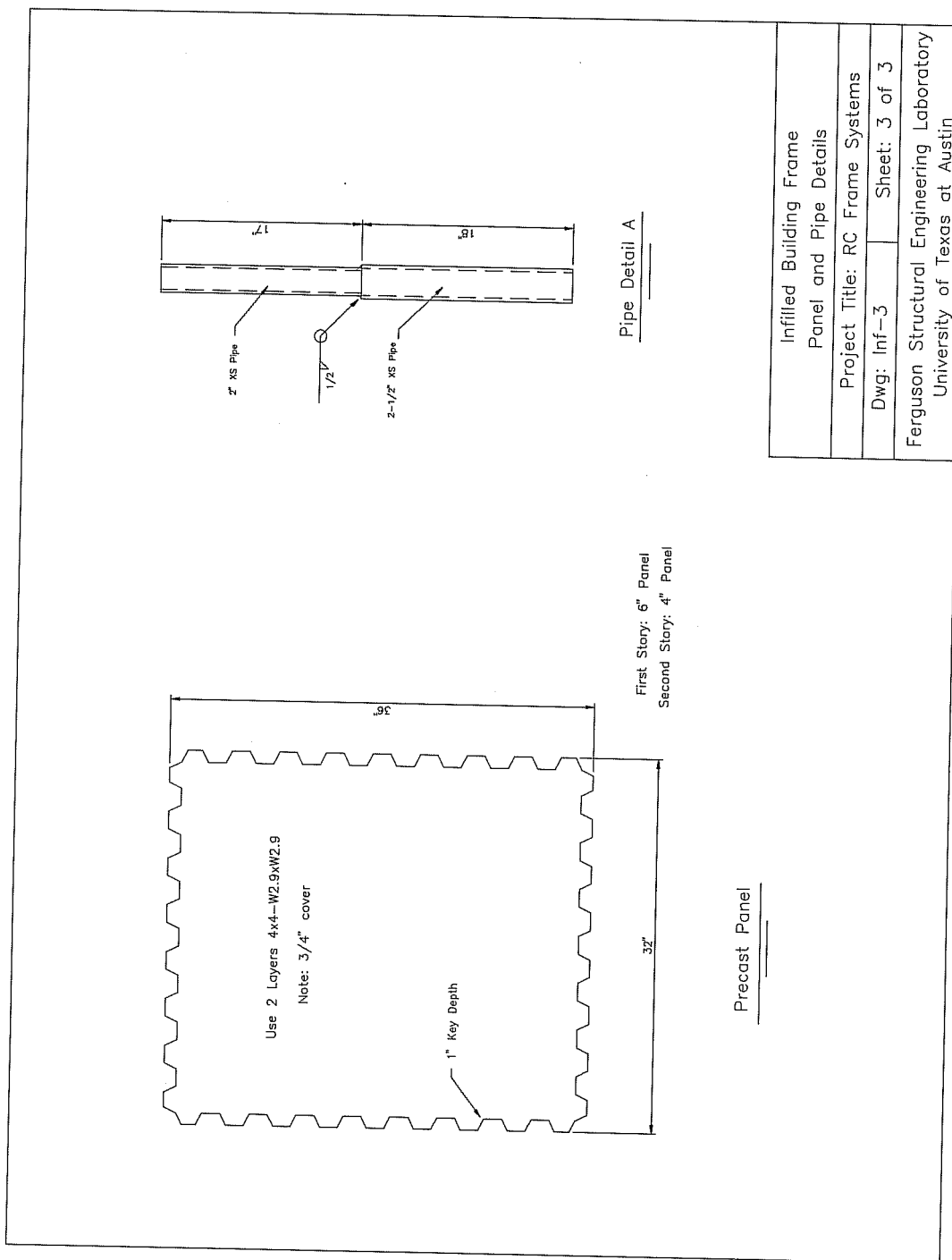


Figure D.3: Panel and Pipe Details

APPENDIX E
LOADING AND BRACING SYSTEM DRAWINGS

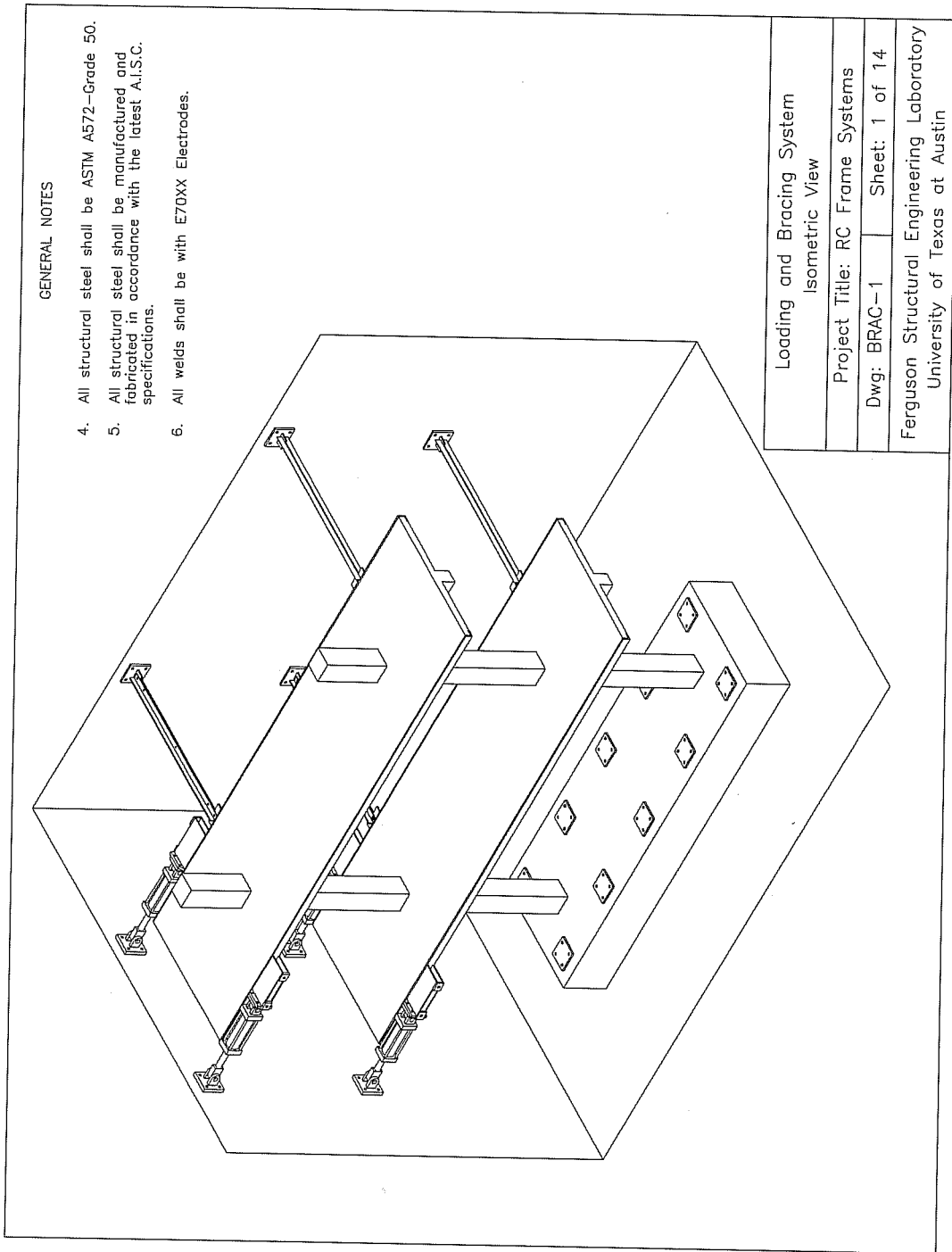


Figure E.1: Isometric View

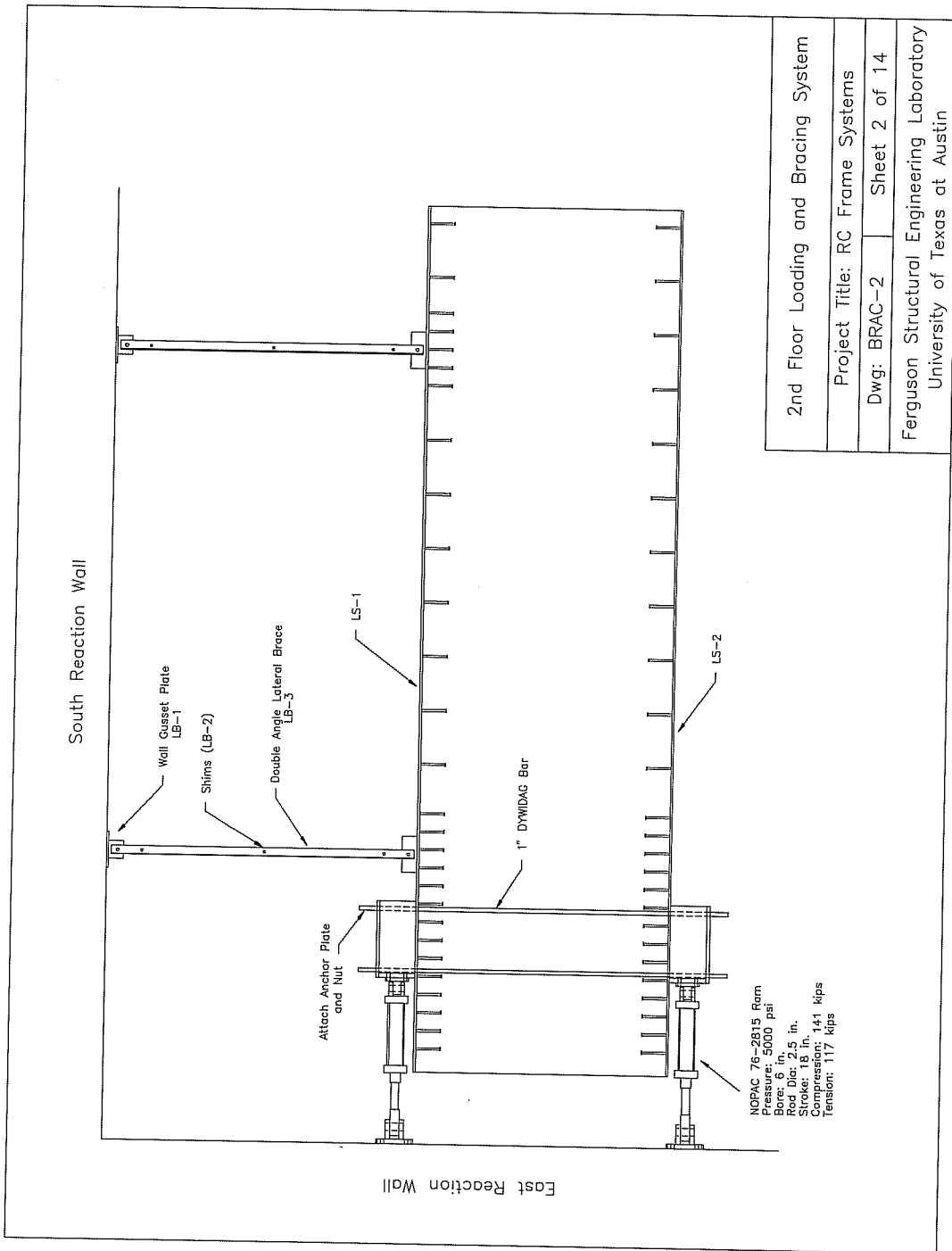


Figure E.2: 2nd Floor Loading and Bracing System

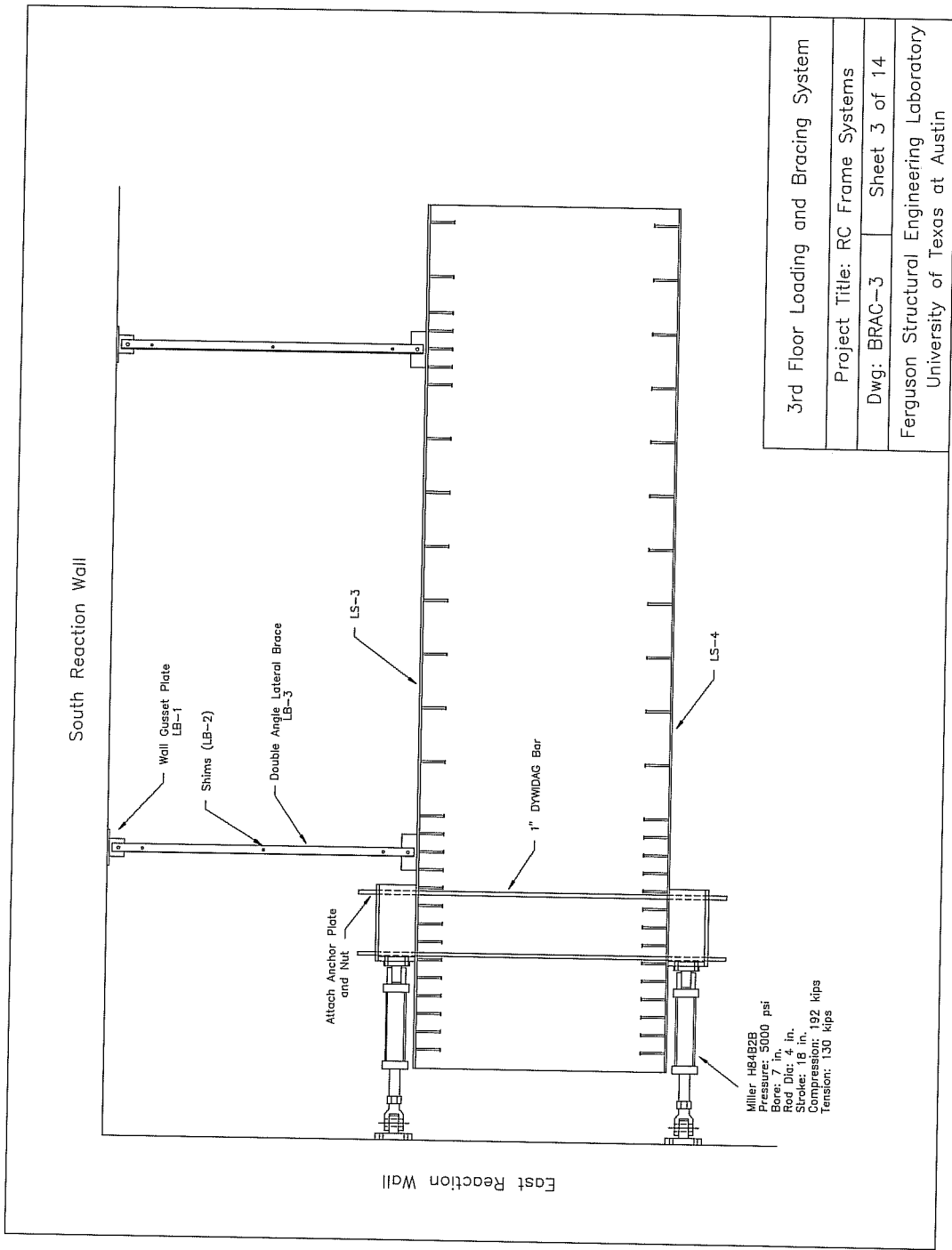
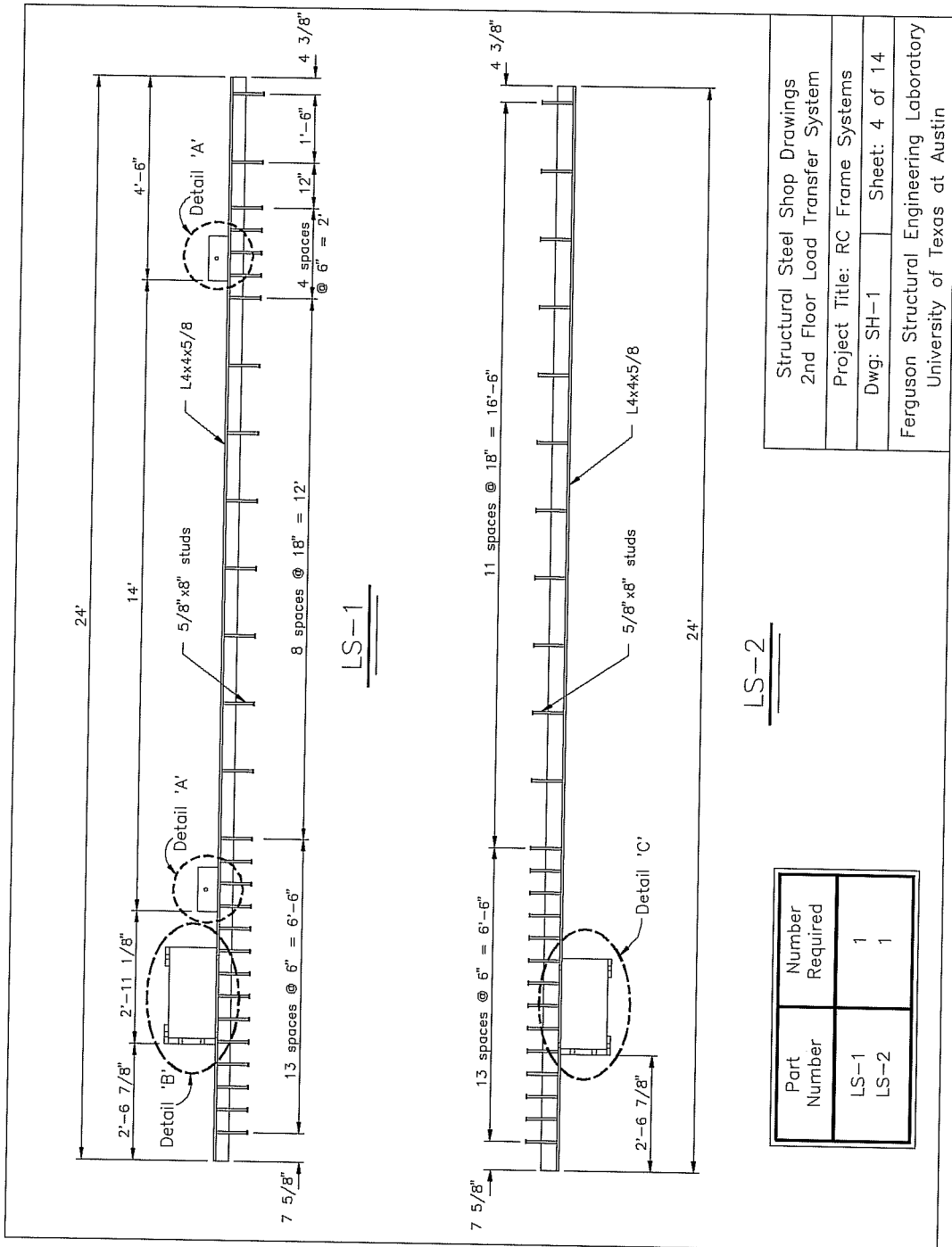


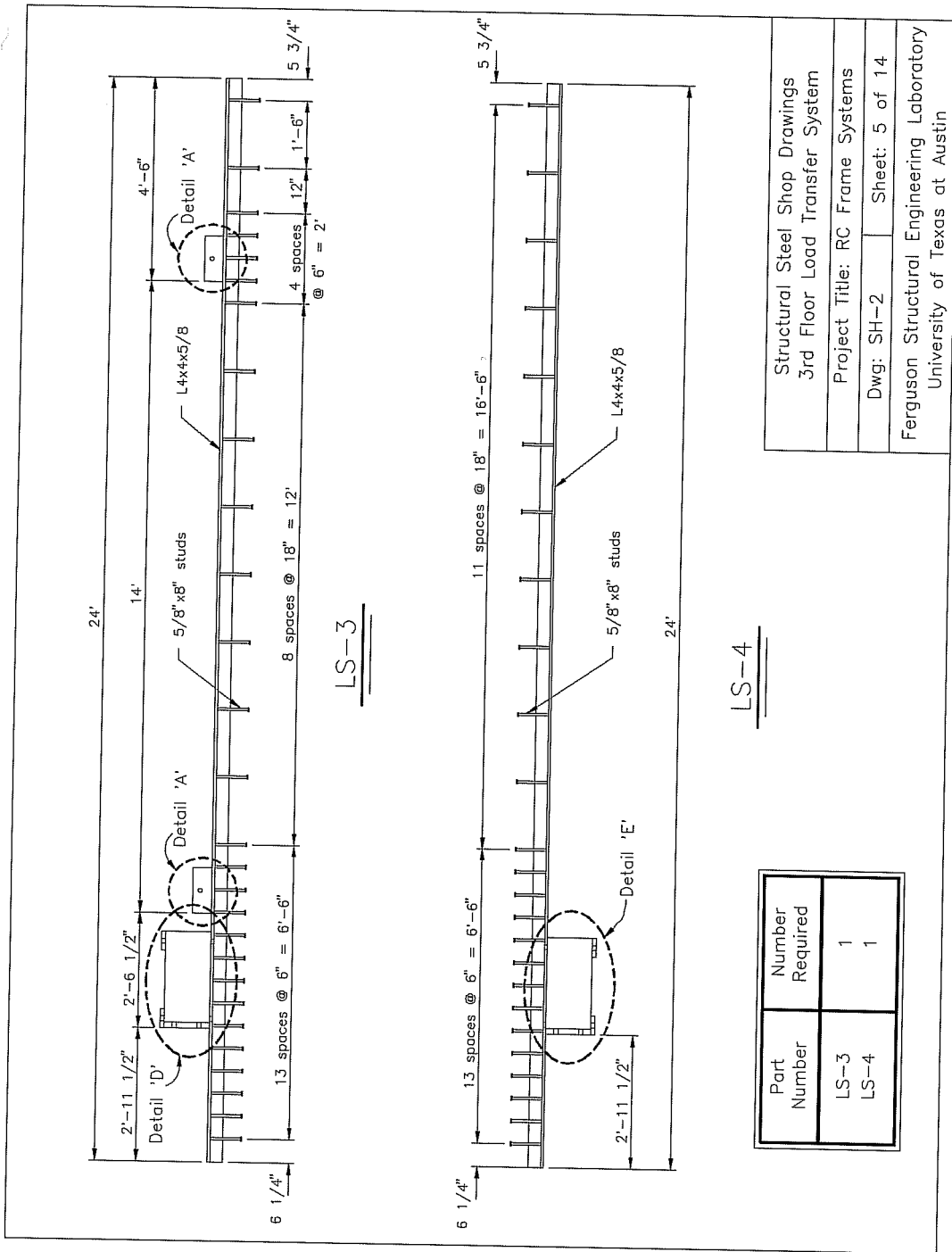
Figure E.3: 3rd Floor Loading and Bracing System



Structural Steel Shop Drawings	
2nd Floor Load Transfer System	
Project Title: RC Frame Systems	
Dwg: SH-1	Sheet: 4 of 14
Ferguson Structural Engineering Laboratory University of Texas at Austin	

Part Number	Number Required
LS-1	1
LS-2	1

Figure E.4: 2nd Floor Load Transfer System



Structural Steel Shop Drawings	
3rd Floor Load Transfer System	
Project Title: RC Frame Systems	
Dwg: SH-2	Sheet: 5 of 14
Ferguson Structural Engineering Laboratory University of Texas at Austin	

Part Number	Number Required
LS-3	1
LS-4	1

Figure E.5: 3rd Floor Load Transfer System

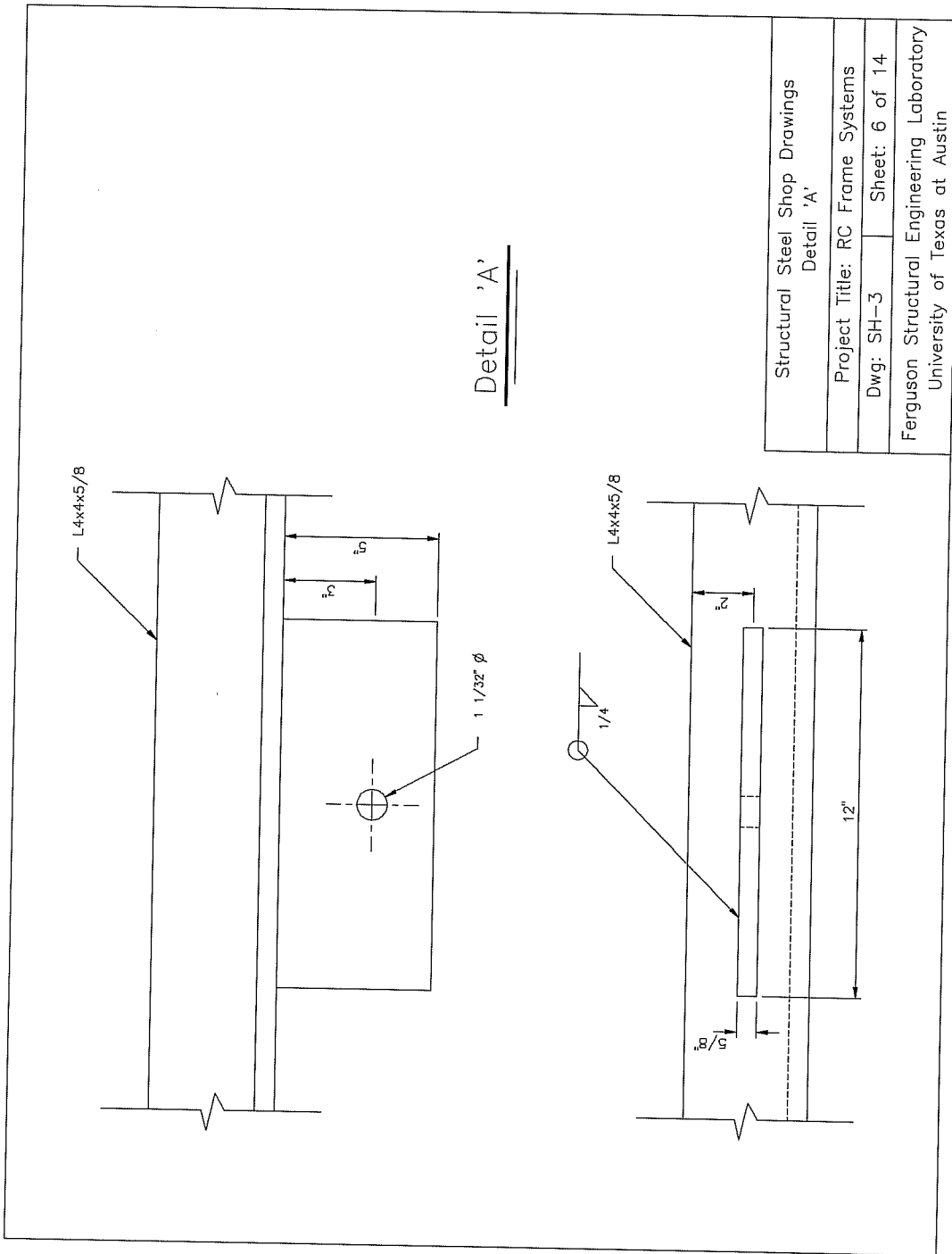


Figure E.6: Detail 'A'

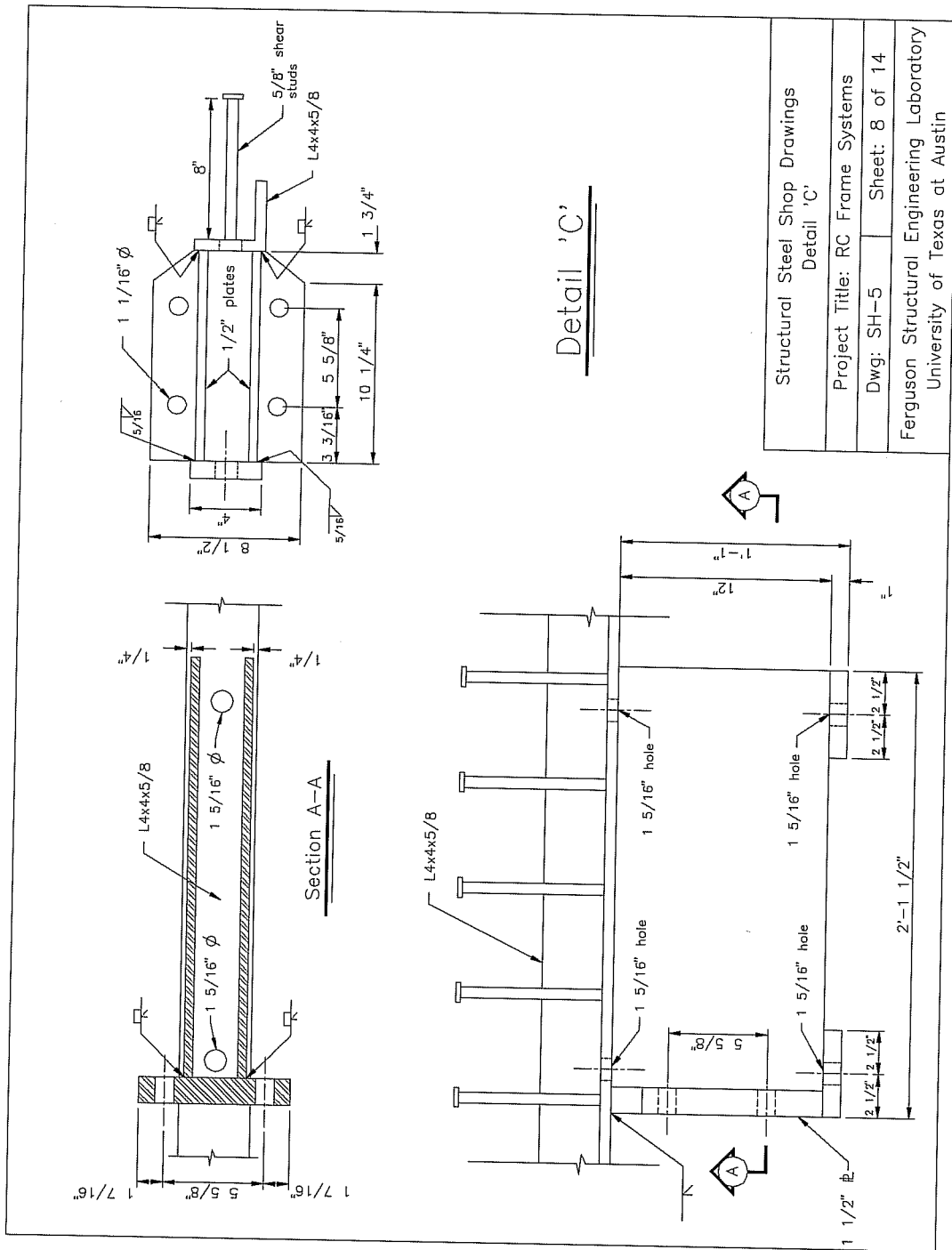


Figure E.8: Detail 'C'

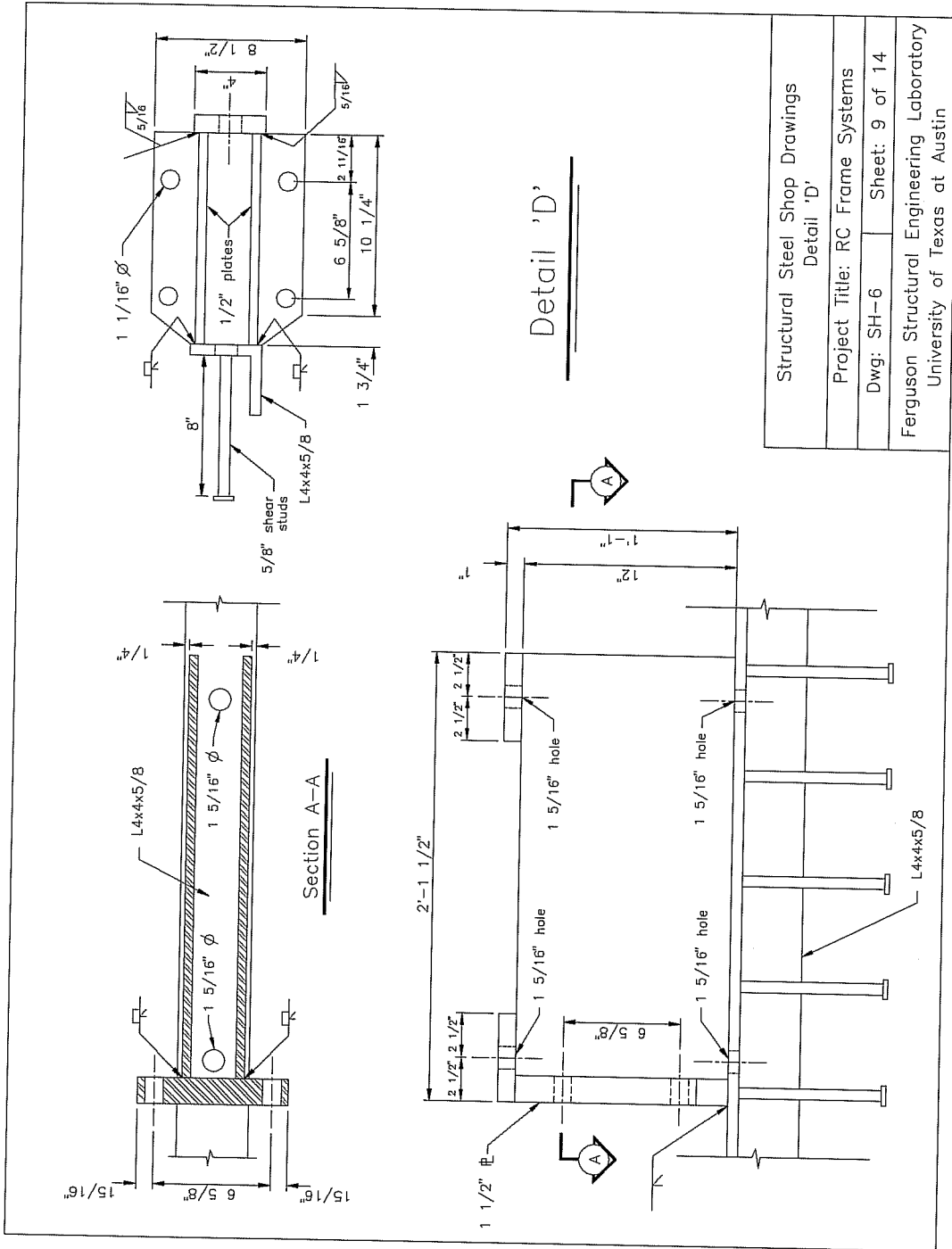


Figure E.9: Detail 'D'

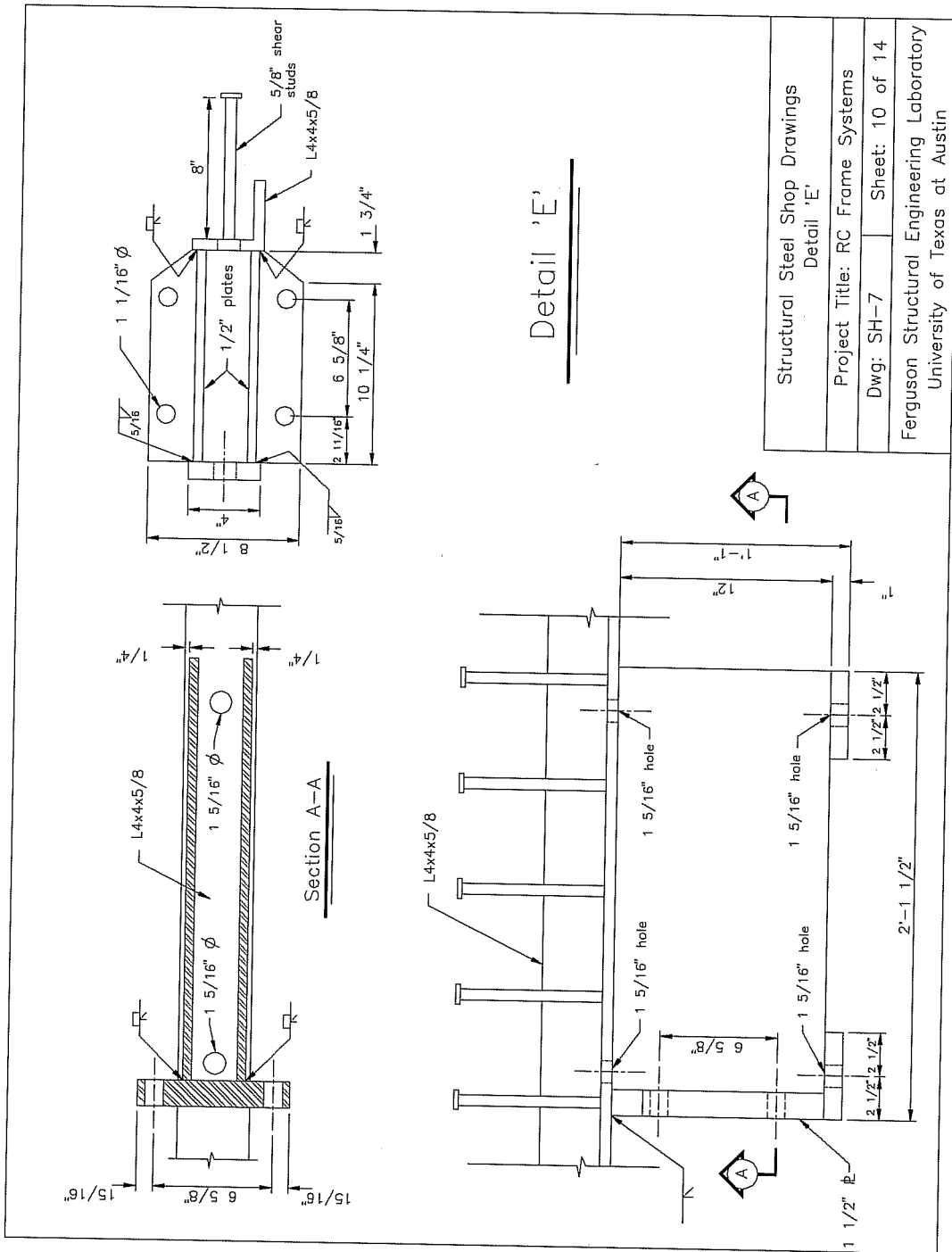


Figure D.10: Detail 'E'

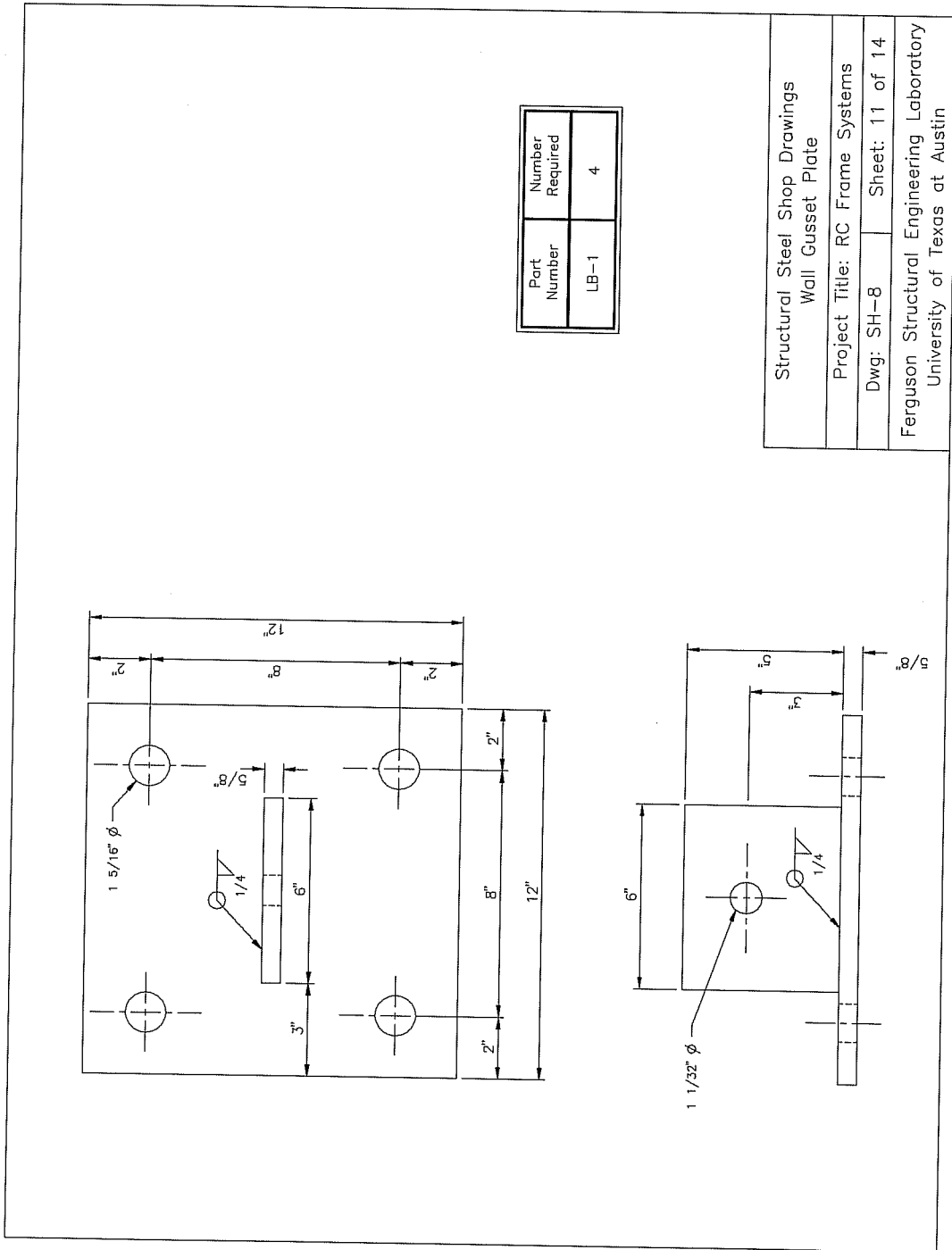
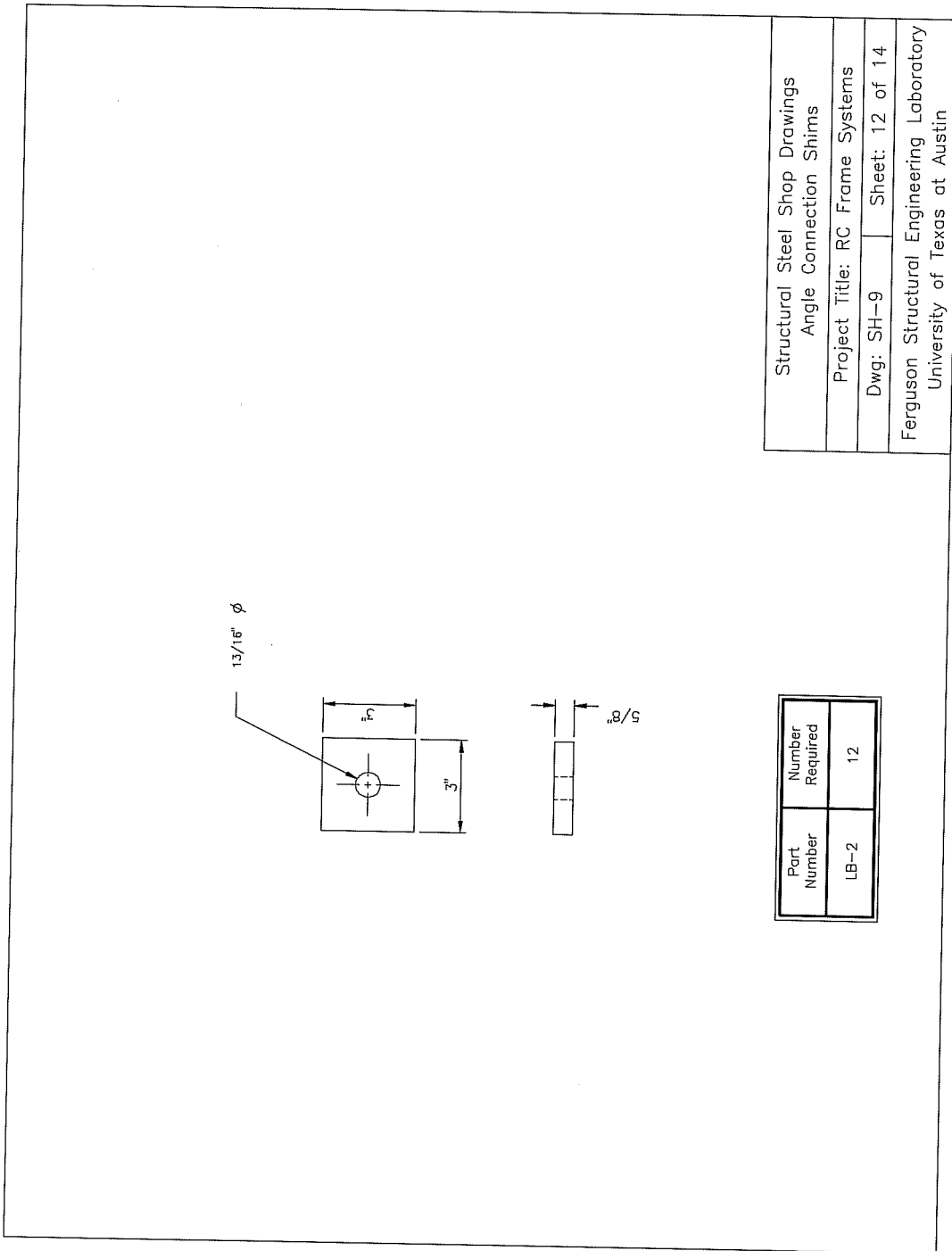


Figure E.11: Wall Gusset Plate



Structural Steel Shop Drawings
 Angle Connection Shims
 Project Title: RC Frame Systems
 Dwg: SH-9 Sheet: 12 of 14
 Ferguson Structural Engineering Laboratory
 University of Texas at Austin

Figure E.12: Angle Connection Shims

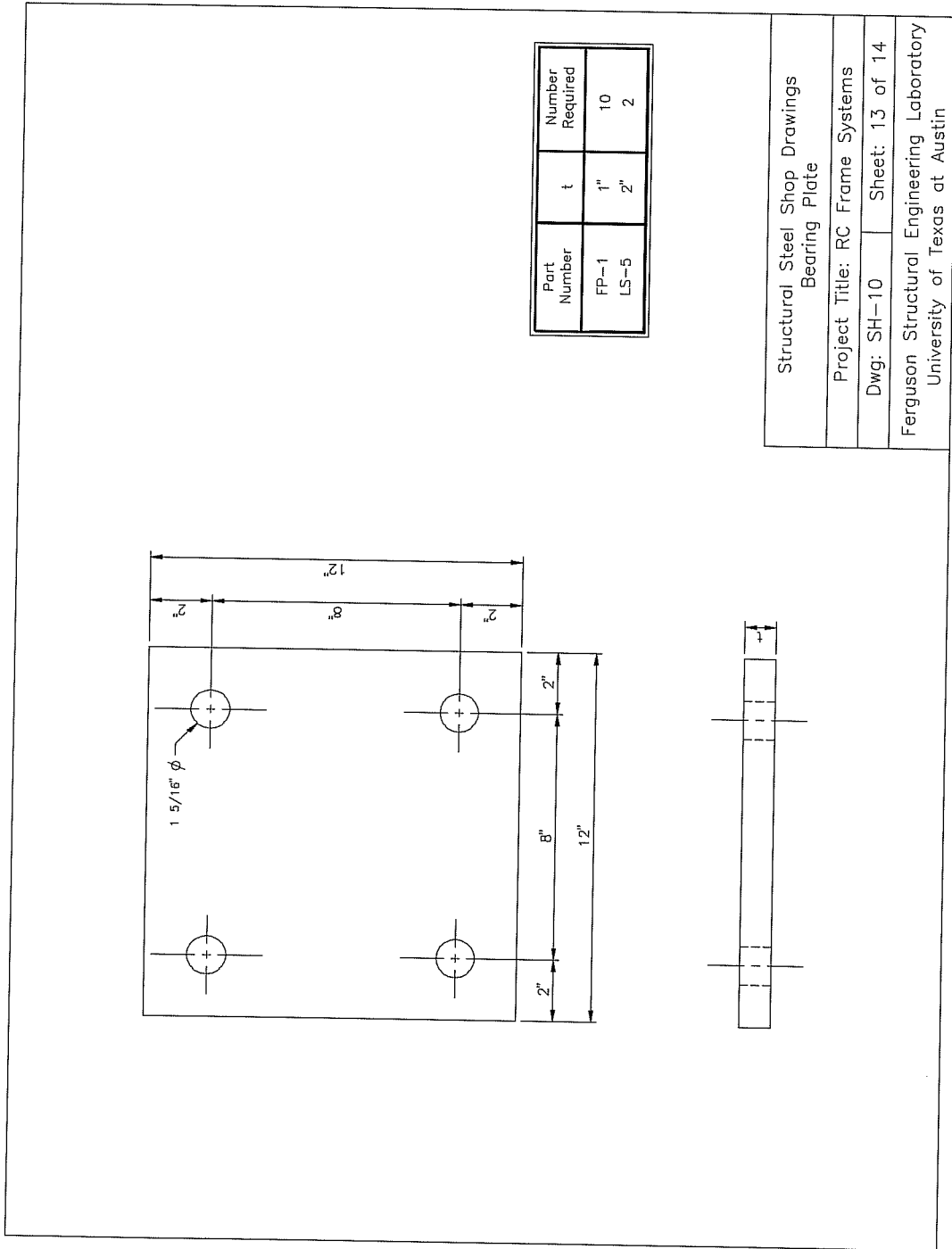


Figure E.13: Bearing Plate

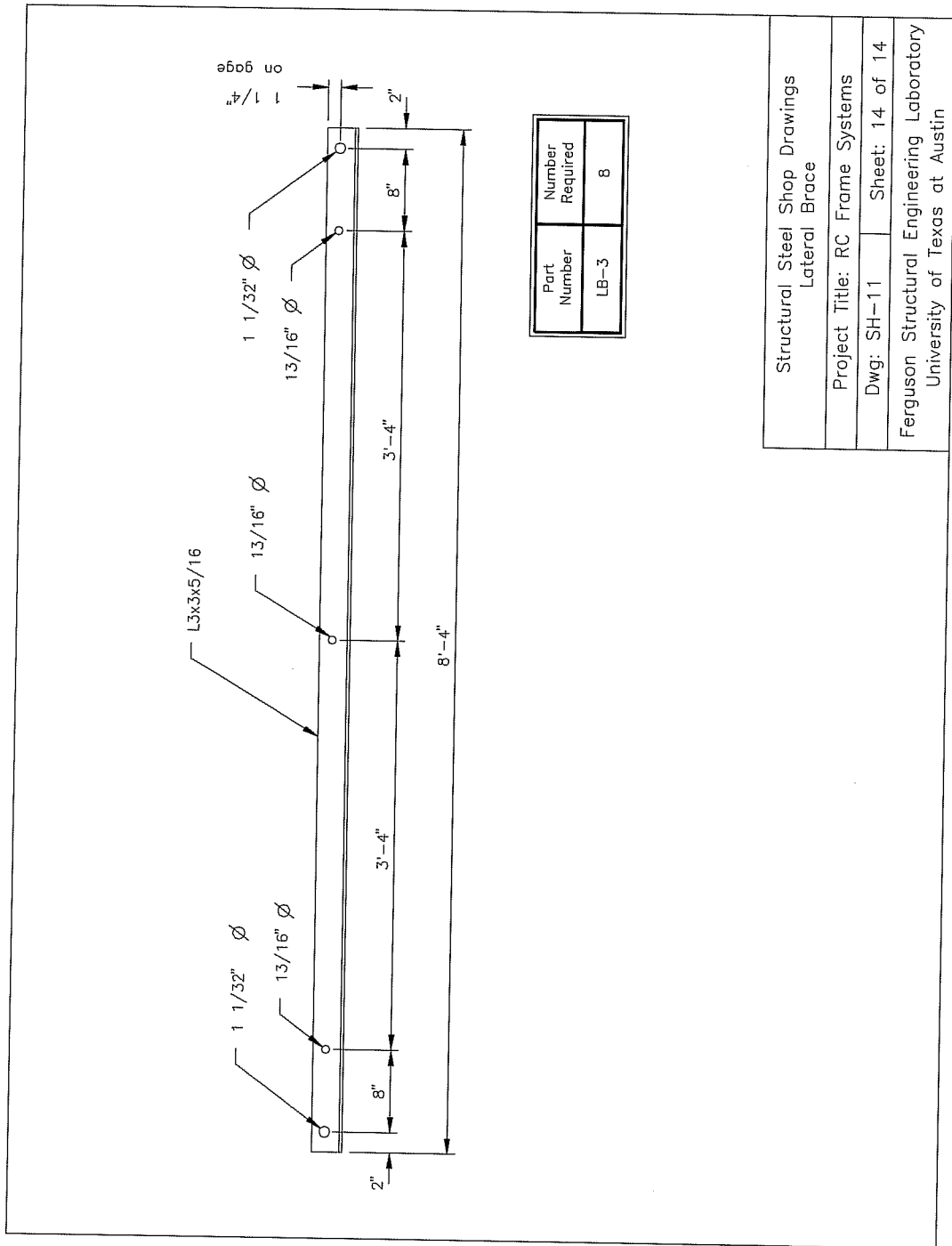


Figure E.14: Lateral Brace

BIBLIOGRAPHY

1. ACI Committee 318, "Building Code Requirements for Reinforced Concrete," ACI 318-56, American Concrete Institute, Detroit, 1956.
2. ACI Committee 318, "Building Code Requirements for Reinforced Concrete," ACI 318-63, American Concrete Institute, Detroit, 1963.
3. ACI Committee 318, "Building Code Requirements for Reinforced Concrete and Commentary," ACI 318-89, American Concrete Institute, Detroit, 1989.
4. AISC, "Manual of Steel Construction -Load & Resistance Factor Design," American Institute of Steel Construction, Inc., Chicago, Ill, 1986.
5. Bakhoun, M.M., Buyukozturk, O., and Beattie, S.M., "Structural Performance of Joints in Precast Concrete Segmental Bridges," *MIT Research Report No. R89-26*, Department of Civil Engineering, MIT, Cambridge, MA, Nov. 1989.
6. Bass, R.A., Carrasquillo, R.L., and Jirsa, J.O., "Interface Shear Capacity of Concrete Surfaces Used in Strengthening Structures," *PMFSEL Report No. 85-4*, University of Texas, Austin, Dec. 1985, 82 pp.
7. Bass, R.A., Carrasquillo, R.L., and Jirsa, J.O., "Shear Transfer across New and Existing Concrete Interfaces," *ACI Structural Journal*, V. 86, No. 4, July-Aug. 1989, pp.383-393.
8. Becker, J.M., and Llorente, C., "Seismic Design of Precast Concrete Panel Buildings," *Proceedings of a Workshop on Earthquake Resistant Reinforced Concrete Building Construction*, Vol. 3, U.C. Berkeley, July 1977.
9. Berg, G.V., Seismic Design Codes and Procedures, Earthquake Engineering Research Institute, 1982.
10. Bergmeister, K., Breen, J.E., Jirsa, J.O., and Kreger, M.E., "Detailing for Structural Concrete," *PMFSEL Report No. 1127-3F*, University of Texas at Austin, May 1993, 300 pp.

11. Birkeland, P.W., and Birkeland, H.W., "Connections in Precast Concrete Construction," *ACI Journal, Proceedings*, Vol. 63, No. 3, Mar. 1966, pp. 345-368.
12. Cholewicki, A., "Loadbearing Capacity and Deformability of Vertical Joints in Structural Walls of Large Panel Buildings," *Building Science*, Vol. 6, 1971, pp. 163-184.
13. Cowper, G.R., "The Shear Coefficient in Timoshenko's Beam Theory," *Journal of Applied Mechanics*, June 1966, pp.335-340.
14. Davis, H.E., Troxell, G.E., and Hauck, G.F.W., The Testing of Engineering Materials, McGraw-Hill, Inc., 1982.
15. FEMA-172, *NEHRP Handbook for Seismic Rehabilitation of Existing Buildings*, Building Seismic Safety Council, Washington, D.C., 1992.
16. FEMA-178, *NEHRP Handbook for the Seismic Evaluation of Existing Buildings*, Building Seismic Safety Council, Washington, D.C., 1992.
17. FEMA-222, *NEHRP Recommended Provisions for the Development of Seismic Regulations for New Buildings*, Building Seismic Safety Council, Washington, D.C., 1991.
18. Gaynor, P.J. "The Effect of Openings on the Cyclic Behavior of Shear Walls," *M.S. Thesis*, The University of Texas at Austin, May 1988, 245 pp.
19. Hofbeck, J.A., Ibrahim, I.O., and Mattock, Alan H., "Shear Transfer in Reinforced Concrete," *ACI Journal*, Vol. 66, No. 2, Feb. 1969, pp. 119-128.
20. Hurd, M.K., *Formwork for Concrete*, SP-4, Fifth Edition, American Concrete Institute, Detroit, 1989.
21. Jimenez, L.R., "Strengthening of RC Frames Using an Eccentric Wall," *M.S. Thesis*, The University of Texas at Austin, May 1989, 67 pp.
22. Kosmatka, S.H. and Panarese, W.C., Design and Control of Concrete Mixtures, Portland Cement Association, 1988.

23. Koseki, K., and Breen, J.E., "Exploratory Study of Shear Strength of Joints for Precast Segmental Bridges," *PMFSEL Report No. 248-1*, University of Texas at Austin, Sept. 1983, 94 pp.
24. Lin, T.Y., and Burns, N.H., Design of Prestressed Concrete Structures, John Wiley & Sons, Inc., New York, 1981.
25. Mast, R.F., "Auxiliary Reinforcement in Concrete Connections," *Proceedings*, ASCE, Vol. 94, ST6, June 1968, pp. 1485-1504.
26. Mattock, A.H., "Shear Transfer in Concrete Having Reinforcement at an Angle to the Shear Plane," *Shear in Reinforced Concrete, SP-42*, American Concrete Institute, Detroit, 1974, pp. 17-42.
27. Mattock, A.H., and Hawkings, N.M., "Shear Transfer in Reinforced Concrete - Recent Research," *Journal, Prestressed Concrete Institute*, V. 17, No. 2, Mar-Apr. 1972, pp.55-75.
28. Mindess, S., and Young, J.F., Concrete, Prentice Hall, Inc., Englewood Cliffs, New Jersey, 1981.
29. Orangun, C.O., Jirsa, J.O., and Breen, J.E., "A Reevaluation of Test Data on Development Length and Splices," *ACI Journal*, March 1977, pp. 114-122.
30. Paulay, T., and Loeber, P.J., "Shear Transfer by Aggregate Interlock," *SP 42-1*, American Concrete Institute, Detroit, 1974, pp. 1-14.
31. Paulay, T., Park, R., and Phillips, M.H., "Horizontal Construction Joints In Cast-In-Place Reinforced Concrete," *SP 42-27*, American Concrete Institute, Detroit, 1974, pp. 599-616.
32. Paulay, T. and Prestley, M.J.N., Seismic Design of Reinforced Concrete and Masonry Buildings, John Wiley & Sons, Inc., New York, 1992.
33. Popov, E.P., Mechanics of Materials, Prentice-Hall, Inc. Englewood Cliffs, New Jersey, 1976.
34. Schlaich, J., Schafer, K., and Jennewein, M., "Toward a Consistent Design of Structural Concrete," *Prestressed Concrete Institute*, Vol. 32, No. 3, May-June 1987, pp. 74-150.

35. SEAOC, *Recommended Lateral Force Requirements and Commentary* ("Blue Book"), Seismology Committee, Structural Engineers Association of California, Sacramento, CA, 1990.
36. Shah, S.N., "Evaluation of Infill Wall Strengthening Schemes for Non-Ductile RC Buildings," *M.S. Thesis*, The University of Texas at Austin, May 1989, 68 pp.
37. UBC, *Uniform Building Code*, International Conference of Building Officials, Whittier, CA, 1991.
38. Valluvan, R., "Issues Involved In Seismic Retrofit of Reinforced Concrete Frames Using Infilled Walls," *Ph.D. Dissertation*, The University of Texas at Austin, December 1993, 293 pp.
39. Zeck, U. "Joints in Large Panel Precast Concrete Structures," *M.S. Thesis*, Department of Civil Engineering, Mass. Inst. of Tech., Cambridge, MA, 1976.
40. Zia, P., "Torsional Strength of Prestressed Concrete Members," *Journal of the American Concrete Institute*, Vol. 57, No. 10, April 1961, pp.1337-1359.

VITA

Robert Joseph Frosch was born in New Orleans, Louisiana, on May 1, 1969, the son of Bessie Gagliano Frosch and Warren Robert Frosch, Jr. After graduating Summa Cum Laude from Holy Cross High School, New Orleans, Louisiana, in 1987, he entered Tulane University in New Orleans, Louisiana. He graduated in May, 1991, as valedictorian of the School of Engineering receiving the degree of Bachelor of Science in Engineering, Summa Cum Laude with Departmental Honors. In September, 1991, he entered the Graduate School of the University of Texas at Austin. He graduated in December, 1992, receiving the degree of Master of Science in Engineering. He is the recipient of the Engineering Foundation Graduate Fellowship, the Engineering Endowed Presidential Graduate Scholarship, the John E. Breen Endowed Presidential Scholarship, the Hemphill/Gilmore Fellowship, and the EERI/FEMA NEHRP Graduate Fellowship. He has worked at the University of Texas at Austin as a Teaching Assistant and as a Graduate Research Assistant at the Phil M. Ferguson Structural Engineering Laboratory. Additionally, he has worked for Modjeski and Masters Consulting Engineers as an Engineering Technician and an Engineer-In-Training. He will continue his career with Modjeski and Masters Consulting Engineers.

Permanent Address: 2012 Etienne Drive
Meraux, Louisiana 70075

This dissertation was typed by the author.

Copyright

by

Robert Joseph Frosch

1996